THE DYNAMICS OF MESO-SCALE ATMOSPHERIC CIRCULATIONS

Aarnout VAN DELDEN

Institute for Marine and Atmospheric Research Utrecht, University of Utrecht, Princetonplein 5, 3584 CC Utrecht, The Netherlands

NORTH-HOLLAND

PHYSICS REPORTS (Review Section of Physics Letters) 211, No. 6 (1992) 251–374. North-Holland

PHYSICS REPORTS

THE DYNAMICS OF MESO-SCALE ATMOSPHERIC CIRCULATIONS

Aarnout VAN DELDEN

Institute for Marine and Atmospheric Research Utrecht, University of Utrecht, Princetonplein 5, 3584 CC Utrecht, The Netherlands

Editor: D. ter Haar Received August 1991

Contents:

Abstract:

A review is given of the dynamics of meso-scale atmospheric circulations. An analysis of the instabilities, oscillations and adjustment processes which are possible in a rotating atmosphere in which the rotation rate does not vary in space, yields several characteristic time scales and length scales which can be used to define the meso-scale. Special attention is paid to showing the relation between the circulation associated with convection, the circulation associated with sea breeze, the circulation perpendicular to a front, and the radial circulation in a tropical cyclone. Other important meso-scale weather phenomena which are discussed are gravity-inertia waves, shallow cumulus convection, downslope winds and thunderstorms.

1. General introduction

During the last 20 years there has been a large increase in the interest in meso-scale atmospheric circulations. This has been stimulated mainly by improvements in measuring capabilities and by the introduction of satellites and supercomputers. Meso-scale circulations are responsible for weather events such as sea breeze, thunderstorms, lee-waves, severe downslope windstorms, polar lows and tropical cyclones. Only very slowly is the newly accumulated knowledge finding its way into textbooks on dynamical meteorology. These textbooks [e.g., Dutton 1976, Holton 1979, Gill 1982, Panchev 1985, Pedlosky 1987] are still devoted for the most part to very large-scale atmospheric circulations, such as planetary Rossby waves, mid-latitude depressions, the jetstream and the general circulation of the earth's atmosphere. Probably this reflects the fact that modern theories concerning these phenomena have reached the adult stage, while many theories on meso-scale phenomena are judged too shaky or not instructive enough to be included in books aimed at introducing the serious student to the core of meteorology. It appears that all this is changing very quickly, now that a significant part of the meteorological community has turned to the study of meso-scale weather phenomena. Since 1983, four conferences on meso-scale meteorology have been organized by the American Meteorological Society, the last one being in June 1990. One can obtain a good impression of the increasing interest in the subject by comparing the reports of the first conference [Emanuel 1984] and the third conference [Barnes and LeMone 1988]. These conferences, in addition to the NATO workshop held near Toulouse (France) in 1982 [Lilly and Gal-Chen 1983], and the Intensive Course on Meso-scale Meteorology given in 1984 [see Ray 1986], have helped to bring together the somewhat provincially operating communities, who have tended to concentrate on special topics such as severe local storms or tropical cyclones.

The first textbook devoted completely to meso-scale weather phenomena was the book by Atkinson [1981], entitled "Meso-scale Atmospheric Circulations". In this book meso-scale circulations are classified into two main categories, namely topographically induced circulations and free circulations. An example of a topographically induced circulation is the circulation associated with a sea breeze. An example of a free circulation is a convection cell. Similar classifications are adopted in more recent books on meso-scale meteorology. For example, Ray [1986] distinguishes between externally generated and internally generated circulations, while Pielke [1984] distinguishes between terrain-induced circulations and synoptically induced circulations.

The latter distinction suggests that ultimately all circulations are forced in some way or another. In this review we ask ourselves: "How does the atmosphere react to forcing, given certain constraints?". The constraints can incidentally also be conceived of as forcing.

The atmosphere reacts to forcing through instabilities and adjustment processes. Adjustment and instability are of course intimately related. Nevertheless, the distinction makes sense because, although a circulation resulting from a flow instability can also be conceived of as an adjustment process, the reverse is not always true.

The chapters encompassing this review are concerned with the following topics: (a) a phenomenological introduction to meso-scale circulations, (b) a review of the equations, approximations and models used to describe meso-scale circulations, (c) instabilities, (d) adjustment processes, and (e) forcing-mechanisms. In the chapters on instabilities and on adjustment processes we will investigate the way in which the rotating atmosphere reacts to forcing, given certain external constraints, such as the boundary conditions and rotation rate. We will refrain from saying too much about the details of the forcing in these chapters. This will be postponed until the last main chapter. In that chapter we will discuss specific meso-scale weather phenomena as illustrations of instabilities and adjustment processes

given certain forcing mechanisms. Examples of forcing mechanisms are mountains, latent heat release and large-scale wind-shear.

We will pay quite a lot of attention to the tropical cyclone, even though this conspicuous phenomenon should, from a dynamical point of view, perhaps be characterized as a large-scale circulation. However, hopefully it will become clear that much can be learnt from a study of the tropical cyclone which can help us to understand the properties of (other) meso-scale circulations.

We will also look in some detail at the Boussinesq approximation to the equations of motion and the equation of continuity. Because this approximation is invoked quite frequently in theoretical or numerical studies of meso-scale circulations, it is worthwhile to pay attention to its validity.

Meteorology is principally an application of physics. Therefore, any person with a solid knowledge of physics, especially fluid dynamics and thermodynamics should be able to read and understand this review. Nevertheless, I think a basic knowledge of meteorology, especially dynamical meteorology (e.g. the first nine chapters of the book by Holton [1979]), will be extremely helpful if not essential in order to fully appreciate the subject matter. Above all, I hope that colleagues and advanced students, especially those who are doing or starting fundamental research on individual meso-scale weather phenomena, will benefit from reading this review. There may not be much in this review which is new to colleagues as far as the individual subjects are concerned, but I hope that the ordering of the material will offer some new perspectives to everybody. This review should possibly be read in conjunction with the more descriptive and observationally oriented book by Atkinson [1981], the book with satellite images by Scorer [1986] and the book with photographs of meso-scale weather phenomena by Scorer and Verkaik [1989].

2. A phenomenological introduction to the meso-scale

In the Meteorology Source Book [Parker 1988], J.M. Fritsch defines meso-scale meteorology as "*that portion of meteorology comprising the knowledge of intermediate-scale atmospheric phenomena, that is, in the size range of approximately 1–200 miles (2–400 km) and with time-periods of typically, but not always, less than 1 day*".

In this review we will be concerned with the following questions. What makes this range of time and size-scales intermediate? Which dynamical processes are characteristic of the meso-scale?

The meso-scale has frequently been identified as coinciding with the so-called spectral gap in the spectrum of atmospheric motions. Soon after spectral Fourier analysis became popular in meteorology results of spectral analysis of meteorological time series began to appear in the literature. The most famous spectrum is shown in fig. 2.1. This spectrum, computed by van der Hoven [1957], is based on a time series of wind measurements made at a fixed point at a height of 100 m. It shows that, on average, there is relatively little energy in the meso-scale range (30 min to one day), compared to the energy in the so-called synoptic scales (more than one day) and the turbulent range (around 1 min). Others, such as Vinnichenko [1970] and Fiedler [1971] have obtained similar spectra. All these investigators found a minimum in the variance spectrum in periods ranging from half an hour to several hours.

The spectral gap is not an expression of the fact that individual (meso-scale) phenomena contain little energy and that they are therefore unimportant; rather it seems to be an indication that these phenomena are highly intermittent [e.g., Ishida 1990]. They occur only if certain conditions are fulfilled. For example, a sea breeze circulation will occur only when the temperature difference between

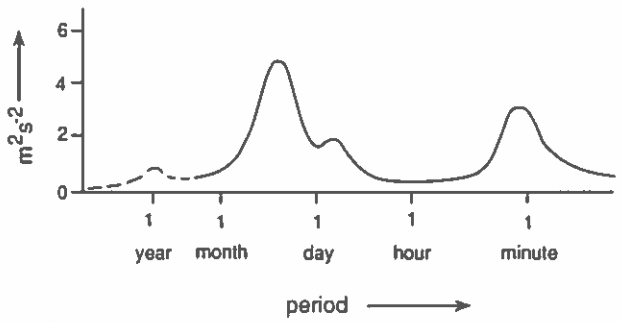

Fig. 2.1. Spectrum of the horizontal wind measured at Brookhaven National Laboratory at a height of 100 m [after Van der Hoven 1957].

the sea and the land is large enough, and even then, other conditions must be met. Thunderstorms, hurricanes, lee-waves and meso-scale convection cells, all of which are examples of meso-scale circulations, occur only in certain areas and in certain seasons. This is in contrast to small scale turbulence in the boundary layer and large scale planetary Rossby waves, which are nearly always present.

If we decide that meso-scale motions are motions large enough to be affected by the rotation of the earth, but small enough *not* to be affected by the curvature (or the sphericity) of the surface of the earth (the so-called β-effect; according to Wipperman [1981], the β-effect can always be neglected for motion-systems with length scales smaller than 2500 km), we can think of only three externally imposed (by the geometry and boundary conditions) constants or parameters in a *static* atmosphere. These are the depth, H (m) (if the upper and lower boundaries are imposed), the Coriolis parameter, f (s^{-1}) ($=2|\Omega| \sin \phi$, where ϕ is the latitude and $|\Omega|$ is the absolute value of the angular velocity of the earth) and the acceleration due to gravity, g ($m\,s^{-2}$). It is better to replace the latter parameter by the so-called Brunt–Väisälä frequency, N (s^{-1}), which contains g, but also takes account of the vertical density stratification, which, of course, also determines the vertical acceleration. Neglecting the curvature of the surface of the earth implies that f is assumed constant. Side boundaries are usually not imposed in the atmosphere. In addition, the large-scale background flow may provide us with certain characteristic parameters; however, for the moment let us restrict our attention to the externally imposed parameters.

It is possible to construct two time scales, τ_1 and τ_2 and two length scales, λ_1 and λ_2 on the basis of the externally imposed parameters. These are

$$\tau_1 = 1/f\,, \quad \tau_2 = 1/N\,, \quad \lambda_1 = H\,, \quad \lambda_2 = HN/f\,. \tag{2.1}$$

τ_1, multiplied by 2π, is usually called the inertial period and at mid-latitudes is equal to about $2\pi \times 10^4$ s (about 18 h); τ_2, multiplied by 2π, is usually called the Brunt–Väisälä period and in the atmosphere its magnitude is usually about $2\pi \times 10^2$ s (about 10 min).

The value of $H = \lambda_1$ may vary according to the location of temperature inversions, which act as a ceiling on atmospheric circulations. One such ceiling is the tropopause at a height of about 10 km. The other length scale, λ_2, is usually called the *Rossby radius of deformation* after Rossby [1937, 1938] and takes on a value of about 10^6 m (1000 km). Instead of λ_2 we can also define a λ_3 as $Hf/N \sim 10^2$ m. This is the smallest length scale which can be constructed from the parameters given above. We will see, however, that λ_3 actually never appears when we analyse the equations governing the motion of the

atmosphere. In the course of this review we shall in fact see that τ_1, τ_2, λ_1 and λ_2 define the bounds of what may be considered as meso-scale meteorological phenomena.

Parameters which may come into play when there is a large-scale background flow, are the flow velocity, $u_0(x, y, z)$ (x, y and z are, respectively, the two horizontal coordinates and the vertical coordinate), the vertical shear, $\partial u_0/\partial z$, and vertical component, ζ_0, of the vorticity associated with this flow. With the help of these two new parameters we can construct additional time and space scales. But, except when u_0, $\partial u_0/\partial z$ and ζ_0 are exceptionally large, these scales invariably lie in between the extremes defined by τ_1, τ_2, λ_1, and λ_2.

An example: sea breeze. Let us be a little more specific and produce some examples of typical meso-scale phenomena. These examples show that it is difficult to give an unambiguous definition of the time and space scales of a particular phenomenon, especially if the phenomenon is not stationary relative to the earth.

Perhaps, the most well-known meso-scale phenomenon is the sea breeze circulation. We will see that this phenomenon possesses most of the properties which are typical for a meso-scale weather system. One characteristic is that it is driven by diabatic heat sources, in this case by the daytime heating of the boundary layer. The time scale of this driving mechanism is of the order of 24 h, which is comparable to the inertial time scale, τ_1. Therefore, the rotation of the earth will affect the circulation. This property may be viewed as a second characteristic of meso-scale circulation. Furthermore, the sea breeze can be viewed as a "hydrostatically balanced" system, i.e. in constructing a theory of this system we can assume that the vertically oriented forces are always in balance. This implies that the sea breeze circulation owes its existence to an imbalance between the forces in the horizontal direction. Of course, a theory based on hydrostatic balance will not account for the detailed structure of the circulation near the so-called sea breeze front [e.g., Kraus et al. 1990], but it will describe the gross features of the circulation quite well (see section 5.2).

The characteristic properties of the meso-scale can be illustrated with a special case of three consecutive sea breeze days (6–8 May 1976) in The Netherlands. On these days air temperatures over land reached values over 30°C, while the adjacent North Sea surface temperature stayed below 10°C. These contrasts led to a very strong sea breeze circulation, penetrating nearly 150 km inland on one of these days. The geography of the coastal area in question is shown in fig. 2.2. Also shown in this figure are the positions of ten measuring stations which were selected for this particular case study (the white circles). The terrain is practically flat west of station 260. There are a few hills no higher than 100 m near station 275. The hourly temperature, measured at the standard height of 1.5 m, is shown in fig. 2.3. In fig. 2.4 the 10 min mean wind speed and direction measured each hour at a height of 10 m are shown for the same period. It can be seen clearly that during the day the wind at the coastal stations blows from directions between south and north through west and during the night it blows from the east. The turning of the sea breeze during the day is due principally to the influence of the earth's rotation (i.e. the Coriolis force) on the circulation. The easterly wind during the night is induced mainly by the large-scale-scale pressure pattern. By "large scale" (also called "synoptic scale" by many meteorologists) we mean horizontal scales larger than about 1000 km. This large-scale pressure pattern is shown in fig. 2.5. At these scales the wind is approximately in geostrophic balance at all times, i.e. the pressure-gradient force and the Coriolis force balance each other very closely. Indeed, geostrophic balance is typical of, and could be used to define the large-scale or synoptic-scale flow [e.g., Charney 1948]. Because of the large area of high pressure to the north of The Netherlands, the large-scale flow is easterly over The Netherlands. This flow functions as a *background* to the smaller-scale sea breeze circulation.

Fig. 2.2. Map of The Netherlands and its vicinity. The positions of the stations are shown by white circles (sea breeze case) and black circles (thunderstorm case) (with thanks to Peter Duynkerke).

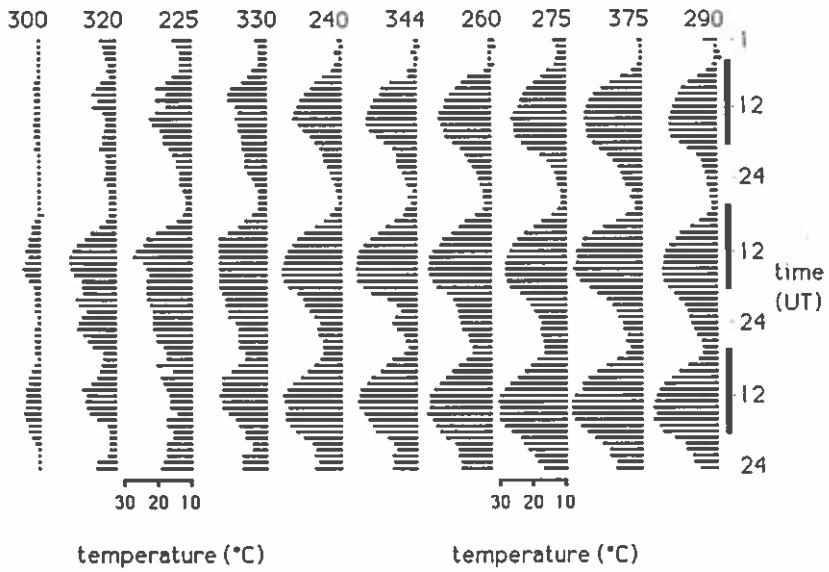

Fig. 2.3. Temperature at a height of 1.5 m as a function of time on 6, 7 and 8 May, 1976 at ten stations in The Netherlands and over the adjacent North Sea (see fig. 2.2). The dark solid lines along the vertical time axis indicate the daylight hours.

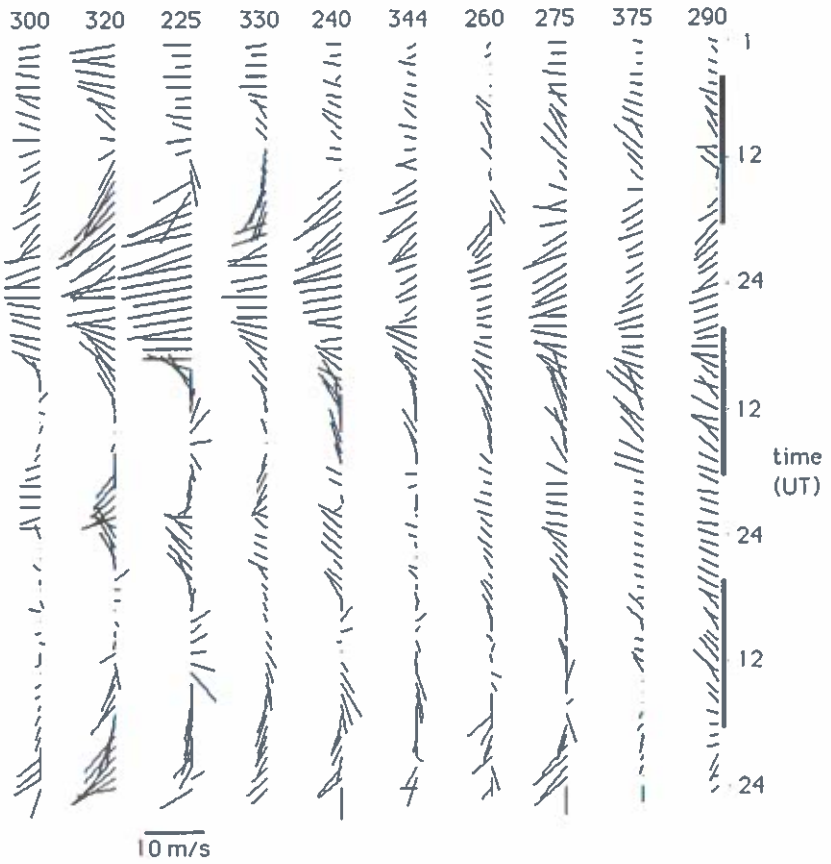

Fig. 2.4. Wind vectors at a height of 10 m as a function of time on 6, 7 and 8 May, 1976 at ten stations in The Netherlands and over the adjacent North Sea (see fig. 2.2). A line directed towards the left indicates a wind from the east. The length of the line is proportional to the wind speed. The dark solid lines along the vertical time axis indicate the daylight hours.

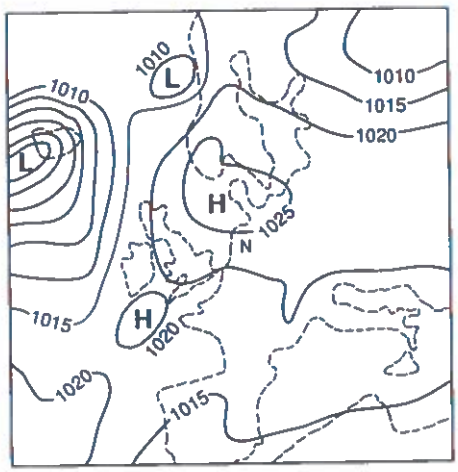

Fig. 2.5. Large-scale surface pressure distribution (in hPa) on May 7, 1976, 00 UT. The letters H and L indicate maxima and minima, respectively. The letter N indicates the location of The Netherlands.

Separating the meso-scale from the other scales. For this particular case, the surface pressure, the temperature and the wind direction and speed (averaged over 10 min) are available each hour at the ten stations shown in fig. 2.2. From these data it is possible to resolve motions with length scales of the order of 20–50 km or larger and with time scales of the order of 2 h or longer. It is important to note that the observation network determines the minimum scales of motion which can be seen. In this context it should be pointed out that some investigators [e.g., Pielke 1984, Joint Centre for Mesoscale Meteorology 1988] have defined the meso-scales as scales of motion too small to be properly defined by the current synoptic observation network but larger than the small-scale circulations within, for example, the boundary layer or cumulus clouds. Ligda [1951], who according to Atkinson [1981] [see also Emanuel 1986a, Browning 1989] introduced the term "meso-scale" into meteorology, coined a similar definition. Although this is not a very satisfactory definition, it does indicate that relatively little is known about the meso-scale (see Atkinson [1981] for a more detailed history of the first steps in the definition of and research on meso-scale meteorology).

If our observation network is fine enough to resolve a meso-scale circulation, as in the sea breeze case discussed presently, we can see whether a clear distinction can be made from the data between this meso-scale circulation and the other scales of motion. In the following an attempt to do this will be described.

Figure 2.6 shows a plot of the surface pressure as a function of time between 0 h UT, 6 May 1976 and 24 h UT, 8 May 1976, at the two extreme stations (300 (sea) and 375 (inland)). Clearly, there is a slow trend in the pressure, associated with the retreat of the high-pressure area towards the north and the advance of a depression from the south. On top of this synoptic trend, which clearly has a time scale longer than three days, there are ripples, associated with phenomena possessing shorter time scales. Although there is little order in these ripples at first sight, one can easily notice, when comparing the two curves, that the station at sea generally records relatively lower pressures during the night than the station inland and vice versa during the day. These pressure variations are associated with the meso-scale sea breeze circulation. Beside this, a periodicity of approximately 12 h can be discerned in

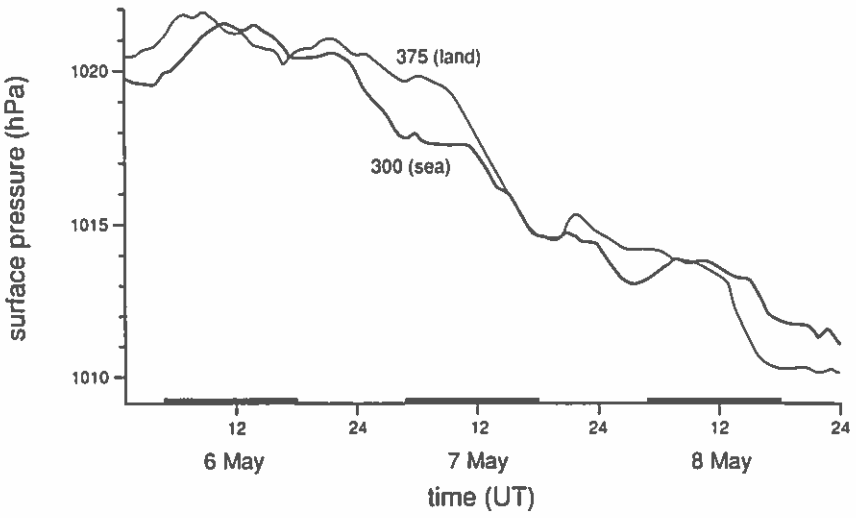

Fig. 2.6. Surface pressure as a function of time (in 1976) at an inland station (375) and a sea station (300) (see fig. 2.2). The dark solid lines along the horizontal time axis indicate the daylight hours.

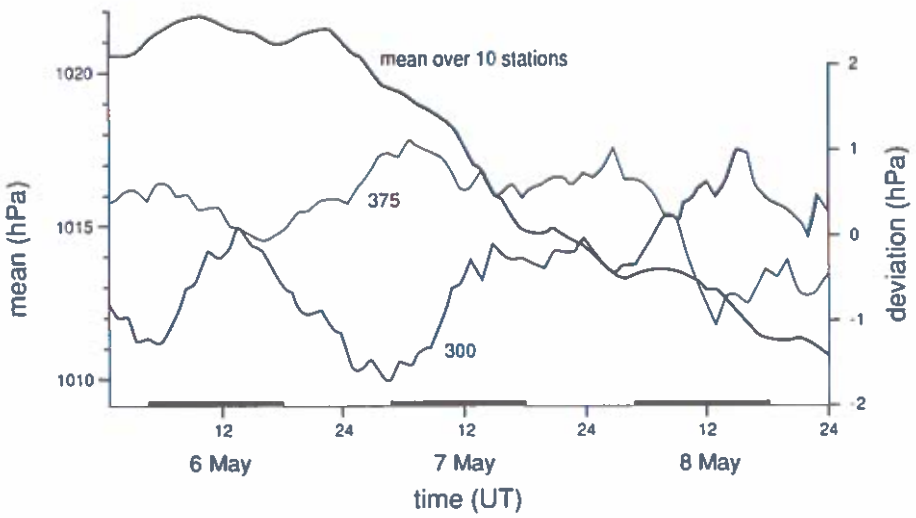

Fig. 2.7. Sea level pressure averaged over ten stations, shown by white circles in fig. 2.2, and the deviation from this mean value at two stations, one at sea (300) and the other over land (375), as a function of time (in 1976). The dark solid lines along the horizontal time axis indicate the daylight hours.

the pressure records, especially at the sea station (300). This periodicity is associated with the atmospheric tide [Chapman and Lindzen 1970, Volland 1988].

The synoptic trend and the tidal trend (both large scale) should be very similar at all stations, irrespective of the position relative to the coast, whereas the variations associated with the meso-scale circulation will depend on the geographical situation. Therefore, if we average the time series of the pressure over all ten stations, we will effectively filter out the meso-scale trend and be left with the large-scale trend (i.e. the synoptic plus tidal trend). The result of this procedure is shown in fig. 2.7 (the thick line). Also shown in fig. 2.7 is the deviation from this mean at stations 300 and 375. Clearly, the

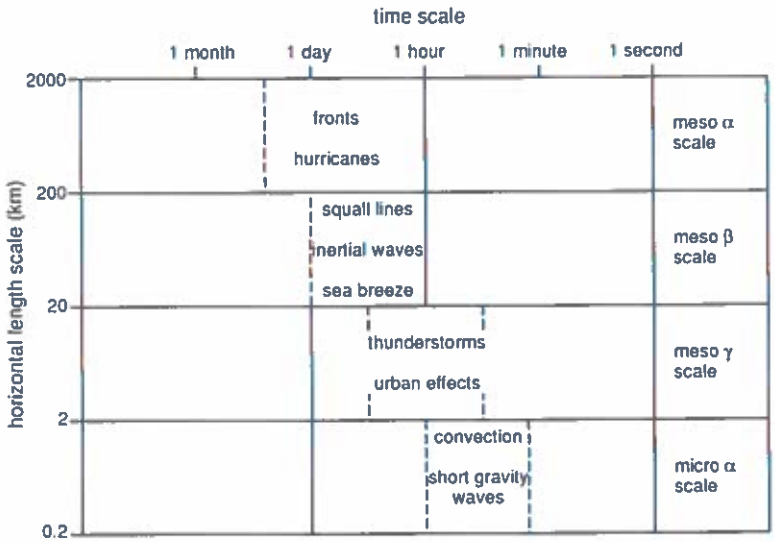

Fig. 2.8. Scale definitions and different processes with characteristic time and horizontal scales [based on Orlanski 1975].

dominant period left after subtracting the tidal and synoptic components is 24 h at both stations. As expected, the two records are out of phase. During the day, the pressure is relatively low over land and relatively high over sea, while the opposite in the case during the night. Apparently, the amplitude of the pressure oscillation associated with the sea breeze is about 1 hPa (1 hPa = 1 mb = 10^2 N/m^2).

During the past few decades several workers have classified weather systems according to their horizontal dimensions, assigning Greek letters to the different classes. The most well-known classification is that of Orlanski [1975] (see fig. 2.8), but Fujita's [1981] terminology is also widely used for reference purposes. These classifications, however, do not say much about the dynamics of these weather systems. The idea that atmospheric motion is composed of several discrete scales of motion,

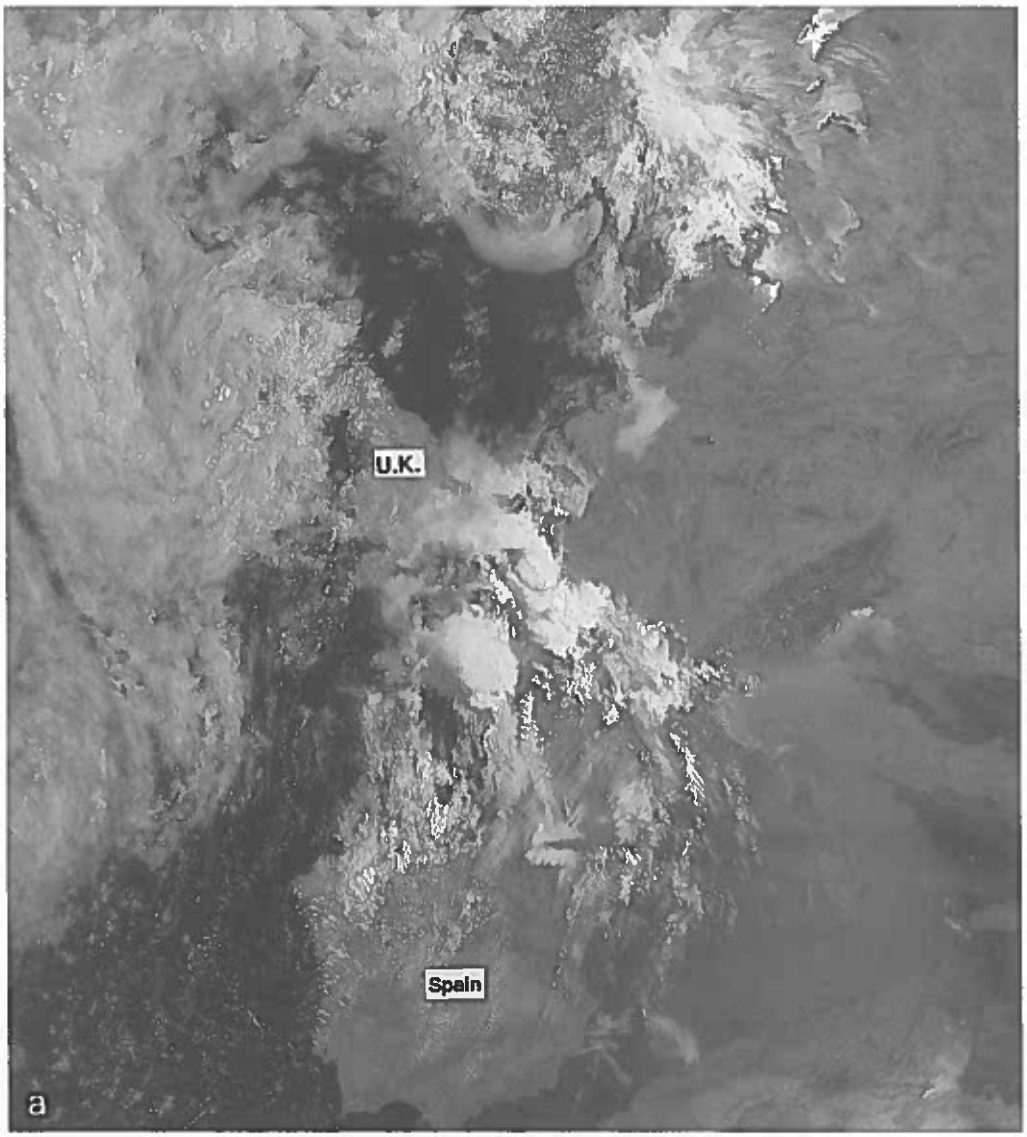

Fig. 2.9. Two photographs of Western Europe made by a polar orbiting satellite on July 11, 1984 at (a) 7 : 48 UT and (b) 14 : 29 UT. Courtesy of the University of Dundee, Scotland.

which may interact with each other, pervades in the minds of meteorologists, but is not always fruitful, and in many cases is probably deceptive. In the case discussed above this view is indeed fruitful. By a simple averaging procedure, we were able to isolate the principal time-scales making up the motion in this case.

Another example: a thunderstorm. As an example of a case in which it is difficult, if not impossible, to do such a thing, consider the thunderstorm showers which passed over exactly the same area, shown in fig. 2.2, on 11 July 1984. Figure 2.9 displays two satellite pictures of the thunderstorms. It can be seen that there are actually two thunderstorms travelling at about the same speed (~94 km h^{-1} or

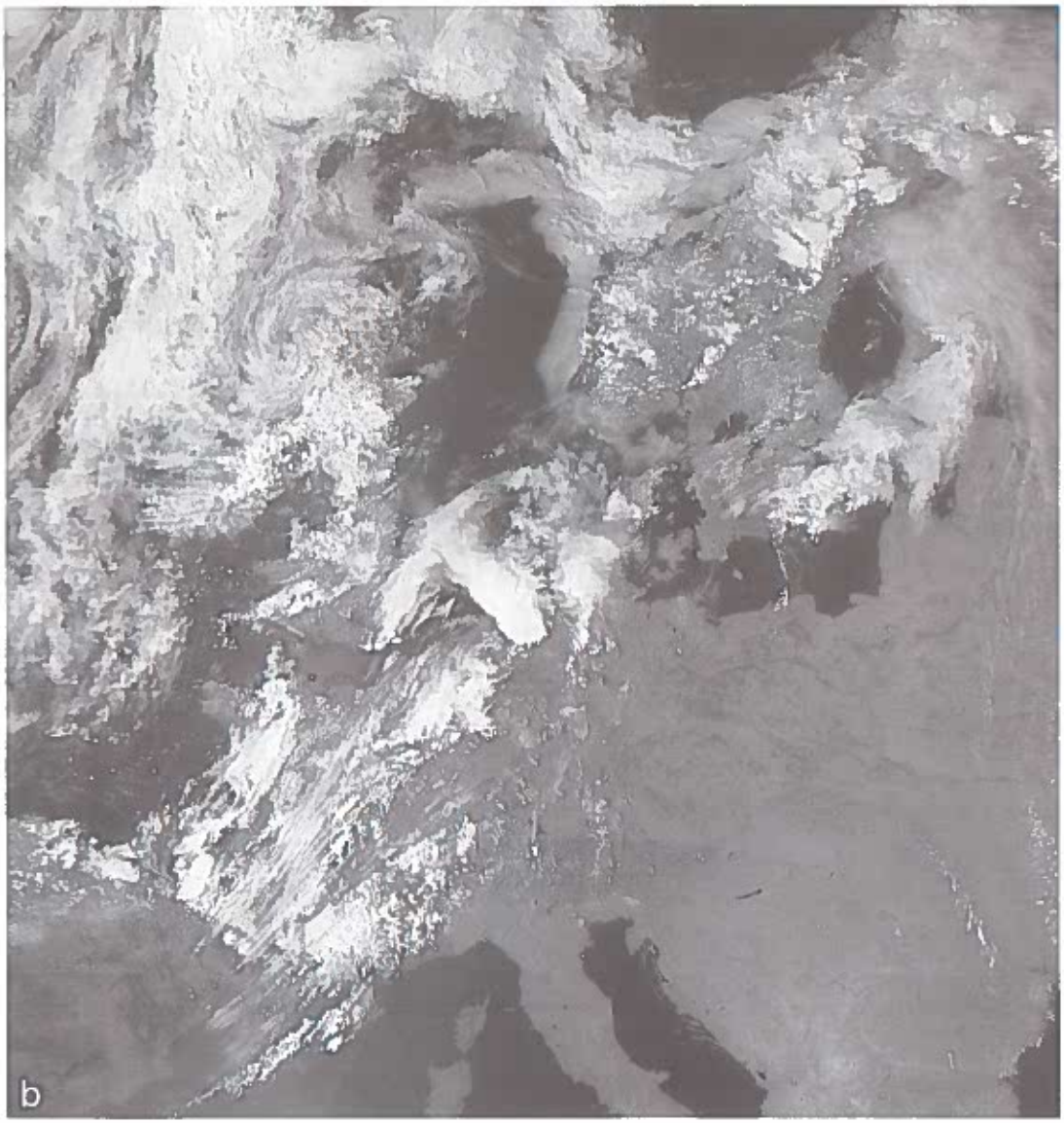

Fig. 2.9. (cont.)

26 m s^{-1}) one after the other from southwest to northeast. The first thunderstorm is dissipating and is already very weak at the time of the second photograph. The very high travelling speed is typical of these systems, which are similar in horizontal (spatial) scale to the sea breeze circulation. The similarity in scale is however not apparent from the measurements at a particular station, as can be seen in fig. 2.10, which shows the pressure as a function of time for four stations in The Netherlands. The thunderstorms are manifest in the pressure records as humps with a certain amplitude and period as if they were solitary waves. The second thunderstorm is the most marked. Zierikzee (325) in the southwest (see fig. 2.2) records a pressure rise of 6 hPa in 35 minutes, followed by a pressure fall of 9 hPa in the next 45 min. De Bilt (260) records a pressure fall of about 5 hPa is less than 3 min. From these pressure records one would of course conclude not that the thunderstorm is short-lived, but rather that it travels fast. In fact, the thunderstorms formed during the night over the Bay of Biscay and intensified strongly over France (see section 6.4). They had existed for at least 12 h when they were crossing The Netherlands.

We will return to this case in section 6.4. Here it serves to illustrate that we must make a distinction between so-called Eulerian and Lagrangian time scales [Emanuel 1986a]. The Eulerian time scale of a system is the time scale we measure at a fixed point in space, i.e. the length of the humps in the pressure records in fig. 2.10. This gives a time scale of about one hour for the individual thunderstorms on 11 July, 1984. The Lagrangian time scale, on the other hand, is the time it takes an air parcel to move once through the entire system, or, if we are dealing with wavelike oscillations, to cover one wavelength. The second thunderstorm on July 11, 1984 extended in the vertical to a height of approximately 14 km, whereas the horizontal extent was about 50 km (see fig. 2.11). A representative particle velocity through the disturbance is about 15 m/s. Such a particle would take less than 3 h to travel through the disturbance.

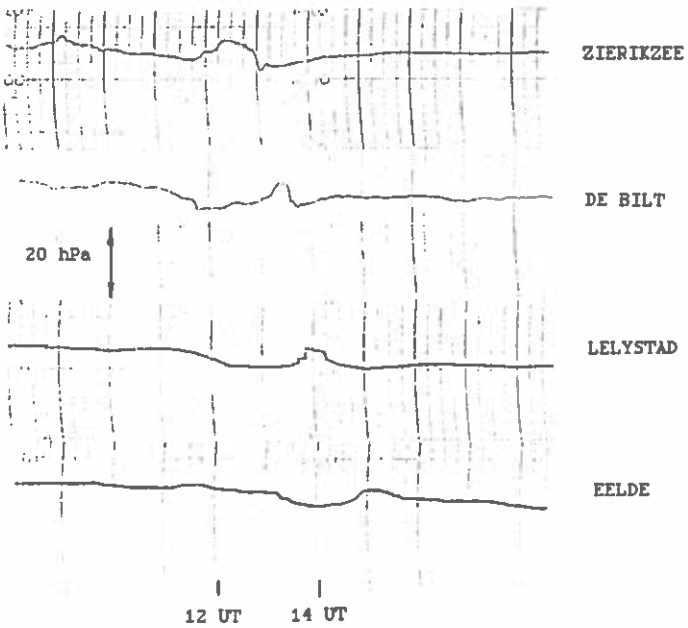

Fig. 2.10. Surface pressure as a function of time at four stations in The Netherlands along the path of the thunderstorms. See fig. 2.11 for the location of the stations.

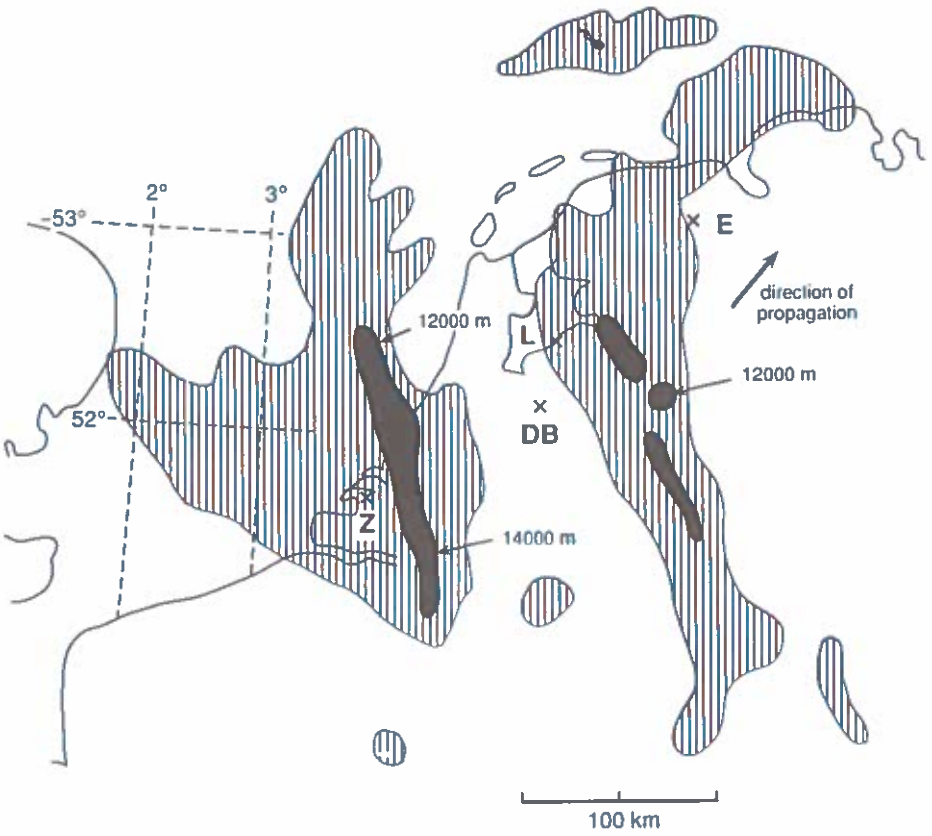

Fig. 2.11. Schematic representation of the precipitation features in the thunderstorms derived from the radar equipment based at De Bilt (DB) on July 11, 1984, 12:32 UT (black: relatively intense precipitation). The other stations indicated are Zierikzee (Z) (325 in figure 2.2), Lelystad (L) (268) and Eelde (E) (280). The complex of thunderstorms is moving in a northeasterly direction. Also indicated are the maximum heights of the echos at several points. For more details on this case, see figs. 6.8 and 6.9.

Another time scale to consider is the total lifetime of a weather system. The sea breeze circulation has a lifetime of about 12 h, after which it becomes a land breeze, or just dies out. The lifetime of a typical fair-weather cumulus cloud is about 1 h, whereas thunderstorms may persist for more than 24 h and tropical cyclones may persist for more than a week. In fact, one of the most persistent Atlantic tropical cyclones on record is Ginger (5 September–5 October 1972) [Fendell 1974]. By dividing the Lagrangian time scale by the total lifetime, we obtain a dimensionless time scale, T, which gives an impression of the coherence in time of the particular system. For an arbitrary eddy in the surface layer of the atmosphere, T will be close to or less than unity. This implies that, after a time equal to the Lagrangian time scale, the eddy has lost its identity. This is a characteristic of incoherence in time and unpredictability, i.e. turbulence. In the case of the fair-weather cumulus cloud, T lies between 1 and 2. For the thunderstorm and the sea breeze, T is of the order of 5. A tropical cyclone is one of the most "time-coherent" meso-scale systems. Its Lagrangian time scale may be about 12 h (see sections 5.5 and 6.7), while its total lifetime is typically 5 to 10 days, which makes $T \sim 10$–20. It should be stressed that T is not the only measure of coherence. As well as coherence in time, there can also be coherence in

space. The coherent motion of billions of fluid molecules in a large area, even if it is only for $T \sim 1$, is just as remarkable as the coherent motion of a few molecules in a small area for $T \gg 1$.

3. Models, equations and approximations

3.1. Basic equations

In this section we will review the models, equations and approximations which are used and applied when investigating meso-scale circulations theoretically. We will also get a first impression of the mechanisms that are responsible for triggering these circulations.

The laws governing the dynamical and thermal behaviour of the atmosphere are conservation of momentum, mass, and energy. These laws can be expressed mathematically as follows [e.g., Batchelor 1967, Holton 1979, Kundu 1990],

$$\mathrm{d}\boldsymbol{v}/\mathrm{d}t = -\alpha\,\boldsymbol{\nabla}p - g\hat{\boldsymbol{k}} - 2\boldsymbol{\Omega} \times \boldsymbol{v} + \mathbf{Fr}\,, \tag{3.1}$$

$$\mathrm{d}\rho/\mathrm{d}t = -\rho\,\boldsymbol{\nabla}\cdot\boldsymbol{v}\,, \tag{3.2}$$

$$\mathrm{d}Q = c_v\,\mathrm{d}T + p\,\mathrm{d}\alpha\,. \tag{3.3}$$

In these equations $\boldsymbol{v}$ is the air velocity, α the specific volume, p the pressure, $\boldsymbol{g}$ the acceleration due to gravity, $\boldsymbol{\Omega}$ the angular velocity of the earth, $\mathbf{Fr}$ the friction force per unit mass, ρ the density ($=1/\alpha$), T the temperature, Q the diabatic heating per unit mass, c_v is the specific heat at constant volume and $\hat{\boldsymbol{k}}$ is the unit vertical vector. Since there are four unknowns ($\boldsymbol{v}$,ρ, T, and p), we have to supplement the above system of equations with one additional equation, namely the equation of state. We can assume that air is an ideal gas. Therefore,

$$p\alpha = RT\,, \tag{3.4}$$

where R is the gas constant for dry air. It is almost impossible to solve the system of equations (3.1–3.4) analytically, except perhaps in very simple special cases. The (approximate) solution, or integration in time, of these equations by computer is possible, but difficult. Analysis of the linearized versions of these equations indicates that the solution contains many kinds of waves, such as sound waves, gravity waves and inertial waves [e.g., Pielke 1984]. Sound waves are of no meteorological significance, but are nevertheless the cause of many of the difficulties in the numerical analysis of these equations. One can make certain approximations to the equations which eliminate (filter out) sound waves from the solution while leaving the interesting part of the solution unaffected. In the next section we will review the various mathematical and physical approximations which are made in the theoretical investigation of meso-scale atmospheric circulations.

3.2. Approximations

The Boussinesq approximation. A very popular approximation to the primitive equations (3.1–3.4) is the so-called Boussinesq approximation. This approximation was originally made by Oberbeck [1879]

and Boussinesq [1903] for a layer of incompressible fluid in the laboratory. By "incompressible" we mean that the density is *not* a function of pressure, in which case the temperature is the most important property determining the density of air. Basically, the Boussinesq approximation states that variations in density, resulting from temperature variations, are only taken into account in the vertical component of the equation of motion. But, even in this equation the density variations are only accounted for when they appear in combination with the acceleration due to gravity. Equations (3.1) and (3.2) in the Boussinesq approximation become [see e.g., Chandrasekhar 1961, Turner 1973]

$$\mathrm{d}\boldsymbol{v}/\mathrm{d}t = -(1/\rho_{\mathrm{m}})\boldsymbol{\nabla}p' + (T'/T_{\mathrm{m}})g\hat{\boldsymbol{k}} - 2\boldsymbol{\Omega}\times\boldsymbol{v} + \mathbf{Fr}\,, \tag{3.5}$$

$$\boldsymbol{\nabla}\cdot\boldsymbol{v} = 0\,. \tag{3.6}$$

In these equations the prime denotes a departure from a reference state (denoted by a subscript, zero) and the subscript, m, refers to a mean of this reference state over the total domain in question. Any variable, $F(x, y, z, t)$, can be written as,

$$F(x, y, z, t) = F_0(z) + F'(x, y, z, t)\,. \tag{3.7}$$

F_{m} is defined as

$$F_{\mathrm{m}} = \frac{1}{H}\int_0^H F_0(z)\,\mathrm{d}z\,, \tag{3.8}$$

where H is the total depth of the domain in question. The reference state is horizontally homogeneous and in hydrostatic equilibrium (see section 3.3). In later sections we will investigate situations where the reference state is also a function of a horizontal coordinate, i.e. $F_0(x, z)$.

In eqs. (3.5) and (3.6), the z-dependence of the density in the reference state is neglected. This is acceptable for a relatively thin layer of fluid in the laboratory where temperature variations between upper and lower boundaries are usually less than 10 K. For variations in temperature of less than 10 K the density of a liquid varies by no more than 1% [Chandrasekhar 1961].

However, it is not possible to apply the so-called Boussinesq equations (3.5) and (3.6) to the compressible atmosphere unless one carefully reconsiders the premises of the approximations. This was done, among others, by Spiegel and Veronis [1960], Ogura and Phillips [1962], and Dutton and Fichtl [1969]. Broadly speaking, the conclusion of these studies was that the Boussinesq approximation for an incompressible fluid is applicable to atmospheric motions which do not extend beyond a height of approximately 1 km. These motions are termed "shallow". The flow associated with a fair-weather cumulus cloud is an example of a shallow circulation. For the so-called deep motions, associated with, for example, a thunderstorm, a slightly different set of equations is applicable. According to the scale analysis given by Dutton [1976], eqs. (3.1) and (3.2) for deep motions become

$$\mathrm{d}\boldsymbol{v}/\mathrm{d}t = -(1/\rho_0)\boldsymbol{\nabla}p' + (T'/T_0 - p'/p_0)g\hat{\boldsymbol{k}} - 2\boldsymbol{\Omega}\times\boldsymbol{v} + \mathbf{Fr}\,, \tag{3.9}$$

$$\boldsymbol{\nabla}\cdot(\rho_0\boldsymbol{v}) = 0\,. \tag{3.10}$$

The main difference between these equations and those applicable to shallow circulations is that the vertical gradient of the reference density is not neglected in the pressure-gradient terms and the continuity equation. Also, the pressure perturbation is not neglected in the buoyancy term [the second term on the right-hand side of eq. (3.9)].

Both forms of the continuity equation, (3.6) and (3.10), guarantee the absence of the meteorologically uninteresting sound waves [Ogura and Phillips 1962]. Due to this property, the term "anelastic" or "sound-proof" is sometimes used to describe the system of equations (3.5, 3.6) or (3.9, 3.10).

Circulation. In order to appreciate the differences in the consequences for the flow between the shallow and the deep approximation, it is worthwhile to look at the equation for the circulation resulting from these approximations. Circulation is defined as,

$$C \equiv \oint \boldsymbol{v} \cdot \mathrm{d}\boldsymbol{s} \,, \tag{3.11}$$

i.e. as the line integral about a closed contour of the component of the velocity which is locally tangent to the contour (see fig. 3.1). An equation for the change in the circulation around the area, A, for shallow and for deep circulations can be deduced from the fact that

$$\frac{\mathrm{d}C}{\mathrm{d}t} = \frac{\mathrm{d}}{\mathrm{d}t} \oint \boldsymbol{v} \cdot \mathrm{d}\boldsymbol{s} = \oint \frac{\mathrm{d}\boldsymbol{v}}{\mathrm{d}t} \cdot \mathrm{d}\boldsymbol{s} \,, \tag{3.12}$$

by applying Stokes theorem [e.g., Holton 1979], and substituting eq. (3.5) or (3.9). The resulting circulation theorems for the shallow and the deep circulations, respectively, are (neglecting friction)

$$\frac{\mathrm{d}C}{\mathrm{d}t} = -\int_A \int 2\boldsymbol{\nabla} \times (\boldsymbol{\Omega} \times \boldsymbol{v}) \cdot \hat{\boldsymbol{n}} \, \mathrm{d}A + \int_A \int g(\boldsymbol{\nabla} B \times \hat{\boldsymbol{k}}) \cdot \hat{\boldsymbol{n}} \, \mathrm{d}A \,, \tag{3.13a}$$

$$\frac{\mathrm{d}C}{\mathrm{d}t} = \int_A \int \frac{\boldsymbol{\nabla}\rho_0 \times \boldsymbol{\nabla}p'}{\rho_0^2} \cdot \hat{\boldsymbol{n}} \, \mathrm{d}A - \int_A \int 2\boldsymbol{\nabla} \times (\boldsymbol{\Omega} \times \boldsymbol{v}) \cdot \hat{\boldsymbol{n}} \, \mathrm{d}A + \int_A \int g(\boldsymbol{\nabla} B \times \hat{\boldsymbol{k}}) \cdot \hat{\boldsymbol{n}} \, \mathrm{d}A \,, \tag{3.13b}$$

where $\hat{\boldsymbol{n}}$ is the unit vector normal to area A (see fig. 3.1) and the buoyancy, B, is defined as

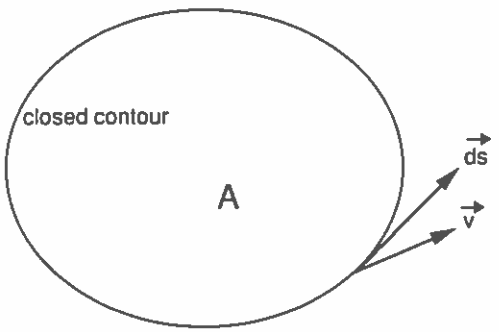

Fig. 3.1. Definition of circulation (see text).

$$B = T'/T_m \quad \text{for shallow flow}, \tag{3.14a}$$

$$B = T'/T_0 - p'/p_0 \approx \alpha'/\alpha_0 \quad \text{for deep flow}. \tag{3.14b}$$

The last equality in (3.14b) is the Boussinesq approximation of the equation of state (3.4).

Circulation can be generated by the Coriolis effect and by the so-called baroclinic effect. The latter effect has two components: one associated with the coupling of horizontal pressure gradients and vertical density gradients (which we will henceforth call the *inertial effect* of vertical variations in density) and the other associated with the coupling of horizontal density (buoyancy) gradients and vertical pressure gradients (which we will henceforth call the *buoyancy effect*). The former component is apparently not present in the equations for shallow flow. Only the equations applicable to deep circulations allow for the generation of circulation in vertical planes due to the fact that isobars are inclined to the horizontal.

The inertial effect is not present in the shallow approximation because the vertical variation of the density has been neglected. It is rather surprising that this is considered possible by many workers, since ρ decreases by about 10% in the lowest kilometer of a neutrally stratified atmosphere. Therefore, when these equations are used to describe the large boundary layer eddies with vertical scales in the order of 1 km, errors as large as 10% may be expected.

The equations in terms of potential temperature and Exner function. A slightly different approximation to the primitive equations (3.1–3.3), which does more justice to the compressibility of air (i.e. the basic vertical variation of density), was proposed by Ogura and Phillips [1962]. Instead of using the pressure, p, and the density, ρ, as variables in the equations, they used the so-called Exner function [e.g., Exner 1925], Π, and the potential temperature, θ. The Exner function is defined as

$$\Pi \equiv c_p (p/p_{ref})^{\kappa}, \tag{3.15}$$

where p_{ref} is a reference pressure and κ is the ratio $R/c_p = (c_p - c_v)/c_p$. The factor c_p is sometimes omitted in (3.15). The potential temperature is defined as,

$$\theta \equiv T(p_{ref}/p)^{\kappa} = c_p T/\Pi . \tag{3.16}$$

From eqs. (3.3) and (3.4) it can be deduced [e.g., Holton 1979] that

$$\mathrm{d}\theta/\mathrm{d}t = (1/\Pi)\,\mathrm{d}Q/\mathrm{d}t . \tag{3.17}$$

Equation (3.1) becomes

$$\mathrm{d}\boldsymbol{v}/\mathrm{d}t = -\theta\boldsymbol{\nabla}\Pi - g\hat{\boldsymbol{k}} - 2\boldsymbol{\Omega}\times\boldsymbol{v} + \mathbf{Fr} . \tag{3.18}$$

If we split Π and θ into a part associated with a reference state and a perturbation, as specified by (3.7), and assume that the reference state is in hydrostatic balance (see section 3.3), the vertical component of eq. (3.18) becomes

$$\mathrm{d}w/\mathrm{d}t = -\theta_0\,\partial\Pi'/\partial z + (\theta'/\theta_0)g + \mathrm{Fr}_z , \tag{3.19a}$$

where we have assumed that $\theta' \ll \theta_0$, w is the vertical component of the flow velocity and Fr_z is the vertical component of the frictional force. We have neglected the vertical component of the Coriolis force because its magnitude is usually much smaller than the buoyancy term. The horizontal component of (3.18) becomes

$$\mathrm{d}u/\mathrm{d}t = -\theta_0\, \partial \Pi'/\partial x + fv + \mathrm{Fr}_x\,, \tag{3.19b}$$

$$\mathrm{d}v/\mathrm{d}t = -\theta_0\, \partial \Pi'/\partial y - fu + \mathrm{Fr}_y\,. \tag{3.19c}$$

Here we have neglected the term involving the vertical velocity in the expression for the horizontal component of the Coriolis force [e.g., Atkinson 1981]. The circulation equation resulting from (3.19) (neglecting friction) is

$$\frac{\mathrm{d}C}{\mathrm{d}t} = -\int_A\int \nabla\theta_0 \times \nabla\Pi' \cdot \hat{\boldsymbol{n}}\, \mathrm{d}A - \int_A\int 2\boldsymbol{\nabla} \times (\boldsymbol{\Omega} \times \boldsymbol{v}) \cdot \hat{\boldsymbol{n}}\, \mathrm{d}A + \int_A\int g(\nabla B \times \hat{\boldsymbol{k}}) \cdot \hat{\boldsymbol{n}}\, \mathrm{d}A\,, \tag{3.20}$$

where the buoyancy, B, is

$$B = \theta'/\theta_0\,. \tag{3.21}$$

We now see that the pressure has vanished from the buoyancy term. This is one advantage of using potential temperature instead of density as a variable. Another advantage stems from the fact that the potential temperature is conserved for dry adiabatic processes (eq. 3.17) and is, therefore, more uniform with height than the density, which, due to compressibility (density depends on pressure), is not conserved. Therefore, the term due to the inertial effect of vertical potential density variations [the first term on the rhs of (3.20)] is usually comparatively unimportant in the well mixed atmosphere, because vertical gradients of potential density (or potential temperature) are comparatively small. In very stable layers (inversions), in which θ_0 increases strongly with height, this term may be important (see section 4.1.1) and, as we will see later (section 5.1), is in fact responsible for wave propagation along these inversions. Outside these special regions and provided horizontal pressure gradients are small (outside hurricanes and thunderstorms this is usually the case), we can safely assume that θ_0 is a constant, which eliminates the first term on the rhs of (3.20) and makes the pressure-gradient term in (3.19) linear. In sections 4.1 and 4.2 we shall see that this simplifies the analysis of this equation considerably. We will investigate the validity of the Boussinesq approximation in more detail in section 4.1.1.

The continuity equation. Turning now to the continuity equation, we can eliminate the density from (3.2) with the help of (3.4), (3.15) and (3.16) to obtain

$$(\mathrm{d}/\mathrm{d}t)(\ln\theta + (1 - 1/\kappa)\ln\Pi) = \boldsymbol{\nabla}\cdot\boldsymbol{v}\,. \tag{3.22}$$

For shallow dry-adiabatic motion Ogura and Phillips [1962] have shown that this equation can be simplified to the incompressible (anelastic) form given in (3.6). As diabatic heat sources become important and the vertical scale of the motion increases, the terms on the left-hand side of (3.22) become increasingly important [see also Lipps and Hemler 1982, Lipps 1990].

An alternative form of the continuity equation, which retains the effect of diabatic heat sources, can be deduced from eq. (3.22), using eq. (3.17). The result is

$$(c_v/R\Pi)\,\mathrm{d}\Pi'/\mathrm{d}t + (c_v/R\Pi)w\,\partial\Pi_0/\partial z + \nabla\cdot\boldsymbol{v} = (1/\theta\Pi)\,\mathrm{d}Q/\mathrm{d}t\,, \tag{3.23}$$

where $\Pi = \Pi_0(z) + \Pi'(x, y, z, t)$. If $\Pi' \ll \Pi_0$ and $\theta' \ll \theta_0$, and if the first term in (3.23) can be neglected, eq. (3.16) and hydrostatic balance of the reference state can be used to write the remaining terms as

$$\nabla\cdot\boldsymbol{v} - (g/c_0^2)w = (1/\theta_0\Pi_0)\,\mathrm{d}Q/\mathrm{d}t\,, \tag{3.24a}$$

or as

$$\nabla\cdot(\rho_0\theta_0\boldsymbol{v}) = (\rho_0/\Pi_0)\,\mathrm{d}Q/\mathrm{d}t\,. \tag{3.24b}$$

In (3.24a) $c_0 = (\gamma RT_0)^{1/2}$ is the speed of sound ($\gamma \equiv c_p/c_v$). It can easily be shown that the diabatic heating term on the rhs of (3.24a) is negligible for heating rates of the order of 1 K/h. Diabatic effects must induce temperature changes of at least 10 K/h before the rhs of (3.24a) is comparable in magnitude to the second term on the lhs of (3.24a), which is the result of compressibility. Since $g/c_0^2 \sim 10^{-4}\ \mathrm{m}^{-1}$ ($-\rho g/c_0^2$ is the adiabatic density lapse rate), the latter term is negligible compared to $\partial w/\partial z$ when the motion is shallow ($H \ll 10^4$ m). Therefore, according to this simple scaling argument, the incompressible form (3.6) of the continuity equation can be used for shallow motion. When the diabatic heating term is neglected, eq. (3.24a) becomes nearly identical to the continuity equation for deep motion (3.10), derived by Dutton [1976].

The so-called pseudo-incompressible continuity equation (3.24b) was recently put forward by Durran [1989] who showed that the use of this equation is justified when the Lagrangian time scale of the disturbance is large compared to the time scale for sound wave propagation and the perturbation pressure is small compared to the vertically varying mean state pressure. No assumption about the magnitude of the perturbation potential temperature or the strength of the mean state stratification is required.

Equations used in numerical models. Most numerical models designed in the last twenty years to simulate, for example, deep cumulonimbus convection, sea breeze circulations, hurricanes, or large-amplitude mountain waves are based (among other) on eqs. (3.17, 3.18, 3.22), although there are some slight technical differences. Examples of such models are those of Steiner [1973], Pielke [1974], Tapp and White [1976], Klemp and Wilhelmson [1978], Durran and Klemp [1983] and Willoughby et al. [1984]. On the other hand, so-called large-eddy numerical models, designed to simulate shallow convective and/or shear turbulence in the atmospheric boundary layer, have been based on equations (3.5, 3.6) [e.g., Deardorff 1974, Nieuwstadt and Brost 1986, van Delden 1988, Schmidt and Schumann 1989, Mason 1989]. Several early models, designed to simulate deep convection, were based on Dutton's [1976] equations (3.9) and (3.10) [e.g., Schlesinger 1975, Clark 1979].

3.3. Balanced circulations

Hydrostatic and geostrophic balance. Models which are based on the set of equations (3.17, 3.18, 3.22) are nearly as complex as reality. They allow for a whole spectrum of motions and waves. For

example, the model devised by Klemp and Wilhelmson [1978] simulates high-frequency sound waves, with periods of less than a few minutes, as well as low-frequency gravity-inertia waves, with periods of several hours.

Generally one is only interested in a specific phenomenon. It is then worthwhile trying to make some assumptions about the balance of forces so as to simplify the equations. For example, in the case of the sea breeze one can assume *hydrostatic balance*, without altering the essential characteristics of the sea breeze (see section 5.2). Hydrostatic balance can be expressed as (see eq. 3.18)

$$\partial \Pi / \partial z = -g/\theta \,. \tag{3.25}$$

This implies that the vertical component of the Coriolis force and friction have been neglected, and $\mathrm{d}w/\mathrm{d}t = 0$. By assuming hydrostatic balance one has, of course, ruled out the possibility of convection, which is a result of the *instability* of the state of hydrostatic balance (see section 4.1.2).

Another balance assumption frequently made in meteorology is *geostrophic balance* [e.g., Eliassen 1984], which implies that the horizontal component of (3.18) is replaced by

$$\theta\, \partial \Pi / \partial x = fv \,, \quad \theta\, \partial \Pi / \partial y = -fu \,. \tag{3.26}$$

We will see later that geostrophic balance is usually a stable equilibrium, implying that return to this state of balance is guaranteed after it is disturbed. Nevertheless, it is rarely well satisfied on the meso-scale. The reason for this is that heat sources and sinks due to phase changes of water or absorption and emission of radiation, or momentum sources and sinks due to terrain inhomogeneities (hills, lakes), may upset geostrophic balance strongly at scales of $\lambda_2 \sim 1000\,\mathrm{km}$ or less (see eq. 2.1), while return to balance takes at least one inertial period, $\tau_1 \sim 18\,\mathrm{h}$ (see eq. (2.1); why this is so will be explained in chapter 5). This is a relatively long time as far as meso-scale phenomena go. On the other hand, meso-scale circulations are usually close to hydrostatic balance. Even though hydrostatic balance is disturbed frequently by, for instance diabatic heating, return to this state of balance is attained in a much shorter time (of the order of the Brunt–Väisälä period, $\tau_2 \sim 10\,\mathrm{min}$, see eq. (2.1)), provided, of course, that the balance is stable, which is actually not always the case (see Chapter 4).

The Rossby number. One can express the fact that meso-scale motions are usually not in geostrophic balance in another way by saying that the Rossby number, defined as

$$\mathrm{Ro} = U/Lf \,, \tag{3.27}$$

where L is a typical horizontal scale and U is a typical velocity scale of the circulation, is of order of unity or larger. Some researchers (e.g., Green and Dalu 1980, Emanuel 1982, Pielke 1984] have suggested that the meso-scale could be defined as coinciding with those motions for which $\mathrm{Ro} \sim 1$. For these motions the horizontal accelerations ($\mathrm{d}u/\mathrm{d}t$) are of the same order of magnitude as the Coriolis forces. Therefore circulations with $\mathrm{Ro} \sim 1$ are not in geostrophic balance, but one cannot ignore Coriolis forces when trying to understand their dynamics. Emanuel [1982] has also defined the Rossby number in a slightly different way by

$$\mathrm{Ro} = \frac{(\mathrm{d}u_0/\mathrm{d}z)H}{Lf} \,, \tag{3.28}$$

where H is the depth of the circulation and $\mathrm{d}u_0/\mathrm{d}z$ is the vertical shear of a mean flow u_0 in the x-direction. Ro, as defined in (3.28), is sometimes referred to as the *thermal Rossby number*, since the vertical wind-shear in a geostrophically and hydrostatically balanced rotating fluid, such as the atmosphere, is directly related to the horizontal thermal gradient by

$$(\partial\theta_0/\partial z)\,\partial\Pi_0/\partial y - (\partial\theta_0/\partial y)\,\partial\Pi_0/\partial z = -f\,\partial u_0/\partial z\,. \tag{3.29}$$

Here we have assumed that the mean state also depends on the horizontal coordinate, y, i.e. the mean state is baroclinic. The thermal Rossby number appears in the context of the problem of the stability of thermal wind balance (see section 4.2).

The question of how the motion field and pressure field adjust to hydrostatic balance is of great importance to the understanding of many meso-scale weather systems, especially the sometimes striking differences in their structure. Think of, for example, the hurricane (see fig. 3.2) and the thunderstorm (see fig. 2.11). Despite the fact that both systems are just a group of deep cumulonimbus clouds, having approximately the same dimensions, their dynamics and appearance on a radar screen are very different. The hurricane or tropical cyclone is a balanced system, which evolves relatively slowly through a succession of balanced states, whereas the thunderstorm is a very unstable (unbalanced) system, i.e. accelerations are relatively large.

One aim of this review is to clarify the mechanisms which lie behind these differences. To this end, it is important to gain an understanding of the conditions under which hydrostatic balance and geostrophic balance and a combination of the two (i.e. thermal wind balance) may exist or may become unstable. Furthermore, if these equilibria are stable, it is also important to gain insight into the way in which they are established, or re-established after being disturbed. These subjects come under the headings "stability" (chapter 4) and "adjustment" (chapter 5), respectively.

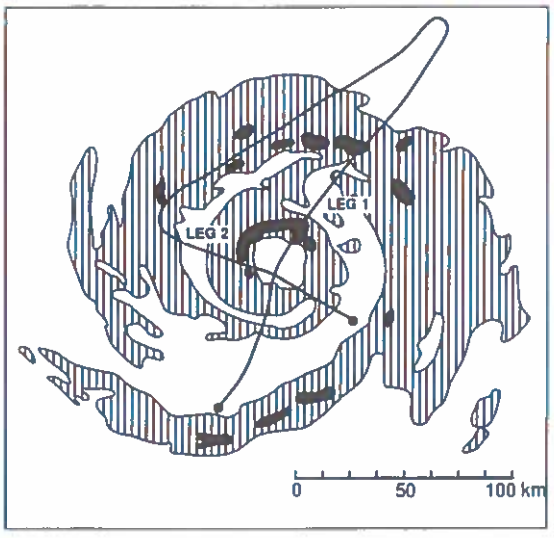

Fig. 3.2. Schematic representation of the precipitation features in hurricane Alicia derived from radar on 18 August 1983, 1:28 UT (black: relatively intense precipitation). The wind is oriented anticlockwise and approximately parallel to the precipitation bands. The solid line indicates the aircraft flight track along which vertical profiles of the vertical velocity were measured. These are shown below in fig. 5.12 [after Marks and Houze 1987].

3.4. Simplified models of the atmosphere

In addition to mathematical approximations, one can also make approximations regarding the physics of a specific problem, using among others the fact that the atmosphere is close to some kind of balanced state. A very popular simplification, which originated in the early years of numerical weather prediction, when computer power was limited, is to assume that the atmosphere consists of only a few layers. This approach works best for relatively large-scale motions in which vertical velocities are much smaller than horizontal velocities. In that case the hydrostatic approximation can usually be made. This, in turn, permits the use of pressure or potential temperature as vertical coordinate. The pressure coordinate has been used most widely, mainly because the continuity equation has a very simple form, and also because density does not appear explicitly (therefore, the complicating effect of compressibility in the equations is partly eliminated) and sound waves are completely filtered out. However, because the earth's surface is not a level of constant pressure, principally because of orography, problems arise when the lower boundary has to be incorporated in the model. Therefore, Phillips [1957] proposed, as vertical coordinate, the pressure normalized by the surface pressure, p_s. This coordinate, denoted by

$$\sigma \equiv p/p_s\,, \tag{3.30a}$$

or, alternately [e.g., Anthes and Warner 1978]

$$\sigma \equiv (p - p_t)/(p_s - p_t)\,, \tag{3.30b}$$

is used in most advanced numerical models for weather prediction.

When orography is relatively steep, as is the case frequently on the meso-state, this so-called sigma coordinate system does not work very well [Kasahara 1974]. A terrain-following coordinate proposed by Gal-Chen and Somerville [1975] is then a much better alternative. This coordinate, defined as

$$\eta \equiv z_t(z - z_s)/(z_t - z_s) \quad \text{or} \quad \eta \equiv (z - z_s)/(z_t - z_s)\,, \tag{3.31}$$

where z_s and z_t are the height of the lower and upper boundary, respectively, has been adopted in many numerical models which are designed to simulate air flow over mountains [Gross 1985, Schumann et al. 1987, Physick 1988]. An even more sophisticated vertical coordinate is used by Adrian and Fiedler [1991] to simulate air flow over very complex terrain.

Another important vertical coordinate (used in numerical meso-scale modelling) is potential temperature (see eq. 3.16). In adiabatic conditions, surfaces of equal potential temperature (called isentropic surfaces or isentropes) are material surfaces (see eq. 3.17). This has the attraction of avoiding vertical advection, which usually is the source of large truncation errors. When modelling the evolution of fronts with strong horizontal contrasts in potential temperature, isentropic coordinates are particularly convenient. Of course there are also some disadvantages, especially concerning the application of boundary conditions. More about the use of this coordinate can be found in Hsu in Arakawa [1990].

The shallow water equations. A very popular, conceptually simple model which is frequently adopted to investigate flow over relatively steep mountains is the so-called shallow water system, or hydraulic model. The atmosphere is approximate by a set of layers of constant density. The so-called hydraulic assumptions are [e.g. Lawrence 1990]: (i) the fluid is inviscid, (ii) the pressure is hydrostatic,

and (iii) within each layer the density is constant and the velocity varies only in the flow direction. An example of such a configuration is shown in fig. 3.3a, taken from Haderlein [1989]. Following Davies [1984], Haderlein modelled the motion of a cold front moving over orography (the Alps) by two isopycnic layers. The cold air is represented by the high-density fluid. The free surface between the two layers, which descends to the ground, represents the frontal surface. Many authors [see Baines 1987] have used this model to investigate the flow over mountains (see fig. 3.3b). The set of equations governing the behaviour of the cold fluid in fig. 3.3b is:

$$\partial u/\partial t + u\,\partial u/\partial x = -g'(\partial/\partial x)(h + h_h) + fv\,, \tag{3.32}$$

$$\partial v/\partial t + u\,\partial v/\partial x = -f(u - u_g)\,, \tag{3.33}$$

$$\partial h/\partial t + (\partial/\partial x)(hu) = 0\,, \tag{3.34}$$

in which we have set all y-derivatives equal to zero [see Gill 1982]. In these equations u and v are the horizontal wind components, h is the height of the free surface, h_h the height of the lower boundary, $g' = g(\rho_1 - \rho_2)/\rho_1$ is the reduced gravity and u_g is the background steady geostrophic wind velocity. There is no geostrophic wind in the y-direction.

Haderlein [1989] and Davies [1984] assign fictitious potential temperatures θ_1 and θ_2 to the two layers, making $g' = g(\theta_2 - \theta_1)/\theta_1$. However, because of compressibility, a layer of constant density cannot be a layer of constant potential temperature (or potential density) if the fluid is air. It can easily be shown that a layer of compressible air with constant density is gravitationally unstable (see section 4.1.2). Egger [1989] has documented the differences between the isopycnic model (in which compressibility is neglected) and the isentropic model (consisting of layers of constant potential temperature). A

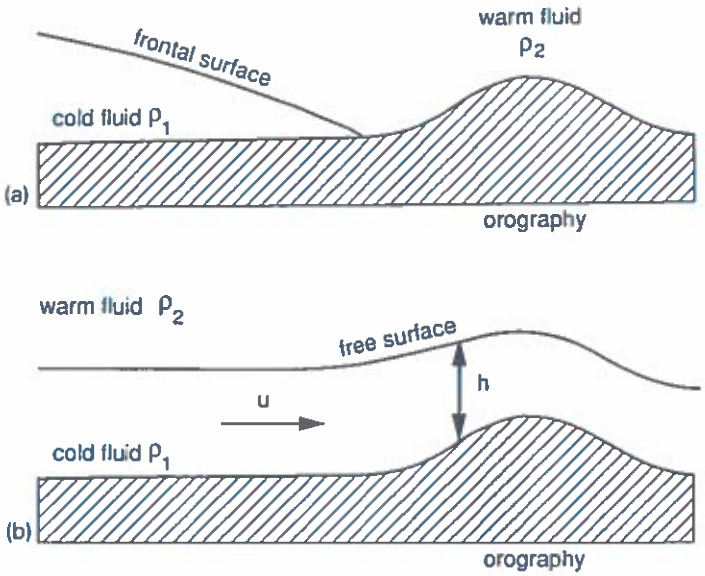

Fig. 3.3. (a) The hydraulic model as used to model a cold front moving over orography. Below the frontal surface the density is ρ_1, while above and to the right of the frontal surface the density is ρ_2 [after Davies 1984, Haderlein 1989]. (b) The hydraulic model as used to simulate flow over mountains.

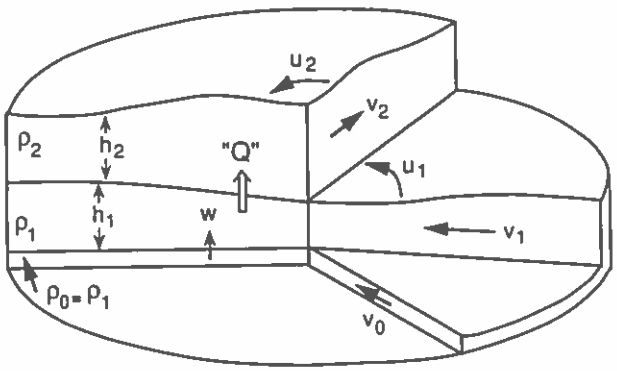

Fig. 3.4. Schematic diagram of Ooyama's [1969] three-layer hurricane model. The variables ρ, h, u, v, w and "Q" are the layer density, the layer thickness, the tangential velocity, the radial velocity, the vertical velocity at the top of the boundary layer (0) and the diabatic mass flux, respectively (see text).

description of an isentropic model can be found in Heimann [1986]. Although the respective model equations are very similar, there are some important differences, especially with regard to the relation between pressure and height. Nevertheless, because of its simplicity, and the ease with which orography is incorporated in the shallow water system, this model has been used to simulate a wide variety of atmospheric circulations, from baroclinic instability [Phillips 1951, Rao and Simons 1970], to tropical cylones [Ooyama 1969, DeMaria and Schubert 1984], fronts [Davies 1984], and flow over mountains [Long 1953b].

Ooyama's tropical cyclone model. It is worth describing the model of Ooyama [1969] because we will refer to it later. Ooyama's tropical cyclone model consists of three axisymmetric superposed shallow-water layers (see fig. 3.4). The thickness of the lower layer, i.e. the boundary layer, is assumed constant. Frictional convergence in this layer will lead to a mass flux into the layer above. The thickness of the upper two layers may vary due to convergence or divergence, or mass fluxes between the layers. The density of the boundary layer is equal to the density of the layer just above, while the density of the upper layer is a factor ε smaller. Diabatic heating ("Q") is represented as a mass flux from layer 1 to layer 2. Due to this, the thickness of the upper layer grows at the cost of the thickness of the lower layer. Thus, the pressure in the upper layer increases while the pressure in the lower layers remains unchanged. Therefore, the mass flux, "Q", mimics the effect of heating on the pressure distribution in the atmosphere. This relatively simple parameterisation of diabatic heating is very ingenious because it also mimics quite realistically the effect of heating on the potential vorticity distribution in the atmosphere. We will return to this subject in section 6.7.

Ooyama's [1969] model was adopted later also by DeMaria and Schubert [1984]. More recently, DeMaria and Pickle [1988] relaxed the incompressible layer assumption and constructed a three-layer model with layers of constant potential temperature.

4. Stability

In this chapter we will be concerned with certain (balanced) steady flow states, such as hydrostatic balance, geostrophic balance, a combination of these two (thermal wind balance), and also with more

general flow conditions with vertical shear imposed by unspecified (background) large-scale and boundary conditions. We will find conditions under which a secondary circulation feeding on the potential and/or kinetic energy of the balanced or background state can exist. The instabilities which give rise to these secondary flows will be termed *static* if they feed only on the potential energy of the background state and *dynamic* if they feed on the kinetic energy of the background state. We will consider two prototype problems. First we will discuss the classical problem of the stability of vertically sheared flow in presence of a potential temperature stratification neglecting Coriolis forces. Stratified shear flow can become unstable due to *thermal instability*, and also due to *dynamic instability* of the shear wind profile. Secondly, we will investigate the stability of geostrophic and hydrostatic balance with respect to certain, so-called *symmetric*, perturbations. Here, inertial forces such as the Coriolis force will introduce new phenomena.

The analysis of these two prototype problems will give us an idea of the time and space scales, as well as of the parameters characterizing the secondary flows and possible oscillations around the specified steady background states. We will find out more about how the characteristic time and space scales, given in eq. (2.1), are related to specific dynamical processes.

In this chapter we will use two methods to analyse the stability of an equilibrium state. The first method is the method of normal modes or, in other words, linear wave perturbation analysis, and the second method is the parcel method. These methods are used very often in meteorology. The parcel method gives considerable physical insight, but requires quite a few approximations and, moreover, does not give any information on the length scale of the circulation resulting from the instability [e.g., Thorpe et al. 1989]. For this information we have to turn to linear wave perturbation analysis, which, unfortunately, is mathematically more involved. In section 6.1 we will discuss a third method to analyse the stability of an equilibrium state, called the slice method.

We will start with linear perturbation analysis. We will derive, analyse and discuss the equation governing wavelike perturbations of a stratified inviscid (no friction) steady sheared flow. This equation is relatively complicated. We will only be able to analyse the effects of stratification and shear separately. In section 4.1.3 we will employ the parcel method to investigate the effects of stratification and shear together.

The discussion in section 4.1.1 will also give some additional information of the validity of the shallow Boussinesq approximation.

4.1. Stability of stratified shear flow

4.1.1. The stability equation in the inviscid case

The method of normal modes. In this section we will investigate the stability of a plane parallel shear flow, $u_0(z)$, in the presence of a potential temperature stratification, $\theta_0(z)$. Typical profiles of $u_0(z)$ and $\theta_0(z)$ are shown in fig. 4.1. To simplify matters, we will neglect friction and the rotation of the earth. We will also assume that there is no diabatic heating. With these assumptions, eqs. (3.17), (3.19a,b), and (3.24a) linearized around the hydrostatically balanced state specified by $u_0(z)$ and $\theta_0(z)$ are

$$\partial u/\partial t = -u_0\,\partial u/\partial x - w\,\partial u_0/\partial z - \theta_0\,\partial \Pi/\partial x\,, \tag{4.1}$$

$$\partial v/\partial t = -u_0\,\partial v/\partial x - \theta_0\,\partial \Pi/\partial y\,, \tag{4.2}$$

$$\partial w/\partial t = -u_0\,\partial w/\partial x - \theta_0\,\partial \Pi/\partial z + (\theta/\theta_0)g\,, \tag{4.3}$$

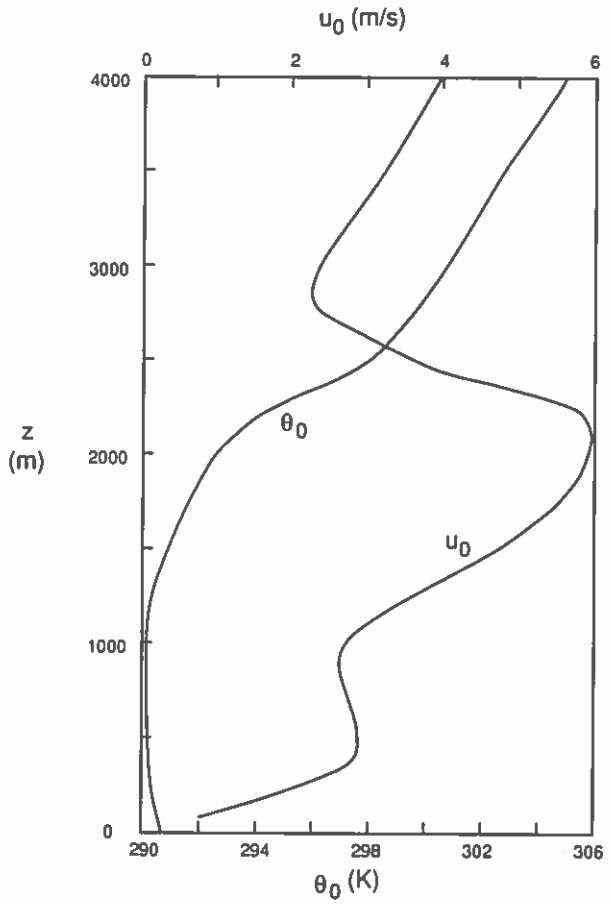

Fig. 4.1. The profiles of potential temperature, θ_0, and the horizontal wind velocity, u_0, measured at Cabauw, The Netherlands, on June 23, 1981, at 9 : 34 UT.

$$\partial\theta/\partial t = -u_0\,\partial\theta/\partial x - w\,\partial\theta_0/\partial z\,, \tag{4.4}$$

$$\partial u/\partial x + \partial v/\partial y + \partial w/\partial z = (g/c_0^2)w\,. \tag{4.5}$$

In the above five equations we have dropped the primes. The variables, u, v, w, Π and θ are small compared to $u_0(z)$, $\Pi_0(z)$ and $\theta_0(z)$, respectively. The linearization is valid as long as u, v, w, θ and Π do not deviate greatly from the reference state.

We now assume wavelike solutions of the form

$$\begin{pmatrix} u \\ v \\ w \\ \theta \\ \Pi \end{pmatrix} = \begin{pmatrix} U \\ V \\ W \\ \Theta \\ P \end{pmatrix} \exp[\mathrm{i}(\alpha x + \beta y - \omega t)]\,, \tag{4.6}$$

where α and β are horizontal wave-numbers in the x- and y-direction, respectively, ω is a frequency or a

growth rate, and U, V, W, Θ and P are height-dependent amplitudes. The system of equations (4.1–4.5) transforms into

$$(-\mathrm{i}\omega + \mathrm{i}\alpha u_0)U + \mathrm{D}u_0 W + \mathrm{i}\alpha\theta_0 P = 0\,, \tag{4.7}$$

$$(-\mathrm{i}\omega + \mathrm{i}\alpha u_0)V + \mathrm{i}\beta\theta_0 P = 0\,, \tag{4.8}$$

$$(-\mathrm{i}\omega + \mathrm{i}\alpha u_0)W + \theta_0\,\mathrm{D}P - (g/\theta_0)\Theta = 0\,, \tag{4.9}$$

$$(-\mathrm{i}\omega + \mathrm{i}\alpha u_0)\Theta + \Gamma W = 0\,, \tag{4.10}$$

$$\mathrm{i}\alpha U + \mathrm{i}\beta V + \mathrm{D}W - (g/c_0^2)W = 0\,, \tag{4.11}$$

where $\Gamma \equiv \mathrm{d}\theta_0/\mathrm{d}z$ is the so-called lapse rate and $D \equiv \mathrm{d}/\mathrm{d}z$. The above system of five ordinary differential equations can be reduced to one differential equation in W of the form

$$\mathrm{D}^2 W + s(z)\,\mathrm{D}W + r(z)W = 0\,, \tag{4.12}$$

with

$$\begin{aligned} s(z) &= \Gamma/\theta_0 - g/c_0^2\,, \\ r(z) &= -k^2 - \frac{\alpha\,\mathrm{D}^2 u_0}{\omega_\mathrm{D}} + \frac{\alpha\Gamma\,\mathrm{D}u_0}{\omega_\mathrm{D}\theta_0} + \frac{g}{c_0^2}\left(\frac{\Gamma}{\theta_0} - \frac{\alpha\,\mathrm{D}u_0}{\omega_\mathrm{D}}\right) + \frac{g\Gamma k^2}{\theta_0\omega_\mathrm{D}^2}\,, \end{aligned} \tag{4.13}$$

where $\omega_\mathrm{D} \equiv \alpha(u_0 - c_x)$, $c_x = \omega/\alpha$ is the phase speed of waves in the x-direction, $k^2 = \alpha^2 + \beta^2$. Equation (4.12) can be transformed into a Helmholtz equation of the form

$$\mathrm{D}^2\mathcal{W} + m^2\mathcal{W} = 0\,, \tag{4.14}$$

where

$$\mathcal{W} = W\exp\left(\frac{1}{2}\int s(z)\,\mathrm{d}z\right), \tag{4.15}$$

$$m^2 = -k^2 - \frac{\alpha\,\mathrm{D}^2 u_0}{\omega_\mathrm{D}} + \frac{g\Gamma k^2}{\theta_0\omega_\mathrm{D}^2} + \frac{\alpha\Gamma\,\mathrm{D}u_0}{\omega_\mathrm{D}\theta_0} - \frac{3\Gamma^2}{4\theta_0^2} + \frac{\mathrm{D}\Gamma}{2\theta_0} - \frac{\alpha g\,\mathrm{D}u_0}{\omega_\mathrm{D}c_0^2} + \frac{g}{2c_0^2}\left(\frac{\Gamma}{\theta_0} - \frac{g}{2c_0^2}\right) \tag{4.16}$$

[e.g., Tolstoy 1973]. Equation (4.14) (with 4.16), together with appropriate boundary conditions, defines the basic eigenvalue problem for inviscid parallel shear flow in the presence of stratification. By solving this problem we can infer the time dependence (i.e. stability) and the vertical structure of inviscid waves in stratified shear flow.

The stability of the wave depends on the imaginary part, c_i, of the phase speed. c_x. If c_i is positive, the wave amplitude will grow exponentially in time, implying that the basic state (u_0, θ_0) is unstable. With regard to the vertical structure of the wave, if m^2 is constant, there are two types of solution to (4.14), depending on the sign of m^2,

$$\mathcal{W} = A\exp(\mu z) + B\exp(-\mu z) \quad \text{if } m^2 < 0\,, \tag{4.17a}$$

$$\mathcal{W} = A\cos(mz) + B\sin(mz) \quad \text{if } m^2 > 0\,, \tag{4.17b}$$

where $\mu^2 = -m^2$. The coefficients A and B are determined by the boundary conditions. If the wave is generated by mountains or hills with dimensions such that $m^2 < 0$ (in which case the boundary conditions are such that the coefficient A is zero), the wave amplitude decays with height. This type of wave is called "evanescent", meaning "vanishing" or "quickly facing" [Gill 1982, p. 143]. When $m^2 > 0$, the solution is wavelike in the vertical, i.e. waves can propagate freely upwards and downwards.

According to (4.16), the sign of m^2 (and therefore the character of the solution) is determined by many different effects. Basically, these are: buoyancy, vertical wind shear, the inertial effect of Γ, and compressibility. In the shallow Boussinesq approximation the inertial effect of Γ is neglected completely. The effect of compressibility in the continuity equation (3.24a) (the term containing c_0^2) is also neglected. The term "shallow" stems from this last approximation. This implies that all terms on the rhs of (4.16) except the first three are neglected. In the following we will examine the validity of this approximation in a little more detail.

Another look at the validity of the Boussinesq approximation. The sign of m^2 depends on the horizontal wavelength of the wave, as well as on the mean background temperature and velocity profiles. Let us compare the order of magnitude of the terms in (4.16). We will do this for the velocity and potential temperature profiles shown in fig. 4.1. Representative values for θ_0, u_0, Γ, $\mathrm{D}\Gamma$, $\mathrm{D}u_0$ and D^2u_0 in the layer between 1000 and 2000 m are 290 K, $4\,\mathrm{m\,s^{-1}}$, $2\times10^{-3}\,\mathrm{K\,m^{-1}}$, $5\times10^{-6}\,\mathrm{K\,m^{-2}}$, $3\times10^{-3}\,\mathrm{s^{-1}}$ and $3\times10^{-6}\,\mathrm{m^{-1}\,s^{-1}}$, respectively. With these values, the fifth and sixth term on the rhs of (4.16) become, respectively.

$$3\Gamma^2/4\theta_0^2 \approx 10^{-10}\,\mathrm{m^{-2}}\,, \quad (\mathrm{D}\Gamma)/2\theta_0 \approx 10^{-8}\,\mathrm{m^{-2}}\,.$$

The last term on the rhs of (4.16) is of the order 10^{-9}. These magnitudes must be compared with the magnitude of the first term on the rhs of (4.16), $k^2 = 4\pi^2/L^2$, where L is the horizontal wavelength. For $L = 100$ m, $k^2 \sim 4\times10^{-3}\,\mathrm{m^{-2}}$; for $L = 1000$ m, $k^2 \sim 4\times10^{-5}\,\mathrm{m^{-2}}$ and for $L = 10\,000$ m, $k^2 \sim 4\times10^{-7}\,\mathrm{m^{-2}}$. Thus, we see that when the horizontal wavelength of the disturbance is about 10 km or less, the fifth, sixth and eighth terms on the rhs of (4.16) can be neglected *in this case*. The upper limit to the horizontal wavelength is determined in the first place by the second derivative with respect to z of the potential temperature. If $\mathrm{D}\Gamma = 0$, the sixth term in (4.16) vanishes. The fifth and eighth terms can be neglected if the horizontal wavelength of the circulation is about 100 km or less. It is stressed that this scale analysis must be repeated for every separate case.

The second, fourth and seventh terms in (4.16) can also be compared without having to make assumptions about $\alpha/\omega_{\mathrm{D}}$. In the layer at 1000–2000 m in the case shown in fig. 4.1 we have

$$\mathrm{D}^2u_0 \approx 3\times10^{-6}\,\mathrm{m^{-1}\,s^{-1}}\,, \quad \Gamma(\mathrm{D}u_0)/\theta_0 \approx 2\times10^{-8}\,\mathrm{m^{-1}\,s^{-1}}\,, \quad g(\mathrm{D}u_0)/c_0^2 \approx 3\times10^{-7}\,\mathrm{m^{-1}\,s^{-1}}\,.$$

Therefore, the fourth and seventh terms can be neglected compared to the second term. The seventh term, however, could become important in a region of large vertical wind-shear. Furthermore, D^2u_0 is very sensitive to slight variations in u_0 and may easily become zero.

The expression for m^2 (4.16), appropriate for the layer at 1000–2000 m in fig. 4.1 and *relatively short horizontal wavelengths*, becomes

$$m^2 + k^2 = -(\mathrm{D}^2 u_0)/(u_0 - c_x) + k^2 N^2/\alpha^2 (u_0 - c_x)^2 \equiv l^2 , \tag{4.18}$$

where

$$N = \sqrt{g\Gamma/\theta_0} \tag{4.19}$$

is the Brunt–Väisälä frequency or *buoyancy frequency* [Turner 1973] which was already introduced in eq. (2.1). The parameter, l, is called the *Scorer parameter* for transient buoyancy waves, after R.S. Scorer [1949], who first demonstrated the importance of this parameter in the dynamics of mountain-generated stationary buoyancy waves.

The fourth, fifth and sixth terms on the rhs of (4.16) arise due to the vertical variation of θ_0. If this variation had been neglected in eqs. (3.19a,b), which is equivalent to the shallow Boussinesq approximation, these terms would not have appeared. In other words, these terms are a manifestation of the inertial effect of vertical potential temperature variation (generation of circulation due to the coupling of vertical potential temperature gradients and horizontal pressure gradients), discussed below eq. (3.14). In the case shown in fig. 4.1, this effect appears to be unimportant in the upper part of the so-called convective layer between $z = 1000$ m and $z = 2000$ m. However, between the heights of 2100 and 2400 m, there is a relatively strong potential temperature inversion in which Γ is an order of magnitude larger than below. In this layer, the fifth term on the rhs of (4.16) certainly cannot be neglected when $L \approx 10$ km. Also, $\mathrm{D}^2 u_0$ is close to zero in this layer, which implies that the fourth and seventh terms cannot be neglected compared to the second term. In most books and publications [e.g., Yih 1980, Atkinson 1981, Drazin and Reid 1982], however, the terms resulting from the inertial effect of vertical potential density variations are neglected under the assumption that θ_0 (or ρ_0 in the case of incompressible flow) varies relatively slowly with height. Usually the latter term on the lhs of the continuity equation (3.24a) is also neglected. This term is responsible for the last two terms (containing the factor g/c_0^2) in the definition of m^2 (4.16).

On the basis of the above analysis, it appears that the shallow Boussinesq approximation, in which the second term on the lhs of (3.24a) is neglected and θ_0 is replaced by a constant θ_m in (3.19a,b,c), is applicable when the circulation has a vertical scale not much greater than about 1 km, and a horizontal scale not greater than about 100 km, provided the vertical potential temperature gradient, Γ, is small. How small depends on the particular situation. The limit on the vertical scale of the circulation is determined by the assumption of incompressibility (the neglect of the term, wg/c_0^2 compared to $\partial w/\partial z$ in eq. (3.24a)). The limit on the horizontal scale of the circulation is determined principally by the neglect of the basic vertical variation of the potential temperature in the equations of motion (3.19a,b,c).

The Taylor–Goldstein equation. If we neglect the basic vertical variation of potential temperature (or potential density) in the equations of motion as well as the basic adiabatic variation in density in the continuity equation, the function $s(z)$ in (4.12) vanishes, implying that $\mathcal{W} = W$. The stability equation becomes

$$\mathrm{D}^2 W + (l^2 - k^2) W = 0 . \tag{4.20}$$

This equation is called the Taylor–Goldstein equation, after Taylor [1931] and Goldstein [1931] although, according to Drazin and Reid [1982], it appears that Haurwitz [1931] also derived a more general version of this equation. In fact, much earlier, Rayleigh [1880, 1883] had already investigated two special versions of this problem: one in which the stratification (θ_0) was neglected and the other in which the background flow, u_0, was neglected.

4.1.2. Waves and instability

Buoyance waves. If there is no background flow ($u_0 = 0$) and if N^2 is constant throughout the atmospheric layer in question and also greater than ω^2, eq. (4.20) possesses wave-like solutions (see eqs. 4.14, 4.17). These waves are termed *buoyancy waves*. The solution of eq. (4.20) in this case can be expressed as $W \sim \mathrm{Re}\{\exp(\mathrm{i}\gamma z)\}$ (where γ is the vertical wave-number), provided the frequency and the wave-numbers are related according to the dispersion relation

$$\omega^2 = k^2N^2/(k^2 + \gamma^2) = N^2 \sin^2\phi \,, \tag{4.21}$$

where ϕ is the angle which the wave vector makes with the vertical. Apparently, the frequency of buoyancy waves cannot exceed N and depends on ϕ, not on the wavelength. This is basically due to the fact that the restoring force is directed along the vertical. If parcels are oscillating at an angle to the vertical, implying that the wave is propagating at an angle to the horizontal, the restoring force will be less than for vertically oscillating parcels. This will lead to a decrease in the frequency of oscillation.

Buoyancy waves belong to a large class of waves which owe their existence to gravity. They are frequently referred to as "internal gravity waves". However, to avoid confusion with another type of internal gravity wave occurring along and below a layer with a large vertical potential temperature gradient, we will stick to the term "buoyancy wave". We will return to this *theoretical* distinction in sections 5.1 and 5.4.

An interesting and complicating property of buoyancy waves is the fact that their phase propagation is perpendicular to their energy propagation. Wave energy is transported with the group velocity. The ratio of the vertical component of the group velocity to the horizontal component of the group velocity can be deduced from (4.21) to be

$$c_{gz}/c_{gx} = -k/\gamma \,.$$

From this equation we see that large-scale *wave-packets* with small k move nearly horizontally while short-scale wave-packets move nearly vertically [e.g., Hines 1972, Tolstoy 1973, Gossard and Hooke 1975, Kundu 1990].

There are many complicating factors affecting buoyancy waves in the atmosphere, the most obvious being the height dependence of the buoyancy frequency, N. For example, waves may be trapped in stable layers, such as the inversion shown in fig. 4.1, if N outside this layer is smaller than the wave frequency. Also, the vertical structure of the background wind plays an important role. For example, when $u_0 = c_x$, we cannot find an acceptable solution to the wave equation (4.20) because the Scorer parameter is infinite. The level where this is the case is called a *critical level*. Numerous experimental, theoretical and numerical investigations have been carried out to find out what happens at the critical level [e.g., Thorpe 1981, Gossard and Hooke 1975, Gill 1982].

Static instability. Buoyancy waves become unstable when $N^2 < 0$, because eq. (4.6) then contains a factor $\exp(\omega_i t)$, where ω_i is the imaginary part of ω. The wave amplitude will grow exponentially when $\omega_i > 0$. This is sometimes referred to as Rayleigh–Taylor instability [Drazin and Reid 1981], or just *static instability*. Rayleigh [1883] showed that instability could occur if $N^2(z)$ was negative somewhere in the layer in question for *any* distribution of $N^2(z)$. Unstable buoyancy waves are in fact synonymous to *convection currents*. Inspection of eq. (4.21) reveals that the growth rate $|\omega_i|$ will attain a maximum when $k^2 \to \infty$. In other words, inviscid convection cells will have very small horizontal wavelengths. However, Rayleigh [1916a] showed that the inclusion of diffusion of heat and momentum by molecules or by turbulent eddies would shift the wavelength of maximum growth rate towards a value in the order of the depth, H, of the layer in which convection is taking place. To be more specific, Rayleigh [1916a] included a term $\kappa\nabla^2\theta$ on the rhs of eq. (3.17) and substituted $\mathbf{Fr} = \nu\nabla^2\boldsymbol{v}$ in eq. (3.18) (κ and ν are diffusion coefficients of, respectively, heat and momentum). Buoyant instability with the effect of diffusion included is usually called *Rayleigh–Bénard instability* [Bénard 1900, Rayleigh 1916a], instead of Rayleigh–Taylor instability.

Assuming stress-free boundaries at the ground and at $z = H$, the solution to eq. (4.20) becomes $W \sim \sin(\pi n z/H)$, where n is the vertical wave-number. The lowest mode ($n = 1$) represents cellular motion spanning the total height of the layer. If $N^2 < 0$, this is the fastest growing mode for a given horizontal wavelength, $L = 2\pi/k$. Figure 4.2 gives a qualitative impression of the growth rate (ω_i) as a function of L in the inviscid case (eq. 4.21) and in the viscous case (both in the absence of background wind-shear). If there is no viscosity or conduction, the preferred horizontal wavelength is infinitely small. On the other hand, if there is viscosity and conduction, the preferred horizontal wavelengths shifts towards values in the order of H, depending on the exact boundary conditions of the temperature and the flow [see Drazin and Reid 1981]. Figure 4.3 gives an impression of the cellular flow resulting from Rayleigh–Bénard instability.

In the last 25 years satellites have clearly revealed that there is a surprising degree of organization in the distribution of cumulus clouds, especially over the ocean during polar air outbreaks [e.g., Agee 1987]. This organization, which strongly resembles the cellular organization of the flow observed in a thin layer of fluid in the laboratory [e.g., Van Dyke 1982, Krishnamurti 1970], can seldomly be detected

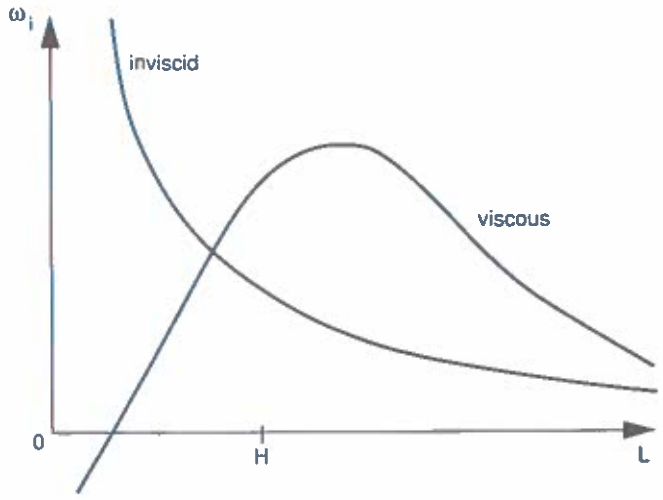

Fig. 4.2. Schematic plot of the growth rate, ω_i, as a function of the wavelength, with viscosity and without viscosity.

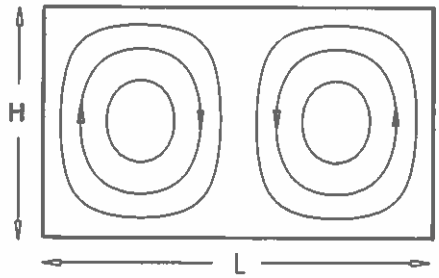

Fig. 4.3. The flow in a convection cell.

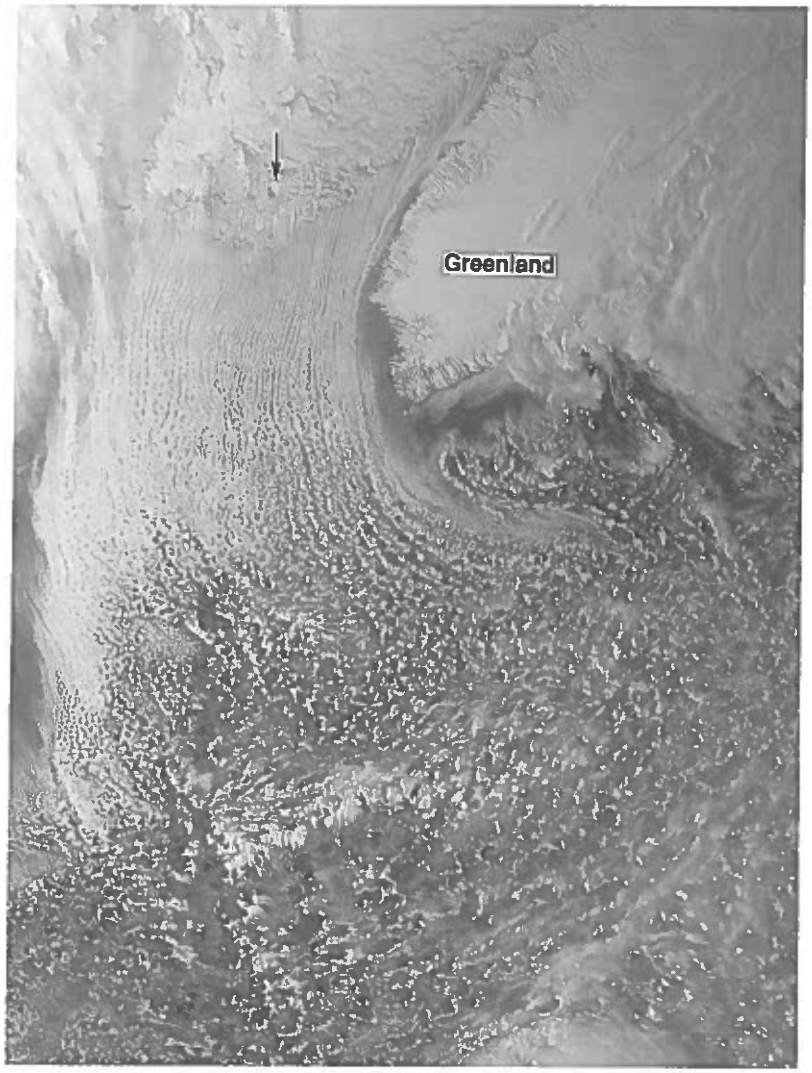

Fig. 4.4. Satellite (NOAA-7) photograph of the north-east Atlantic ocean and Greenland made on 19 February, 1984, at 17:03 UT. The arrow indicates the mean wind direction in the convective layer. Courtesy of the University of Dundee.

by eye from the ground, because the horizontal scale is too large. An example of such a case is shown in fig. 4.4. Here air is flowing from the ice edge over a relatively warm sea surface. Due to the great difference in temperature between the seawater and the air, vigorous convection currents develop. When these convection currents reach the lifting condensation level, clouds appear. In the first instance these clouds are almost invariably organized into streets (two-dimensional cells) oriented in the direction of the background wind. After the air has been flowing over sea for a while the cloud-streets start breaking up and gradually three-dimensional cellular patterns develop, quite similar to what is observed in the laboratory. In many cases these three-dimensional cloud patterns consist of an array of cells in which a thin ring of clouds surrounds a large clear area. These cells are called "open cells". Also possible are so-called "closed cells", which are complementary to open cells. In closed cells the clouds are concentrated in the middle and are surrounded by a clear area. The degree of cloud cover in closed cells is generally much larger than in open cells, hence the terms "open" and "closed".

Longitudinal (oriented parallel to the mean wind direction) cloud streets usually occur when there is a strong shear in the background wind (see e.g., Asai [1970a,b] and section 4.1.4). Numerical models of three-dimensional shallow convection indicate that planform selection is also related to the shape of the static (in the absence of convection) temperature profile $\theta_0(z)$ [Veltischev and Zelnin (1975), van Delden 1988]. Open cells are preferred when the greatest static instability is located adjacent to the lower boundary, whereas closed cells are preferred when the greatest static instability is located adjacent to the upper boundary. The (shape of the) static temperature profile is determined by processes other than convection, such as diabatic heating (due to radiation and latent heat release), large-scale vertical motion and changing boundary conditions. The transition from streets (or rolls) to open cells, seen in fig. 4.4, is probably determined by the reduction of the shear in the background flow and by the steadily increasing sea-surface temperature as the air flows southwards. The latter effect induces a static temperature profile which is extremely unstable near the sea surface. This favours the transition to open cells.

Atmospheric convection cells differ principally from Rayleigh–Bénard cells in two respects. They generally have a larger aspect ratio (width divided by height). Rolls in the atmosphere may have an aspect ratio of about 10 while three-dimensional cells may have aspect ratios up to about 50 [Agee 1987]. Also, atmospheric cells are frequently highly asymmetric in the horizontal, in the sense that the horizontal dimension of the upward motion generally differs greatly from the horizontal dimension of the downward motion. Modelling studies [van Delden 1985, Chlond 1988] reveal that latent heat release in the updraught can induce both the large aspect ratio and the asymmetry of atmospheric convection cells. This effect, and other effects of diabatic heating, will be discussed further in chapter 6.

4.1.3. Dynamic instability

Inflection point instability. Departing from a simplified form of the Taylor–Goldstein equation (4.20), Rayleigh [1880] proved an important theorem about the growth of wave-like perturbations in the presence of a shear flow ($u_0 \neq 0$) in a neutral environment ($N^2 = 0$). This theorem (see Drazin and Reid [1981] for the proof) states that *transverse* perturbations (i.e. roll-like motions organized perpendicular to the mean wind direction) will grow only if u_0 contains an inflection point, i.e. if $D^2 u_0$ changes sign somewhere. This is not to say that instability will always occur if this condition is fulfilled. It is a necessary, but not sufficient condition. A stronger form of this theorem is due to Fjørtoft [1950], who demonstrated [see Drazin and Reid 1981] that if u_0 is a continuous function of z with only one inflection point, then a necessary, but not sufficient condition for instability is that

$$(D^2u_0)[u_0 - u_0(z_s)] \leq 0\,, \tag{4.22}$$

where z_s is the height at which $D^2u_0 = 0$. Fjørtoft's condition (4.22) is illustrated in fig. 4.5. Another way of stating this *dynamic instability* (if it occurs) is that an inviscid fluid cannot support a vorticity maximum. The fluid develops transverse waves to relieve this vorticity maximum.

It is important to note that in the above we have considered an inviscid fluid. The extension of these results to a viscous fluid is not straightforward because the influence of viscosity is not necessarily stabilizing. Flows that are stable in the absence of viscosity may be unstable in the presence of viscosity and vice versa.

Dynamic instability in the presence of stratification (the parcel method). In the previous two sections we have considered independently the effect of wind-shear and the effect of stratification on the growth of wavelike perturbations. In the next two sections we will consider briefly the case when there is both shear and stratification in the background state.

Let us find out first which non-dimensional parameter(s) govern(s) this combined problem, using the parcel method. Following Miles [1986], consider two air parcels of unit volume located at different heights, z and $z + \Delta z$, respectively, moving in a height-dependent background flow, $u_0(z)$. In order to "mix" the two air parcels at a height $z + \gamma\,\Delta z$ $(0 \leq \gamma \leq 1)$, the lower parcel has to move up a distance $\gamma\,\Delta z$ while the upper parcel has to move down a distance $(1 - \gamma)\,\Delta z$. In a stable environment $(N^2 > 0)$ Fjørtoft's condition (4.22) will certainly not be the only condition for instability, because work has to be done against the buoyancy forces. The work done in raising a parcel of unit volume that is in equilibrium at $z = z_1$ to $z = z_1 + \zeta$ against the downward buoyancy force, F, is

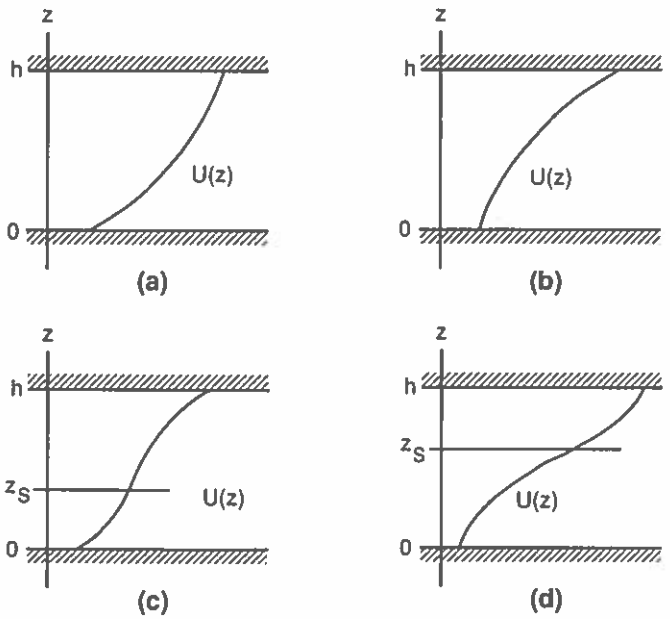

Fig. 4.5. (a) Stable: $U_0'' < 0$; (b) stable: $U_0'' > 0$; (c) stable: $U_0'' = 0$ at z_s but $U_0''(U_0 - U_s) \geq 0$; (d) possibly unstable: $U_0'' = 0$ at z_s and $U_0''(U_0 - U_s) \leq 0$ [from Drazin and reid 1981].

$$W = \int_{z_1}^{z_1+\zeta} F \, \mathrm{d}z \, . \tag{4.23}$$

Here

$$F = g[\rho_{\mathrm{pot}}(z_1) - \rho_{\mathrm{pot}}(z_1 + \zeta)] = -g\zeta \, \mathrm{d}\rho_{\mathrm{pot}}/\mathrm{d}z + \mathrm{O}(\zeta^2) \, , \tag{4.24}$$

where

$$\rho_{\mathrm{pot}} \equiv \rho_0 (p_{\mathrm{ref}}/p)^{c_v/c_p} \tag{4.25}$$

is the potential density of the environment ($\rho_{\mathrm{pot}} = p_{\mathrm{ref}}/R\theta_0$) [see Gill 1982, pp. 54, 55]. In the absence of diabatic processes, a compressible parcel of air conserves its potential density. It follows that

$$W = -\tfrac{1}{2} g(\mathrm{d}\rho_{\mathrm{pot}}/\mathrm{d}z)\zeta^2 \, . \tag{4.26}$$

The net work done in the mixing of the two parcels is

$$\Delta W = -\tfrac{1}{2} g(\mathrm{d}\rho_{\mathrm{pot}}/\mathrm{d}z)\{(\gamma \, \Delta z)^2 + [(1-\gamma)\, \Delta z]^2\} \geq -\tfrac{1}{4} g(\mathrm{d}\rho_{\mathrm{pot}}/\mathrm{d}z)(\Delta z)^2 \, . \tag{4.27}$$

Due to conservation of momentum, the velocity of the mixed air parcel must be $[u_0(z) + u_0(z + \Delta z)]/2$ (here we have neglected variations in density). Hence, the net change in kinetic energy is

$$\Delta K = -\tfrac{1}{4} \rho_{\mathrm{pot}} (\Delta u_0)^2 \, , \tag{4.28}$$

where $\Delta u_0 = u_0(z + \Delta z) - u_0(z)$. This kinetic energy is available for the mixing process. If $\Delta K < \Delta W$, mixing will *not* take place. This corresponds to

$$\mathrm{Ri} \equiv \frac{N^2}{(\partial u_0/\partial z)^2} > 1 \, , \tag{4.29}$$

where Ri is the so-called non-dimensional *Richardson number*, is a sufficient condition for stability of stratified shear flow. It can easily be verified that

$$N^2 = -(g/\rho_{\mathrm{pot}}) \, \mathrm{d}\rho_{\mathrm{pot}}/\mathrm{d}z \, . \tag{4.30}$$

A necessary, but not sufficient condition for instability is $\mathrm{Ri} < 1$. The dynamical instability which may occur in buoyantly stable conditions (for $0 < \mathrm{Ri} < 1$) is usually called *Kelvin–Helmholtz instability*.

The criterion (4.29) was derived in different ways by many authors [e.g., Richardson 1920, Abarbanel et al. 1984, Miles 1986]. However, starting with the Taylor–Goldstein equation (4.20), Miles [1961] and Howard [1961] have rigorously derived $\mathrm{Ri} > 0.25$ as a sufficient condition for stability. This focuses attention on the realm $0.25 < \mathrm{Ri} < 1$ for intensive theoretical and experimental investigation.

Investigations into the stability of a stratified parallel shear flow began with Helmholtz, who determined the stability criteria for an unbounded atmosphere with a step-discontinuity in wind speed

and density. Kelvin showed that the resulting disturbance developed a braided or "cat's eye" pattern [for the references, see Chandrasekhar 1961]. The papers by Miles and Howard, mentioned above, were milestones. Howard [1961] was able to show, among other things, that the phase speed of an unstable mode must match the speed of the background flow somewhere. At such a level, called a critical level (see section 4.1.2), the Doppler shifted frequency, ω_D (see the definition above eq. (4.14)), of the perturbation becomes zero. Subsequent analysis by many other investigators dealt with more general continuous wind speed and density profiles and realistic boundary conditions. The results of these investigations in which the computer was indispensable, are quite complicated, especially when compressibility is taken into account [e.g., Davis and Peltier 1976]. As an example of the complexity of the problem, Howard and Maslowe [1973] showed that if the stratification, Γ, varies with height, stable stratification ($\Gamma > 0$) can in some circumstances be destabilizing due to the vorticity generated by non-homogeneity.

The unstable Kelvin–Helmholtz disturbance grows by extracting energy from the mean flow. Eventually it breaks to dissipate the energy in turbulence. However, if the stratification remains stable away from the shear zone, the possibility exists that the shear energy can be used instead to generate an internal wave, which can carry the energy over great distances from the shear layer.

4.1.4. Static and dynamic (in)stability in the presence of dissipation

The effect of wind-shear on buoyant instability (Asai's analysis). In the previous two sections we have discussed the influence of stable stratification on dynamical instability. In this section we will look at the same problem from the opposite point of view, i.e. we will investigate the influence of wind-shear on static (buoyant) instability. This problem was discussed in a series of papers by Asai [1970a,b]. We will give a short review of the results obtained by Asai.

Let us define the operator, $G(u)$, as follows:

$$G(u) \equiv (\partial/\partial t + u_0\,\partial/\partial x - \nu\nabla^2)u\,. \tag{4.31}$$

Equations (4.1–4.3), including the effect of turbulent viscosity (assuming a constant viscosity coefficient, ν), can be rewritten as

$$G(u) = -\theta_0\,\partial\Pi/\partial x - w\,\mathrm{d}u_0/\mathrm{d}z + \nu\,\mathrm{d}^2u_0/\mathrm{d}z^2\,, \tag{4.32}$$

$$G(v) = -\theta_0\,\partial\Pi/\partial y\,, \tag{4.33}$$

$$G(w) = -\theta_0\,\partial\Pi/\partial z + (\theta/\theta_0)g\,. \tag{4.34}$$

Remembering that G is a linear operator only in the x- and y-direction, we now differentiate (4.32) with respect to x, (4.33) with respect to y, and (4.34) with respect to z. Adding the results and using the continuity equation (4.5), we obtain a Poisson equation for the Exner function,

$$\theta_m\,\nabla^2\Pi + 2(\mathrm{d}u_0/\mathrm{d}z)\,\partial w/\partial x + (g/\theta_m)\,\partial\theta/\partial z = 0\,. \tag{4.35}$$

This equation shows that Π (or p) is determined by the shear as well as by the stratification or buoyancy. The pressure perturbations resulting from the interaction of the vertical motion with the mean vertical shear are termed *dynamic*, while the pressure perturbations resulting from buoyancy are

termed *static*. Aircraft measurements of the perturbation pressure fields around the cloud base of convective clouds due to LeMone et al. [1988a,b] showed that the pressure perturbation variations in and around these clouds are principally dynamically induced. Pressure perturbation extrema measured in deep sheared cumulus clouds were typically 1 hPa, with a range from 0.2 to 9.5 hPa. In contrast, in shallow clouds with little wind-shear the extrema were of the order of 0.1 hPa. In section 6.3 we will discuss the important role played by dynamic pressure perturbations in thunderstorms.

Asai [1970a,b], like many others who did studies on the stability of steady wind-shear profiles in combination with stratification, substituted θ_m for θ_0. This approximation, together with the use of the incompressible adiabatic version of the continuity equation (3.6), leads to the elimination of Π from the problem. This is attained by operating with $\partial/\partial z$ on (4.35) and with ∇^2 on (4.34) and subtracting, yielding

$$G(\nabla^2 w) = (\mathrm{d}^2 u_0/\mathrm{d}z^2)\,\partial w/\partial x + (g/\theta_m)\,\nabla_H^2 \theta\,. \tag{4.36}$$

An equation for the vertical component of the vorticity, ζ $(=\partial v/\partial x - \partial u/\partial y)$, is easily obtained from eqs. (4.32) and (4.33):

$$G(\zeta) = (\mathrm{d}u_0/\mathrm{d}z)\,\partial w/\partial y\,. \tag{4.37}$$

Equations (4.36) and (4.37) define the dynamical part of Asai's problem. We need an equation for the potential temperature to complete the formulation. The linearized potential temperature equation, including the effects of turbulent heat diffusion (again, assuming a constant coefficient of turbulent heat transfer, κ) is,

$$\partial\theta/\partial t + u_0\,\partial\theta/\partial x - \kappa\,\nabla^2\theta = -w\,\mathrm{d}\theta_0/\mathrm{d}z + \kappa\,\mathrm{d}^2\theta_0/\mathrm{d}z^2\,. \tag{4.38}$$

If the basic temperature profile is linear (i.e. Γ is constant), the last term in (4.38) vanishes.

Let us now define the following units of length $\{L\}$, time $\{t\}$ and temperature $\{T\}$:

$$\{L\} = H\,,\quad \{t\} = H/u^*\,,\quad \{T\} = \Gamma H = \Delta\theta\,, \tag{4.39}$$

where u^* is a characteristic velocity of the basic flow, as indicated in fig. 4.6. In terms of these units the perturbation equations (4.36–4.38) become

$$(\partial/\partial t + u_0\,\partial/\partial x - \mathrm{Re}^{-1}\,\nabla^2)\nabla^2 w = (\mathrm{d}^2 u_0/\mathrm{d}z^2)\,\partial w/\partial x + \mathrm{Ri}\,\nabla_H^2\theta\,, \tag{4.40}$$

$$(\partial/\partial t + u_0\,\partial/\partial x - \mathrm{Re}^{-1}\,\nabla^2)\zeta = (\mathrm{d}u_0/\mathrm{d}z)\,\partial w/\partial y\,, \tag{4.41}$$

$$(\partial/\partial t + u_0\,\partial/\partial x - \mathrm{Pr}^{-1}\,\mathrm{Re}^{-1}\,\nabla^2)\theta = -\Gamma w\,, \tag{4.42}$$

where we have the dimensionless parameters

$$\mathrm{Re} = Hu^*/\nu \quad \text{(the Reynolds number)}\,, \tag{4.43}$$

$$\mathrm{Pr} = \nu/\kappa \quad \text{(the Prandtl number)}\,, \tag{4.44}$$

$$\mathrm{Ri} = g\Gamma H^2/\theta_m (u^*)^2 \quad \text{(the Richardson number)}. \tag{4.45}$$

There is a relationship between Re, Ri and another dimensionless parameter, known as the Rayleigh number Ra,

$$\mathrm{Ra} = -\mathrm{Pr}\cdot\mathrm{Ri}\cdot\mathrm{Re}^2 = -g\Gamma H^4/\theta_m \nu\kappa\,. \tag{4.46}$$

Asai [1970a,b] assumed a mean potential temperature profile with a constant lapse rate (Γ is constant) and substituted perturbations of the form,

$$\begin{bmatrix} w \\ \zeta \\ \theta \end{bmatrix} = \begin{bmatrix} W \\ Z \\ \Theta \end{bmatrix} \exp[\mathrm{i}(\alpha x + \beta y - \omega t)]\,, \tag{4.47}$$

where, as in eq. (4.6), $W(z)$, $Z(z)$ and $\Theta(z)$ are height-dependent amplitudes. Substituting this into the system (4.40–4.42) yields a system of three ordinary differential equations for $W(z)$, $Z(z)$ and $\Theta(z)$. With suitable boundary conditions at $z = 0$ and $z = 1$, this system can be transformed into a set of algebraic equations by approximating the derivatives of W, Z and Θ with respect to z by finite differences using about 20 intervals. Requiring the solution of this set of algebraic equations to be nontrivial yields a frequency equation for ω. The imaginary part of ω represents the growth rate of the perturbations. More about this numerical method of solution can be found in Asai [1970a].

Results. The basic velocity profiles chosen for investigation by Asai [1970b] were,

$$u_0(z) = \tfrac{1}{2}[1 - (2z-1)^2]^n\,, \quad n = 1, 2, \ldots, \tag{4.48}$$

in addition to a profile with linear shear (profile (c) in fig. 4.6). The profiles (4.48) are symmetric about mid-level ($z = 1/2$), having a maximum of 1/2, and vanishing at the top and bottom. When $n = 1$,

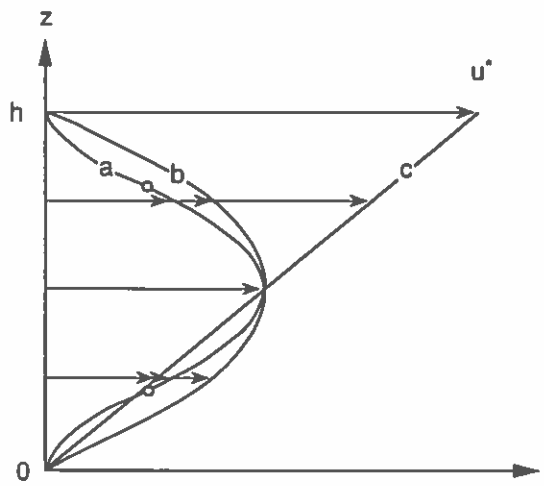

Fig. 4.6. The profiles of the basic flow for three cases whose stability properties are studied, (a) a shear flow with points of inflection indicated by circles, (b) a plane Poiseuille flow, and (c) a Couette flow [from Asai 1970b]. To transform to nondimensional units (4.39) we choose $H = h$.

(4.48) gives a parabolic profile without inflection points (a plane Poiseuille flow). When $n = 2$, (4.48) yields a jet-like profile with two inflection points. The jet becomes sharper as n increases. Asai [1970b] only investigated the cases $n = 1$ ((b) in fig. 4.6) and $n = 2$ ((a) in fig. 4.6). It is very important to keep in mind that we will not refer to any mechanism maintaining the basic flow with such profiles.

Asai [1970b] assumed that the perturbations had to satisfy perfectly conducting and stress-free top and bottom boundary conditions. There is some inconsistency here, because the mean flow does not satisfy these boundary conditions. Figures 4.7a,b,c show the growth rates of wavelike perturbations as a function of the Richardson number and the total horizontal wave-number, k $(=(\alpha^2 + \beta^2)^{1/2})$, for the basic velocity profiles shown in fig. 4.6, with $\alpha = \beta$, $\mathrm{Ra} = 10^4$ and $\mathrm{Pr} = 1$.

The unstable domain in case (a) can be divided into two portions, one for large values of $-\mathrm{Ri}$ and the other for small values of $-\mathrm{Ri}$. Counterparts of the former instability domain can be observed in both cases (b) and (c). However, no low-$(-\mathrm{Ri})$ instability domain can be seen in either (b) or (c). The former instability domain is associated with buoyant instability modified by shear, while the latter, low-$(-\mathrm{Ri})$, instability domain must be associated with the inflection points in the basic velocity profile (a). The wave-number of maximum instability, k_c $(=2\pi/L_c)$, is about 3 to 4 in cases (a) and (b) $(1.5 < L_c < 2.2$, in non-dimensional units). In the case of linear shear (plane Couette flow), $2.5 < L_c < 8$. This implies that circulations, which are the result of buoyant instability in the presence of shear, will have aspect ratios (L/H) of 1.5 to 8.

It is interesting to examine the growth rates of perturbations of different form. Figure 4.8 shows the growth rates as a function of the ratio β/α, for the different velocity profiles, when $\mathrm{Ri} = -1$, $\mathrm{Ra} = 10^4$, $\mathrm{Pr} = 1$ and $k = 2$. Evidently, shear inhibits the growth of buoyantly unstable perturbations oriented transverse to the mean flow. This is especially the case when the shear is constant. In other words, in

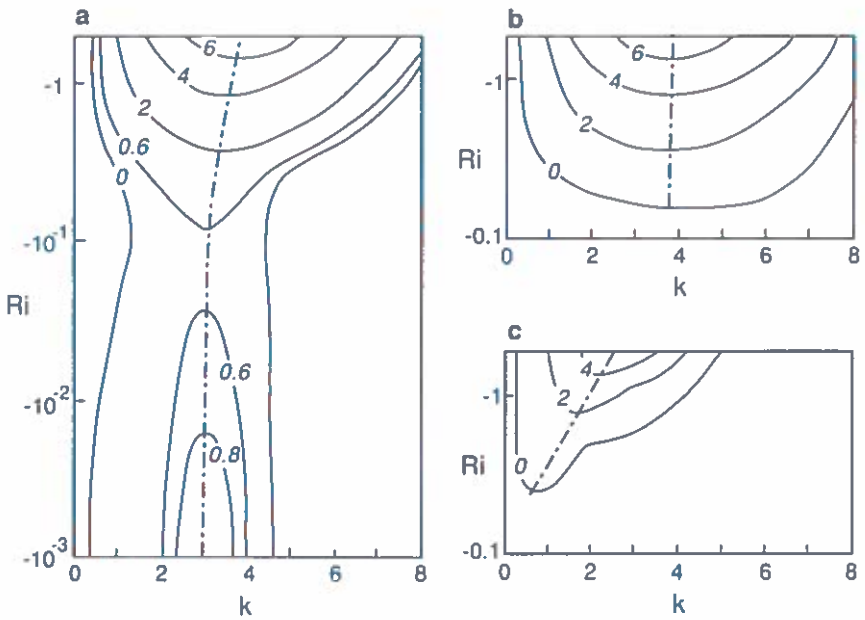

Fig. 4.7. Stability diagram for the shear profiles shown in fig. 4.6. Solid lines indicate the amplification rate in units of $10^{-1}\,\mathrm{s}^{-1}$ as a function of Ri and k. The dashed-dotted line indicates a preferred wave number for a given value of Ri [from Asai 1970b].

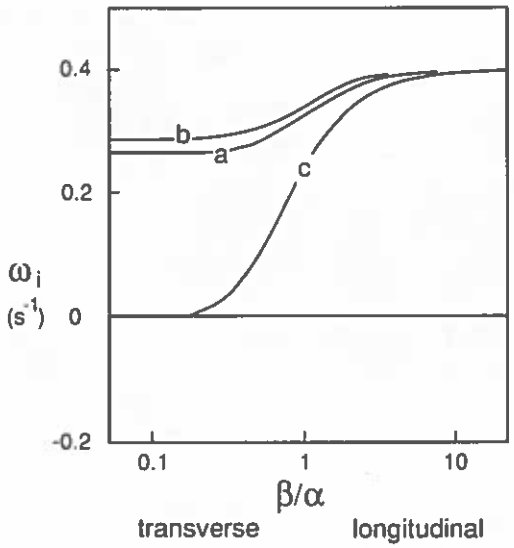

Fig. 4.8. Variations of the amplification rate, ω_i, with wave number ratio, β/α, for the shear profiles shown in fig. 4.6 ($k = 2$, $Ra = 10^4$ and $Ri = -1$) [from Asai 1970b].

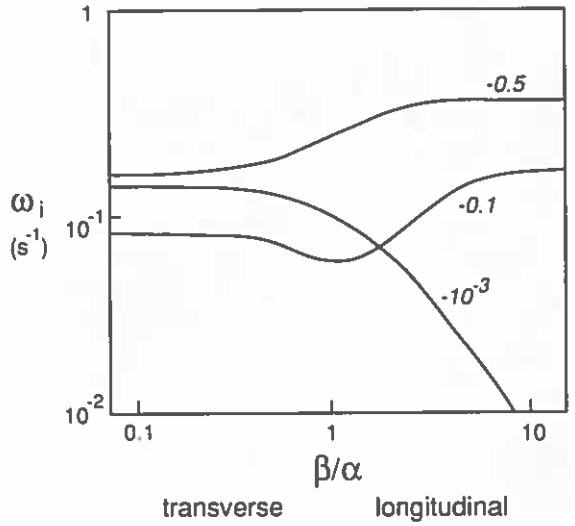

Fig. 4.9. Variation of the amplification rate with β/α for different values of Ri for the shear profile (a) shown in fig. 4.6. Here $Ra = 10^4$ and $k = 2\sqrt{2}$ [Asai 1970b].

constant shear, convection will preferably appear in the form of rolls oriented along the mean wind (longitudinal rolls).

Figure 4.9 shows the growth rates of perturbations as a function of the ratio β/α for case (a) with $Ra = 10^4$, $k = 2\sqrt{2}$ for a set of different negative Ri-values. Apparently, the transverse mode is preferred when $-Ri$ is small (dynamical instability), whereas the longitudinal mode is preferred when $-Ri$ is large (buoyant instability), although in the latter case the preference is not so clear cut.

Some observations. In the atmosphere cloud streets are almost always organized parallel to the mean wind direction (see, e.g., fig. 4.4). Occasionally, however, transverse cloud streets are observed, such as on the satellite image shown in fig. 4.10, which shows a view of northwestern France in a west to northwesterly flow. As is typical on a spring day, convection is active only over land due to strong solar heating. Transverse cloud streets are excited due to buoyant instability soon after the air reaches the coast of northwestern France. According to the theory of Asai [1970a,b], the mean wind profile must have a jet-like character with at least one inflection point. The radio sounding made at Trappes (see fig. 4.11a) shows that this is indeed the case below the temperature inversion (in the cloud layer). Fjørtoft's condition (4.22) is satisfied at the inflection point above the jet. More to the south(east) there is a transition to so-called popcorn cumuli. As expected, the wind profile measured at Bordeaux, which is representative for this area, have very little shear and no inflection points below the temperature inversion (see fig. 4.11b). A word of caution is in place here. The basic, *static* (in the absence of growing perturbations) part of the wind profile cannot in fact be observed when this profile is linearly unstable, because the perturbations will act to modify it. Therefore, the temperature and wind profiles, shown in fig. 4.11, are the sum of a static part and a dynamic part. In the above example it has been tacitly assumed that the static part dominates over the dynamic part.

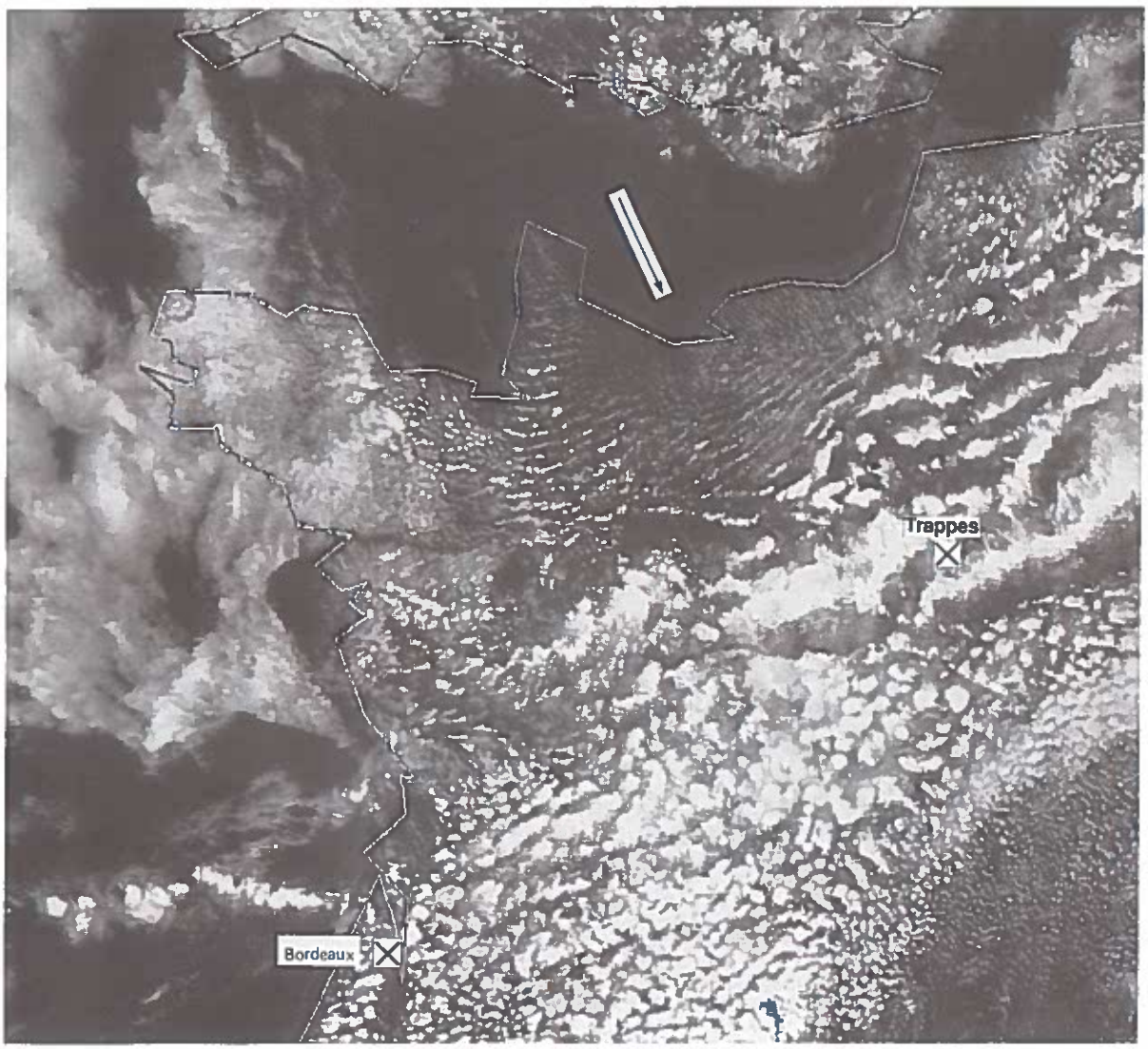

Fig. 4.10. Satellite (NOAA-9) photograph of north-west France made on 28 March 1983, at 13:21 UT. The locations of the measuring stations, Trappes and Bordeaux are shown by the crosses. The mean wind direction at 1000 m is indicated by the arrow. Courtesy of the KNMI, De Bilt.

The stability of the Ekman boundary layer (analyses due to Lilly, Etling and Brown). Because of the rather unrealistic boundary conditions and velocity profiles, the limited parameter range Asai investigated, and many other uncertainties regarding the applicability of the model problem to the atmosphere, no more than qualitative conclusions can be drawn from Asai's [1970a,b] work on the effect of wind-shear on convection.

A steady wind profile, which is thought to be more realistic, is obtained when it is assumed that there is an equilibrium between the pressure gradient force, the Coriolis force, and the viscous force. Solving the equations corresponding to this equilibrium subject to appropriate boundary conditions, assuming the diffusion coefficients, ν and κ, are constant, yields the so-called Ekman spiral velocity profile [see

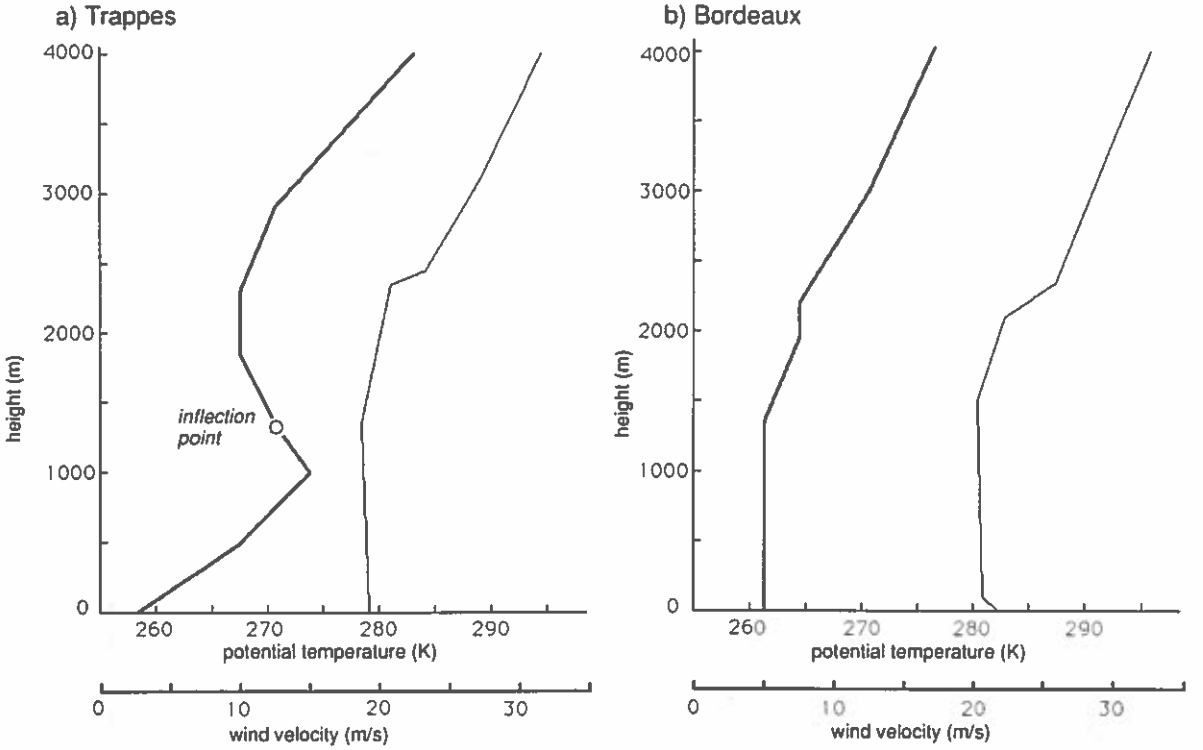

Fig. 4.11. Vertical profiles of the dominant component of the wind speed (thick solid line) and the potential temperature (thin solid line) measured at (a) Trappes (dominant wind direction is 340°) and (b) Bordeaux (dominant wind direction is 300°) on 28 March 1983 at 12 UT. The variation of the wind direction with height is negligible.

Holton 1979]. This is one of the few analytical steady state solutions of the equations of motion applicable to the atmosphere. However, the ideal Ekman spiral is hardly ever observed in the atmosphere, partly because the eddy diffusion coefficients are not constant with height, and also because it is an unstable solution under many circumstances [e.g., Faller 1963]. This stems from the fact that the Ekman wind profile contains an inflection point.

Lilly (1966) was the first to investigate systematically the stability of the Ekman wind profile. He did this for the special case of neutral static (buoyant) stability ($\Gamma = 0$). Using essentially the same numerical method as Asai [1970a,b], described in the previous section, he investigated the growth of small *two-dimensional* perturbations with a roll-axis orientation-angle ε, counterclockwise from the direction of the geostrophic wind vector superposed on Ekman spiral wind profile (see fig. 4.12). The computations revealed that the neutral Ekman layer is most unstable to two-dimensional perturbations with $-30° < \varepsilon < 15°$. The preferred orientation angle depends strongly on the Reynolds number, $\mathrm{Re} = v_g D/\nu$, where v_g is the geostropic windspeed and D is the Ekman layer depth $(=\sqrt{2\nu/f})$. Lilly [1966] discovered that the instability at high Re was of the inflection point type (giving a preferred $\varepsilon \sim 15°$), while the instability at low Re was of a completely different type. He named the latter type "parallel instability", because the secondary circulation abstracts energy from the mean flow component parallel to the roll-axis through the Coriolis force.

Brown [1970] calculated numerically the shape and intensity of the secondary flow resulting from

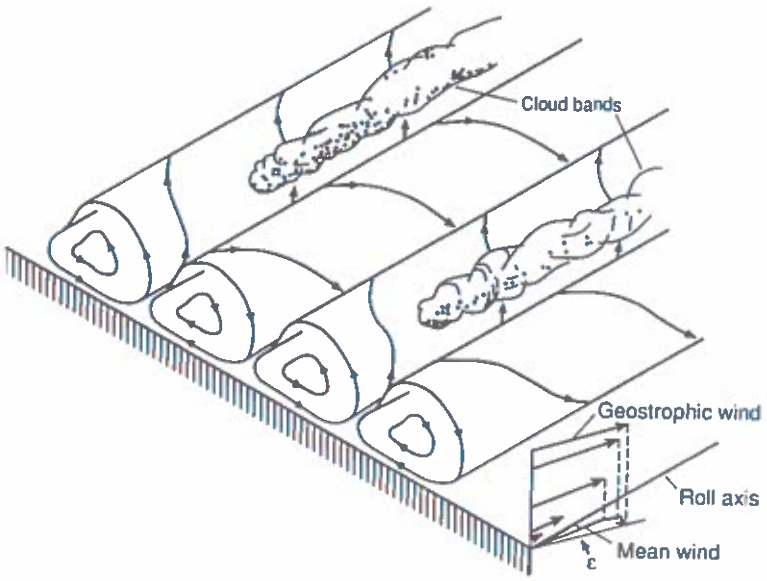

Fig. 4.12. Typical secondary flow in the planetary boundary layer resulting from the instability of the Ekman boundary layer [from Brown 1972].

Ekman layer instability and found that the rolls had a height of about $4D$ to $5D$ and an aspect ratio (width divided by height) of about 2.5. The typical secondary flow is shown in fig. 4.12.

The effect of stratification on Ekman layer instability has been investigated by several authors, beginning with Etling [1971], Brown [1972], Kaylor and Faller [1972] and Asai and Nakasuji [1973]. To give an impression of this effect, fig. 4.13 shows the neutral stability curves (where $\omega_i = 0$) for $\varepsilon = 14°$, calculated by Etling [1971], for different values of Ra (in which $H = D$ and Γ is constant) as a function of Re and α, where α is the non-dimensional wave-number ($=2\pi D/L$) in the direction perpendicular to the roll-axis. To the right of these curves there is instability. When the stratification is stable ($\mathrm{Ra} < 0$), the parallel mode is unstable at lower Re than the inflection point mode, even at an angle, ε, which is

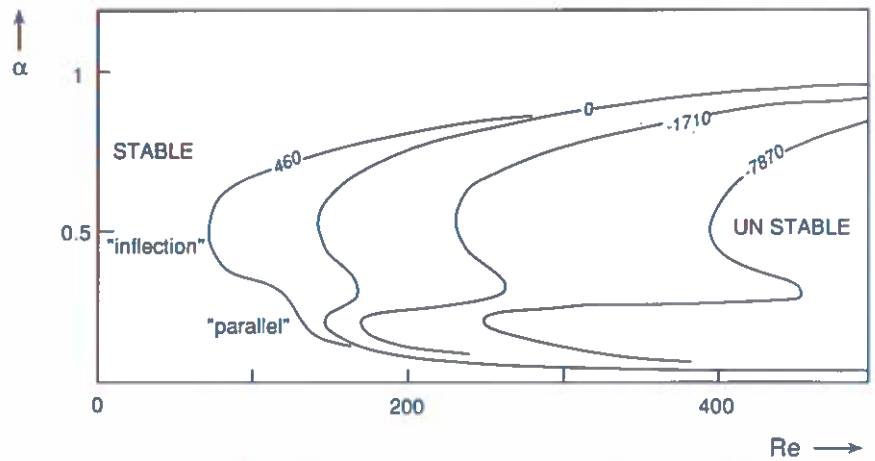

Fig. 4.13. Neutral curves, $\omega_i = 0$, for different values of Ra (in which $H = D$) for $\varepsilon = 14°$ [from Etling 1971].

more favourable for the growth of the inflection point mode. However, the results of Etling [1971] also show that, once the inflection point mode is unstable, its growth rate generally exceeds by far the growth rate of the parallel mode. The wavelength of maximum parallel instability is about $30D$, more than twice as large as the wavelength of maximum inflection point instability.

Brown [1972] showed that when $\mathrm{Ra} > 0$ the preferred wavelength shifts to slightly smaller values ($\sim 10D$) and the preferred orientation becomes more parallel to the geostrophic wind. In fact buoyant instability quickly starts to dominate the growth of the disturbance.

More information on this topic can be found in the review by Brown (1980).

4.2. Symmetric stability of thermal wind balance

Statement of the problem. In previous sections we have considered the stability of a steady state characterized by height (z)-dependent temperature and wind profiles. We assumed that the secondary flows, which develop as a result of instabilities of these steady states, possess time scales short enough for the Coriolis force to be unimportant. Because meso-scale systems may have lifetimes of the order of a day, it is obvious that this is a rather limited problem to investigate in this context. Therefore, in this section we will consider a problem which applies to weather systems with time scales of at least several hours. In this problem inertial forces, such as the Coriolis force, play a crucial role. More specifically, we will investigate a simplified version of baroclinic (in)stability, namely *symmetric baroclinic instability*. The analysis of this problem will yield additional wavelengths, frequencies and non-dimensional parameters, governing the behaviour and of many meso-scale weather systems, such as the sea breeze and the tropical cyclone.

Let us specify a background steady state, denoted by $u_0(y, z)$ and $\theta_0(y, z)$, which is in hydrostatic and geostrophic equilibrium with a large-scale pressure field, $\Pi_0(y, z)$. Since hydrostatic and geostrophic balance can be expressed as

$$\partial \Pi_0/\partial z = -g/\theta_0 , \quad \theta_0\, \partial \Pi_0/\partial y = -f u_0 , \tag{4.49}$$

respectively, thermal wind balance (3.29) can be written as

$$-(f u_0/\theta_0)\, \partial \theta_0/\partial z + (g/\theta_0)\, \partial \theta_0/\partial y = -f\, \partial u_0/\partial z . \tag{4.50}$$

The first term on the lhs of (4.50) can be neglected compared to the second term if $|\partial \theta_0/\partial y| \gg |(f u_0/g)\, \partial \theta_0/\partial z|$. Substituting typical values of u_0 ($\sim 10\ \mathrm{m\,s^{-1}}$), g ($10\ \mathrm{m\,s^{-2}}$), $\partial \theta_0/\partial z$ ($5 \times 10^{-3}\ \mathrm{K\,m^{-1}}$) and f, we obtain $\partial \theta_0/\partial y \gg 5 \times 10^{-7}\ \mathrm{K\,m^{-1}}$. Hence, if the horizontal temperature-gradient is much greater than about $10^{-3}\ \mathrm{K\,km^{-1}}$, which is usually the case in situations we are thinking of (fronts, sea breeze circulations), we can express thermal wind balance as

$$(g/\theta_m)\, \partial \theta_0/\partial y = -f\, \partial u_0/\partial z . \tag{4.51}$$

Here we have replaced θ_0 by a mean value, θ_m, over the domain in question.

We will superpose disturbances $u(y, z, t)$, $v(y, z, t)$, $w(y, z, t)$, $\theta(y, z, t)$ and $\Pi(y, z, t)$ which are *independent of* x, i.e. disturbances symmetric with respect to the x-axis, and proceed to derive an equation governing the growth or decay of these disturbances. Therefore, we are looking at the circulation perpendicular to the basic flow, u_0, or, in the terminology of section (4.2.4), at longitudinal

rolls (see fig. 4.14). Our starting point is the relatively simple set of inviscid equations for shallow flow linearized around the background state,

$$\partial u/\partial t = -v\,\partial u_0/\partial y - w\,\partial u_0/\partial z + fv\,, \tag{4.52}$$

$$\partial v/\partial t = -\theta_m\,\partial \Pi/\partial y - fu\,, \tag{4.53}$$

$$\partial w/\partial t = -\theta_m\,\partial \Pi/\partial z + (\theta/\theta_m)g\,, \tag{4.54}$$

$$\partial \theta/\partial t = -v\,\partial \theta_0/\partial y - w\,\partial \theta_0/\partial z + (1/\Pi_m)\,\mathrm{d}Q/\mathrm{d}t\,, \tag{4.55}$$

$$\partial v/\partial y + \partial w/\partial z = 0\,. \tag{4.56}$$

In (4.52) we have neglected the term involving the vertical velocity in the Coriolis force. This is justified as long as $\partial u_0/\partial z \gg 2|\Omega|\cos\phi \sim 10^{-4}\,\mathrm{s}^{-1}$. In (4.55) we have replaced Π by a constant mean value, Π_m. The variation of θ_0 is neglected in the momentum conservation equations (4.52–4.54). We have seen earlier (sections 3.2 and 4.1.1) that neglecting the vertical potential temperature variations in the pressure gradient terms amounts to neglecting the generation of circulation in a vertical plane due to the tilting to the horizontal of (disturbance) isobaric surfaces. Note that considering only symmetric disturbances (i.e. longitudinal rolls) makes this set of equations relatively simple. If the disturbances were also dependent on x, we would in fact be left with the ordinary baroclinic instability problem [e.g., Holton 1979, Stone 1966]. If the disturbances were only dependent on x and z, we would be left with the Kelvin–Helmholtz instability problem (see sections 4.1.3 and 4.1.4).

Another approximation that is made in the above set of equations is the use of the incompressible form of the continuity equation. This allows us to introduce a stream function $\psi(x, z, t)$, such that

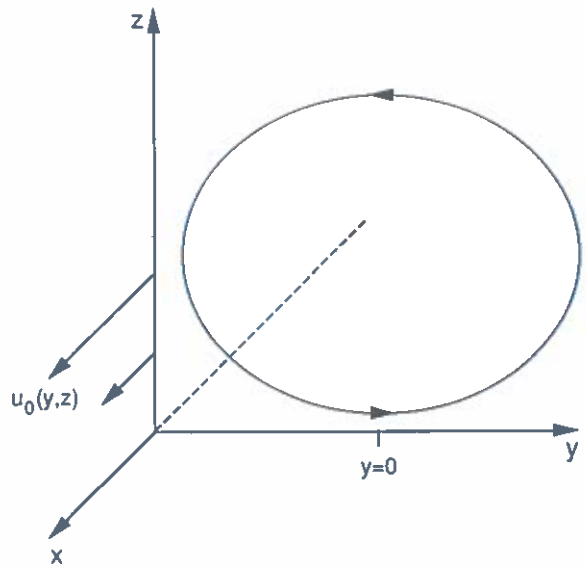

Fig. 4.14. Circulation in the y–z plane resulting from the symmetric instability of the mean baroclinic current $u_0(y, z)$.

$$v = \partial\psi/\partial z\,, \quad w = -\partial\psi/\partial y\,. \tag{4.57}$$

Equations (4.53) and (4.54) can easily be combined to form an equation for the secondary circulation. The result is

$$(\partial^2/\partial t^2)\nabla^2\psi = -f\,\partial u/\partial z - (g/\theta_m)\,\partial\theta/\partial y\,, \tag{4.58}$$

where we have assumed that f is constant and where $\nabla_i^2 = \partial^2/\partial y^2 + \partial^2/\partial z^2$. The above equation shows that the secondary circulation is forced by departures from thermal wind balance. By differentiating (4.58) with respect to time and using (4.52) and (4.55) we obtain the following important linear equation for the secondary circulation:

$$\frac{\partial^2}{\partial t^2}\nabla^2\psi = -F^2\frac{\partial^2\psi}{\partial z^2} + 2S^2\frac{\partial^2\psi}{\partial y\,\partial z} - N^2\frac{\partial^2\psi}{\partial y^2} - \frac{g}{\Pi_m\theta_m}\frac{\partial}{\partial y}\frac{\mathrm{d}Q}{\mathrm{d}t}\,, \tag{4.59}$$

where

$$F^2 = f(f - \partial u_0/\partial y)\,, \tag{4.60}$$

$$S^2 = (g/\theta_m)\,\partial\theta_0/\partial y = -f\,\partial u_0/\partial z\,, \tag{4.61}$$

$$N^2 = (g/\theta_m)\,\partial\theta_0/\partial z\,. \tag{4.62}$$

F, S and N are frequencies. N (the Brunt–Väisälä or buoyancy frequency) has been introduced earlier (see section 4.1.1). The other frequencies are the *inertial frequency*, F, and the *baroclinic frequency*, S. Typical atmospheric values of these frequencies [Hoskins 1978] are

$$F \sim 10^{-4}\,\mathrm{s}^{-1}\,, \quad S \sim 0.5\times 10^{-3}\,\mathrm{s}^{-1}\,, \quad N \sim 10^{-2}\,\mathrm{s}^{-1}\,.$$

Thus, the time scale associated with convection and buoyancy waves, $1/N$, is one to two orders of magnitude smaller than the other two time scales. However, if we realize that the relative vorticity of the background flow is $\zeta_0 = -\partial u_0/\partial y$, we immediately see that the inertial frequency, which is associated with adjustment to geostrophic balance, can increase significantly if the (background) flow possesses positive (cyclonic) vorticity.

Mathematical analysis. For the moment we will assume no diabatic heat sources ($\mathrm{D}Q/\mathrm{d}t = 0$). In an unbounded domain we will look for solutions of the form (see fig. 4.15)

$$\exp(\mathrm{i}\omega t)\exp[\mathrm{i}\alpha(y\sin\phi + z\cos\phi)]\,, \tag{4.63}$$

where the angle, ϕ, is defined as in section 4.1.2, below eq. (4.21). When we substitute (4.63) into (4.59) we obtain an equation for the frequency,

$$\omega^2 = N^2\sin^2\phi - 2S^2\sin\phi\cos\phi + F^2\cos^2\phi\,. \tag{4.64}$$

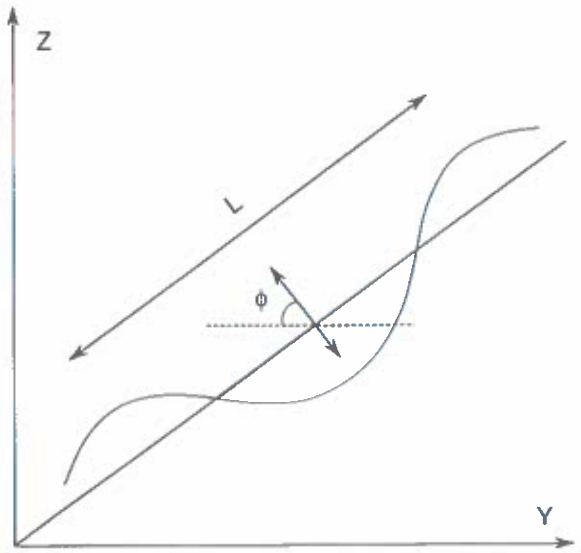

Fig. 4.15. Geometry of a vertically propagating wave with wavelength L. Particles oscillate as indicated by the arrows at an angle, ϕ, to the horizontal.

Note again (see also eq. 4.21) that the frequency, ω, is independent of the absolute value of the wave-number, α. When $S = 0$ and $F = 0$, we are left with the dispersion relation (4.21) for pure buoyancy waves. When $S = 0$ and $N = 0$, only so-called *inertia waves* are possible. Inertia oscillations in the horizontal owe their existence primarily to the earth's rotation. However, inertia oscillations can also be sustained if the vertical vorticity of the mean flow is positive. When only $S = 0$, we are left with the dispersion relation for so-called *buoyancy–inertia waves*, a mixture of buoyancy and inertia oscillations. The time series of the wind direction measured on May 7 and on May 8 at station number 225, shown in fig. 2.4, is characteristic for the passage of an inertia (–buoyancy) wave. The passage of the wave is marked by winds from the south prior to the passage of the wave-crest and winds from the north after the passage of the wave-crest. The passage of the wave-crest at a particular point can be identified with the onset of the sea breeze at that particular point. We will elaborate further on the relation between inertia–buoyancy waves and the sea breeze in section 5.2.

In the general case ($N \neq 0$, $F \neq 0$, $S \neq 0$) we may write, after doing some straightforward algebra [Ooyama 1966],

$$2\omega^2 = N^2 + F^2 - A\cos[2(\phi - \phi_1)]\,, \tag{4.65}$$

where

$$\cos(2\phi_1) = (N^2 - F^2)/A\,, \quad \sin(2\phi_1) = 2S^2/A\,, \tag{4.66}$$

$$A = [(N^2 - F^2)^2 + 4S^4]^{1/2}\,. \tag{4.67}$$

The minimum frequency, $\omega_{\min}$, corresponds to $\phi = \phi_1$ (with $A > 0$):

$$2\omega_{\min}^2 = N^2 + F^2 - [(N^2 + F^2)^2 - 4q]^{1/2}\,, \tag{4.68}$$

where q is defined as

$$q = F^2N^2 - S^4 , \tag{4.69}$$

which is proportional to *Ertel's potential vorticity*[*]. Instability can set in only when $\omega^2 < 0$, i.e. when either

$$N^2 + F^2 < 0 \quad \text{or} \quad q < 0 . \tag{4.70}$$

Interpretation. The potential vorticity of the background state is composed of two terms: one (F^2N^2) is associated with the vertical component of the vorticity and the vertical stratification, and the other (S^4) is associated with the horizontal component of the vorticity and the horizontal temperature gradient (baroclinicity). If there is no baroclinicity ($S = 0$), (4.70) reveals that instability will set in if either N^2 or F^2 is negative. If only F^2 is negative (and $N^2 = 0$), the instability is called *inertial instability*. This instability is in fact analogous to the so-called *centrifugal instability* of a circular balanced vortex, first addressed by Rayleigh [1916b] (see also Drazin and Reid [1982]). If only N^2 is negative (and $F^2 = 0$), the instability is called buoyant instability or hydrostatic instability (see section 4.1.2). A special and new situation arises when N^2 and F^2 are both positive, i.e. when the flow is inertially stable and buoyantly stable, but nonetheless the potential vorticity is negative due to strong baroclinicity (high values of S^2). In this case the instability is called *symmetric baroclinic instability*. It is also referred to as "Helmholtz instability" [Godske et al. 1957].

The orientation of the disturbance with maximum growth rate can be found from eq. (4.66) with $\phi_1 = \phi$ and $A > 0$. We have the following special cases:

(i) Pure buoyant instability: $N^2 < 0$, $S^2 = 0$ and $0 \le F^2 < |N^2|$ gives $\cos(2\phi) = -1$, or $\phi = \pi/2$, implying a maximum growth rate in the vertical direction.

(ii) Pure inertial instability: $F^2 < 0$, $S^2 = 0$ and $0 \le N^2 < |F^2|$ gives $\cos(2\phi) = 1$, or $\phi = 0$, implying a maximum growth rate in the horizontal direction.

If there is baroclinicity, the orientation of the disturbance with maximum growth rate lies somewhere between the horizontal and the vertical. To find out more about this orientation, we rewrite the instability criterion, $q < 0$, in terms of the slope of the potential temperature surfaces and the slope of the absolute momentum surfaces. The absolute linear momentum (per unit mass),

$$M = u - fy , \tag{4.71}$$

is a conserved quantity within the framework of the model defined in this section. This can easily be derived from the x-component of the equation of motion.

The atmosphere is usually stratified with respect to both M and θ. The stability of the atmosphere with respect to small disturbances depends on both types of stratification. This can be understood by means of the following considerations. The slope of surfaces of equal M_0 is

$$\left(\frac{\partial z}{\partial y}\right)_{M_0} = -\frac{\partial M_0/\partial y}{\partial M_0/\partial z} = -\frac{\partial u_0/\partial y - f}{\partial u_0/\partial z} = -\frac{F^2}{S^2} . \tag{4.72}$$

[*] Ertel's potential vorticity in the atmosphere is defined as $\omega_a \cdot \nabla\theta/\rho$, i.e. as the scalar product of the absolute vorticity and the potential temperature gradient divided by the density. It is conserved for adiabatic, inviscid processes [Ertel 1942, Pedlosky 1987].

The slope of the background isentropes (surfaces of equal potential temperature) is

$$\left(\frac{\partial z}{\partial y}\right)_{\theta_0} = -\frac{\partial \theta_0/\partial y}{\partial \theta_0/\partial z} = -\frac{S^2}{N^2} . \tag{4.73}$$

Remember that the subscript zero refers to the time-independent environment. In view of (4.72, 4.73) the instability condition, $q<0$, can be written as,

$$(\partial z/\partial y)_{\theta_0}/(\partial z/\partial y)_{M_0} > 1 . \tag{4.74}$$

In other words, the slope of the potential temperature surfaces must be greater than the slope of the absolute momentum surfaces.

A parcel of air will conserve both M (as long as motions remain symmetric) and θ. If M_0 and θ_0 surfaces are congruent, conservation of both can be achieved while the parcel remains in balance with its environment if it moves along this surface. If M_0 and θ_0 surfaces are not congruent, the following two cases can be distinguished [Bennetts et al. 1988]: (a) M_0 surfaces steeper than θ_0 surfaces, (b) θ_0 surfaces steeper than M_0 surfaces.

If a parcel of air is displaced from its equilibrium level it will try to return to a position where the environment has exactly the same values of M and θ. There are two different restoring mechanisms. Restoration with respect to θ is achieved through the buoyancy force and the vertical pressure gradient force, while restoration with respect to M is achieved through horizontally oriented forces (pressure gradient force and Coriolis forces).

Take, for example, case (a) (fig. 4.16a). Consider a parcel of air displaced upwards and to the right along a line at an angle to the horizontal which lies between the angles made by, respectively, the θ_0 and M_0 surfaces. Because θ_0 increases with height, the parcel becomes colder than its environment and therefore sinks back. Since M_0 decreases with increasing y, the parcel comes into a region where M_0 is lower. The velocity, u, of the parcel is greater than the velocity, u_0, of the environment. Therefore, the environmental pressure gradient force is too weak to balance the Coriolis force on the parcel, which implies that the net force is towards lower y in the direction of higher M_0. Hence, the parcel returns to

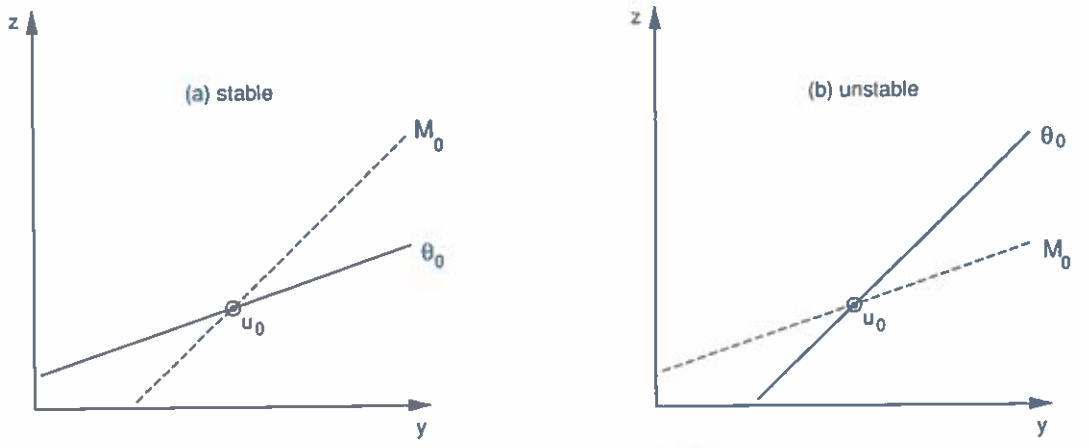

Fig. 4.16. Stable (a) and unstable (b) background distributions of absolute momentum, M_0, and potential temperature, θ_0. The equilibrium position of the parcel referred to in the text is indicated by a circle.

its original position. Note that we have neglected the effect of perturbation pressure gradient forces in this argument (for a discussion of this approximation, see Thorpe et al. [1989]).

In case (b) (fig. 4.16b) a similar displacement has the opposite effect. The parcel now enters a region of lower potential temperature and therefore rises further. It also enters a region of higher absolute momentum. To restore the equilibrium the parcel must move in a direction of decreasing M_0, which implies that the original displacement is magnified. The parcel is accelerated both in the horizontal and in the vertical direction. This only happens if the initial displacement is oriented at an angle between θ_0 surfaces and M_0 surfaces. Because θ_0 and M_0 surfaces in the vicinity of fronts are generally tilted at a relatively small angle to the horizontal, the motion resulting from symmetric baroclinic instability is slanted (see fig. 4.17). Therefore, this motion is frequently referred to as *slantwise convection* [e.g., Emanuel 1983a,b].

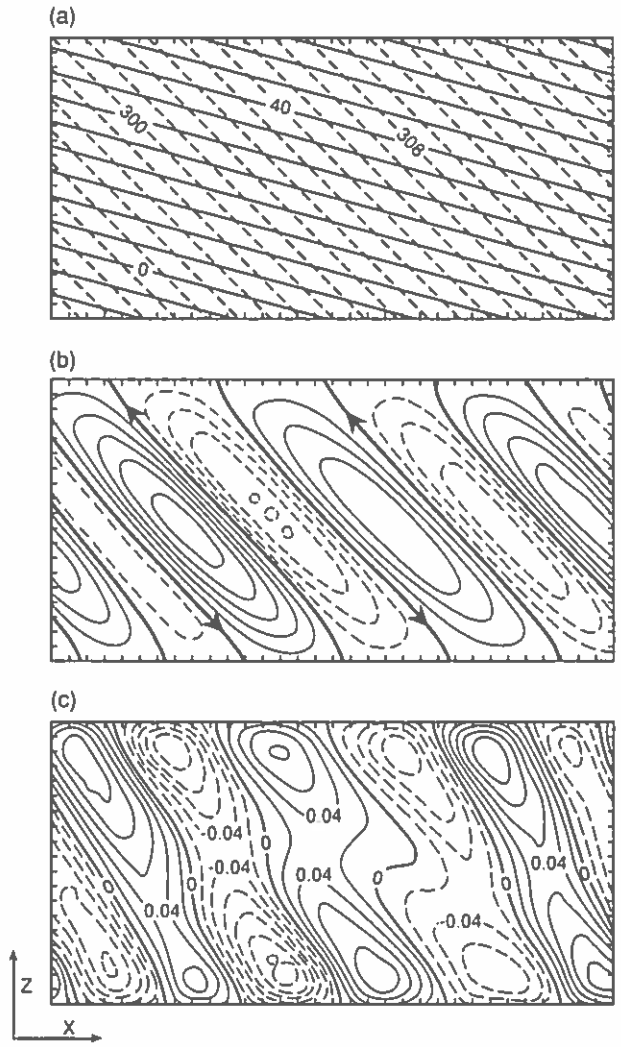

Fig. 4.17. Results from a numerical simulation of symmetric baroclinic instability. (a) Initial distribution of M (solid line) and θ in the full domain 3 km by 300 km (contour interval in M is 5 m s^{-1} and in θ it is 1 K), (b) the stream function field after $t = 10$ h (contour interval 0.002 m^2 s^{-1}). (c) potential temperature deviation after 10 h (contour interval 0.04 K) [from Thorpe and Rotunno 1989].

If H is the vertical scale of the two-dimensional roll-like motion resulting from symmetric baroclinic instability, two length scales can be deduced from eqs. (4.72) and (4.73). These are

$$L_\theta^2 = |N^2H^2/S^2|\,, \quad L_M^2 = |S^2H^2/F^2|\,. \tag{4.75}$$

If we substitute representative values of F ($10^{-4}\,s^{-1}$), N ($10^{-2}\,s^{-1}$) and H (3000 m) and assume neutrality (i.e. $q=0$, thus $S^4 = N^2F^2$), the two length scales become identical, i.e. 300 km. This is a typical meso-scale length scale. In fact, symmetric baroclinic instability is the only clear meso-scale instability. This led Emanuel [1982] to suggest a dynamical definition of the meso-scale, namely those motions for which the Rossby number, as defined in eq. (3.28), is of order unity.

Because potential vorticity is conserved in adiabatic, inviscid flow, the instability criterion, $q<0$, has some interesting consequences. The motions resulting from this instability will never relieve the instability unless there are nonconservative processes. Therefore, nonconservative processes, such as friction, must play a crucial role. This matter has been investigated by Thorpe and Rotunno [1989].

The instability criterion, $q<0$, or (4.74) can be written in yet another way, i.e. as

$$\mathrm{Ri} < (1 - f^{-1}\,\partial u_0/\partial y)^{-1}\,, \tag{4.76}$$

where the Richardson number, Ri, is defined as in (4.29). If the basic state has zero vorticity ($\partial u_0/\partial y = 0$), it is unstable to symmetric disturbances if $\mathrm{Ri}<1$. The critical Richardson number ($\mathrm{Ri}_{crit}=1$) for marginal (neutral) stability is identical to the critical Richardson number derived in section 4.1.3, for Kelvin–Helmholtz instability. However, the two cases are different. In the present section we are considering disturbances oriented parallel to the mean wind direction, whereas in section 4.1.4 we investigated disturbances oriented *perpendicular* to the mean wind direction.

When the basic flow possesses positive vorticity ($\partial u_0/\partial y < 0$), the critical Richardson number increases, implying that the flow becomes more stable to symmetric disturbances. This flow property, which is of some importance for the dynamics of tropical cyclones, has been called "stiffness" by Hoskins [1974] and Schubert and Hack [1982], and "rotational rigidity" by others [e.g., Stern 1975].

Purely symmetric baroclinic instability is rare in the atmosphere. On the meso-scale the atmosphere is usually statically (buoyantly) and inertially stable. However, this does not mean that the theory described above is irrelevant. We will see later (section 6.1) that diabatic heat sources, such as latent heat release due to condensation, or sensible heat fluxes, may trigger symmetric instability. Furthermore, even if instability does not occur, diabatic heat sources may *force* a steady secondary circulation. Basically, this is due to the fact that these heat sources upset the existing equilibrium of forces. A secondary circulation is then needed to re-establish the equilibrium. This readjustment is not a trivial process because the atmosphere does not react to forcing in a simple way like a damped pendulum, in the sense that it hardly ever returns exactly to its original equilibrium state after being forced away from this equilibrium state. Therefore, diabatic heating (or other non-conservative processes) will trigger a slow evolution from one equilibrium state to another equilibrium state. The process of *adjustment to balance in a stable atmosphere* is the topic of the next chapter.

5. Adjustment

In the previous chapter we were concerned with the stability and instability of certain prototype background or large-scale states. Usually the background atmospheric stratification and flow are such

that disturbances generated by, for example, diabatic heat sources and sinks do not amplify. This is the same as saying that the background state is stable. Nevertheless, these nudgings and pullings, which may be quite appreciable, do upset the balance of forces in the background state. If the forcing acts relatively abruptly, the response is in the form of oscillations around the equilibrium. If the forcing acts slowly and gently, the atmosphere responds with a (relatively) steady circulation leading to a gradual (without oscillations) readjustment to a new equilibrium. In this chapter I hope to convince the reader that the topic of adjustment to geostrophic and hydrostatic balance is central to the understanding of the characteristics and differences of meso-scale circulations. I hope also that this will refine the concept of meso-scale.

5.1. Geostrophic adjustment in the shallow-water layer model

Characteristic time scales and length scales. In order to illustrate the adjustment process, let us first consider the behaviour of a rotating shallow homogeneous layer of fluid which is disturbed by mass extraction. This will have the same effect as throwing a stone into a pond. The free surface is depressed by the stone and surface gravity waves are excited and propagate away from the source. In a system which is not rotating, all of the potential energy, imparted initially to the system by the stone, is radiated away by the waves. However, in a rotating system in which potential vorticity (absolute vorticity divided by the layer depth) is conserved, the disturbed mass field adjusts to a geostrophic equilibrium. Only a fraction of the potential energy is radiated away. These statements can be illustrated with the results of several numerical simulations with the shallow fluid system described in section 3.4 (see fig. 3.3b).

The configuration in these particular experiments is shown in fig. 5.1. The whole system is rotating with an angular velocity equal to $\Omega = f/2$. The equations of motion for the lower layer are given in section 3.4 (eqs. 3.32–3.34) in which $u_g = 0$ and $h_h = 0$. We will extract a specified volume of mass from the lower layer. To incorporate this effect into the model, the continuity equation becomes

$$\partial h/\partial t = -\partial hu/\partial x + Q\,, \tag{5.1}$$

instead of (3.34). In this equation Q represents the volume of mass extracted per unit time and area. All y-derivatives are assumed to be zero. It is well known [e.g., Gill 1982, section 7.3] that the linearized shallow water equations with $Q = 0$ support *surface gravity-inertia waves* with phase-speeds, c, given by

$$c^2 = f^2/\alpha^2 + g'\bar{h}\,, \tag{5.2}$$

where α is the wave-number and $\bar{h}$ is the mean depth of the lower layer. Evidently, the effect of

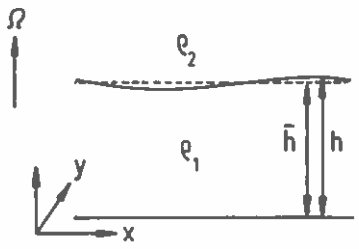

Fig. 5.1. Geometry of the shallow slab-symmetric rotating layer of fluid (see text).

rotation on the speed of these dispersive waves is more important than the effect of stratification if

$$L > 2\pi\sqrt{g'\bar{h}}/f = 2\pi\lambda\,, \tag{5.3}$$

where $L = 2\pi/\alpha$ is the wavelength. λ is called the Rossby radius of deformation. This important length scale, which was introduced in a different form in chapter 2 (eq. 2.1), also appears when we consider the frequency, ω, of surface gravity-inertia waves, given by

$$\omega^2 = \alpha^2 c^2 = f^2 + 4\pi^2 g'\bar{h}/L^2\,. \tag{5.4}$$

It is easily deduced that the system possesses two fundamental limiting frequencies. If $L \gg 2\pi\lambda$, the waves are nearly inertial, with frequency

$$\omega_F^2 = f^2\,. \tag{5.5}$$

If $L \ll 2\pi\lambda$, then the waves become pure surface gravity waves with frequency

$$\omega_G^2 = 4\pi^2 g'\bar{h}/L^2\,. \tag{5.6}$$

Note that the inertial frequency, ω_F, is independent of the horizontal scale of the disturbance, while the gravity wave frequency, ω_G, is not. This is the reason why the reaction of a rotating fluid system to large-scale disturbances is primarily in the form of inertial waves, which means that the reaction is noted most strongly in u and v (i.e. in the vorticity), whereas the reaction to small-scale disturbances is primarily in the form of gravity waves, which means that it is noted most strongly in u and h (i.e. in the divergence).

The group velocity of surface gravity inertia waves is equal to $g'h\alpha/\omega$. If $g' = 0$, we are left with pure inertia waves which apparently have zero group velocity and, therefore, do not transport energy.

Response to forcing: a simple numerical experiment. The importance of the length scale, λ, and the inertial time scale, $1/\omega_F$, can be illustrated with the results of some numerical integrations of eqs. (3.32, 3.33, 5.1) with $v = u = 0$ and $h = 2000\,m$ initially and $g' = 1\,\mathrm{m/s^2}$ and $u_g = 0$. We will vary the rotation rate, f (i.e. λ), and the time scale of the mass extraction, while keeping the total volume of mass extracted during the integration time constant. The mass extraction term is specified as follows:

$$Q = Q_0(x)/\tau \quad \text{if } t \le \tau\,; \qquad Q = 0 \quad \text{if } t > \tau\,, \tag{5.7}$$

where Q_0 is the total volume of mass extracted per unit area, and τ is the time in which this is accomplished. Q_0 is plotted as function of x in fig. 5.2. The horizontal scale of the forcing, L_Q, is approximately equal to 150 km. It is very important to note here that when we extract mass, we are simultaneously introducing potential vorticity. Potential vorticity in the hydraulic model is defined as the absolute vorticity divided by the depth of the fluid. Because potential vorticity is materially conserved, the fluid will not adjust to the steady state of rest, but will adjust to geostrophic equilibrium [Gill 1982].

Equations (3.32, 3.33, 5.1) are integrated on a grid of 240 points in the x-direction. The grid distance is 10 km and the time step is 2 min. Details of the numerical procedure can be found in van Delden [1989a].

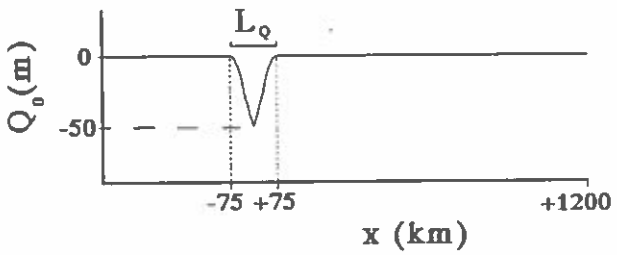

Fig. 5.2. Total volume per unit mass extracted as a function of x.

In fig. 5.3 the height, h is plotted as a function of x every 8 min for three cases. In case (a) the rotation rate is representative for a motionless atmosphere at mid latitudes. The length scale of the forcing is very short compared to λ. Also, the time scale of the forcing is very short compared to $1/\omega_F$. As expected, waves are excited which propagate away at a speed approximately equal to 45 m/s. However, some potential energy is caught in the so-called "geostrophic equilibrium mode". This potential energy is spread out over a distance of the order of λ.

In case (b), the rotation rate (f) is increased tenfold, while all other parameters are identical. Therefore, λ is smaller than L_Q. We see that, although there are dispersive gravity-inertia waves propagating away from the forcing region, an appreciable amount of balanced potential energy is left in a relatively small area.

In case (c), which differs from case (b) only in the prescribed forcing time, τ, which is now 400 min ($>1/\omega_F$), the gravity-inertia waves have such small amplitudes that they cannot be resolved by the graphics, although the same amount of potential energy as in case (b) is left in the geostrophic mode (in this very simple model). Therefore, in the context of this model, the time scale, τ, does not influence the final geostrophic equilibrium. It only influences the wavelength, and therefore the amplitude, of the waves. In the next section we will discuss a different model which permits buoyancy waves instead of surface gravity waves. In this model the forcing frequency is indeed crucial in the energy partition between transient and steady motions.

Some differences between interfacial gravity-inertia waves and buoyancy-inertia waves. The gravity waves shown in fig. 5.3, which propagate along and below the interface between the two layers shown in fig. 5.1, are fundamentally different from the buoyancy waves which were discussed in sections 4.1.2 and 4.2. This can clearly be seen when comparing the respective dispersion relations, (4.21) for buoyancy waves and (5.6) for surface gravity waves. Buoyancy waves have frequencies depending on the direction of propagation, or, stated the other way around, propagate in a direction determined by the frequency. The driving force is the sum of the *vertical* perturbation pressure gradient force and the buoyancy force. Surface or interfacial gravity waves in shallow fluid layers are hydrostatic. They have frequencies which are inversely proportional to the horizontal wavelength. They propagate along and below a discontinuity in density or potential temperature, such as the tropopause, or a subsidence inversion. Therefore, the inertial effect of the vertical gradient in (potential) density (see section 3.2) plays a crucial role in generating and maintaining these waves. The driving force is the *horizontal* pressure gradient force. Ultimately, of course, both buoyancy waves and surface gravity waves owe their existence to gravity. This is why they are both frequently referred to simply as *gravity waves*.

We must keep in mind that buoyancy waves and interfacial gravity waves are *theoretical constructions*. The distinction between the two types of wave arises in theory, on the one hand because certain

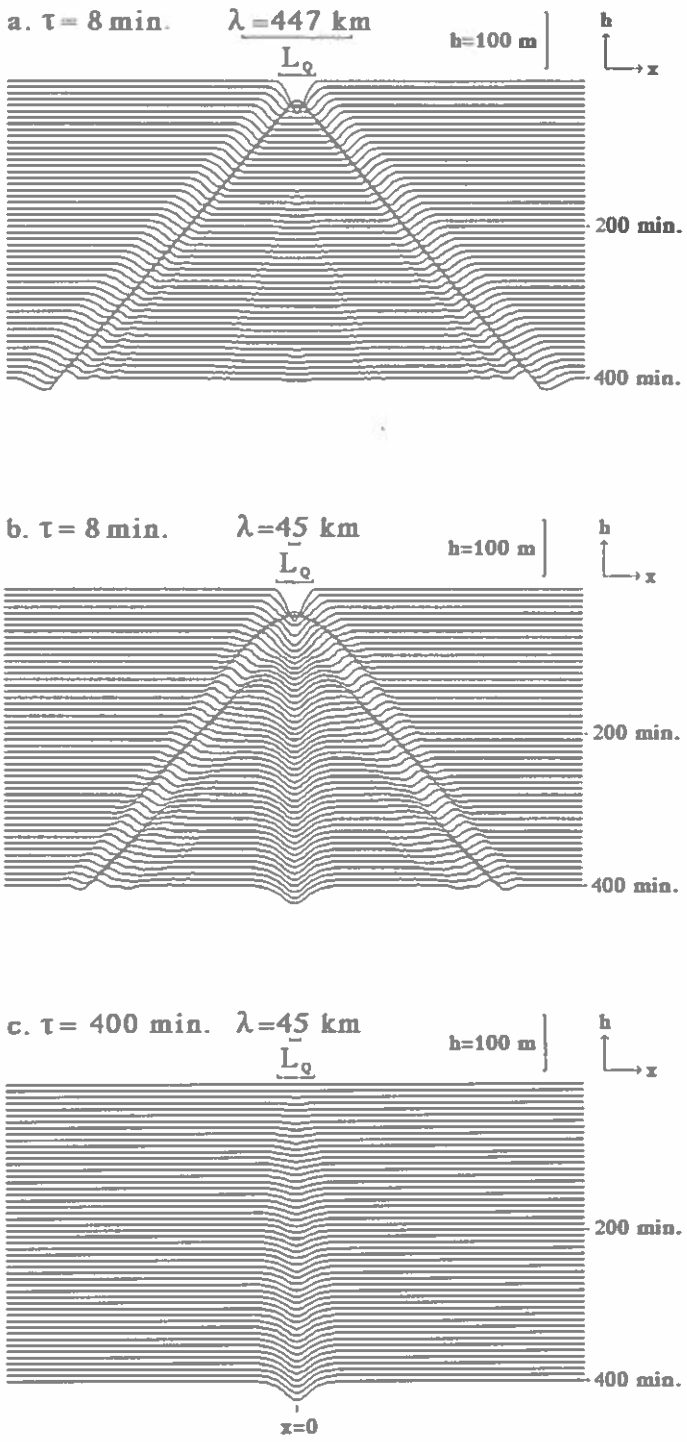

Fig. 5.3. The reaction of the rotating shallow layer of fluid to forcing (Q), with a horizontal scale L_Q and a time scale τ. The level of the free surface is shown every eight minutes. (a) $f = 0.0001\ s^{-1}$, $\tau = 8$ min ($L_Q/\lambda \approx 0.3$, $\tau f \approx 0.05$); (b) $f = 0.001\ s^{-1}$, $\tau = 8$ min ($L_Q/\lambda \approx 3$, $\tau f \approx 0.5$); (c) $f = 0.001\ s^{-1}$, $\tau = 400$ min ($L_Q/\lambda \approx 3$; $\tau f \approx 2.4$). The values of the other parameters are $L_Q = 150$ km, $g' = 1\ m\ s^{-2}$ and $\tilde{h} = 2000$ m.

terms in the equations of motion and continuity are neglected (e.g. in the Boussinesq approximation; see section 3.2 and 4.1.1), and on the other hand because of certain assumptions in the physics of the problem (e.g., in the model shown in figure 5.1). In reality, however, this distinction is impossible. Real gravity waves will probably resemble buoyancy waves when the stratification is relatively weak (N^2 is small), and when the horizontal wavelength is relatively small, because these are the conditions for the validity of the Boussinesq approximation on which the theory of buoyancy waves is based (see section 4.1.1). With increasing horizontal wavelength and with increasing intensity of the stratification (e.g., in a temperature inversion) the gravity wave in reality will probably behave more and more like an interfacial gravity wave (horizontal propagation, less dispersion).

Inertia waves in the continuously stratified case and in the shallow water layer model also differ as far as the dispersion properties are concerned. As noted earlier, surface inertia waves do not transport energy because they travel horizontally. Inertia waves in the continuous model, on the other hand, may travel vertically. The group velocity of these waves is not zero. Therefore, vertically propagating inertia waves transport energy horizontally.

Due to the different dispersion properties of buoyancy-inertia waves compared to interfacial gravity waves, we expect a different geostrophic adjustment process in a model which only permits the former type of wave. Therefore it is worth discussing geostrophic adjustment in such a model. We will do this in the following section, especially with the sea breeze in mind.

We will return to the problems involved in relating the theory of gravity waves to reality in sections 5.4 and 6.5.

5.2. Adjustment to thermal wind balance in the shallow Boussinesq model

Linear theory of the sea breeze. A model which allows for buoyancy waves and inertia waves is the configuration which was introduced in section 4.2. We can apply this configuration to the sea breeze situation if we assume that the coastline is given by the line $y = 0$ in fig. 4.14 with the land to the right of this line. Equation (4.59) then describes the circulation perpendicular to the coast. Assuming, for simplicity that background baroclinicity is negligible ($S = 0$), this equation can be written as

$$\frac{\partial^2}{\partial t^2}\nabla^2\psi = -F^2\frac{\partial^2\psi}{\partial z^2} - N^2\frac{\partial^2\psi}{\partial y^2} - \frac{g}{\Pi_m\theta_m}\frac{\partial}{\partial y}\frac{\mathrm{d}Q}{\mathrm{d}t}\,. \tag{5.8}$$

This is a linearized equation. It is, therefore, valid only for small-amplitude motions. Assuming inertial and static stability ($F^2 > 0, N^2 > 0$), motions will arise only as a result of a horizontal gradient in diabatic heating. In this section we will assume that this diabatic heating is weak enough so that the linear model remains valid.

The sea breeze is forced by horizontal gradients in diabatic heating. This forcing introduces baroclinicity, $\partial\theta/\partial y$, which upsets thermal wind balance (4.51). This in turn sets off buoyancy-inertia waves and a readjustment to thermal wind balance. In the new balanced state, a vertical gradient in M (defined in eq. (4.71)) is required to balance the horizontal temperature gradient introduced by the heating. The sea breeze is in fact a manifestation of this process of adjustment to thermal wind balance. However, thermal wind balance is never attained because the period of the forcing is too short. This can be understood as follows.

Let us ignore, for the moment, the actual process by which heat is transferred to the air. Following Rotunno [1983], the diabatic heating term can simply be prescribed as a function of space and time by

$$dQ/dt = Q_1(y, z)\exp(-i\omega t)\,, \tag{5.9}$$

i.e. the atmosphere in the vicinity of the coast is forced at the frequency, ω. Since eq. (5.8) is linear, $\psi = \psi_1(y, z)\exp(-i\omega t)$. Equation (5.8) then becomes,

$$(N^2 - \omega^2)\frac{\partial^2\psi_1}{\partial y^2} + (F^2 - \omega^2)\frac{\partial^2\psi_1}{\partial z^2} = -\frac{g}{\Pi_m\theta_m}\frac{\partial Q_1}{\partial y}\,. \tag{5.10}$$

The character of the solution of this equation depends on the magnitude of the forcing frequency, ω, compared to the fundamental frequencies, F and N. If $\omega^2 \ll N^2$, in which case the time scale of the forcing is much larger than the period of the possible buoyancy waves, (5.10) becomes

$$\frac{\partial^2\psi_1}{\partial y^2} + \frac{F^2 - \omega^2}{N^2}\frac{\partial^2\psi_1}{\partial z^2} = -\frac{g}{\Pi_m\theta_m}\frac{\partial Q_1}{\partial y}\,. \tag{5.11}$$

This is tantamount to having made the hydrostatic approximation in (4.54). In other words, if the system is forced with a low frequency such that $\omega^2 \ll N^2$, hydrostatic balance will not be significantly upset. The flow will be able to readjust immediately (adiabatically) to hydrostatic balance. In the case of the sea breeze, the period of the forcing is determined by the diurnal cycle, which is 24 h. This implies that $\omega = 0.73 \times 10^{-4}\ s^{-1}$, which is indeed much smaller than the typical value of $10^{-2}\ s^{-1}$ for N. The sea breeze may thus be regarded as a so-called hydrostatic circulation.

In the absence of background flow vorticity, $F = f$. Since $f \sim 10^{-4}\ s^{-1}$, the inertial frequency is of the same order of magnitude as the forcing frequency. Therefore, the sea breeze circulation is never able to reach geostrophic equilibrium because the circulation is forced away from this equilibrium in the same time as it takes to (re)adjust to this equilibrium. In fact, the response of the atmosphere depends critically on whether f (or F if the background flow possesses vorticity) is greater or less than ω. There are three types of solution to (5.11):

(1) When $\omega^2 < F^2$, (5.11) is elliptic. The solution is such that the motion is confined to the neighbourhood of the forcing.

(2) When $\omega^2 > F^2$, (5.11) is hyperbolic. The solution is oscillatory, i.e. the response to the forcing is in the form of inertia-buoyancy waves propagating away from the source region.

(3) When $\omega = F$, the solution to (5.11) is singular. Resonance occurs. Effects of friction must be included. These will eliminate the resonance.

Let us specify $Q_1(y, z)$ and $\psi_1(y, z)$ by

$$Q_1(y, z) = Q_0(y)\sin(\pi z/H)\,, \quad \psi_1(y, z) = \psi_0(y)\sin(\pi z/H)\,, \tag{5.12}$$

with $Q_0 > 0$ for $y > 0$, $Q_0 = 0$ for $y \le 0$, i.e. there is heating over land and no heating over sea. The solution of eq. (5.11) together with (5.12) is of the form

$$\begin{aligned} &\psi_0(y) \approx A\exp[-\pi(F^2 - \omega^2)^{1/2}y/NH] \quad \text{for } y > 0\,, \\ &\psi_0(y) \approx A\exp[\pi(F^2 - \omega^2)^{1/2}y/NH] \quad \text{for } y < 0\,. \end{aligned} \tag{5.13}$$

A is a constant determined by the boundary conditions. If $\omega^2 < F^2$ this solution tells us that the

intensity of the circulation decays exponentially away from the coast. The e-folding distance is proportional to

$$L = NH/\sqrt{F^2 - \omega^2}\,. \tag{5.14}$$

The sea breeze circulation is confined to a distance of the order of L from the coast. L reaches a minimum when ω approaches zero or when $\omega^2 \ll F^2$, i.e. when geostrophic balance is assumed from the start. The horizontal scale representative of the circulation generated by the land–sea contrast is then given by

$$\lambda = NH/F\,. \tag{5.15}$$

The parameter, λ, is again the Rossby radius of deformation. This parameter was already introduced in chapter 2 (eq. 2.1) as the largest length scale that could be deduced from the basic parameters governing the flow in a rotating reference frame with constant angular velocity. It was again introduced in a different form in the previous section. The definition of λ in (5.15) differs from the definition of λ in (5.3) because of the different dispersion properties of surface gravity waves and of buoyancy waves. The effect of the background rotation (the Coriolis force) on the flow field is to make waves evanescent instead of propagating when $\omega < F$. The "wave" amplitude decays most rapidly with distance when the flow is allowed to adjust perfectly to geostrophic balance. This is the case if the time scale associated with the forcing is very large compared to the inertial time scale.

Let us substitute into (5.15) some typical values for N ($10^{-2}\,s^{-1}$), H (2000 m) and F ($10^{-4}\,s^{-1}$) which apply to the sea breeze situation. We then obtain $\lambda \approx 200$ km. This means that the sea breeze circulation will adjust to geostrophic balance (that is, the wind will blow parallel to the coast) over a distance of the order of 200 km. Further away from the coast, the effects of the temperature contrast across the coast will hardly be noticeable. However, since ω is actually not very different from F, sea breeze effects may possibly be noticed in the form of inertia-buoyancy waves over much larger distances, certainly at lower latitudes. In fact, at a critical latitude, ϕ, where $\omega = F$ (if $F = f$ this is $\phi \approx 30°$), the character of the solution to (5.11) changes drastically. According to eq. (5.11) no steady sea breeze is possible when $|\phi| < 30°$. The potential energy introduced into the atmosphere by the diurnal heating is dispersed by buoyancy-inertia waves.

Effects of friction. Although the "sea breeze" is sometimes observed as a "wave", especially in Australia [Clark 1989], steady sea breezes are certainly observed in the tropics [Arakawa 1969, Schwerdtfeiger 1976, Lloyd 1990]. The effect of friction can explain this discrepancy with inviscid theory [e.g., Walsh 1974, Dalu and Pielke 1989]. With eddy diffusion of momentum and heat included in the equations of motion and potential temperature, Emanuel [1979, 1983c] derived the following expression for the radius of deformation:

$$\lambda = 2\pi\sqrt{\mathrm{Pr}}\,NH/F^2(1 + \mathrm{Ta}^{-1})\,, \tag{5.16}$$

where

$$\mathrm{Ta} \equiv H^4F^2/\pi^4\nu^2\,, \tag{5.17}$$

is the so-called *Taylor number* and Pr is the Prandtl number defined in (4.44). This suggests that the condition for the oscillatory solution becomes

$$\omega^2 > F^2 + \pi^4 \nu^2 / H^4 . \tag{5.18}$$

With $\nu \approx 10\,\mathrm{m^2/s}$ and $H \approx 1000\,\mathrm{m}$, the second term on the rhs of (5.18) is of order of magnitude of $10^{-8}\,\mathrm{s^{-1}}$. Therefore, according to (5.18) a steady sea breeze is possible at all latitudes, even at the equator, where $F = 0$.

The above linear theory of the land and sea breeze ignores several important dynamical and thermodynamical effects, which are usually important in reality. One of these effects is the interaction with the large-scale flow perpendicular to the coast. This interaction strongly determines the onset of the sea breeze and the formation of the sea breeze front. Another effect which is treated very crudely here is the heat transfer from the earth's surface to the atmosphere. Furthermore, we have said nothing about the influence of the form of the coastline and the orography. For this and many other, especially observational, details of the sea breeze, Atkinson's [1981] book should be consulted.

5.3. The meso-scale as a transition regime between dynamical regimes

In this section we will try to define the meso-scale on the basis of what we have learnt in the previous two sections. We have seen that the response of the stable atmosphere to forcing depends critically on the duration or frequency as well as on the length scale of the forcing.

First let us look again at the dynamics in terms of the horizontal scale relative to the Rossby radius of deformation, λ, and the depth of the circulation in question. Following Ooyama [1982], we can distinguish three dynamical regimes: a balanced regime, an unbalanced regime, and a transition regime. Systems which fall into the *balanced regime*, have horizontal dimensions much greater than λ. If the forcing is not applied too abruptly, the response to forcing in this regime is non-oscillatory and relatively weak (see fig. 5.3c). In other words, external forcing does not greatly affect the structure of balanced systems. These systems are said to be "dynamically large" [Frank 1983]. At the other extreme, we encounter the *unbalanced regime* associated with "dynamically small" motions resulting from instabilities with horizontal scales of the order of H or smaller. Generally speaking, these circulations are not in hydrostatic balance, and may even be the result of hydrostatic instability, in which case the theory of geostrophic adjustment, discussed in sections 5.1 and 5.2, is not applicable. Furthermore, the Lagrangian time scale and the coherence time scale, T, of these circulations (defined in chapter 2) are so small that inertial forces, associated with background rotation, cannot exert a systematic and lasting influence.

In between the balanced regime and the unbalanced regime, we have a *transition regime*, which can be identified as the *meso-scale*. Systems falling into this regime have Lagrangian time scales large enough to allow for the effects due to inertial forces, and length scales small enough to be significantly affected by external forcing. In this regime the period or frequency of the forcing critically determines the character of the response or the type of motion system which develops. If the forcing, ω, is smaller than F (slow forcing), a meso-scale system will adjust to, or remain in approximate geostrophic and hydrostatic balance (provided, of course, N^2 is positive). This will, however, not be the case if $\omega > F$.

In an atmosphere which is basically at rest, the inertial period $2\pi/F$ varies from about 69 h at 10° latitude (and more at even lower latitudes) to 15.6 h at 50° latitude and nearly 12 h at the poles. The

geostrophic adjustment process, therefore, takes nearly three days near the intertropical convergence zone (at about 10° latitude). Cloud clusters moving along this zone, which function as meso-scale heat sources, would have to persist for more than three days before a balanced flow would emerge. Very few cloud clusters persist as recognizable, reasonably steady entities for longer than three days [Chang 1970]. In the light of these facts it is evident that a balanced system such as a tropical cyclone will not emerge spontaneously out of every cloud cluster in the tropics.

The dynamics of the atmosphere can be represented in fig. 5.4 as a horizontal line indicating the dynamical regimes as function of wavelength for a given value of the Rossby radius of deformation. Clearly the meso-scale range of scales decreases as λ decreases. When λ approaches H, the meso-scale vanishes and so does the scale separation in space between the balanced regime and the unbalanced regime. This may in fact occur in the core of a tropical cyclone. For example, measurements in the lower part of the core of hurricane Gloria (1985) yielded a value for the vorticity of $10^{-2}\,s^{-1}$ [Franklin et al. 1988]. The local Rossby radius inside such a cyclone is in the order of 10 km. Therefore, latent heat release inside an individual cumulonimbus cloud functions as a dynamically large perturbation to the balanced flow associated with the cyclone.

At the same time the inertial period, the time needed for adjustment to geostrophic balance (although in this case it is actually gradient wind adjustment, i.e. the centrifugal term is also involved), approaches the time scale needed for adjustment to hydrostatic balance (F approaches N). The implications of these facts can be inferred from eq. (5.10). With (5.12), this equation can be written as

$$d^2\psi_0/dy^2 - [(F^2 - \omega^2)/(N^2 - \omega^2)](\pi^2/H^2)\psi_0 = \{\text{source}\}\,. \tag{5.19}$$

The term on the rhs of (5.19) represents the diabatic heating term. Roughly speaking, this equation describes the radial circulation forced by diabatic heating in a tropical cyclone in which curvature effects

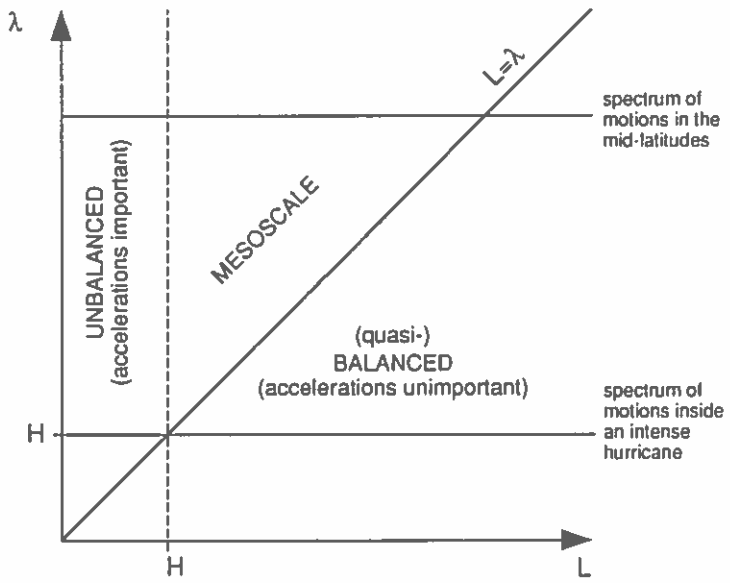

Fig. 5.4. Characteristics of the motion as a function of the horizontal wavelength, L, and the local Rossby radius of deformation, λ [based on Ooyama 1982]. H is the depth of the circulation.

are neglected. The coordinate, y, must then be interpreted as the radial coordinate (see section 5.5). The solution of (5.19) is hyperbolic, i.e. oscillatory, if the frequency of the diabatic heating ω (see eq. 5.9) lies in between the buoyancy and the inertial frequencies. Therefore, the chance of buoyancy-inertia wave excitation due to diabatic heating becomes smaller as the gap between these two frequencies narrows. Ultimately, the reaction is practically elliptic, that is, confined to the neighbourhood of the forcing. It is very probable that the impossibility of propagating buoyancy-inertia wave excitation in a broad band of forcing frequencies is advantageous for the growth of the balanced cyclone. The exact character of the response to forcing in these circumstances cannot be deduced from these simple arguments and equations. In the extreme case that $F > N$, even an individual cumulus cloud or simple buoyancy oscillation in the vertical falls into the balanced regime. The behaviour of buoyancy-inertia waves in these rather bizarre circumstances is not very well understood. It is complicated by the fact that the local inertial frequency varies by several orders of magnitude over radial distances of the order of 100 km (for more details see [Willoughby 1977, 1978, 1988, Willoughby et al. 1984] and sections 5.5 and 6.7).

5.4. *Unbalanced flow*

Meso-scale gravity-inertia waves. Basically, there are two types of meso-scale circulation: (a) unbalanced (unstable or oscillatory) circulations in which parcel accelerations are of crucial importance, and (b) balanced (relatively steady) circulations in which parcel accelerations are negligible. Sections 5.4 and 5.5 of this chapter on adjustment will be devoted to showing some examples of these circulation types.

In the present section we will pay attention to the first category, i.e. the unbalanced systems, which, in view of the mathematics, could also appropriately be called "hyperbolic systems". The most obvious example of this type of system is a gravity-inertia wave. Uccellini and Koch [1987] have presented an overview of thirteen case studies revealing the existence in the atmosphere of gravity-inertia waves, taking the form of a singular wave of depression or a wave packet (a series of progressive disturbances). The wave periods ranged from 1 to 4 h and the observed horizontal wavelengths were 70–500 kms. The perturbation pressure amplitudes measured at the earth's surface associated with these waves were 0.2–7 hPa. The waves had a relatively long duration (3–16 wave periods) and affected very large areas (10^4–10^6 km^2). Uccellini and Koch [1987] concluded that the generation of these waves in most cases must be related to a *jet streak* (speed maximum) in the jetstream with strong vertical and horizontal wind-shear. According to these authors, convection and topographical forcing did not seem to be a likely source of these waves.

There are, however, a few conceptual problems in the theoretical interpretation of these waves. It is not at all clear whether these waves are similar to interfacial (surface) waves, as discussed in section 5.1, or more like buoyancy waves, as discussed in section 4.1.2. Because of the large wavelength, the complete stability equation (4.14) for gravity waves in the presence of vertical wind-shear should be applied (i.e. the shallow Boussinesq approximation is not applicable). This yields a very complicated eigenvalue problem. The factor, m^2, in (4.14) depends on so many parameters (e.g., u_0, Du_0, D^2u_0, θ_0, $D\theta_0$, $D^2\theta_0$), which all depend on z, that there seems no hope for a general solution to this equation. Theoretical studies have been concerned almost exclusively with the much more simple Taylor–Goldstein equation (4.20) [see Drazin and Reid 1982, Einaudi et al. 1978]. Several investigators [e.g., Lalas and Einaudi 1976] have computed the stability properties of certain large-scale flows, such as jetstreams, with the help of a relatively complete stability equation, including the inertial effect of

vertical density variation. But, because a strong inversion was not present in their specific reference state, the latter effect was of course unimportant. Nevertheless, according to Uccellini and Koch [1987], the general presence of an inversion below 2 km height suggested that this feature was needed for the maintenance of the waves. For waves with wavelengths of several hundreds of kilometres the Coriolis force will also be important. A further question is whether the waves discussed by Uccellini and Koch [1987] are the product of an instability of a specific large-scale balanced state, or the transient response in a stable atmosphere to certain relatively rapid changes in the large-scale state. Due to the difficulty of defining a large-scale steady state, it is very difficult, if not impossible, to rigorously separate these two processes. So far there have been no reports of attempts to make numerical simulations of these large-scale gravity waves and their generation (at least to the author's knowledge). Thus, we still seem to be very unacquainted with large-scale transient gravity waves. More about this subject will be said in section 6.5 on mountain waves.

Another example of an unbalanced circulation system is the so-called morning glory, the name given to the spectacular low roll clouds that occur early in the morning, most frequently towards the end of the dry season, in the southern part of the Gulf of Carpentaria region of northern Australia [Smith 1988] (see Simpson [1987] for some nice photographs). They seem to be associated with solitary wave disturbances at the leading edge of an undular bore (a bore consisting of a series of smooth waves at the leading edge) that propagates on a low-level maritime stable layer at a speed of about 10 m s^{-1} [Christie 1989] (see figure 5.5). Morning glory-like phenomena have also been observed in Oklahoma [Haase and Smith 1984] and in Germany [Haase 1991]. Crook and Miller [1985] and Rottman and Simpson [1989] have suggested that the morning glory is generated by some type of gravity current moving into an existing inversion or stable layer. The gravity current can be characterized as a current of relatively

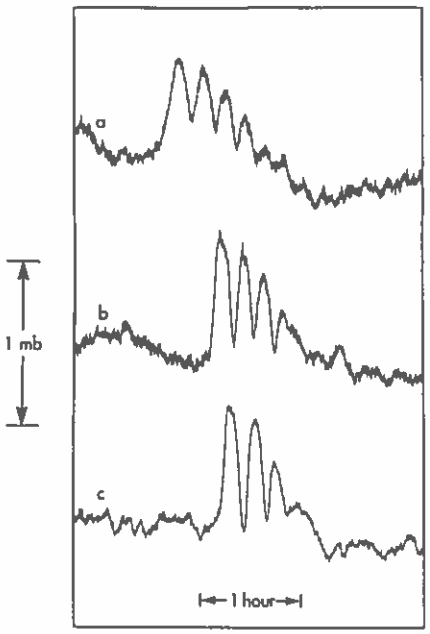

Fig. 5.5. Surface micropressure records corresponding to amplitude-ordered morning-glory solitary-wave disturbances at Edward River on the eastern side of the Gulf of Carpentaria. Onset times, source azimuths and propagation speeds are as follows: (a) 2152 EST 15 September 1983, 28°, 5.9 m s^{-1} (b) 2120 EST 18 September 1983, 31°, 6.3 m s^{-1}; (c) 2117 EST 24 September 1983, 35°, 7.2 m s^{-1} (1 mb = 1 hPa) [Christie 1989].

heavy fluid intruding into a layer with a lower mean density under the influence of gravity. The force driving the current is, of course, the horizontal pressure gradient, just as in the case of a surface gravity wave. However, the gravity current can be distinguished from the surface gravity wave by the fact that it mainly transports mass, while the gravity wave mainly transports energy. Sea breeze fronts [e.g., Kraus et al. 1990] and cold thunderstorm outflows [e.g., Kessler 1985] are typical examples of atmospheric gravity currents. Rottman and Simpson [1988] conducted laboratory experiments to show how a gravity current can generate a bore in the stable layer ahead. The experiments compared reasonably well with observations of atmospheric bores generated by thunderstorm outflows and sea breeze fronts. It must be stressed that the scale of these phenomena is much smaller than that of the wave phenomena cited by Uccellini and Koch [1987].

Other examples of atmospheric waves are mountain lee-waves and convection waves. The names given to these waves obviously refer to the generating mechanism. We will defer the discussion of lee-waves to section 6.5. Convection waves [e.g., Erickson and Whitney 1973] are excited by convection currents bumping into a stable layer aloft. They were discovered by glider pilots as so-called thermal waves. With the help of aircraft observations Keuttner et al. [1987] found these waves to have the following characteristics: horizontal wavelength: 5–15 km; vertical motion amplitude: 1–3 $m\,s^{-1}$; vertical wind-shear: 0.003–0.01 s^{-1}; vertical extent of the wave system: >9 km. Therefore, these waves are in effect buoyancy waves, possibly modified by background wind-shear [see also Bradbury 1990].

Convection. The meso-scale gravity waves, the morning glory, transient mountain lee-waves and convection waves are all unbalanced oscillatory types of motion occurring in a stable background atmosphere. They owe their existence to some kind of short scale (in time and space) external forcing. Another class of motion systems occurs when the background state is unstable. Unbalanced motion systems may then arise spontaneously. For example, convection currents are the result of an unstable balance of forces in the vertical direction. The deviations from this balance are governed by eq. (3.19a), which in the absence of the Coriolis force and friction can be written as

$$w\,\mathrm{d}w/\mathrm{d}z = -\theta_0\,\partial\Pi'/\partial z + Bg\,. \tag{5.20}$$

Assuming that the pressure in a parcel with buoyancy, B, adjusts to the environmental pressure at all levels (i.e. $\Pi' = 0$), it can easily be deduced that a parcel starting its ascent at a level z_1 with vertical velocity w_1, will have a velocity w_2 at a height z_2 given by

$$w_2^2 = w_1^2 + 2 \times \mathrm{CAPE}\,, \tag{5.21}$$

where the convective available potential energy (CAPE) is defined by

$$\mathrm{CAPE} \equiv g \int_{z_1}^{z_2} B\,\mathrm{d}z\,. \tag{5.22}$$

The magnitude of CAPE can be as large as 4500 $m^2\,s^{-2}$, but in deep convective conditions it generally ranges between 1500 and 2500 $m^2\,s^{-2}$ [Weisman and Klemp 1986]. This includes the effect on B of the release of latent heat due to condensation or freezing (see section 6.1). A value of 2500 $m^2\,s^{-2}$ would, according to (5.21), translate to a maximum possible updraught of about 70 $m\,s^{-1}$ if $w_1 = 0$. Such strong

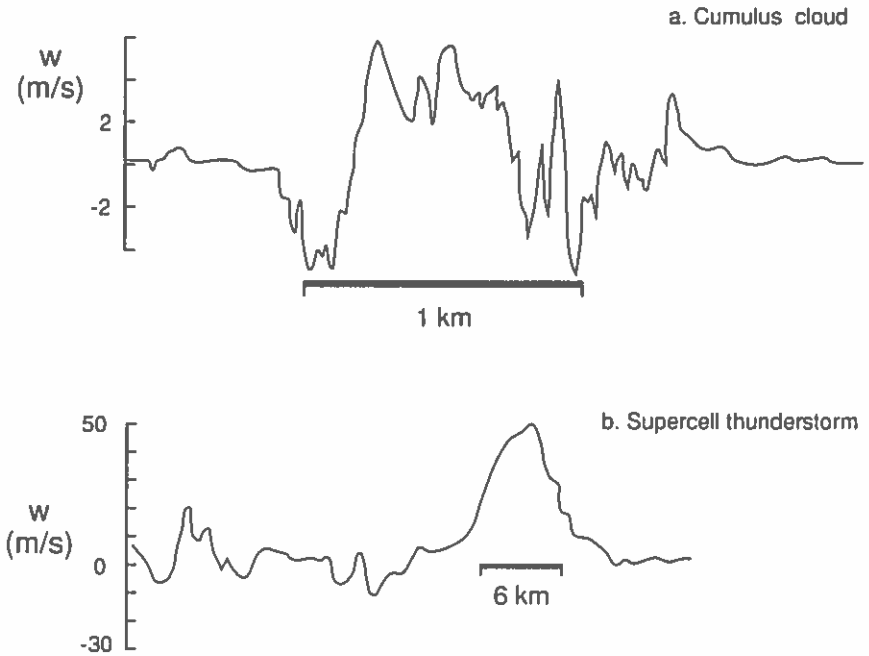

Fig. 5.6. The vertical motion measured from an aeroplane in (a) a fair-weather cumulus cloud, 1.5 km deep, over a track about 250 m below the cloud top [from Telford and Warner 1962], and (b) a supercell thunderstorm over a track about 6000 m above the ground [Musil et al. 1986].

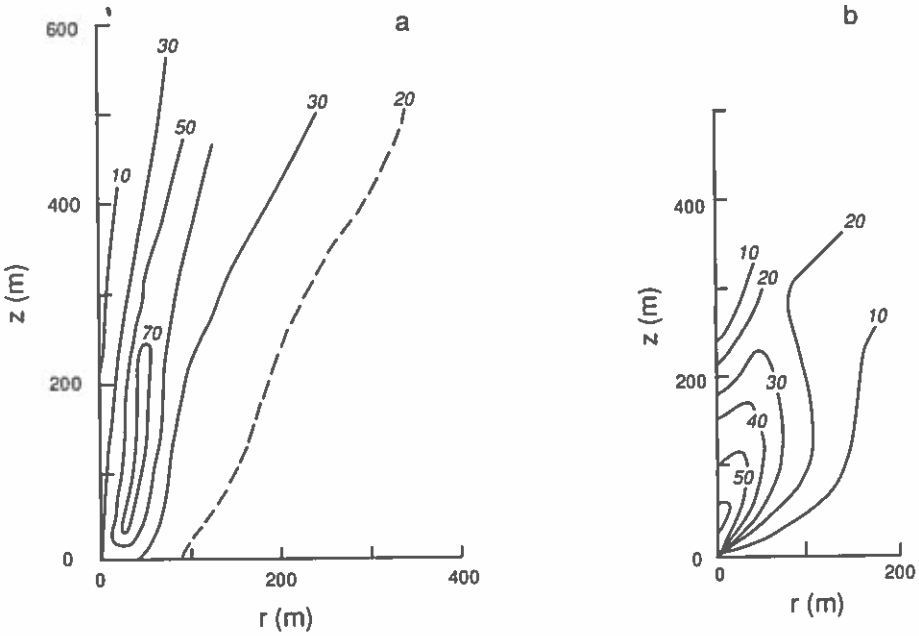

Fig. 5.7. Hoeker's [1960] photogrammetric analysis of the 1975 Dallas tornado showing (a) tangential and (b) vertical velocities in $m\,s^{-1}$ [from Davies-Jones 1985].

updraughts are never observed because of friction and water loading (see section 6.2). However, sometimes updraught intensities in thunderstorms come surprisingly close to this value, as can be seen in fig. 5.6b [Browning 1986]. Maximum horizontal wind speeds in hurricanes are of the same order of magnitude! Updraughts in ordinary non-precipitating cumulus clouds are usually of the order of $3\ \mathrm{m\ s^{-1}}$ (see fig. 5.6a). Updraughts of the order of $50\ \mathrm{m\ s^{-1}}$ are also observed at heights of about 100 m in tornadoes (see fig. 5.7). The accelerations associated with these intense updraughts can be deduced from the lhs of (5.20). For the cumulus cloud, the thunderstorm cloud and the tornado depicted in fig. 5.6a, fig. 5.6b and fig. 5.7, respectively, we have: cumulus cloud: $\mathrm{d}w/\mathrm{d}t \approx 0.01\ \mathrm{m\ s^{-2}} \ll g$; thunderstorm: $\mathrm{d}w/\mathrm{d}t \approx 0.25\ \mathrm{m\ s^{-2}} < g$; tornado: $\mathrm{d}w/\mathrm{d}t \approx 25\ \mathrm{m\ s^{-2}} > g$. Since pressure perturbations (p' or Π') in cumulus clouds are small [LeMone et al. 1988a,b] (see section 4.1.4), the vertical accelerations found in these clouds are solely due to the buoyancy force. In fact, a rather small potential temperature perturbation, θ', of about 0.3 K is needed to get a vertical acceleration of $0.01\ \mathrm{m\ s^{-2}}$. If accelerations in thunderstorms and tornadoes were only due to buoyancy, this would require a potential temperature perturbation, θ', of about 7.5 K for the thunderstorm cloud and about 750 K (!) for the tornado. Excess potential temperatures in clouds much greater than 10 K are hardly ever observed. Therefore, the vertical acceleration in a tornado must be due principally to a vertical pressure gradient (see section 6.3).

5.5. *Balanced flow*

We have seen that forced and self-excited unbalanced flows are characterized by relatively large accelerations. In the case of forced flows, these accelerations are due to the fact that the forcing is abrupt relative to the time required for readjustment to balance (see fig. 5.3a,b). If, on the other hand, the forcing is relatively slow, the structure can adjust continuously to a new state of balance. The result is a system which evolves through a succession of balanced states without experiencing oscillations (see fig. 5.3c). We will see in this section that many theories of slowly evolving systems in which accelerations are negligible assume that the forcing is felt instantly at its full strength in all parts of space. This implies that the system remains in approximate balance at all times. Due to this, these systems are frequently described by differential equations of the elliptic type. Therefore, in view of the mathematics, we could call these weather systems elliptic systems.

Forced secondary circulations in balanced baroclinic zones (fronts). In order to obtain more insight into the dynamics of forced balanced flows, let us return to a situation similar to that depicted in fig. 4.14. We will follow the pioneering theoretical studies of fronts by Sawyer [1956] and Eliassen [1959, 1962]. Sawyer investigated the situation shown in fig. 5.8. On a straight geostrophic current, $\bar{U}(y, z, t)$, similar to the basic current $u_0(y, z)$ investigated in section (4.2), he superposed a geostrophic (balanced) deformation field (following an idea of Bergeron [1928]) and an ageostrophic (unbalanced) symmetric (x-independent) circulation denoted by a subscript a. Thus, the velocity field is given by the following expression:

$$\boldsymbol{v} = \{\bar{U}(y, z, t) + Ax, -Ay + v_a(y, z, t), w_a(y, z, t)\}\ . \tag{5.23}$$

Note that $\bar{U}$ depends on time. The deformation field is represented by the terms containing the constant factor A. It can easily be seen that this deformation field is non-divergent and irrotational. The along-front velocity conforms with geostrophy at all times. This approximation is now called the

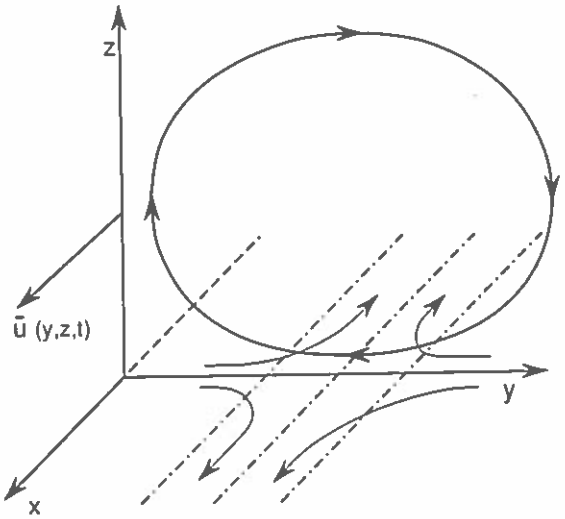

Fig. 5.8. The secondary (vertical) circulation forced by the deformation field in a frontal region. The dash-dotted lines represent isentropes in the plane $z = 0$. Also shown in this plane is the deformation field (the arrows). $\bar{U}$ is the geostrophic flow (see the text).

geostrophic momentum approximation or *semi-geostrophic approximation* [Eliassen 1948, Hoskins 1975]. It is valid as long as the term $v\,\partial v/\partial y$ and $w\,\partial v/\partial z$ can be neglected compared to the pressure gradient term and the Coriolis term in the y-component of the momentum equation.

The approximate equations of motion (neglecting friction) and the temperature equation are, respectively (see eqs. 3.17, 3.19),

$$\mathrm{d}u/\mathrm{d}t = -\theta_\mathrm{m}\,\partial \Pi'/\partial x + fv\,, \tag{5.24a}$$

$$\mathrm{d}v/\mathrm{d}t = -\theta_\mathrm{m}\,\partial \Pi'/\partial y - fu\,, \tag{5.24b}$$

$$\mathrm{d}w/\mathrm{d}t = -\theta_\mathrm{m}\,\partial \Pi'/\partial z + (\theta'/\theta_\mathrm{m})g\,, \tag{5.24c}$$

$$\mathrm{d}\theta'/\mathrm{d}t = (1/\Pi_\mathrm{m})\,\mathrm{d}Q/\mathrm{d}t\,. \tag{5.24d}$$

Here we have made the same approximations as in section 4.2. That is, we have again split the potential temperature and the Exner function into a constant mean value, denoted by the subscript m and a perturbation, denoted by a prime (the Boussinesq approximation). We have neglected the potential temperature perturbation, θ', in the pressure gradient terms and we have assumed that $\Pi \approx \Pi_\mathrm{m}$ in the potential temperature equation. Sawyer assumed that the temperature field remains independent of the along-front coordinate, x. The geostrophic momentum approximation implies that

$$\theta_\mathrm{m}\,\partial \Pi'/\partial y + f\bar{U} + fAx = 0\,. \tag{5.25}$$

The deformation field is also geostrophic. Therefore,

$$\theta_\mathrm{m}\,\partial \Pi'/\partial x + fAy = 0\,. \tag{5.26}$$

In addition to this Sawyer assumed that the flow remains in hydrostatic balance. In view of (5.24c) this leads to

$$\theta_m \, \partial \Pi' / \partial z = (\theta' / \theta_m) g \, . \tag{5.27}$$

Relations (5.25) and (5.27) imply thermal wind balance, i.e.

$$f \, \partial \bar{M} / \partial z + (g / \theta_m) \, \partial \theta' / \partial y = 0 \, , \tag{5.28}$$

where the linear absolute momentum associated with the current $\bar{U}$ is defined as

$$\bar{M} = \bar{U} - fy \, . \tag{5.29}$$

The equation for $\bar{M}$ can be derived from (5.24a) and (5.26). The result is

$$\partial \bar{M} / \partial t + v_a \, \partial \bar{M} / \partial y + w_a \, \partial \bar{M} / \partial z = - A(\bar{U} + Ax) + Ay \, \partial \bar{U} / \partial y \, . \tag{5.30}$$

It can easily be shown that the second term on the right-hand side of (5.30) functions as a source of total absolute linear momentum. The cross-frontal geostrophic velocity field implies an along-front pressure gradient which acts as a source of momentum. Differentiating (5.28) locally with respect to time and using eq. (5.30) and eq. (5.24d) (in which we neglect the along-front temperature gradient), we obtain an equation for the cross frontal circulation as follows:

$$F^2 \frac{\partial^2 \psi}{\partial z^2} - 2S^2 \frac{\partial^2 \psi}{\partial x \, \partial z} + N^2 \frac{\partial^2 \psi}{\partial y^2} = - \frac{2Ag}{\theta_m} \frac{\partial \theta'}{\partial y} - \frac{g}{\Pi_m \theta_m} \frac{\partial}{\partial y} \left(\frac{\mathrm{d}Q}{\mathrm{d}t} \right) , \tag{5.31}$$

where

$$F^2 = -f \, \partial \bar{M} / \partial y \, , \quad S^2 = (g / \theta_m) \, \partial \theta' / \partial y \, , \quad N^2 = (g / \theta_m) \, \partial \theta' / \partial z \tag{5.32}$$

(compare these definitions with (4.60–4.62)). The stream function ψ is defined in terms of v_a and w_a by equations analogous to (4.57). This equation describes the secondary circulation which is needed to maintain a current in geostrophic and hydrostatic balance in the presence of heat sources and sources of momentum due to confluent or diffluent advection. The equation is frequently referred to as the *Eliassen–Sawyer equation*. Equation (5.31) together with appropriate boundary conditions (e.g. $\psi = 0$ on a closed curve surrounding the frontal zone) has a unique solution if it is of the elliptic type, i.e. if the quantity, $q = F^2 N^2 - S^4 > 0$. Note that this criterion coincides with the second criterion in (4.70) for the stability of a baroclinic current with respect to symmetric disturbances. The above criterion is nearly always satisfied in the atmosphere. This ensures that transverse circulations will only arise in response to the forcing terms on the right-hand side of eq. (5.31). We may then say that we are dealing with a balanced weather system, which is continuously disturbed by sources of momentum and heat. The geostrophic momentum approximation is valid as long as the forcing is not too abrupt.

Let us, for the moment, neglect the effect of diabatic heating and investigate the effect of the so-called geostrophic forcing due to the geostrophic deformation field. If $A > 0$, the deformation field has the effect of intensifying the horizontal temperature contrast across the front. With $\partial \theta / \partial y < 0$ (see

fig. 5.8), the forcing term on the right-hand side of (5.31) becomes positive. It can be shown [e.g., Eliassen 1962, 1990] that the solution of (5.31) with a positive term on the right-hand side gives an ageostrophic circulation which is thermodynamically direct, i.e. with potentially warm air rising and potentially cold air sinking. This circulation is drawn in fig. 5.9. Obviously, it will tend to weaken the front (i.e. have a frontolytic effect). However, in areas (indicated in fig. 5.9 by the letters A and B) where the forced circulation induces convergence, gradients of θ and M will tend to increase. At the ground a front-parallel jet will thus be formed towards the warm side of the front, whereas higher up in the troposphere a jet will be formed on the cold side of the front. The gradients associated with these jets will tend to become stronger as time progresses [e.g., Garner 1989] until a balanced state is reached in which frontolysis due to turbulent diffusion counteracts frontogenesis due to large scale deformation [e.g., Williams 1974].

Beside confluent motion and convergence there are ot course many other processes which may contribute to frontogenesis (for a recent paper on this subject see, e.g., [Thorpe 1990]). The above theory is relatively crude due to the restriction to two-dimensions. Hoskins and Draghici [1977] and recently Davies-Jones [1991] have extended it to three dimensions. We will see in section 6.4 that the situation becomes quite complicated when the temperature varies across the front, or when the front is not straight. We will not go into further details here. There is a huge body of literature on the subject [e.g., Hoskins 1982, Keyser and Shapiro 1986, Newton and Holopainen 1990].

Tropical cyclones. Several years prior to the investigation of fronts by Sawyer, Eliassen [1952] had already derived and analysed an equation similar to (5.31) for the steady transverse (radial) circulation (also called secondary circulation) in a balanced circular symmetric vortex such as a tropical cyclone. Figure 5.10 shows a cross section running through the axis of a typical tropical cyclone. The secondary circulation extends to a radius of about 900 km, although it is by far the most intense for $r < 150$ km, where the greatest radial pressure gradients are observed. Not shown is the much weaker but very important thermally indirect branch of the secondary circulation inside the eye. Frequently, the high cloud shield does not extend as far out as shown in this figure. The secondary circulation is not self-excited due to some kind of hydrodynamic instability, but is forced by heat and momentum sources [Shapiro and Willoughby 1982] in the same way as the cross-frontal circulation described earlier in this section. The forcing upsets the existing state of balance, i.e. gradient wind and hydrostatic balance, which may be expressed in cylindrical coordinates as

$$u^2/r + fu = \theta\, \partial \Pi / \partial r\,, \tag{5.33}$$

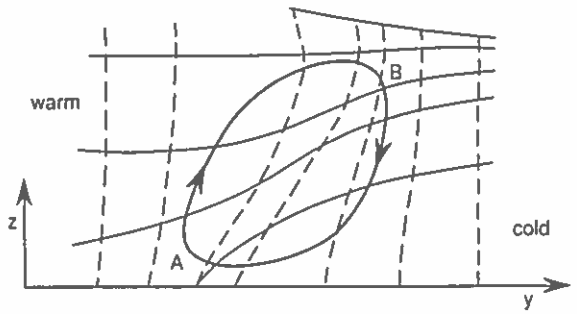

Fig. 5.9. The potential temperature distribution (isentropes: solid lines) and absolute momentum distribution (dashed lines) across a frontal region in the presence of a geostrophically forced secondary circulation [based on figure 9.3 in Eliassen 1990].

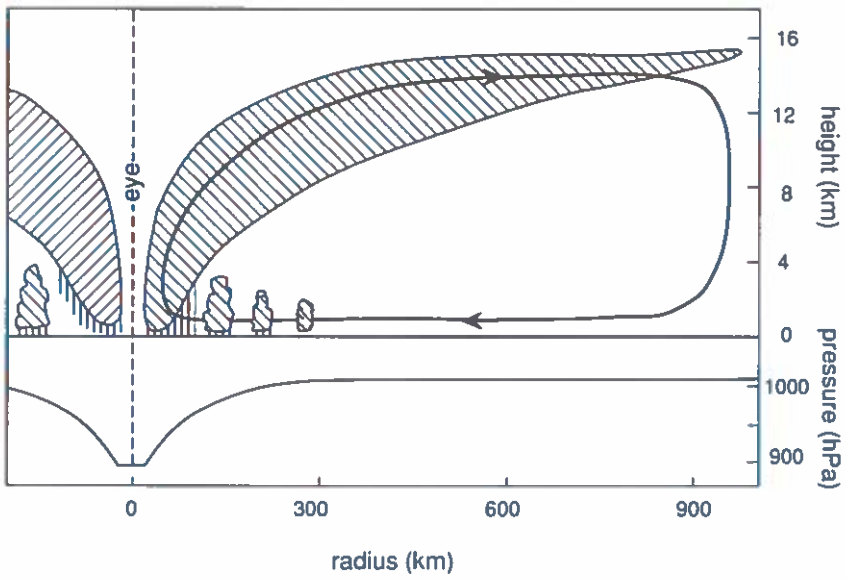

Fig. 5.10. Secondary circulation and surface pressure in a hurricane [based on a schematic picture in Eliassen and Kleinschmidt 1957].

$$\partial \Pi / \partial z = -g/\theta \,, \tag{5.34}$$

where u is now the tangential component of the velocity. The secondary circulation is required to maintain these equilibria. Note that there is an inconsistency here because a radial circulation is incompatible with exact gradient wind balance. If $v \neq 0$ and $w \neq 0$, two extra terms, $-v\,\partial v/\partial r$ and $-w\,\partial v/\partial z$, are required on the lhs of (5.33). If v and w are small, however, these terms can be shown to be of very little importance in the balance. This is the gradient wind balance version of the geostrophic momentum approximation.

The gradient wind relation (5.33) is observed to be a good representation of the radial balance of forces in relatively intense hurricanes [Willoughby 1979, 1990b, Sheets 1982, Jorgensen 1984]. As an example, fig. 5.11 shows a comparison of the observed azimuthal average tangential wind and the gradient wind computed from the observed azimuthal average isobaric height at flight level in hurricane Alicia (1983) (see also figs. 3.2 and 5.12). The validity of gradient wind balance at this level is impressive*).

The validity of hydrostatic balance in a hurricane, on the other side, is not a trivial matter. It is, nevertheless, an important assumption in the theory of tropical cyclone growth because it allows for a clear distinction between the cyclone mode of motion and cumulus convection (see section 6.7). The clouds observed in the eye-wall of a tropical cyclone have the same dimensions as thunderstorm clouds and produce enormous amounts of rain. Frank [1977] estimated that the average rainfall within the inner 200 km radius of a typhoon (the name given to tropical cyclones occurring around the Philippines and Japan) averages about 100 mm per day. Nevertheless, vertical velocities observed in these clouds are very weak compared to those observed in a typical thunderstorm cloud (see figs. 5.6 and 5.12). The

*) There is some controversy on the degree of balance in a hurricane and its implications [see Gray 1991, Willoughby 1991]. Here we only intend to show, following Willoughby [1990b, 1991], that gradient wind balance is a reasonable assumption in a theory of tropical cyclone dynamics.

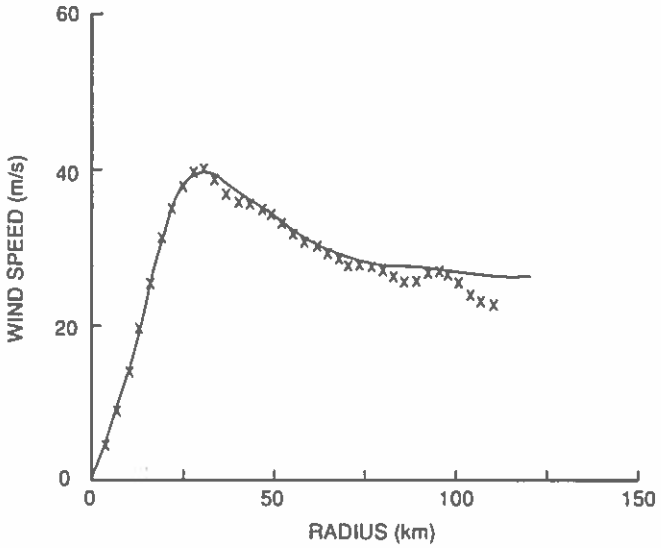

Fig. 5.11. The time-mean axisymmetric swirling (tangential) wind (solid line) and the mean gradient wind (crosses) at the 850 hPa pressure level measured in hurricane Alicia in the time interval 11 : 59 to 18 : 18 UT, 17 August 1983 [from Willoughby 1990b].

most intense updraughts ($w \approx 10$ m/s) are found at altitudes above 10 km coinciding with the area where the highest outflow velocities ($v \approx 6$–9 m/s) are observed [Marks and Houze 1987]. These high velocities are indicative of small-scale hydrostatic or symmetric baroclinic instability. Elsewhere the radial and vertical velocities are usually a factor 10 smaller than the vertical velocities in clouds with similar dimensions in thunderstorms. This suggests that the clouds in an intense tropical cyclone are not principally the result of hydrostatic instability (or CAPE; see eq. 5.22), but are the visual manifestation of the vertical component of the *forced secondary circulation*. We will elaborate further on the exact nature of this secondary circulation and the way in which it is forced in section 6.7. Here we only want to show that hydrostatic balance is an acceptable approximation in a theory of tropical cyclones.

The equations governing the primary (azimuthal) and secondary circulations in an axisymmetric balanced tropical cyclone are given by (5.33, 5.34), in addition to

$$\partial u/\partial t + v\,\partial u/\partial r + w\,\partial u/\partial z + v(f + u/r) = 0\,, \tag{5.35}$$

$$\partial(r\rho_0 v)/\partial r + \partial(r\rho_0 w)/\partial z = 0\,, \tag{5.36}$$

$$\partial\theta/\partial t + v\,\partial\theta/\partial r + w\,\partial\theta/\partial z = (1/\Pi)\,\mathrm{d}Q/\mathrm{d}t\,, \tag{5.37}$$

where v is the radial flow (positive outwards) and we have assumed that $\partial\rho_0/\partial z = -g\rho_0/c_0^2$ (see section 3.2, below eq. (3.24a)). From gradient wind balance (5.33) and hydrostatic balance (5.34) we can deduce that the cyclone must be in thermal wind balance according to

$$(2u/r + f)\,\partial u/\partial z = (g/\theta)\,\partial\theta/\partial r + (u/\theta)(u/r + f)\,\partial\theta/\partial z\,. \tag{5.38}$$

Because $g \gg u(u/r + f)$ and $\partial\theta/\partial r \sim \partial\theta/\partial z$ inside a tropical cyclone, the second term on the rhs can be

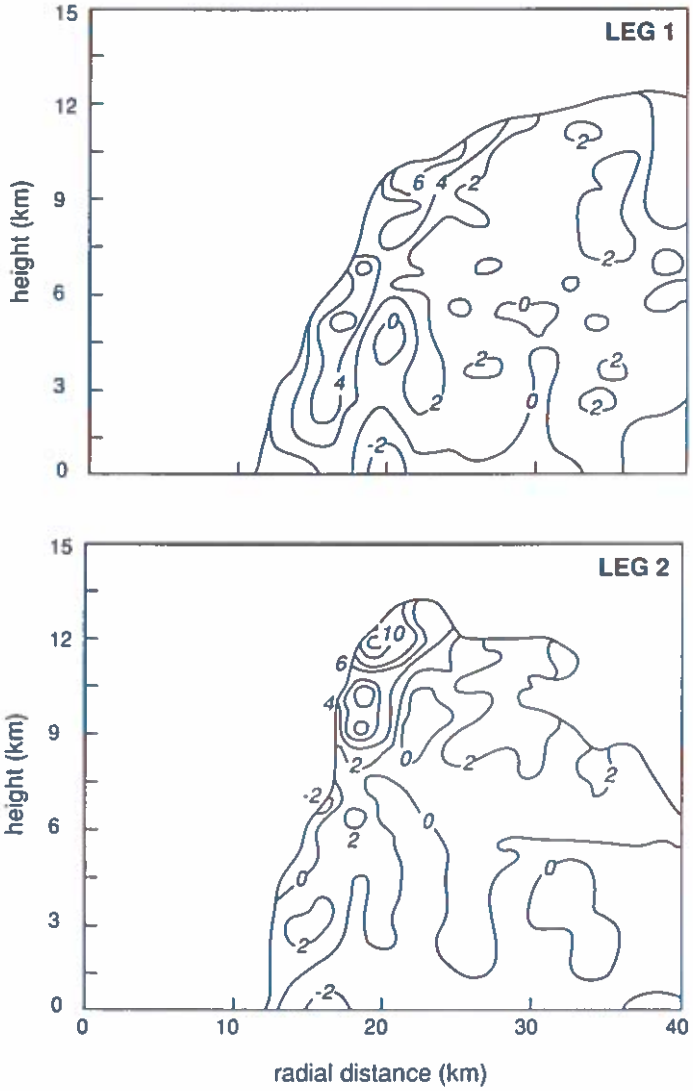

Fig. 5.12. Vertical velocity in m s^{-1} in hurricane Alicia (1983) derived from airborne Doppler radar along two radial flight legs (see fig. 3.2) through the eye. The vertical velocity cannot be measured inside the clear eye [from Marks and Houze 1987].

neglected. We see that the high temperatures in the centre of the cyclone (fig. 5.13), which make $\partial\theta/\partial r < 0$, are directly related to the *decrease* of u with height via the thermal wind relationship. The fact that this is observed in all mature tropical cyclones confirms the hypothesis that the tropical cyclone is close to hydrostatic and gradient wind balance. The decrease of the tangential wind speed with height entails a decrease of the inertial stability with height. We will see in section 6.7 that this promotes the intensification of the cyclone.

Differentiating (5.38) with respect to time and using (5.35–5.37) yields a diagnostic equation for the secondary circulation similar to the slab-symmetric case (eq. 5.31). The general form of this equation is

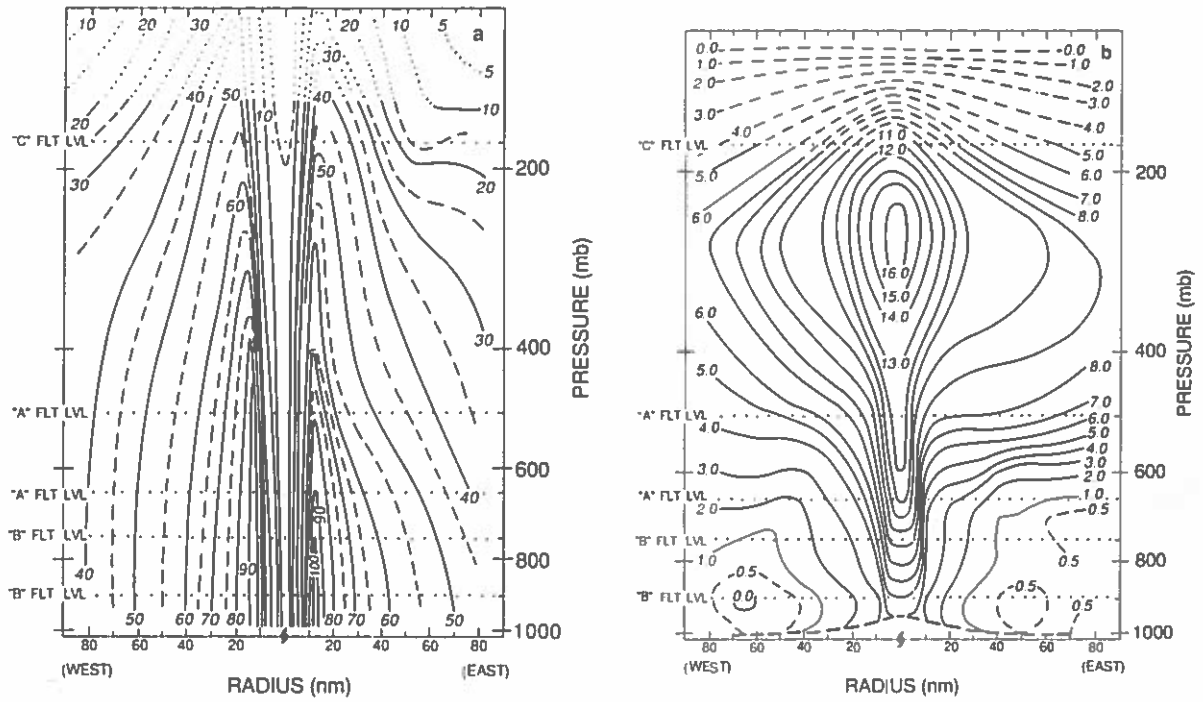

Fig. 5.13. Vertical-radial cross section of (a) azimuthal or tangential winds (in knots, 1 knot $\approx 0.5\,\mathrm{m\,s^{-1}}$) and (b) temperature anomaly (K) in hurricane Hilda (1964) [Hawkins and Rubsam 1968].

$$A\,\partial^2\psi/\partial z^2 + 2B\,\partial^2\psi/\partial r\,\partial z + C\,\partial^2\psi/\partial r^2 + D\,\partial\psi/\partial r + E\,\partial\psi/\partial z + G = 0\,, \tag{5.39}$$

where ψ is the streamfunction, defined in terms of w and v as

$$w = (1/\rho_0 r)\,\partial\psi/\partial r\,, \quad v = -(1/\rho_0 r)\,\partial\psi/\partial z \tag{5.40}$$

to satisfy (5.36). In eq. (5.39), A is related to the inertial stability of the vortex: $r^{-3}\,\partial M_a^2/\partial r = 2M_a\zeta_{abs}/r^2\ [\mathrm{s}^{-2}]$, where M_a is the angular momentum per unit mass, defined for an axisymmetric vortex as

$$M_a \equiv ur + \tfrac{1}{2}fr^2\,. \tag{5.41}$$

A is also called the "Rayleigh discriminant" (e.g., Drazin and Reid 1981]. B is related to the baroclinicity of the vortex, $\partial\theta/\partial r$, C is related to the static stability, $\partial\theta/\partial z$, and G is related to the forcing (diabatic heating). The parameters D and E are also functions of the distributions of θ and u in the cyclone.

Equation (5.39) was derived first by Eliassen [1952] with pressure as a vertical coordinate instead of z [see also Yanai 1964]. A steady solution exists only when the distributions of θ and u are such that the vortex is statically, inertially and baroclinically stable. This is the same as saying that eq. (5.39) must be elliptic [Eliassen 1952]. This is the case if $AC - B^2 > 0$ (compare this with (4.70) and (5.21)). Estoque [1962] and Rosenthal [1963] and many others subsequently attempted to find numerical solutions of

(5.39) for distribution of u and θ representative of tropical cyclones. Later this equation was used to diagnose the secondary circulation in a numerical model of a balanced axisymmetric tropical cyclone [Ooyama 1969, Sundquist 1970]. These models integrated in time the equation for the tangential velocity (5.35) and used eq. (5.39) to diagnose the secondary circulation needed to preserve balance in the presence of processes such as diabatic heating and friction. Such models are numerically very stable because they do not permit unbalanced motions such as gravity waves. In the early days of numerical modelling, this was very desirable because computer power did not allow for the high degree of resolution required to simulate gravity waves. In spite of this, the models gave a very faithful picture of the growth of a weak balanced vortex into a mature tropical cyclone, demonstrating, once again, that

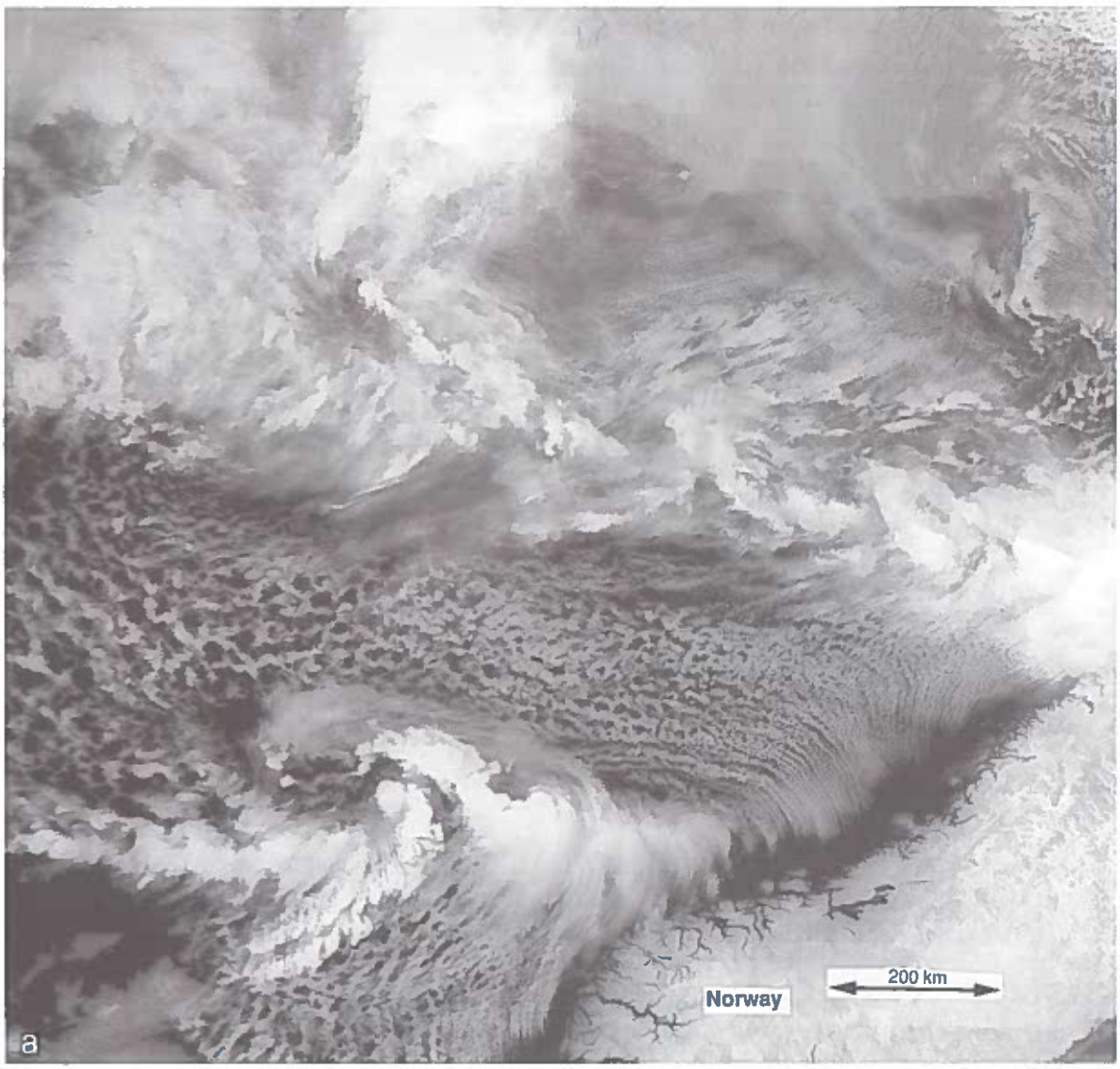

Fig. 5.14. Satellite (TIROS-N, infrared) photograph of a polar low: (a) in its formative stage over the Norwegian sea on 30 December 1978, 14 : 31 UT; (b) making landfall at the Dutch coast on 2 January 1979, 14 : 01 UT. Courtesy of the University of Dundee.

the tropical cyclone is indeed a balanced structure which evolves slowly from one balanced state to the other. Naturally, the models could not simulate the genesis of a vortex.

An example of a balanced meso-scale vortex. Another example of a balanced meso-scale weather system is the polar low [Rasmussen and Lystad 1987, Twitchell et al. 1989], which may be considered, with some reservations, as the high-latitude version of the tropical cyclone (see Emanuel and Rotunno 1989, Rasmussen 1989]. In order to facilitate a comparison between the different meso-scale circulations, we will discuss shortly a polar low occurring over the same area (The Netherlands and surroundings) as the other meso-scale circulations discussed in this review (the sea breeze and the thunderstorm; see chapter 2 and section 6.4). Figure 5.14 displays two satellite images of a polar low. The first image (fig. 5.14a) was taken on 30 December, 1978. At that time the polar low was forming over the Norwegian sea (in the lee of the Norwegian mountains) in an area of large-scale horizontal convergence (for a discussion of the rather unique large-scale weather pattern, see Kurz [1979]). Cold

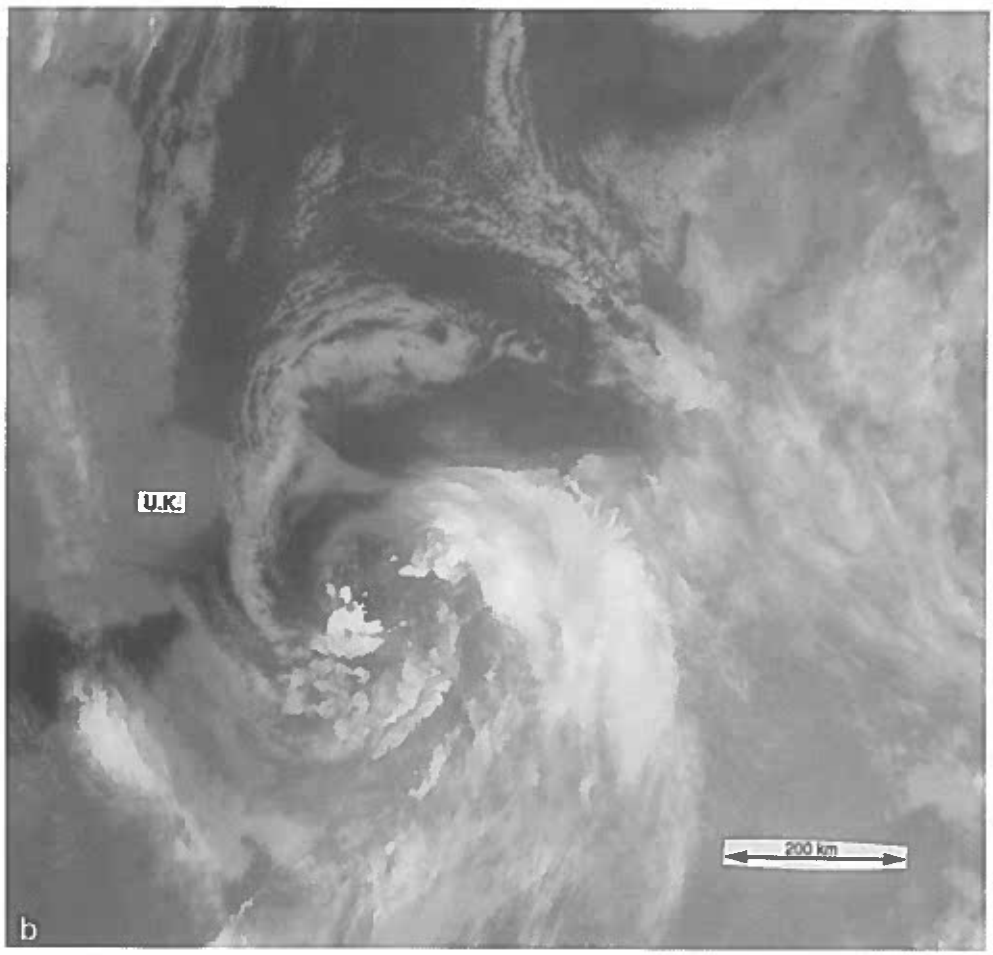

Fig. 5.14. (cont.)

continental air was flowing around the southern tip of Norway and colliding with slightly warmer air coming from the northeast. The Norwegian mountains, large-scale baroclinicity, intense sensible heating and latent heat release were probably all playing a role in the formation of the polar low. On 1 January 1979, the large-scale conditions changed and the polar low was steered into the North Sea by the large-scale flow. After travelling towards the south east, with its centre remaining about 50 to 100 km to the east of the British coast, it finally made landfall at the Dutch coast at approximately 14 UT on 2 January 1979 (see fig. 5.14b). Figure 5.15a shows a map of the weather at the surface at this time. The minimum surface pressure measured near the centre of the cyclone at 14 UT was 1007.5 hPa. Windgusts of up to 31 m s $^{-1}$ were measured along the coast to the southwest of the centre. Showers with thunder, rain, hail and snow were observed in the southwest quadrant of the cyclone, while a band of continuous snowfall was observed principally in the northeast (see fig. 5.14b). This band is a result of baroclinicity, i.e. relatively warm air is forced to glide up over the cold continental air near the earth's surface. A clear area, resembling an eye, with a diameter of about 60 km, can be observed in the centre of the cyclone. The situation at the ground four hours later is shown in fig. 5.15b. The cyclone has travelled approximately 200 km in a southeasterly direction, while the central surface pressure has risen by about

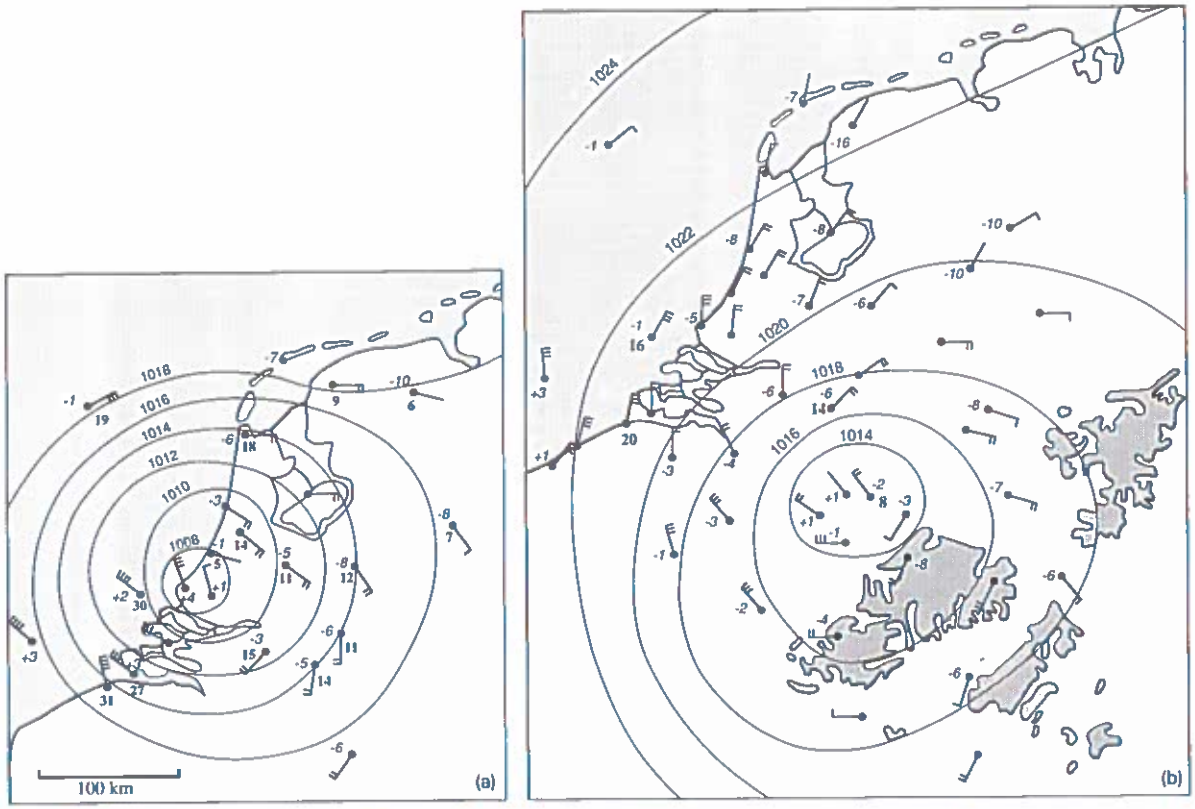

Fig. 5.15. Surface weather maps of January 2, 1979 at (a) 14 UT, and (b) 18 UT. Isobars are shown by solid lines with values indicated in hPa. A dot marks the position of a weather station as well as the end point of the wind vector. The barbs attached to the wind vector indicate the 10 min mean windspeed, ff, measured at a height of 10 m: no barb corresponds to ff < 2.5 m s $^{-1}$; one barb corresponds to 2.5 ≤ ff < 5 m s $^{-1}$ and one further barb is added for every 5 m s $^{-1}$. Numbers in bold indicate the maximum wind speed (in m s $^{-1}$) measured during the previous hour. Numbers in italics indicate the temperature at a height of 1.5 m. Dark shading in (b) indicates areas where the height of the earth's surface is greater than 400 m.

5 hPa. The system has weakened, presumably bacause it has lost its supply of energy, namely the sensible heat and the latent heat from the sea. An interesting feature is the pocket of relatively warm air in the centre of the cyclone. Note also that the horizontal dimension of this cyclone and the accompanying cloudcluster is of the same order of magnitude as the thunderstorm complex shown in figs. 2.9 and 2.11.

Fronts, tropical cyclones and polar lows are good examples of a balanced meso-scale weather system. The evolution of these systems is governed by small departures from the state of balance. These departures are the result of relatively weak forcing acting on a relatively large time-scale. Sometimes the qualifications, "semi-geostrophic" (when the geostrophic momentum approximation is made, e.g., Hoskins [1975]) or "quasi-static" [Eliassen 1948], or "quasi-hydrostatic" [Orlanski 1981], or in general, "quasi-equilibrium" [Cullen et al. 1987], are given to these circulations to emphasize the fact that the departures from balance, however small, are important to the dynamics of these circulations. In this review we will stick to the term "balanced", even though this does not necessarily mean that there is exact balance. As is also stated by Garner [1991], the term "balanced" then refers to the exclusion of gravity-inertia waves and convection from the theory.

6. Forcing

Now that we have a general understanding of the instabilities and the adjustment processes that are possible on a local scale (neglecting the sphericity of the earth) in the atmosphere, we can go into more detail on the specific way in which these instabilities and adjustment processes can be triggered or forced. Perhaps the most important forcing mechanism is diabatic heating or cooling. This may be due to condensation of water vapour or freezing of liquid water, absorption of solar radiation, emission of infrared radiation or fluxes of sensible heat from the earth's surface. Another important forcing agent is topography (such as mountains, hills, coastlines and valleys). The large-scale background flow can also act as forcing agent, especially when this flow possesses vertical wind-shear and/or acts frontogenetically.

We will start with latent heat release due to condensation. We will describe how this process affects static buoyant instability and baroclinic symmetric instability. In section 6.2 we will discuss some effects of rainwater loading and evaporation of raindrops on the dynamics of convection currents. Next, we will treat the role played by background vertical wind-shear in sustaining severe thunderstorms and also the role played by upper level jet streaks propagating along large-scale fronts in promoting these storms.

Subsequently we will turn to topography. We will discuss, relatively briefly, the dynamical effect of mountains and valleys on the flow, illustrating the confusion that still exists about the nature of gravity waves in the atmosphere. After that we will list the wide variety of ways in which friction influences meso-scale circulations. Finally, we will return to the versatile role played by diabatic heating in generating meso-scale circulations. The ideal example to illustrate the ways in which diabatic heating effects the flow in the atmosphere is the tropical cyclone. In order to explain the growth of a tropical cyclone we must address the role of diabatic heating as a source of pressure perturbations and as a source of potential vorticity, as well as a source of buoyancy.

6.1. Latent heat release and conditional instability

Cumulus convection. The effect of latent heat release due to condensation of water vapour on the flow has been investigated by a large number of authors since the American meteorologist Espy recognized is as an important form of energy in storms in the nineteenth century [Kutzbach 1979]. In this section we will discuss the role of *latent heat release as a source of buoyancy*.

Consider a saturated atmosphere in which there is rising and falling motion. Condensation and, thus, latent heat release will only take place in the updraught. It can be shown that the *latent heat released is closely proportional to the upward velocity*, w [Holton 1979]. Hence, the potential temperature equation (3.17) in these circumstances becomes

$$\mathrm{d}\theta'/\mathrm{d}t = -(\theta_0/g)N^2 w \quad \text{if } w<0\,; \qquad \mathrm{d}\theta'/\mathrm{d}t = -(\theta_0/g)N_\mathrm{m}^2 w \quad \text{if } w>0\,. \tag{6.1}$$

Here we have assumed that $\theta = \theta_0(z) + \theta'$ (and likewise for Π). N_m is the moist Brunt–Väisälä frequency, defined as

$$N_\mathrm{m}^2 = N^2 + (gL/\theta_0 \Pi_0)\,\partial r_\mathrm{s}/\partial z\,, \tag{6.2}$$

where L is the latent heat of condensation and r_s is the saturated mixing ratio of water vapour. To arrive at this expression, we have assumed that the change in r_s following the motion is mainly due to ascent [see Holton 1979]. There are more accurate definitions of N_m available in the literature [Durran and Klemp 1982], but the present definition is sufficiently accurate to illustrate the principle influence of moisture on atmospheric circulations.

Because $\partial r_\mathrm{s}/\partial z < 0$, N_m^2 may easily become negative, even if N^2 is positive but not too large. In these circumstances the atmosphere is statistically or buoyantly unstable only with respect to saturated upward motion. This is called *conditional or latent instability*. The word "conditional" or "latent" refers to the condition that the air must be saturated. Usually an ascending air parcel is not saturated until a so-called lifting condensation level is reached. Air parcels must overcome a kind of *potential barrier* before the latent instability can be released. This has some interesting consequences for the intensity of atmospheric convection [Oerlemans 1983].

The asymmetry between the stability properties of the saturated updraught and the dry downdraught will obviously have an important influence on the flow pattern of convection in a conditionally unstable atmosphere. This has been investigated theoretically and numerically by many authors [e.g., Bjerknes 1938, Lilly 1960, Kuo 1961, 1965a, Asai and Kasahara 1967, Yamasaki 1974, Asai and Nakasuji 1977, van Delden 1985, Oerlemans 1986, Bretherton 1987, Chlond 1988]. These studies were concerned with aspects of moist convection, such as the preferred aspect ratio and plan-form of the convection cells and the preferred radius of the updraught. In order to highlight the most important features of these studies, we will follow an argument put forward by Bjerknes [1938] (see also Godske et al. [1957] and Charney [1973]). This argument is based on the so-called slice method referred to earlier in the introduction to chapter 4. We will assume for the moment that all the condensed water in the atmosphere falls out immediately.

Let us schematically denote the area of rising motion at a fixed level by A_+, and the area of sinking motion by A_-. Let the typical upward displacement be l_+ and a concomitant downward displacement be l_-. From mass continuity $l_+ A_+ = l_- A_-$, assuming that the density is constant throughout the fluid. The work per unit mass, W_-, required to overcome the buoyancy forces in the downward displacement

is given by $W_- = \frac{1}{2}N^2 l_-^2 A_-$ (see section 4.1.3, eqs. (4.26, 4.30)). The work per unit mass by the buoyancy forces in the upward displacement is $W_+ = \frac{1}{2}N_m^2 l_+^2 A_+$. Instability in a conditionally unstable atmosphere ($N_m^2 < 0$, $N^2 > 0$) will occur only when $|W_+| > |W_-|$, i.e. when

$$|N_m^2| A_- > |N^2| A_+ , \tag{6.3}$$

where we have used mass continuity. This is Bjerknes' [1938] instability condition for moist convection. The instability will be most intense when A_+/A_- approaches zero. This implies that updraughts in a conditionally unstable atmosphere will preferably be very narrow, whereas downdraughts will be very broad. Turbulent diffusion or entrainment will limit the updraught area A_+ to a finite value. Theoretical and numerical studies due to Kuo [1965a], Yamasaki [1974] and van Delden [1985] have revealed that the radius of the updraughts attains a steady value approximately equal to the depth of the conditionally unstable layer. The downdraught radius, or spacing of the clouds, on the other hand, may grow to very large values, differing greatly from one updraught to the other [Chlond 1988]. Figure 6.1 shows how a field of updraughts emerges from the random forcing in a two-dimensional model of moist convection. It is worth noting that buoyancy wave propagation is possible in the unsaturated area [Bretherton and Smolarkiewicz 1989, Huang 1990]. This makes atmospheric convection much more complicated than ordinary laboratory Rayleigh–Bénard convection (see section 4.1.2).

By analogy with dry adiabatic motion, where potential temperature is constant following the motion, we can define an equivalent potential temperature, θ_e, which is constant following saturated ascent. To this end, we simply define

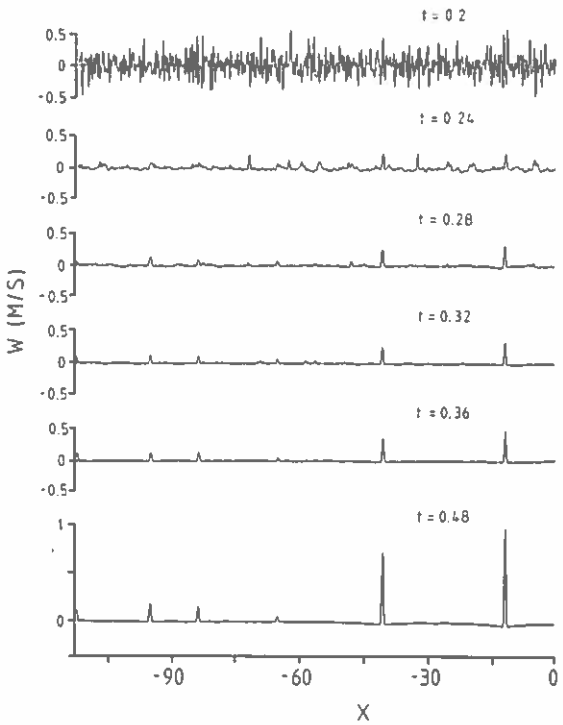

Fig. 6.1. Time series of the vertical velocity as a function of x (in units of H) (see fig. 4.3) in the middle of a conditionally unstable layer according to a numerical model of moist convection between two horizontal, perfectly conducting, stress-free boundaries [van Delden 1985]. (The time unit is equal to $\kappa\nu/g\alpha H^3$.)

$$N_m^2 = [g/(\theta_e)_0]\,\partial(\theta_e)_0/\partial z\,, \tag{6.4}$$

which implies, using (6.2) and (4.19), that

$$\theta_e = \theta \exp(Lr_s/\theta H)\,. \tag{6.5}$$

It should be noted that there are a lot of subtleties involved in the definition and derivation of θ_e and N_m, which have been bypassed here for the sake of conciseness (details can be found in [Durran and Klemp 1982]). The criterion for static instability of a *saturated updraught* (independent of the environment) is

$$\partial\theta_e/\partial z < 0\,. \tag{6.6}$$

Conditional symmetric baroclinic instability; *rainbands*. In a balanced saturated frontal zone, where the above criterion is not satisfied, we may expect that symmetric baroclinic instability is possible if equivalent potential temperature surfaces are steeper than momentum surfaces (see section 4.2). Warm saturated air contains more moisture than cold saturated air. Therefore, the horizontal gradient in θ_e will be larger than the horizontal gradient in θ. Thus, a moist atmosphere may become baroclinically unstable with respect to symmetric perturbations earlier than a dry atmosphere. Bennetts and Hoskins [1979] called this process "*conditional symmetric instability*". They invoked this instability mechanism to explain the formation of frontal rainbands e.g., Browning et al. 1973]. In such an unstable frontal zone, an air parcel travels along a surface of constant $(\theta_e)_0$ conserving absolute momentum (see eq. 4.71). The Coriolis force acting on the parcel in the transverse (y) direction (see fig. 4.14) will immediately exceed the environmental pressure gradient. The parcel will therefore accelerate further away from the equilibrium. Basically, the instability may be described as inertial instability along surfaces of constant θ_e.

Since the pioneering paper by Bennetts and Hoskins [1979], after preparatory work by notably Sawyer [1956], Eliassen [1959, 1962] and Hoskins [1974], several authors have tried to simulate numerically the circulation resulting from conditional symmetric instability. One notable example of such a simulation is described by Saitoh and Tanaka [1987]. Their simulation reproduces many observed features of frontal rainbands [e.g., Houze and Hobbs 1982], lending considerable support to the hypothesis that these bands are ultimately due to conditional symmetric instability.

However, detailed comparison of the theory with observations of meso-scale cloud bands in frontal (baroclinic) zones is difficult. Aircraft measurements are needed to resolve the associated motion, temperature and moisture fields. Bennetts and Ryder [1984] attempted to do this and constructed a schematic diagram, displayed in fig. 6.2, of a cloud band resulting from conditional symmetric instability based on theory and observations. The observations clearly revealed the strong slope of the circulation, demonstrating that baroclinicity is an important feature of the flow. Bennetts and Ryder [1984] divided the atmosphere into three layers: a conditionally, statically unstable boundary layer; a middle weakly baroclinic zone, marginally stable with respect to saturated ascent; and an upper stable layer. They suggested that conditional symmetric instability develops in the middle layer. The ascending air in this layer is inclined at typically a few degrees to the horizontal and the vertical velocity has a magnitude of a few tens of cm/s. As a consequence, a band of relatively shallow clouds develops in the region shown in fig. 6.2. Several cumulonimbus clouds may also be found in this layer. These are excited, either in the conditionally unstable lower layer and overshoot into the upper layers, or in locally statically unstable

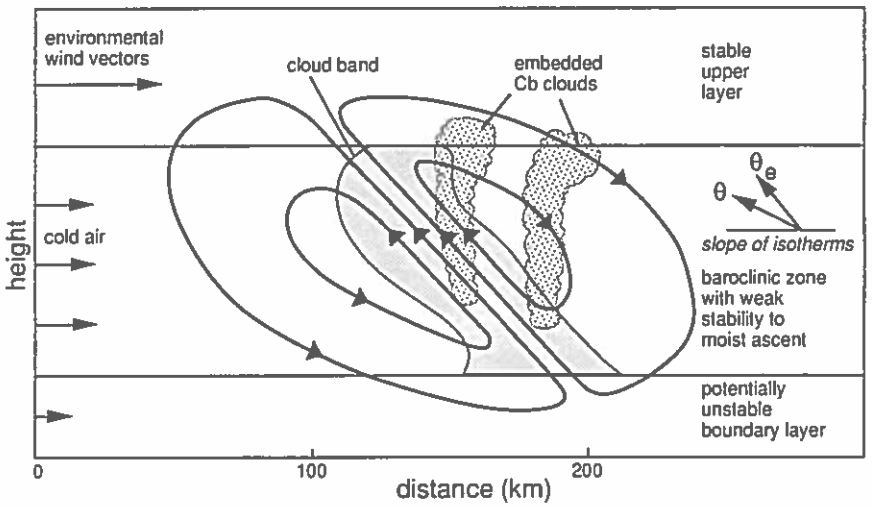

Fig. 6.2. Schematic diagram of the mesoscale cloud bands found in the case study of Bennets and Ryder [1985]. Cb cloud = cumulonimbus cloud.

regions developing at the top of the cloud band resulting from conditional symmetric instability [see also Saitoh and Tanaka 1987]. The measurements made by Bennetts and Ryder [1984] were too coarse to allow for a clear distinction between the motions associated with ordinary upright (or static) conditional instability and the motions associated with conditional symmetric baroclinic instability. More details and references on the problem of rainband formation in frontal zones can be found in the paper by Parsons and Hobbs [1983] and by Browning [1990].

6.2. Water loading, rainfall and evaporation

Cumulonimbus convection. In the theories discussed in the previous section we assumed that the condensed water vapour falls out of the atmosphere immediately as rain. In reality this does not happen until the liquid water mixing ratio, r_ℓ, has exceeded a certain threshold value. The liquid water present in a moist updraught reduces the upward buoyancy, B, by an amount equal to gr_ℓ. This may make the buoyancy force negative, in which case the updraught cannot be maintained and the cloud dies out. Liquid water mixing ratios of 0.5 g m^{-3} are not uncommon in ordinary non-precipitating cumulus clouds [Rogers and Yau 1989, Cotton and Anthes 1989]. As far as its effect on buoyancy is concerned, this is equivalent to a negative temperature perturbation of about 0.15 K if $\rho = 1$ kg m^{-3}. Ludlam [1980] reports measurements of total concentration of condensed water at high levels (above 8 km) in severe thunderstorms over Oklahoma of about 10 g m^{-3} and in one case 44 g m^{-3}.

Except for liquid water loading, as it is called, cooling due to evaporation and melting of falling rain, snow and hail also have a strong negative influence on the upward buoyancy. In fact Kessinger et al. [1988] estimated that 22% of the downward acceleration in a strong downdraught (a so-called downburst) beneath a thunderstorm cloud was due to condensate loading and 78% was due to cooling as a result of melting and evaporation.

Obviously, these processes are not very advantageous for the maintenance of the updraught or cloud. Numerical model simulations (see fig. 6.3) have shown that the lower part of the cloud will tend to collapse within one hour [Takeda 1971, Ogura and Takahashi 1971]. A circulation with a sign opposite to that of the original circulation is generated by the rain water loading and the cooling due to

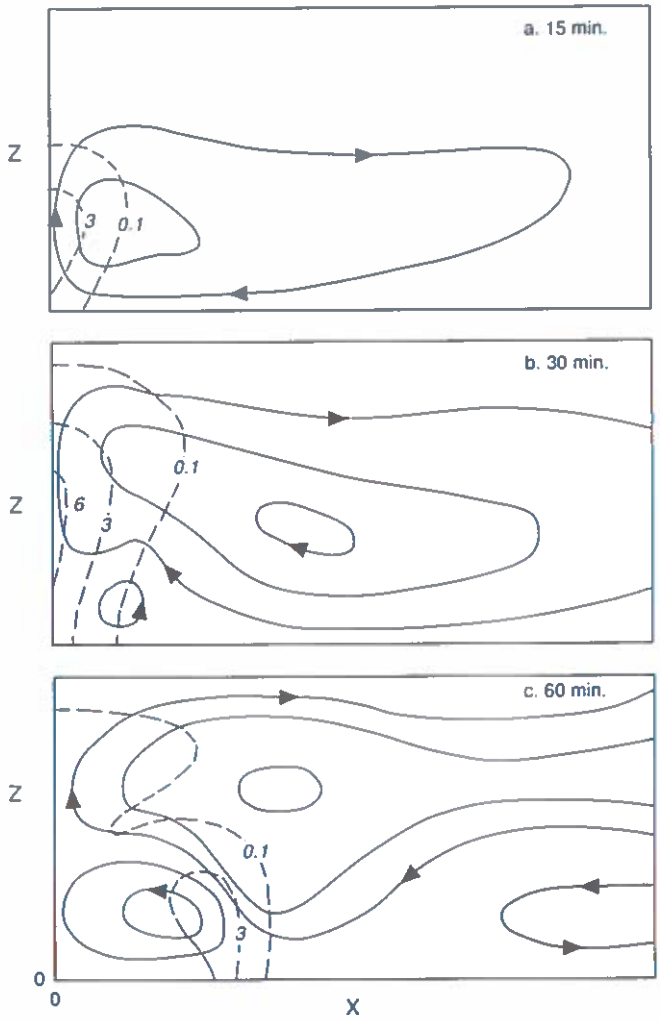

Fig. 6.3. The streamline pattern (solid lines) in a numerical simulation of an isolated shower. The model is two-dimensional and slab-symmetric around $x = 0$. Rain water content in g m^{-3} is indicated by dashed lines [from Takeda 1971].

evaporation. The updraught associated with this "*cold pool*" *circulation* is detached from the original updraught. This eventually generates a new cloud beside the old dissipating cloud.

Despite this, thunderstorms producing large amounts of rain may persist for many hours. In the following section we will discuss the role of environmental vertical wind-shear in promoting the longevity of these meso-scale weather systems.

6.3. Vertical wind-shear

Types of thunderstorm. In the absence of vertical wind-shear, an ordinary buoyantly driven cumulus or cumulonimbus cloud would grow, produce rain and decay over a period of about 1 h. Severe thunderstorms in these circumstances are only produced when CAPE (see section 5.4) is large

[Kingsmill and Wakimoto 1991]. Byers and Braham [1949] referred to these relatively short-lived thunderstorms as "air-mass" thunderstorms. Since the pioneering study by Byers and Braham it has become ever more clear that more than just a large degree of CAPE is needed to produce a severe thunderstorm that persists longer than 1 h. It appears that vertical wind-shear is a crucial factor.

Vertical shear of the large scale wind may force the cloud into a configuration that prevents the updraught from becoming detached from the ground. In this section we will give a short review of the effect of wind-shear on deep convection. This can serve simply as an illustration. The subject is very complicated and, on the theoretical side, it relies heavily on computer simulation.

Results of linear theory, discussed in sections 4.1.3 and 4.1.4, suggest that, except when condition (4.22) is satisfied, non-precipitating clouds would probably grow more slowly in shear than in uniform flow. However, when rain is involved, vertical wind-shear, with weak wind speeds below and high wind speeds aloft, promotes the lifetime of clouds because it allows for a spatial separation of the updraught from the evaporating downdraught and rainshaft, as shown in fig. 6.4.

The picture of a thunderstorm in figure 6.4 corresponds most closely to a so-called squall line. One can, in fact, distinguish several types of thunderstorms, such as (a) air-mass thunderstorms, (b) squall lines, (c) multicellular thunderstorms, (d) supercell thunderstorms and (e) meso-scale convective complexes. In reality this division is, of course, not so clear-cut. Most large unbalanced deep convective weather systems have properties of all five types mentioned above. The convective systems displayed in figs. 2.9 and 2.11 have many properties in common with multicellular thunderstorms (in the early stages; see fig. 2.9a) and with squall lines (in the later stages; see fig. 2.9b).

Interaction of the cold pool with unidirectional shear (the squall line). Although it is not known precisely why thunderstorms occur in concert along a line to form a squall line, this fact does allow for a considerable simplification of the theory. As a first and good approximation we can assume that the squall line is a convection roll organized perpendicular to the mean wind. According to studies by Moncrieff [1978] and Seitter and Kuo [1983], the mean wind-shear causes the updraught to lean *down*shear. The squall line moves with a speed greater than the mean wind at low level but slower than the mean wind at high level. The level at which the mean wind speed is equal to the cloud-propagation speed is referred to as the *steering level*. The steering level for the thunderstorms of July 11, 1984, shown in figs. 2.9 and 2.11, for example, is about 4 km. The clouds are fed below this level with warm,

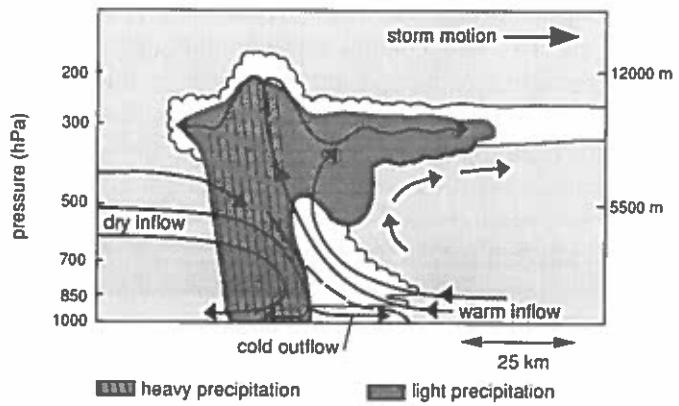

Fig. 6.4. Cloud boundaries and simplified circulation (arrows denote flow) of a typical mature squall-line-type thunderstorm. Vertical scale has been exaggerated fivefold compared with the horizontal scale [from Parker 1988].

relatively humid air from the front (see fig. 6.4). Due to the downshear tilt, the rain will fall into this inflow stream, which will of course inhibit further storm growth. However, in certain conditions the environmental wind-shear can interact constructively with the circulation generated by the cold pool so that the storm can persist and even grow. Thorpe et al. [1982] and Rotunno et al. [1988] identified these conditions with the help of numerical simulations. They discovered that strong wind-shear in the lowest one or two kilometers (below the steering level) and little vertical wind-shear above would produce the most long-lived storms. This represents the optimal state for long-lived squall lines. The absence of shear above the steering level prevents the storm from leaning downshear and reduces the inhibiting effect of shear on the updraught. The effect of the low-level relative countercurrent with shear is more subtle. The cold pool circulation and the circulation associated with the low-level shear in the optimal state have opposite signs. According to Rotunno et al. [1988] and Weisman et al. [1988], this is favourable to the updraught and also keeps it in place relative to the storm [Wilhelmson and Klemp 1978, Thorpe and Miller 1978].

The condition for an optimal state is expressed by Rotunno et al. [1988] as

$$\Delta u_0^2 \approx 2 \int_0^H (-B)\, \mathrm{d}z \equiv c^2 , \tag{6.7}$$

where Δu_0 represents the difference in the mean wind velocity across the low level environmental shear layer, B $(=g(\theta'/\theta_0 - r_1))$ represents the full buoyancy term, including the effect of rain water loading, and the integral is taken within the cold pool and integrated from the surface to a height, H, defined to be level where the negative buoyancy first vanishes. For $c/\Delta u \gg 1$ (i.e. shear is weak relative to the cold pool circulation), lifting at the head of the pool is weakened. For $c/\Delta u \ll 1$, lifting also decreases due to the strong wind-shear.

Thunderstorm splitting. In unidirectional shear conditions for long-lived storms are quite critical. The cold pool circulation and the low-level shear must maintain a delicate balance. The storm must somehow maintain its identity as a line of clouds oriented perpendicular to the environmental wind. It is possible that imbalances in the jet over a frontal zone, which set off gravity-inertia waves, principally take care of this organization [Zhang and Fritsch 1988, Bluestein and Jain 1985] (see also section 6.4). In the absence of such large-scale forcing, the rainwater loading effect will induce a *splitting* of the updraught as shown in fig. 6.5a. Two new counter-rotating updraughts are formed which travel to the right and left, respectively. The right moving updraught takes on positive vertical vorticity, whereas the left moving updraught acquires anticyclonic vertical vorticity. This can be understood with the help of the linearised vertical vorticity equation (4.37), which expresses the change in ζ due to tilting to the vertical of horizontal environmental vorticity due to horizontal gradients in the vertical velocity. The most intense rotation around a vertical axis is thus created on the flanks of the updraught. From (4.37) it follows that the ζ will be positive if $\partial w/\partial y > 0$, which is precisely the case on the right flank of the original updraught.

The interaction of the updraught with the environmental shear creates *dynamic pressure perturbations*. Following Rotunno and Klemp [1982], this can be understood from the linear diagnostic equation (4.35) for the pressure, which, neglecting buoyancy and stratification, becomes

$$\nabla^2 \Pi = -(2/\theta_m)(\partial u_0/\partial z)\, \partial w/\partial x . \tag{6.8}$$

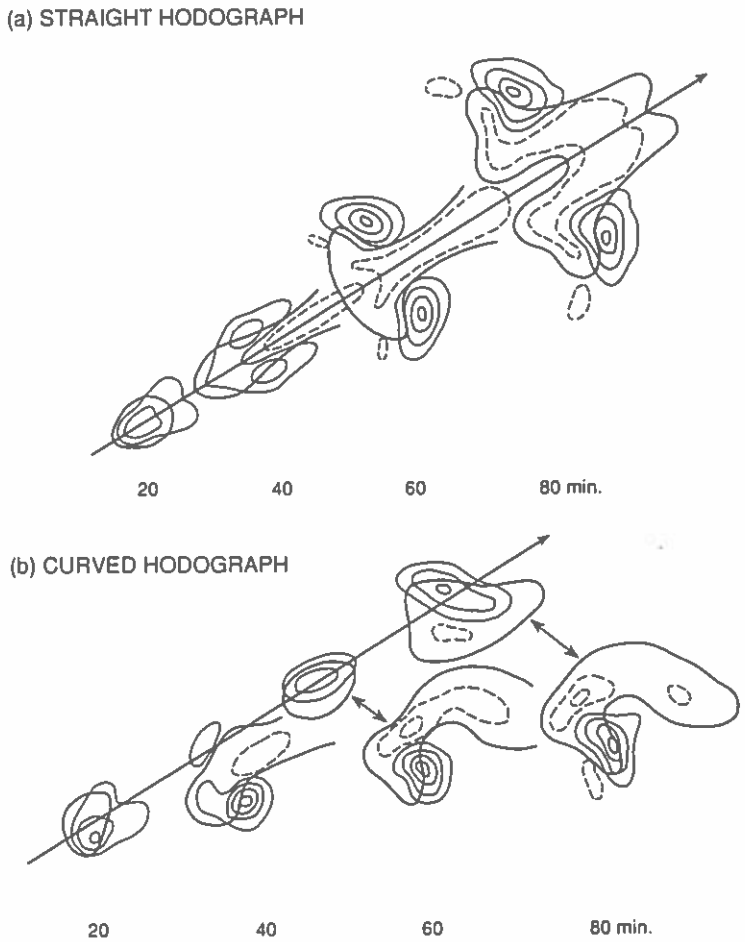

Fig. 6.5. Horizontal contour plots of vertical velocity at 2.25 km above ground level at different times in a numerical simulation with the three-dimensional cloud model described by Klemp and Wilhelmson [1978] for two cases: (a) with an environmental wind which increases in speed but not in direction with increasing height, and (b) with an environmental wind which increases in speed and veers clockwise with increasing height. Updraughts (solid lines) and downdraughts (dashed lines) are contoured at 4 m s^{-1} increments. The heavy line is the outline of the 0.5 g m^{-3} rainwater field [from Rotunno and Klemp 1982].

If we assume that Π can be written as $A \exp[i(kx + nz)]$, we can easily deduce that $\nabla^2 \Pi \approx -\Pi$. This implies that

$$\Pi \approx (\partial u_0/\partial z)\, \partial w/\partial x\,. \tag{6.9}$$

If $\partial u_0/\partial z > 0$, Π will be positive on the upshear side of the updraught and negative on the downshear side. This leads to a negative vertical pressure gradient on the downshear side, promoting updraught propagation downshear. But, since the updraught disappears due to rainwater loading, this does not happen.

The effect of turning of wind-direction with height (*rotating supercell thunderstorms*). The dynamic pressure gradients do, however, play an important role when the environmental wind turns with height.

In most cases of deep convection in North America and Europe, the wind direction turns clockwise with height. This induces negative vertical dynamic pressure gradients on the right-hand side of the storm. This in turn favours the growth of the right-moving updraught and suppresses the left moving updraught (see figure 6.5b). This effect is strongest with very intense vertical shear. The cyclonically rotating right moving storm may turn into a so-called *supercell thunderstorm*, which is the most violent type of thunderstorm (see fig. 6.6). The rotation and the dynamically induced vertical pressure gradient help to produce tornadoes. Supercell storms occur most frequently in the southern interior states of North America to the east of the Rocky mountains. They are relatively rare in Europe. Occasionally they do, however, arise over France, and subsequently affect the neighbouring countries to the north and east [Wessels 1968].

The meso-scale convective complex. Another type of convective weather system, which does not require large environmental vertical wind-shear, was identified by Maddox [1980]. It is termed *meso-scale convective complex* (MCC). The MCC has a more circular form than the squall line (at least on satellite images) and travels relatively slowly. It has a relatively long lifetime (>12 h), acquires a large areal extent ($>10^5$ km^2) and produces tremendous amounts of rain at one location [McAnelly and Cotton 1989]. MCCs result from mergers and interactions between groups of storms that develop in different locations. Some MCCs are initially squall lines that acquire MCC characteristics [Maddox et al. 1986]. Presumably large-scale low-level convergence induced by, for example, a cold core upper level cyclone, keeps these systems going in the first few hours of their lifetime. Orographic lifting may also contribute to the long lifetime. Due to the slow movement of the MCC, prolonged and intense latent heating occurs in the middle of the troposphere over a fixed area comparable to the local Rossby radius of deformation. This induces dynamically large-scale pressure and temperature perturbations followed by a partial adjustment of the flow to geostrophic balance [Cotton et al. 1989]. In the later stages of the lifetime of an MCC, a cyclonic warm-core vortex appears at mid-levels. At higher levels, an anticyclonic circulation develops, which may sometimes become inertially unstable. The cyclonic circulation at

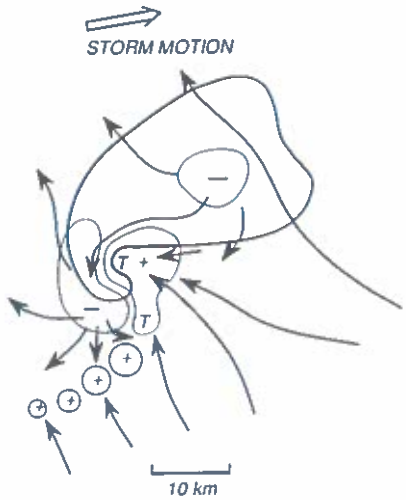

Fig. 6.6. Schematic plan of a tornadic supercell thunderstorm. The solid line encompasses the radar echo. Regions with strong vertical motion are enclosed by thin solid lines and marked with a plus sign or a minus sign. The flow near the ground is indicated by arrows. Tornadoes are most likely to form at the points marked by a T [adapted from Lemon and Doswell 1979, Davies-Jones 1985].

mid-levels can frequently be seen in the cloud pattern of decaying MCCs on satellite images [e.g., Zhang and Fritsch 988, Menard and Fritsch 1989]. MCCs have many features in common with tropical cloud clusters [Cotton et al. 1989] and with torrential rainstorms occurring in the autumn over the warm Mediterranean sea and adjacent coast (for example, more than 1000 mm in 36 h at one place on the east coast of Spain in 1987), frequently in connection with a large-scale cold-core cyclone [Rivera 1990, Llasat and Puigcerver 1990].

6.4. Frontogenesis and jet streaks

Geostrophically forced ageostrophic circulations around jet streaks. Intense deep convection usually occurs in the vicinity of a well-developed intensifying cold front [Ludlam 1980]. Because the cross-front temperature gradient is not uniform along the front, the upper level jet, associated with this front, is typified by concentrations of stronger wind in the jet streaks alternating with weaker winds [Riehl et al. 1954, Palmén and Newton 1969]. In this section we will discuss the way in which these variations promote or force the formation of severe thunderstorms. We will not discuss the formation of fronts themselves. For that we refer to Hoskins [1982], Orlanski et al. [1985] and section 5.5.

Due to geostrophic imbalances, secondary circulations perpendicular to the jet axis are set up at the entrance and exit regions of the jet streaks [Bluestein 1986, Ewenz and Kraus 1990]. Parcels of air travelling through the upper level jet core accelerate into the jet streak through unbalanced (ageostrophic) motion directed towards lower pressure. After passing through the region of maximum winds, the parcels decelerate through ageostrophic motion towards higher pressure. The secondary circulation is thermally direct in the entrance or confluence region and thermally indirect in the exit region or delta of the jet streak (see fig. 6.7). In the exit region, the secondary circulation is frontogenetic because the downward motion on the warm side of the front causes further adiabatic warming, while the upward

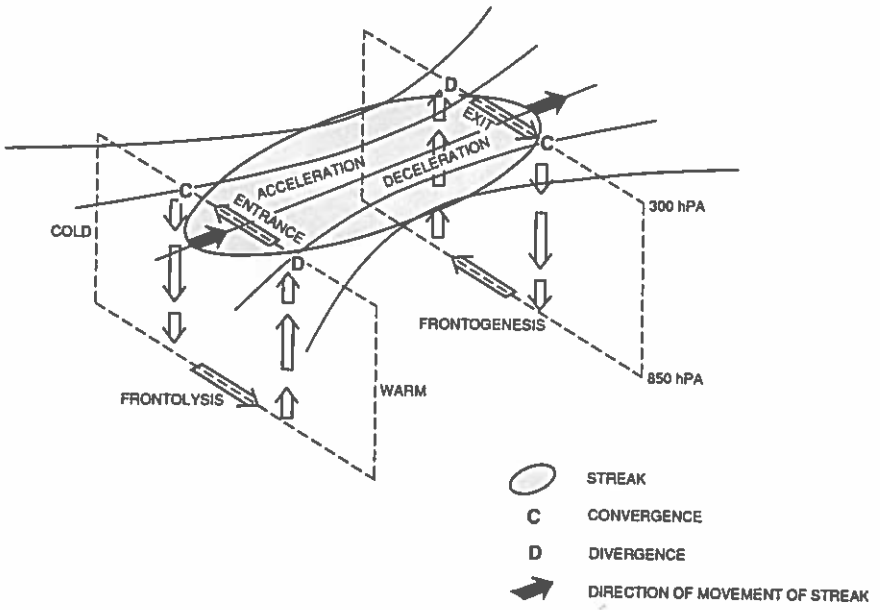

Fig. 6.7. The geostrophically forced (see section 5.5) circulation in the vicinity of a jet streak in a baroclinic zone. Thin solid lines are streamlines. (With thanks to P. Esser.)

motion on the cool side of the front causes further adiabatic cooling. In the entrance region the situation is reversed, i.e. the secondary circulation is frontolytic, provided of course that the temperature stratification is stable. Hence, the jet streak progresses forward, along the current. Simultaneously, due to the secondary circulation relatively cool air is advected into the exit region of the jet streak at upper levels while relatively warm air is advected into the exit region of the jet streak at lower levels. Hence, the stratification is destabilised. Again, the opposite is the case in the entrance region of the jet streak. Clearly, the left exit region of the jet streak is the most favourable for deep convection [Beebe and Bates 1955].

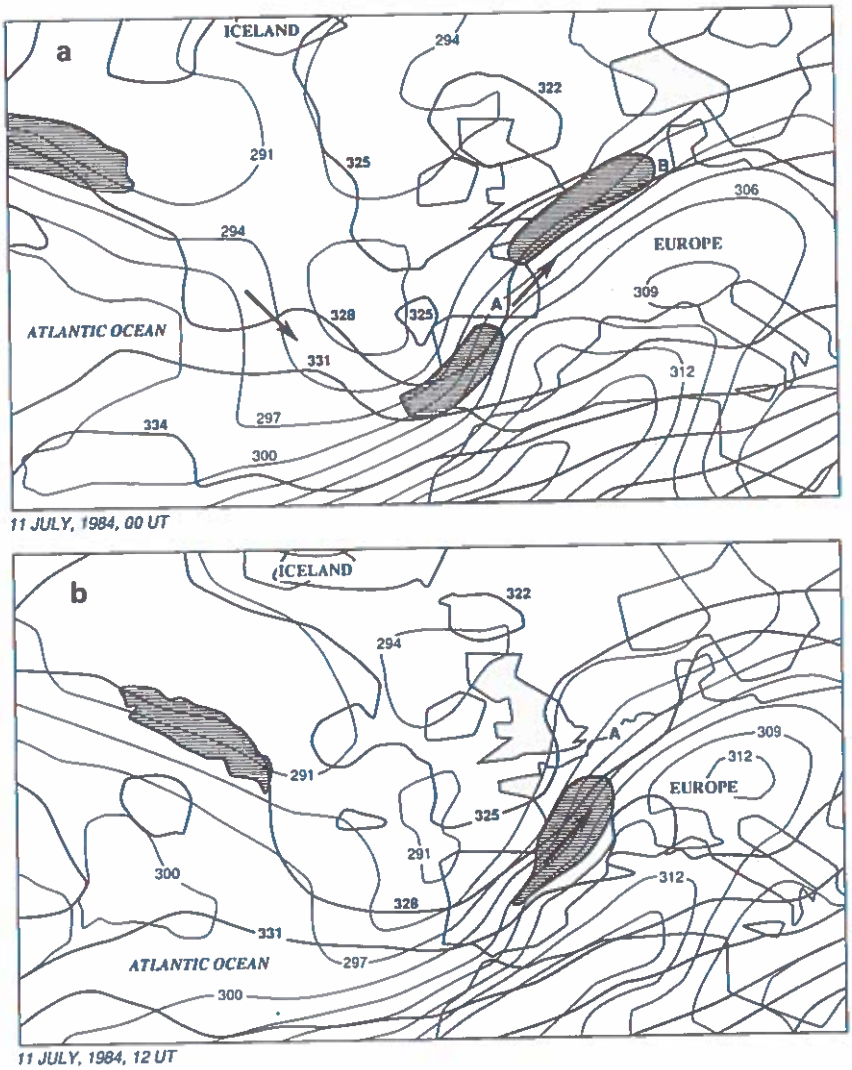

Fig. 6.8. The potential temperature distribution at 300 hPa (about 9500 m) (thick solid line) and at 850 hPa (about 1500 m) over western Europe on July 11, 1984, at (a) 00 UT and (b) 12 UT. The numbers indicate potential temperature in K (eq. (3.16) with $p_{ref} = 1000$ hPa). Regions with a wind speed greater than 45 m s^{-1} (jetstreaks) are enclosed by very thick solid lines and hatched. The letters A and B indicate the position of thunderstorm complexes. The arrows indicate the direction in which the wind is blowing at 300 hPa (approximately parallel to the isentropes). Based on the analysis performed at the ECMWF in Reading, UK.

A case study of thunderstorms forced by a jet streak. The above qualitative theoretical considerations are illustrated quite clearly by the thunderstorm case (July 11, 1984) which was introduced in chapter 2 (e.g., fig. 2.9). These thunderstorms formed in and remained coupled to the exit region of an upper level tropospheric jet streak. Figure 6.8 shows the position of the jet streaks at 300 hPa (about 9500 m) over the Atlantic ocean and western Europe according to the analysis made by the European Centre for Medium Range Weather Forecasts (ECMWF) for this day at 00 UT and 12 UT, respectively. We see that two jet streaks were located over western Europe at 00 UT. The thunderstorms at this time were located precisely in the exit regions of these jet streaks. The thunderstorm, marked B in fig. 6.8a, had brought 17 mm of rain to De Bilt two hours earlier. A cluster of cumulonimbus clouds was just forming at point A in the exit region of the jet streak over Spain. In 12 h (see fig. 6.8b) this jet streak traveled about 1000 km towards the north east. This makes its speed of travel about 83 km h^{-1} (23 m s^{-1}). During this time the group of cumulonimbus clouds became more organized, but despite this, remained coupled to the exit region of the jet streak. Clearly, the intense convection at point A needed the favourable conditions created by the large-scale flow at higher levels in order to subsist.

The surface conditions in the vicinity of the jet on July 11, 1984 reveal some very interesting additional details associated with this case (see fig. 6.9). At 06 UT (figs. 6.9a and 2.9a) the thunderstorm

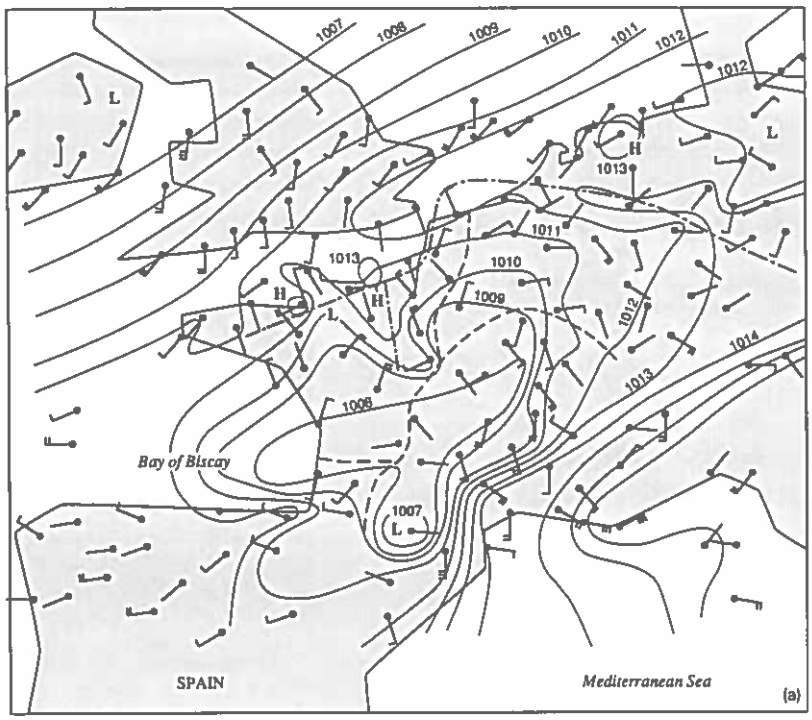

Fig. 6.9. Surface weather maps of July 11, 1984 at (a) 06 UT, (b) 12 UT and (c) 18 UT. Isobars are shown by solid lines with values indicated in hPa. The letters H and L denote surface pressure maxima and minima, respectively. A dot marks the position of a weather station as well as the end point of the wind vector. The barbs attached to the wind vector indicate the 10 min mean windspeed, ff, measured at a height of 10 m: no barb corresponds to ff < 2.5 m s^{-1}; one barb corresponds to 2.5 ≤ ff < 5 m s^{-1} and one further barb is added for every 5 m s^{-1}. Dashed lines mark zones of surface convergence and dotted-dashed lines mark zones of surface divergence. [Note: the analysis of the pressure field and the convergence/divergence lines has been performed on the basis of an observation network with more than double the density of that shown on these maps.] See also figs. 2.9–2.11.

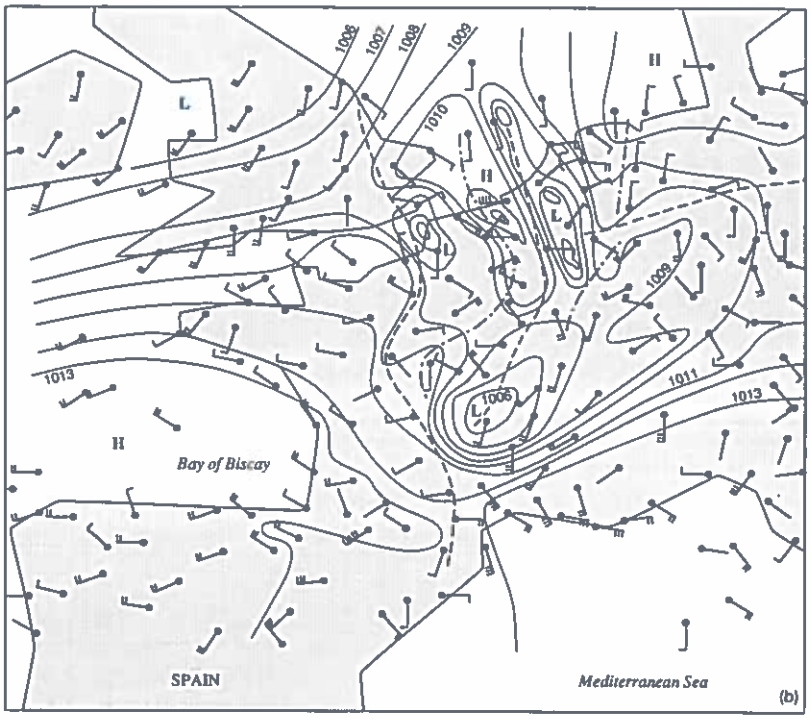
1008
1007
1008
1009
1010
L
H
H
1009
1013
1006
1011
1013
H
Bay of Biscay
SPAIN
Mediterranean Sea
(b)

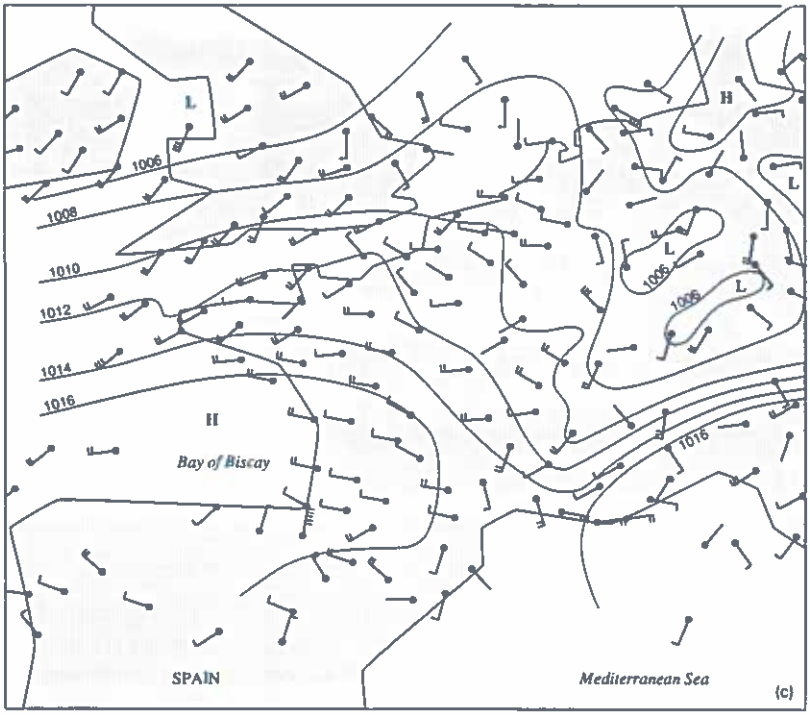
L
1006
1008
1010
1012
1014
1016
H
H
L
L
1006
1006
L
1016
H
Bay of Biscay
SPAIN
Mediterranean Sea
(c)

Fig. 6.9. (cont.)

complex was centred over Normandy in a region of weak synoptic horizontal surface-pressure gradients between the large depression over Ireland and a shallow (i.e. only discernible below a height of about 1500 m) wake low in the lee of the Pyrenees. The low-level convergence line running from south to north right through central France is an indication of both the secondary circulation induced by the jet streak and the outflow from the thunderstorms induced by the rain. Six hours later (fig. 6.9b) the thunderstorms are seen over the Benelux countries as a series of meso-scale highs and lows in the pressure field (see also fig. 2.10). The shallow low has moved away from the Pyrenees remaining directly below the jet streak. This suggests that there is some connection between this low and the jet streak. The low-level secondary horizontal circulation induced by the jet streak is indeed cyclonic (see fig. 6.7). Probably, this circulation is reinforced by the presence of the shallow low. Whatever the precise cause of the movement of this low, frequently referred to as the "thundery low" in England and The Netherlands [e.g., Ludlam 1980], in conjunction with the jet streak, this configuration is certainly very favourable for further intensification of the thunderstorms because it maintains a warm low level flow of air from the southeast.

We see, therefore, that large synoptic scale processes, especially at higher levels in the atmosphere, and meso-scale processes are intimately related in forcing and maintaining intense long-lived convective storms. Areas in the world which are notorious for severe thunderstorms are the high plains in the United States, and northern India. In both these areas, intense thunderstorms with cloud-top heights approaching 20 km [Weston 1972] are clearly related to regions of upper-level (about 300 hPa) divergence in the jetstream [Ramaswamy 1956, Witney 1977, McNulty 1978, Uccellini and Johnson 1979, Uccellini 1980, Kocin et al. 1986].

Jet streaks and associated upper-level short-wave troughs also promote the development of comma-shaped cloud patterns (so-called comma clouds) in cold air masses over a relatively warm ocean [Businger and Reed 1989]. These comma clouds have a horizontal scale of about 500 km. They occur very frequently over the North Pacific in the winter half of the year. In the literature they are frequently associated with polar lows (see section 5.5 and Twitchell et al. [1989]).

More details on the dynamics of fronts, jets and jet streaks and their relation to meso-scale weather events, especially in the United States, where a lot of work has been done on this topic, can be found in the papers by Shapiro [1981], Newton and Trevisan [1984], Bluestein [1986], Keyser [1986] and Keyser and Shapiro [1986]. More about recent developments in the theory of thunderstorms can be found in the papers by Lilly [1986, 1990], Klemp [1987], the recent book by Cotton and Anthes [1989], and the books edited by Kessler [1985] and Ray [1986].

6.5. Topography

Time-scales and length-scales associated with flow over mountains. Because major mountain ranges, such as the Alps and the Canadian Rockies, and major valleys, such as the Rhône valley in France, have meso-scale dimensions, $L \approx 50$–500 km, one can expect these topographic features to generate meso-scale weather phenomena. This expectation is reinforced when one realizes that an air parcel, travelling in a large-scale flow at a typical speed, u_0, of about 10 m/s in the troposphere, takes $L/u_0 \approx 1.4$ to 14 h to cross a mountain range with the above-mentioned dimensions, which is precisely a typical meso-scale range of time scales.

In this section we will discuss some dynamical effects of mountains and valleys on the large-scale flow in the atmosphere. Effects due to diabatic heating will not be drawn into the discussion. Examples of

meso-scale weather phenomena due to the presence of mountains and valleys are lee gravity waves, downslope winds, valley winds, lee vortices and cyclones, and vortex streets.

The response of the atmosphere to mountain forcing depends, among others, on the time, L/u_0, mentioned above, relative to the intrinsic frequencies, N and F. If u_0, N and F are constant, we can, following Queney [1948] [see also Gill 1982], distinguish five regimes:

(i) Potential flow regime ($L/u_0 < 2\pi/N$). In this case the atmosphere is forced at a frequency exceeding the cut-off frequency, N (see eq. 4.21). The reaction is evanescent. The air parcels follow the topography exactly, while the amplitude of the vertical displacements decays with height.

(ii) Non-hydrostatic wave regime ($L/u_0 \geq 2\pi/N$). If the atmosphere is forced with a frequency of the order of N, buoyancy waves are generated in which air parcels oscillate nearly vertically. For lower frequencies ($<N$) are parcels are set into a more oblique oscillation.

(iii) Hydrostatic non-rotating wave regime ($2\pi/F \gg L/u_0 \gg 2\pi/N$). This regime can only exist if the natural frequencies, N and F, differ by several orders of magnitude. It is most applicable to equatorial regions, where F is usually small.

(iv) Rotating wave regime ($L/u_0 \leq 2\pi/F$). In this case the atmosphere reacts primarily in the form of inertial waves.

(v) Balanced flow regime ($L/u_0 > 2\pi/F$). In this regime, solutions are again evanescent, i.e. propagating waves are not possible. Disturbances forced by the mountain adjust to geostrophic or gradient wind balance.

Relevant nondimensional parameters. The first two cases can be defined also in terms of a *Froude number*, Fr, defined by Clark and Peltier [1977] as

$$\mathrm{Fr} = 2\pi u_0/LN\,. \tag{6.10}$$

The potential flow regime corresponds to $\mathrm{Fr} > 1$, while the non-hydrostatic wave regime corresponds to $\mathrm{Fr} \leq 1$. At larger time-scales the earth's rotation becomes more important than stratification. Therefore, the inertial frequency becomes the relevant time scale instead of the Brunt–Väisälä frequency. Thus, the latter two regimes can be defined in terms of a *Rossby number*,

$$\mathrm{Ro} = 2\pi u_0/LF\,. \tag{6.11}$$

Regime (iv) is characterized by $\mathrm{Ro} \geq 1$ and regime (v) is characterized $\mathrm{Ro} < 1$.

Stationary and transient response. The basis of present-day theories on mountain waves was constructed in the 1940s and 1950s principally by Queney [1948], Scorer [1949] and Long [1953a]. The approach of the former two authors, however, was quite different from that of the latter author. Queney and Scorer tackled the problem by applying the linear theory of a continuously stratified fluid, as described in section 4.1. In contrast, Long used hydraulic theory (eqs. 3.32–3.34).

There is, however, one point of resemblance. All three authors were concerned almost exclusively with the stationary response of the air flow to forcing by mountains. They neglected the transient response. The term "stationary" means that local time-derivatives are zero. For waves this implies that the horizontal phase velocity, c_x, is zero.

The difference between the transient and the stationary response as well as several other typical effects of mountains on fluid flow can be illustrated with the help of the one-layer hydraulic model,

described in section 3.3. This model was also employed in section 5.1 to illustrate the geostrophic adjustment process. The governing equations are eqs. (3.32–3.34). Let us place a bell-shaped mountain with a maximum height, H_b, in the middle of the domain ($x = 0$). Starting with a mean flow velocity, u_g, and a free surface which is horizontal in the x-direction, we can integrate eqs. (3.32–3.34) on the computer to find out what happens afterwards. The result is shown in fig. 6.10. Initially, the flow is partly *blocked* by the mountain. Transient surface gravity waves are excited, which propagate in opposite directions away from the mountain. The wave propagating downstream is a wave of depression, whereas the wave propagating upstream is a wave of elevation. The latter wave leaves behind a region with lower flow velocities and higher free-surface elevations. Thus, a horizontal pressure gradient is set up with high pressure upstream and low pressure downstream from the mountain. Due to this pressure difference, there is a strong acceleration of the flow ($\partial u/\partial x > 0$) immediately behind the mountain crest. Further away downstream, however, there is a sudden transition back to the initial state. This so-called *hydraulic jump* is a non-linear phenomenon. The conditions for the formation of a hydraulic jump can be deduced from eqs. (3.32–3.34), by setting the local time derivatives equal to zero. After eliminating $\partial h/\partial x$ from (3.32) and (3.34), one obtains an expression for the steady acceleration,

$$\frac{\mathrm{d}u}{\mathrm{d}x} = \frac{u}{h(1-\mathrm{Fr}^2)}\left(\frac{\mathrm{d}h_b}{\mathrm{d}x} - \frac{fv}{g'}\right), \tag{6.12}$$

where the Froude number, Fr, is defined in the context of this model as

$$\mathrm{Fr} \equiv u/\sqrt{g'h}\,. \tag{6.13}$$

The hydraulic jump corresponds to the point where Fr = 1, so that, according to (6.12), $\mathrm{d}u/\mathrm{d}x$ becomes infinite if $\mathrm{d}h_b/\mathrm{d}x - fv/g' \neq 0$. In fact, in the case shown in fig. 6.10, there are two points at which Fr = 1. The first point is located close to the mountain crest, where $\mathrm{d}h_b/\mathrm{d}x - fv/g' = 0$. Here there is a

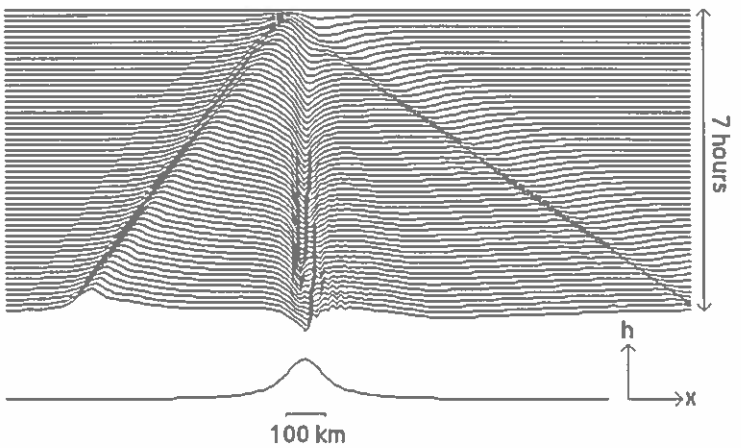

Fig. 6.10. The level of the free surface as a function of time in a numerical integration of the one-layer hydraulic model starting with a horizontal free surface everywhere, a constant geostrophic velocity, $u_g = 12\ \mathrm{m\,s^{-1}}$, and a bell-shaped mountain with a height, H_b, of 300 m in the middle of the domain. The mountain profile is shown below. The fluid depth far from the mountain is 1000 m. The values of other parameters are $g' = 1\ \mathrm{m\,s^{-1}}$ and $f = 0.0001\ \mathrm{s^{-1}}$. The magnitude of the Froude number (see eq. 6.13) far upstream is 0.38.

smooth transition from *subcritical* flow ($Fr < 1$) to *supercritical* flow ($Fr > 1$). The second point marks the transition back to the imposed upstream and downstream subcritical flow conditions. This last transition cannot take place smoothly, hence the hydraulic jump or bore.

Severe downslope winds. The transition from subcritical to supercritical flow is the most interesting because this leads to very high downslope fluid velocities. Due to the fact that the positive pressure gradient spreads out upstream, the acceleration of the fluid (i.e. $du/dx > 0$) begins a certain distance upstream from the crest. This effect *accelerates* the fluid *upslope* until the Froude number reaches the critical value first *near* the crest (if $f = 0$, $Fr = 1$ at the crest). On the leeward side both $1 - Fr^2$ and dh_b/dx change sign so that, according to (6.12), the acceleration continues downslope. This may lead to very high flow speeds on the lee slope of the mountain.

The acceleration of the flow on the upslope side does not always induce a transition from subcritical to supercritical flow over the crest. For relatively low mountains and small upstream Frounde numbers the flow remains subcritical everywhere. All we see then is a slight depression of the free surface above the mountain. The different regimes characterizing single-layer flow over an obstacle in a non-rotating fluid are summarized in fig. 6.11. Except for Fr, the relative height of the obstacle also governs the behaviour of the fluid. The diagram presented in fig. 6.11 has been obtained on the basis of theoretical, experimental and numerical investigations carried out by, among others, Long [1954, 1970, 1972], Houghton and Kasahara [1968] and Baines [1987]. Note that the solution presented in fig. 6.10 corresponds to the transition between two regimes. In fact, if we continue the integration, the system will tend towards the subcritical regime. For a study on the effect of background rotation on one-layer flow over topography, see Baines and Leonard [1989].

Long [1953b] applied the hydraulic model to the atmosphere, in particular to explain the violent downslope winds and turbulence observed in the flow over the Sierra Nevada range in the United States. Intense downslope windstorms are observed frequently in many parts of the world. One of the most well-known examples is the so-called bora wind occurring along the steep coast of Yugoslavia. This windstorm develops when cold continental air is forced over the coastal mountain range and out

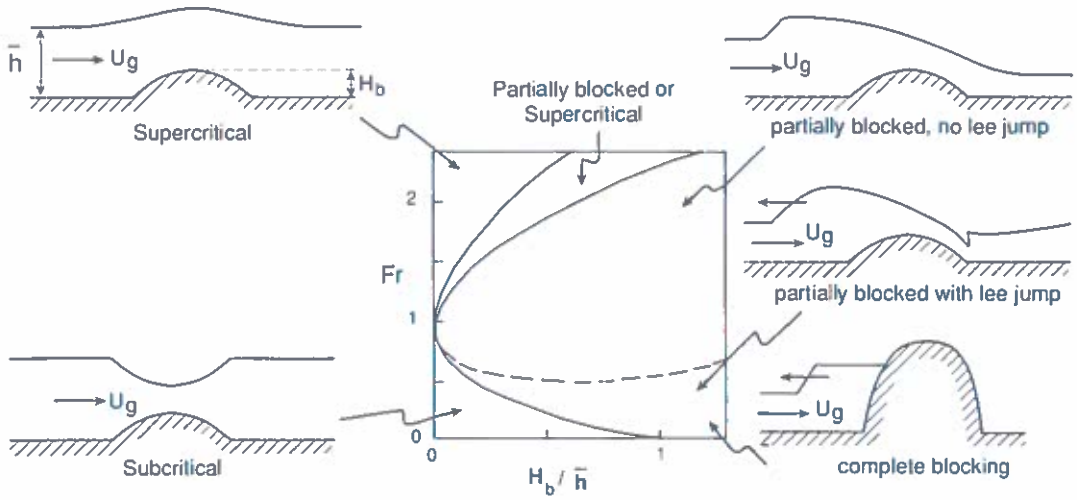

Fig. 6.11. Regime diagram of the flow of a shallow layer of fluid with constant density over an isolated hill as a function of Froude number far upstream and the non-dimensional height of the hill [adapted from Baines 1987].

over the relatively warm Adriatic sea. The acceleration of the flow starts already where the mountains begin to rise and continues over the crest and down the other side [Smith 1987]. The concept of blocking and of transition from subcritical to supercritical flow offers a very plausible explanation of these phenomena. This appears to be confirmed by numerical simulations of two-dimensional continuously stratified flow over a mountain ridge [Durran 1986a, Klemp and Durran 1987].

Very violent downslope winds have also been observed near Boulder, Colorado. In one case, which is particularly well documented by Lilly [1978], windspeeds of up to 55 m s^{-1} were measured on the eastern slopes of the Rocky Mountains (see fig. 6.12a). The analysis of the potential temperature field for this case, displayed in fig. 6.12b, suggests that the hydraulic model gives a good first-order accurate description of these phenomena.

An alternative explanation was put forward by Peltier and Clark [1983] and Clark and Peltier [1984]. They interpreted the severe downslope winds in terms of resonant growth of non-linear mountain buoyancy waves. Vertically propagating buoyancy waves excited by the topography can be reflected at a critical level, where $u_0 = c_x$, if the Richardson number is not too large [Thorpe 1981]. In the case of stationary waves, the critical level corresponds to a level of mean wind reversal ($u_0 = 0$). By performing numerical simulations of two-dimensional flow over a ridge, Clark and Peltier [1984] showed that the reflected wave could interfere constructively with the incident wave if the critical level was located at certain discrete heights above the ground. This could, in turn, induce violent winds near the ground and enhanced pressure drag on the mountain.

Although subsequent investigations, such as Durran [1986a], Klemp and Durran [1987] and Bacmeister and Pierrehumbert [1988], have confirmed these remarkable numerical results, these authors have also obtained results with sophisticated numerical models which indicate that severe downslope winds also develop when the resonant wave amplification mechanism proposed by Peltier and Clark is not possible. There has been much debate in the past fifteen to twenty years about the mechanisms responsible for these winds [e.g., Lilly and Klemp 1980, Peltier and Clark 1980, Durran 1986, Smith 1989a]. It is now thought that the mechanism which produces the violent downslope wind is probably not related to resonant growth of buoyancy waves, but is fundamentally similar to what happens in the hydraulic model when there is a transition from subcritical to supercritical flow near the mountain crest [Klemp and Durran 1987]. The issue is, however, still not completely resolved. Probably, part of the difficulty lies in the fact that the results obtained with sophisticated numerical models are interpreted either in terms of the "language" of the linearized shallow Boussinesq model or within the framework of the non-linear, but physically simplified, hydraulic model. Both these models have severe limitations (see sections 3.2, 3.4 and 4.1.1).

An effect which appears crucial in producing strong downslope winds is the blocking of the low level air flow by the mountains. If this air cannot flow around the mountain, as in the case of the bora [Smith 1987], the pressure upstream from the mountain will rise until the air is able to flow over the crest. Another factor which seems to be of importance according to Durran [1986a] is the presence of an inversion layer such as that shown in fig. 4.1, and also between 500 and 600 mb in fig. 6.12b. The pressure gradient which is set up due to the blocking is confined principally to levels below the inversion. Therefore, only the layer below the inversion is accelerated. Figure 6.11 shows that the thickness of this layer relative to the mountain height determines the response on the lee-side. This has been tested and confirmed in numerical simulations described by Klemp and Durran [1987].

Dynamically forced strong valley winds (mistral). An analogous situation arises in a valley with a constriction. Blocking by the constriction can induce a transition from subcritical to supercritical flow

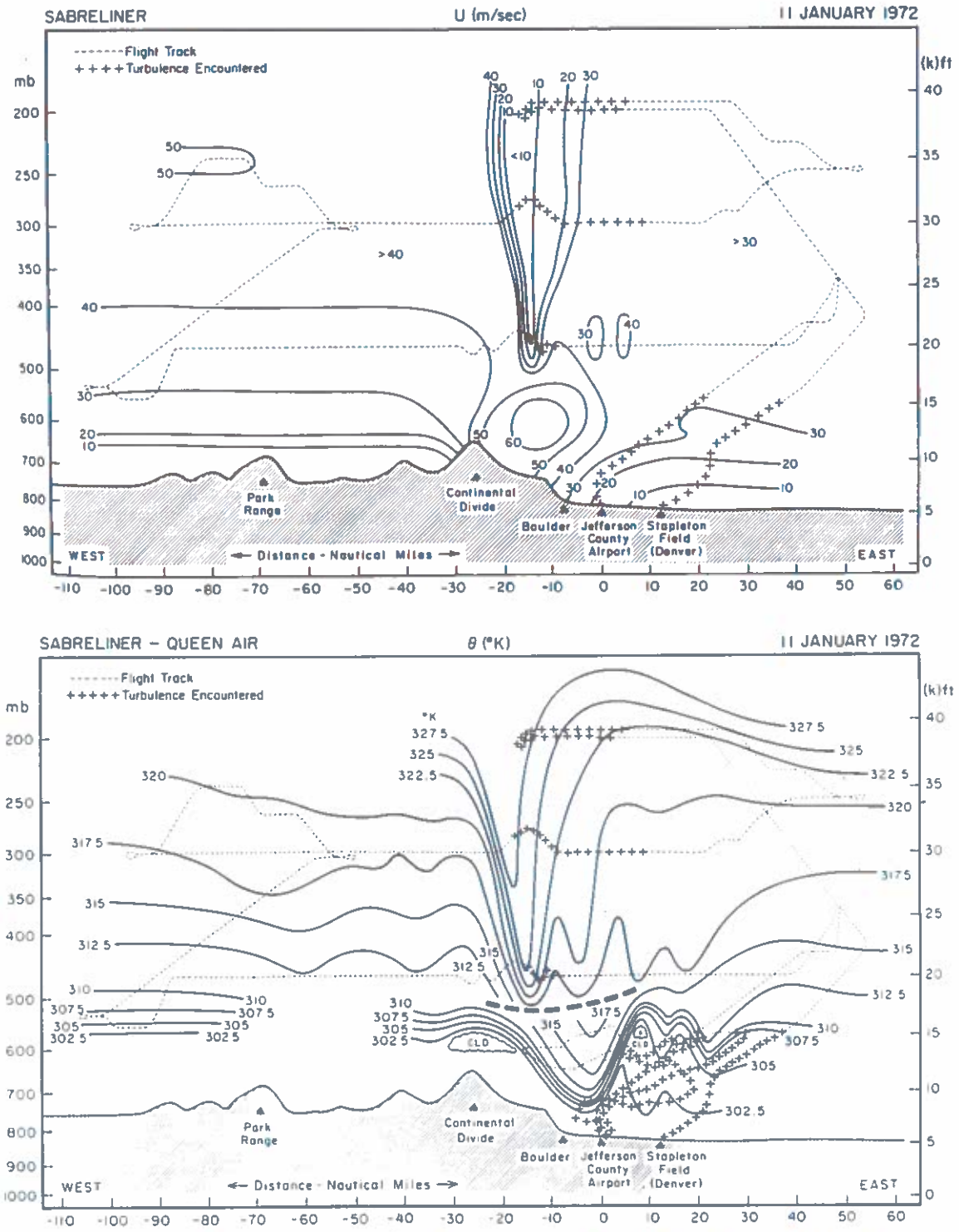

Fig. 6.12. (a) Analysis of the westerly wind component (m s^{-1}) on 11 January 1972, made from aircraft flight data and radio sondes. (b) Analysis of the potential temperature field (solid lines), corresponding to (a). The dashed lines show the aircraft track, with periods of significant turbulence shown by pluses. The heavy dashed line separates data taken by the Queen Air at lower levels before 22 : 00 UT from that taken by the Sabreliner in the middle and upper troposphere after 00 : 00 UT (12 January) [Lilly 1978].

leading to continued acceleration of the air down the valley when the valley-width increases. Pettre [1982] hypothesized that this effect produces the famous mistral wind in the Rhône valley in southern France. Observations show that winds are relatively weak upstream from the constriction, near Valence, while there is a sudden increase in the wind downstream from the constriction. The acceleration continues until a maximum wind speed is reached about 100 km downstream from Valence. A sudden transition back to calmer conditions, similar to a hydraulic jump, is frequently observed near Nîmes, about 150 km from Valence. Observations compiled by Pettre [1982] seem to indicate, that, here too, a potential temperature inversion at relatively low levels is required to produce violent mistral winds.

Foehn. One very conspicuous aspect or property of downslope winds is that some are warm and others are cold. The bora and mistral are relatively cold winds while the well known foehn, occurring in the lee of the Alps, is warm. The warmth of the foehn has been attributed in the past to the release of latent heat in the air rising from the ground at the upwind side of the mountain range. This has been demonstrated to be a false hypothesis [Siebert 1990]. The mechanism producing warm foehn is in fact probably identical to the mechanism producing the cold bora [e.g., Igawa and Nagasawa 1989]. Although the bora is felt as a cold wind, this is only relative to the originally warm air found along the Adriatic coast. The foehn is felt as a warm wind because it replaces a relatively cold layer of air near the ground in the lee of the Alps. In all cases the air reaching the ground in the lee of the mountain range comes from higher altitudes.

Nonhydrostatic resonant lee-waves. Early studies of disturbances produced by mountains were directed towards finding a theory which could explain the relatively small-scale non-hydrostatic *lee-waves* frequently visible as a series of parallel cloud bands (with a spacing in the order of 10 km) being mountain ranges [e.g., Scorer 1986, Cruette 1976]. Because the amplitude of these phenomena is relatively small, linear Boussinesq theory, as described in section 4.1.1, was adopted by the pioneers in this field to investigate this problem [e.g., Queney 1948, Scorer, 1949]. Since the horizontal structure of the wave field is determined by the structure of the mountain, which is not necessarily sinusoidal, this structure was not specified a priori as was done in section 4.1.1. For two-dimensional Boussinesq flow over a ridge this yields a wave equation of the form,

$$\partial^2 W/\partial x^2 + \partial^2 W/\partial z^2 + (l^2 - k^2)W = 0\,, \tag{6.14}$$

where $W(x, z)$ is the amplitude of the wave (compare this equation to (4.20); see also Gill [1982, p. 284]). Scorer [1949] was the first to point out the relevance of the parameter l. He investigated two-dimensional stationary small-amplitude buoyancy waves, excited by a weak ridge. The Scorer parameter for these waves becomes

$$l^2 = N^2/u_0^2 - (\mathrm{D}^2 u_0)/u_0\,. \tag{6.15}$$

Equation (6.14) possesses wave-like solutions as long as the wavelength is such that $k^2 < l^2$. In an environment where $l^2 < k^2$, waves with wave-number, k, cannot be sustained. Thus, if the Scorer parameter decreases with height, all but the longest waves will be trapped and reflected. This will produce a *downstream* train of stationary buoyancy mountain waves, which are usually referred to as *resonant lee-waves.* Stationary buoyancy waves upwind of the mountains are not possible because the horizontal group velocity of stationary waves is directed downstream (i.e. $|c_{gx}| < |c_x|$).

Flow around mountains. Because of limitations on computer power and analytical intractability, very few studies on the problem of flow over and around three-dimensional mountains have been undertaken until relatively recently. When air encounters a three-dimensional obstacle, it can not only flow over the obstacle, it can also flow around it. If the fluid is stably stratified, a so-called *dividing streamline* may be formed which separates the upper layer flowing over the hill from the lower layer flowing around the hill [Sheppard 1956, Snyder et al. 1985]. For a simple background flow with constant u_0 and constant N, the dividing streamline height h_c is given by

$$h_c \equiv H_h(1 - \text{“Fr”}) , \tag{6.16}$$

where “Fr” is defined in yet another way according to

$$\text{“Fr”} = u_0/NH_h , \tag{6.17}$$

where H_h is the maximum height of the obstacle [Etling 1989]. The Froude number “Fr” has been placed in quotation marks in order to distinguish it from the other Froude numbers defined in (6.10) and (6.13). There have been some critical comments in the literature on the many definitions of the Froude number used in different contexts [e.g., Baines 1987]. It might be best to reserve the term Froude number for the ratio of the flow velocity to the phase speed of some wave, as in (6.13). The “Froude number” defined above clearly does not meet this requirement. Rather, it is a measure of the ratio of the mean velocity to the perturbation velocity induced by the mountain, and thus a measure of non-linearity. We will not decide here which is the best definition of Fr, since the different definitions are still used by the different specialists studying flow over and around mountains.

According to eq. (6.16) a dividing streamline will only exist for “Fr” $\ll 1$. The air below the height, h_c, will have insufficient kinetic energy to overcome the potential energy barrier, induced by the stable stratification, and to flow over the mountain top. The air flowing around the obstacle will form counter-rotating vortices in the lee, while the air flowing over the obstacle will produced gravity waves. Theses two principal flow patterns are easily recognized in the cloud pattern on satellite photographs [e.g., Scorer 1986]. In high “Froude number” flow over relatively steep islands the gravity waves are frequently seen as so-called ship waves (see fig. 6.13a). In low “Froude number” flow, lee-vortices form

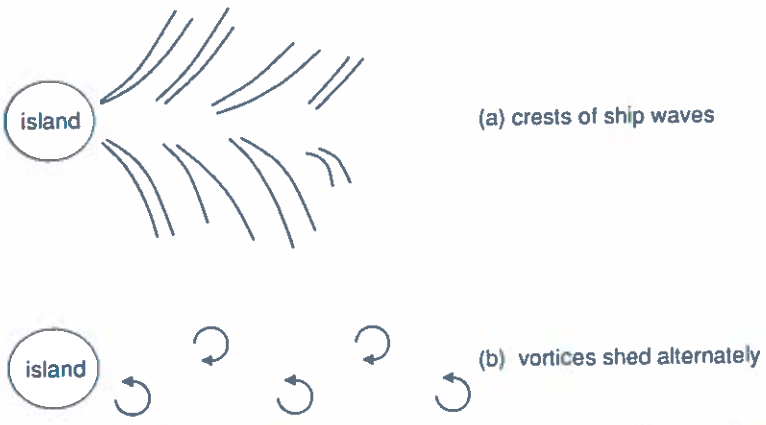

Fig. 6.13. (a) The crests of “ship” waves behind an isolated obstacle at high Froude numbers. (b) Vortices shed alternately by the same obstacle at low Froude numbers.

especially when there is a strong potential temperature inversion below the mountain top. The vortices are shed alternately, forming vortex streets (see fig. 6.13b). The similarity with the von Kármán vortex streets, observed in fluid flow behind a cylinder [e.g., Tritton 1988, Van Dyke 1982, Kundu 1990] is remarkable. It is, however, not entirely clear whether the two phenomena can be attributed to the same mechanism. For the von Kármán vortices the production of vertical vorticity is due to the viscous stress at the side walls of the cylinder and the subsequent viscous boundary layer separation. Laboratory experiments have revealed vortex shedding in a stably stratified flow around obstacles with slopes of 1/4 to 2. Because the steepest islands have slopes of 1/5 or less, the experimental results cannot be carried over directly to the atmosphere [Etling 1989, 1990].

Recently, Smolarkiewicz and Rotunno [1989a] have shown that lee-vortices can also be explained without invoking the traditional arguments on the separation of the frictional boundary layer. They used a numerical model of inviscid, *stress-free* flow past a bell-shaped (round) three-dimensional hill. They demonstrated that vertical vorticity is produced on the lee-side owing to the tilting of horizontally oriented vorticity produced baroclinically as isentropes deform in response to the flow over the hill.

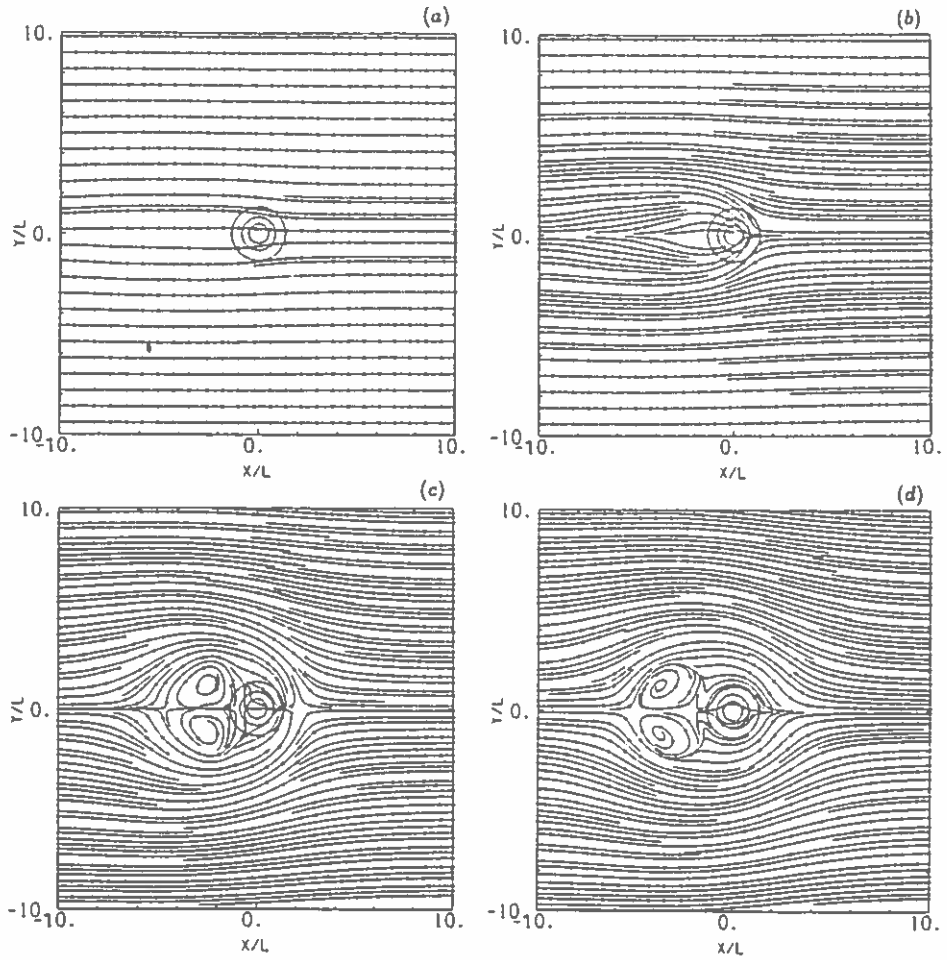

Fig. 6.14. Steady state streamlines at the lower surface for "Fr" = (a) 2.2, (b) 0.66, (c) 0.22, (d) 0.055. Concentric contours in the centre of the domain represent the height of the obstacle with contour interval $0.25H_h$ [Smolarkiewicz and Rotunno 1989a]. $H_h = 0.12L$.

This interpretation is rather controversial [Smith 1989b, Smolarkiewicz and Rotunno 1989b]. Figures 6.14 and 6.15 show some of their results. Evidently, lee-vortices are produced only when "Fr" < 0.5. In fig. 6.15 it can be seen that gravity waves are produced only when "Fr" is large. The domain is probably too small to verify whether the wave crests form a ship wave pattern. Apparently, vortex shedding does not occur in the model simulations reported by Smolarkiewicz and Rotunno [1989a]. In this context the very recent study by Schär and Smith [1991] should be mentioned. Here it is shown that the shedding of vortices is due to a hydrodynamic instability which results from the presence of potential vorticity in the wake of the obstacle. This potential vorticity is created due to internal dissipation in the fluid.

In a continuation of their study, Smolarkiewicz and Rotunno (1990) investigated the zone of *flow reversal* on the windward side of a three-dimensional obstacle. This is a characteristic feature of low "Froude number" flow. Here too, the numerical model experiments indicated quite clearly that frictional boundary layer separation is not needed for upwind stagnation and flow reversal. The flow

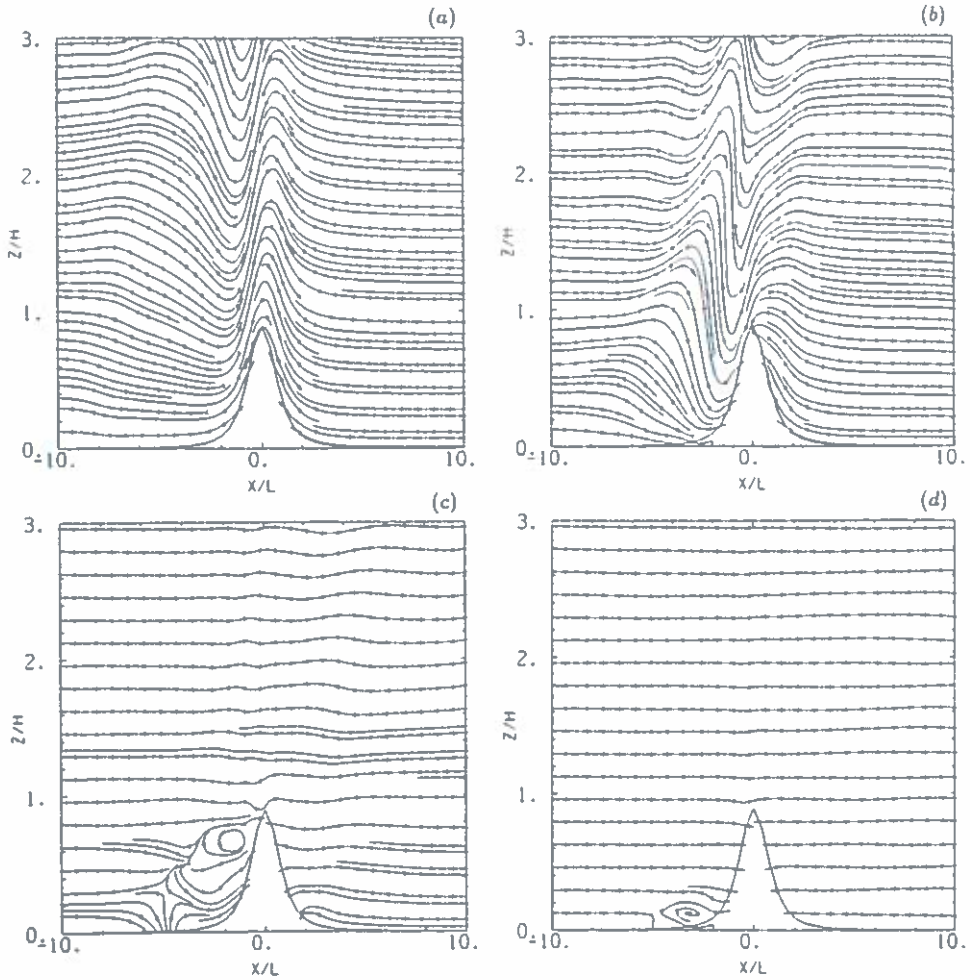

Fig. 6.15. Steady state streamlines in a vertical cross section through the centre plane for "Fr" = (a) 2.2, (b) 0.66, (c) 0.22, (d) 0.055 [Smolarkiewicz and Rotunno 1989a]. $H_b = 0.12L$.

reversal is only observed when the aspect ratio, β (across-stream length divided by the along-stream length), is greater than one. Lee-vortex formation seems to be independent of β, although the lee-vortices become much larger and more marked when β increases. The upwind flow reversal when $\beta > 1$, tends to destabilize the atmosphere, thus promoting the formation of upwind rainbands. Such rainbands are regularly observed offshore from Hawaii [Smolarkiewicz et al. 1988, Rasmussen et al. 1989].

Topography can influence the flow on the meso-scale in many ways, especially in combination with diabatic heating (thermally induced valley and slope winds; katabatic winds) and friction. More details about the topics discussed in this section can be found in the reviews by Smith [1979, 1989a], Durran [1986b, 1990], Chopra [1973] and Hunt et al. [1991], in the books by Turner [1973], Barry [1981], Gill [1982] and Pichler [1984], and in the book edited by Kuhn [1989]. Thermally induced wind systems in mountainous terrain are not discussed in this review. Details on these phenomena can be found in the classical review by Defant [1951], in the recent reviews by Vergeiner and Dreiseitl [1987], Kraus [1987], Whiteman [1990] and Egger [1990a], and in the special issue of *Meteorology and Atmospheric Physics* edited by Davies and Pichler [1990].

6.6. *Friction*

So far we have said very little about friction and dissipation, not because it is unimportant, but more because a physically sound theory on the nature of friction and dissipation in meso-scale weather systems is lacking, even though a large amount of literature exists on this topic (for a philosophical review see [Scorer 1988]). To do justice to all the literature would make this review excessively long. Here we will only list a few of the very differing roles played by friction, some of which we have already discussed earlier.

Frictional forces play both a destructive and a constructive role. An obvious example of the destructive role is the fact that friction converts kinetic energy to heat. A more subtle example is the fact that internal viscous diffusion causes dispersion of gravity waves. This effect may even eliminate the gravity waves altogether (see section 5.2). The constructive role of friction is exemplified by the fact that internal eddy viscous diffusion determines the minimum horizontal wavelength of convection cells (the so-called small-scale cut-off wavelength; see section 4.1.2, fig. 4.2), thus shifting the peak in the growth rate curve to a finite wavelength and providing a mechanism for the organization of the flow. Furthermore, friction or viscous diffusion is responsible for various hydrodynamic instabilities, such as the parallel instability of the Ekman layer discussed in section 4.4.4. Frictional convergence at coastlines is in part responsible for the formation of a meso-scale weather system called the *coastal front* [Bosart et al. 1972, Roth 1981, Roeloffzen et al. 1986, van den Berg 1987, Pike 1990]. Frictional convergence in vortices such as polar lows and tropical cyclones leads to cloud formation, latent heat release and, in certain circumstances, further growth of the vortex [Charney and Eliassen 1964, Ogura 1964, Ooyama 1969]. Frictional convergence due to the direct stress which the earth's surface exercises on the air flow, may even be responsible for the formation of the eyewall in a tropical cyclone [Eliassen 1971, Anthes 1971, Yamasaki 1977, Anthes 1982]. The sensitivity of downslope windstorms to the asymmetry of the mountain shape arises primarily through surface friction effects [Miller and Durran 1991]. Friction and turbulent heat fluxes may also redistribute potential vorticity [Shapiro 1976, Danielsen 1990]. We will see in the next section that mechanisms affecting the distribution of potential vorticity strongly influence the dynamics of the atmosphere.

6.7. Diabatic heating

Theories of tropical cyclone growth. Diabatic heating has been discussed in more than one context in previous sections of this review. We will now make a kind of synthesis of these somewhat scattered discussions and remarks by describing the role played by diabatic heating in the growth of a tropical cyclone. We will use the concepts which were introduced earlier, especially in section 4.2, and the observations discussed in section 5.5.

We have seen in section 5.5 that a tropical cyclone is characterized by a high positive relative vorticity at low levels together with low surface pressure. Other characteristics are: (1) the warm core (see fig. 5.13), (2) the axisymmetry (see fig. 3.2), (3) gradient wind balance (see fig. 5.11) and thermal wind balance (see fig. 5.13), (4) the eye (see fig. 3.2).

The problem of the growth of a tropical cyclone has been an important topic of research since the last century when it was generally thought that all cyclones have a warm core and therefore must be a result of heating [for a historical account see Kutzbach 1979, Palmén and Newton 1969, ch. 5, Hoskins 1990, Uccellini 1990]. In the first half of this century, this so-called "thermal theory of cyclones" (also referred to as "convective cyclone theory" by e.g., Dunn [1951] and Riehl [1951]), was pushed into the background when the connection between the genesis of mid-latitude cyclones and regions of strong baroclinicity was discovered. With the theory of baroclinic instability, put forward by Charney [1947] and Eady [1949], this idea broke through definitively (for a review of progress since then, see Reed [1990]). However, since baroclinicity is usually very weak in the tropics, this theory obviously did not apply to tropical cyclones. Therefore, the thermal cyclone theory was kept alive and reserved principally for the tropics. But serious conceptual problems continued to frustrate researchers who worked on this topic in the nineteen fifties and the early sixties. The problem was that the thermal theory at that time could not really make the distinction between buoyant cumulus convection and the growth of a tropical cyclone [e.g., Bergeron 1954]. The first serious theoretical breakthrough with this problem came in the nineteen sixties with the papers by, notably, Charney and Eliassen [1964], Ogura [1964], Ooyama [1964, 1969] and Kuo [1965b]. These authors took a rather bold step: they constructed models of a tropical cyclone in which the motion was assumed to be in hydrostatic balance and in gradient wind balance at all times (see for example the description of Ooyama's model in section 3.4). Charney, in his conversation with George W. Platzman [see Lindzen et al. 1990, pp. 69, 70], states:

"*. . . I became interested in the mechanism of generation of hurricanes and this led to the notion of CISK* [*Conditional Instability of the Second Kind*] *. . . I worked on the problem and one of the things that led me to the formulation of CISK was the idea that the forces in a hurricane must be in essential balance, that you were dealing with a balanced flow, not an inertial gravity oscillation . . .* [*Earlier authors*] *had dealt with hurricane motions as a sort of gigantic convection cell. I knew that couldn't be correct, but I was still puzzled by the existence of conditional instability. But it was really Ooyama who pointed out that, despite the fact that the individual cumulus cells were conditionally unstable, that the hurricane as a whole was stable.*"

The balance assumption was the crucial new step made in 1960s. This assumption does permit accelerations in the tangential direction, but these are constrained by the condition of thermal wind balance (see section 5.5). In other words, the tangential accelerations and the accompanying radial circulation are only required to keep the vortex in thermal wind balance in the presence of diabatic heating and sources or sinks of angular momentum. Linear analysis together with computer integrations of these models reproduced many of the salient features of mature tropical cyclones.

The assumption of hydrostatic balance was probably the most controversial, because it explicitly

excluded vertical accelerations and convection from the model. In the early 1960s there were no detailed measurements of vertical velocities in tropical cyclones (as those shown in fig. 5.12). It was generally thought that the magnitudes of the vertical velocities and vertical accelerations in the eyewall clouds of a tropical cyclone were comparable to the vertical velocities and vertical accelerations in the most intense thunderstorms (see fig. 5.6b). The assumption was therefore difficult to justify. Despite this it was hypothesized that the motions associated with the cumulus clouds could be regarded as unbalanced turbulence compared to the balanced motions associated with the vortex, and that this unbalanced turbulence by itself is unimportant to the evolution (the growth and decay) of the vortex. Therefore, the motion in the model was assumed to be in balance at all times. Recent measurements (see section 5.5) are showing that the balance assumption is in fact quite accurate as far as relatively intense cyclones are concerned. It seems, therefore, that the bulk of the eyewall clouds are a direct result of the *forced* upward motion, not of hydrostatic conditional instability.

Diabatic heating due to latent heat release in cumulus clouds as well as heating due to turbulent sensible heat fluxes from the sea surface are treated alike in the balanced model, namely as a *prescribed heat source*. The way in which the heat source is prescribed poses great theoretical problems, because this heat source (especially the latent heat release) is determined strongly by the unbalanced part of the motion field (see eq. 6.1). Many authors [e.g., Ooyama 1969] have related the heating to the boundary layer convergence.

But, whatever the precise relation between heating and balanced motion, this heating serves as a continuous disturbance to the state of balance (especially gradient wind balance). According to the balanced model, the (inertially and hydrostatically) stable atmosphere reacts to this effect by adjusting to a new state of balance, which in many cases, but not all [see van Delden 1989a,b], is such that the vortex intensifies. This forced adjustment is accomplished by a secondary (radial) circulation, as shown in fig. 5.10 and described mathematically by eq. (5.39). The vortex evolves slowly through a succession of balanced states.

Since convection itself is neglected, it is better to use the term "balanced thermal cyclone theory" instead of the term "convective cyclone theory" to designate the theory put forward by the above-mentioned authors between 1964 and 1969. It is referred to by many as "Conditional Instability of the Second Kind" (CISK)*). The balanced thermal cyclone theory emphasises that it is diabatic heating (which encompasses both latent heat release and sensible heating) which is important to the growth of the cyclone, not convection.

In this section we will show that diabatic heating in a rotating environment may influence the motion field in more than one way. In order to understand the dynamics of cumulus convection and conditional instability (see section 6.1) we need only to allude to the role of diabatic heating (latent heat release) as a source of buoyancy. But, as far as the tropical cyclone is concerned, the role of diabatic heating as a

*) The term "Conditional Instability of the Second Kind" was introduced by Charney and Eliassen [1964]. The linear analytical theory associated with this concept, as put forward by these authors, has unfortunately led to much confusion. Some have even rejected CISK as a "useless hypothesis" [e.g., Emanuel 1991]. Some assumptions made by Charney and Eliassen [1964] are indeed doubtful or confusing. However, Charney and Eliassen as well as Ooyama [1964] should get credit for focussing on the role played by diabatic heating and frictional convergence, as well as for making the far from trivial assumption of thermal wind balance. With this assumption the dynamics of the cyclone was separated from the much more complicated dynamics of cumulus convection. In other words, the tropical cyclone was classified as a "balanced" weather system. Using the ideas put forward by Charney and Eliassen, subsequent authors constructed numerical models which produced realistic simulations of the nonlinear evolution of a tropical cyclone [e.g., Ooyama 1969, Sundquist 1970]. It should be noted that Eliassen and Kleinschmidt [1957] and Yanai [1964] had also made an explicit distinction between unbalanced and balanced motions in a tropical cyclone. According to these authors, the structure and growth (not the genesis!) of a tropical cyclone could be explained by considering explicitly only the balanced part of the motion.

source of upper tropospheric pressure perturbations as well as a source and/or sink of potential vorticity are probably more important than its role as a source of buoyancy.

Diabatic heating as a source of buoyancy. We will proceed with the tropical cyclone later in this section. Let us first summarize the effect of a diabatic heat source in a *non-rotating* atmosphere. As long as diabatic heat sources are limited in extent and in duration, they will function principally as a *source of buoyancy*. Heated air parcels will temporarily be out of equilibrium with the environmental vertical pressure gradient and will, therefore, be accelerated vertically. In a *stably stratified* non-rotating atmosphere two cases can be distinguished:

(1) The evanescent or potential flow case. This is the case if the time-scale of the forcing is shorter than the buoyancy period. The heated air parcel will rise until it is again in hydrostatic balance with the environment. However, since the heating is applied over a relatively short period, it will not lead to significant thermodynamic changes.

(2) The oscillatory case. If the time-scale of the forcing is longer than the buoyancy period, the heated air parcel will oscillate around the initial position with a period proportional to the forcing time scale. The frequency, ω, of the buoyancy wave which is produced by the heating is given by the dispersion relation for buoyancy waves, eq. (4.21). The heated air parcel will oscillate at an angle to the horizontal in order to match the dominant frequency of the forcing. The potential energy, or buoyancy, will ultimately be radiated away with these buoyancy waves.

In a *rotating* atmosphere, a new eigenfrequency enters into the problem. The dispersion relation for waves in the Boussinesq approximation becomes

$$\omega^2 = N^2 \sin^2 \phi + F^2 \cos^2 \phi \tag{6.18}$$

(see eq. 4.64). In polar coordinates the inertial frequency, F, can be expressed as follows,

$$F^2 = r^{-3}\, \partial M_a^2 / \partial r = (2M_a/r^2)\zeta_{abs} \tag{6.19}$$

(see the definition of the parameter A below eq. (5.39)). Assuming $F < N$, we can now distinguish three cases:

(1) Potential flow regime, $\omega > N$. The atmosphere readjusts to hydrostatic balance without producing oscillations.

(2) Wave regime, $F < \omega < N$. The atmosphere reacts in the form of buoyancy-inertia waves. The potential energy is radiated away by these waves.

(3) Gradient wind adjustment regime, $\omega < F$. Waves are not possible. The atmosphere adjusts to gradient wind balance (5.33), which can be expressed in terms of the angular momentum, M_a, as

$$M_a^2/r^3 - \tfrac{1}{4} f^2 r = \theta\, \partial \Pi / \partial r\,. \tag{6.20}$$

In a *baroclinic* balanced vortex in which there is a radial gradient in potential temperature, sources of buoyancy will produce oscillations around thermal wind balance (eq. 5.38). Thermal wind balance can be expressed in terms of M_a and θ as

$$(M_a^2/r^3 - \tfrac{1}{4} f^2 r)\, \partial\theta/\partial z + g\, \partial\theta/\partial r = (2M_a\theta/r^3)\, \partial M_a/\partial z\,. \tag{6.21}$$

The first term on the left-hand side is nearly always much smaller than the second term on the left-hand side (see section 5.5). So, approximately

$$\partial M_a^2/\partial z \approx (gr^3/\theta)\,\partial\theta/\partial r\,. \tag{6.22}$$

This is equivalent to making the shallow Boussinesq approximation. The frequency of the oscillations is given by eq. (4.64) in which S is now the frequency associated with the baroclinicity of the vortex. For an axisymmetric vortex S can be expressed as

$$S^2 = (g/\theta_0)\,\partial\theta_0/\partial r\,. \tag{6.23}$$

In a symmetric baroclinic vortex, ω^2, may become negative if $q<0$ (see section 4.2, eq. (4.70), and [Fjørtoft 1946, 1950, Ooyama 1966]). In the Boussinesq approximation q is related to Ertel's potential vorticity, Ω_{pot}, by

$$q = (2\rho g M_a/\theta_m r^2)\Omega_{pot}\,, \tag{6.24}$$

where Ω_{pot} can be expressed as

$$\Omega_{pot} = \frac{1}{\rho r}\left(\frac{\partial M_a}{\partial r}\,\frac{\partial\theta}{\partial z} - \frac{\partial M_a}{\partial z}\,\frac{\partial\theta}{\partial r}\right) \tag{6.25}$$

[e.g., Shutts 1981]. Recall that potential vorticity is conserved in adiabatic inviscid flow.

If the baroclinicity is sufficiently strong, q will become negative and symmetric disturbances will grow without limit (instability). It can be shown (see section 4.2 and Ooyama [1966]) that this criterion is equivalent to the condition

$$(\partial z/\partial r)_\theta > (\partial z/\partial r)_{M_a}\,. \tag{6.26}$$

In other words, the slope of the potential temperature surfaces must be greater than the slope of the angular momentum surfaces. This will only happen in the outflow leg of a relatively intense balanced warm-core cyclone.

Diabatic heating as a source of pressure perturbations. In a statically stable atmosphere the M_a and θ surfaces are oriented as shown in fig. 6.16. Movement of air parcels at an angle to M_a surfaces will be hampered by the horizontal pressure gradient force and the inertial forces, while movement at an angle to the isentropes will be hampered by the environmental hydrostatic vertical pressure gradient force. How then is the initial growth of a vortex possible?

The answer to this question lies in the fact that diabatic heating also serves as a source of pressure perturbations. Due to these pressure perturbations, air parcels can flow across ambient angular momentum surfaces and, thus, change the angular momentum distribution in a cyclone.

Suppose a circular heat source is centred at $r=0$ and at a certain unspecified height in the troposphere (see fig. 6.17a). In the vertical (r–z) plane this will induce an upward bulging of isobars above the heat source and a downward bulging of isentropes in the heating area. Neglecting further

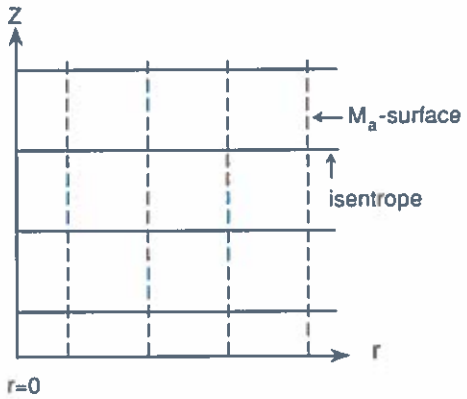

Fig. 6.16. The distributions of angular momentum, M_a (dashed line), and potential temperature (solid line) as a function of height (z) and horizontal distance (in this case the radius r) in a statically stable barotropic rotating atmosphere. θ increases upwards and M_a increases with increasing r.

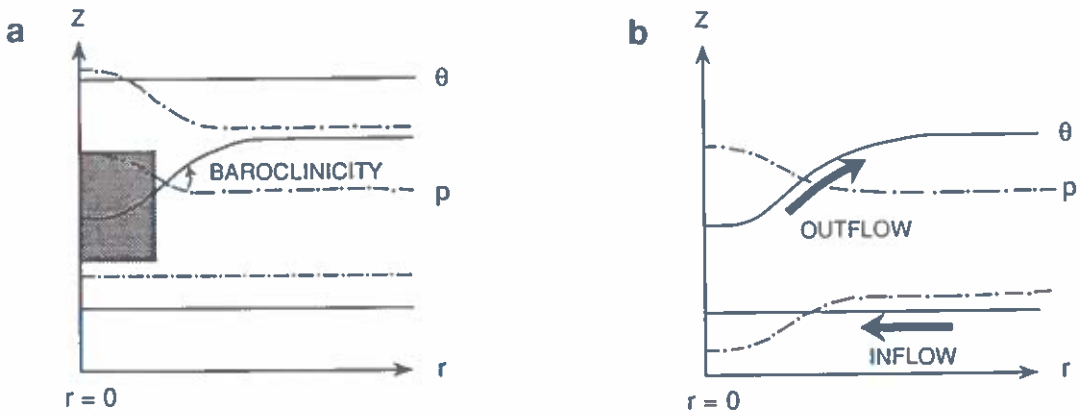

Fig. 6.17. (a) The distributions of potential temperature (θ) and pressure (p) as functions of r and z after the dark region has been heated. (b) The direction of the flow as a result of this heating and the new pressure distribution resulting from this flow.

diabatic effects, this will lead to an outflow of air along isentropes above the heat source. This outflow will lead to a pressure drop below and therefore inflow (see fig. 6.17b). In a non-rotating atmosphere this inflow will cancel the initial pressure drop. However, in a rotating atmosphere ($f \neq 0$) the pressure drop at low levels will be only partially cancelled, because ambient air with finite angular momentum, $M_a = fr^2/2$ (assuming that the air at large radii is at rest), is advected into the heating area. Since M_a is conserved, the tangential velocity, u, must increase as air is drawn into the heating area. The inertial forces acting on an air parcel in an axisymmetric vortex are the Coriolis force and centrifugal force. Both will act to decelerate an inward travelling air parcel. The net inertial force per unit mass F_I, can be expressed in terms of M_a and r as

$$F_I = M_a^2/r^3 - \tfrac{1}{4} f^2 r \,. \tag{6.27}$$

We see that the outward force increases drastically as the parcel comes closer to the axis ($r = 0$) (see fig. 6.18). A pressure gradient is needed to counteract this force. Therefore, the pressure gradient initially

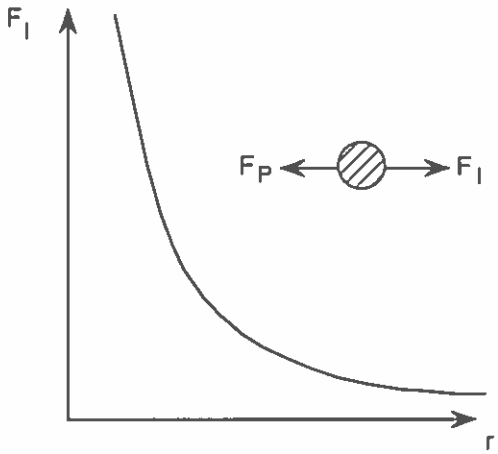

Fig. 6.18. The inertial force, F_I, on an air parcel as a function of r for a fixed finite value of the angular momentum, M_a.

set up by the outflow aloft will not be completely offset by the inflow. That is, in the final adjusted state there is a balance between the inertial forces and the pressure gradient force.

Let us assume that the outflow aloft can maintain a steady constant pressure gradient force, F_P, at low levels at a radius $r = r_c$. We can then calculate the radius of origin, R_0, of air parcels with just enough angular momentum to produce a balance between F_I and F_P at $r = r_c$, i.e.

$$(M_a)_0^2/r_c^3 - \tfrac{1}{4} f^2 r_c = F_P \,, \tag{6.28}$$

where $(M_a)_0$ is the angular momentum of the air parcel at $r = R_0$. Solving eq. (6.28) for R_0, using the definition of M_a, (5.41), yields

$$R_0 = -u_0/f + (u_0^2/f^2 + r_c^2\sqrt{4F_P/f^2 r_c + 1})^{1/2} \,, \tag{6.29}$$

where u_0 is the tangential velocity of the air parcel at $r = R_0$. Note that if F_P is positive (in a low-pressure system), this equation has a solution, but if F_P is sufficiently negative (in a high-pressure system), there is no solution. If $u_0 = 0$,

$$R_0 \approx (4F_P r_c^3/f^2)^{1/4} \,. \tag{6.30}$$

By analogy with the Rossby radius of deformation, we will call this length scale the *radius of influence*.

Figure 6.19 visualizes the dependence of the radius of influence on F_P for two values of u_0. We see that, for representative pressure gradients per unit mass of 0.01 m s^{-2} (if $\rho = 1$ kg m^{-3} this is equivalent to 10^{-2} Pa m^{-1} or 1 hPa per 10 km) to 0.2 m s^{-2}, R_0 lies in between 40 km and nearly 100 km if $u_0 = 0$. These typically are meso-scale dimensions. If the air parcel has a finite tangential velocity, u_0, before it is drawn into the area where the steady pressure forcing is taking place, the radius of origin is considerably less. It may even become smaller than r_c. This implies that air must be drawn from inside the vortex if tangential velocities are sufficiently high.

In reality, some angular momentum will however be lost due to frictional dissipation in the boundary layer. Therefore, an air parcel arrives in the centre of the cyclone with a lower value of M_a than it had

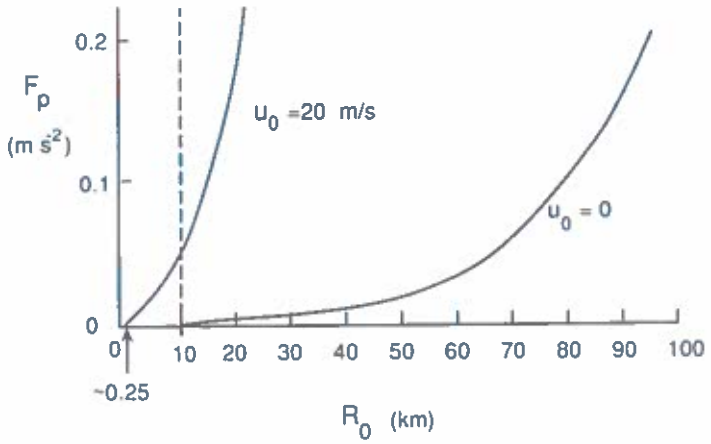

Fig. 6.19. Dependence of the radius of influence on the pressure gradient force, F_p, for two values of u_0 (r_z = 10 km and $f = 10^{-4}$ s^{-1}). See the text for further information.

when it started its journey inwards. This implies that the air parcel must in fact have a larger radius of origin in order to achieve balance.

Diabatic heating as a source or sink of potential vorticity. The initiation of a vortex requires quite a bit of pressure forcing. It is thus not surprising that tropical cyclones are never observed to appear spontaneously and grow exponentially in intensity right from the start. As many writers [e.g., Riehl 1951] have pointed out, intense tropical cyclones always evolve from some disturbance of lesser intensity, which may have been in existence for a long time. However, once the intensification has started, further intensification will require less and less effort. The reason for this has to do with the warm core. The isentropes will become more and more inclined to the horizontal as the vortex intensifies. Because the vortex strives towards thermal wind balance, this must be accompanied by a concurrent tilting to the vertical of M_a surfaces. The M_a and θ surfaces will thus come closer and closer together (see fig. 6.20). This will reduce the ambient symmetric stability and thus facilitate the outflow. Air parcels, moving along isentropes, will hardly have to deviate from the prevailing M_a surface. This argument suggests that the chances of further deepening of the vortex increase as the core becomes warmer. A cold-core vortex will probably not deepen at all due to diabatic heating. To understand this requires a short discussion of the role of diabatic heating as a sink of potential vorticity.

The potential vorticity is proportional to the tangent of the angle between the θ surfaces and M_a surfaces (see section 4.2, eqs. (4.72, 4.73)). This implies that the potential vorticity decreases as the vortex becomes warmer (see fig. 6.20 and eq. (6.25)). This suggests that the diabatic heating functions as a sink of potential vorticity. Figure 6.21a shows the change in the potential temperature profile if there is a heat source at the earth's surface. The decrease of N at low levels due to such a heat source will indeed lead to a decrease in the potential vorticity. When the heat source is located higher up in the atmosphere, the effect on the potential vorticity distribution is a little more complicated (see fig. 6.21b). In this case the potential vorticity decreases above the heat source while it increases below the heat source. It should be remarked that there is still some discussion on the interpretation of the effect of diabatic heating and diffusion on the potential vorticity distribution [see Haynes and McIntyre 1987, 1990, Danielsen 1990].

The most important sources of heat in a tropical cyclone are the sensible heat flux from the ocean

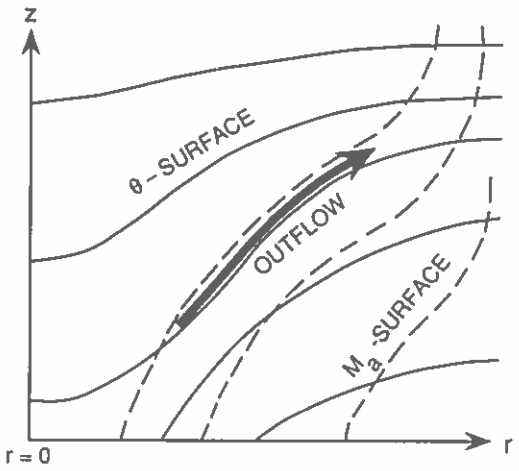

Fig. 6.20. The distributions of angular momentum, M_a (dashed line), and potential temperature (solid line) in a stable baroclinic warm core cyclone. Compare this figure with fig. 6.16.

and latent heat release due to condensation in cumulus clouds. Although the importance of latent heat release has been stressed the most in the past, it is becoming increasingly clear recently that the sensible heat flux from the ocean is probably much more important. Emanuel [1986b], Rotunno and Emanuel [1987] and Emanuel and Rotunno [1989] have stressed this point for both the polar low and the tropical cyclone. These authors even go so far as to assert that latent heat release plays no role in vortex intensification. They claim that the net effect of latent heat release, adiabatic cooling and condensate loading are not sufficient to make the rising air positively buoyant compared to the subsiding air in the environment. In other words, CAPE ≤ 0, in spite of latent heat release (see eq. 5.22). The assertion makes clear that the secondary circulation is not a convection cell driven by buoyant instability. Rather, it is driven by upper-level positive pressure perturbations caused by the heating and expansion of the air below. One result of the forced secondary circulation is that potentially warm air is advected into the eye from the stratosphere. The warm core is principally a result of this effect.

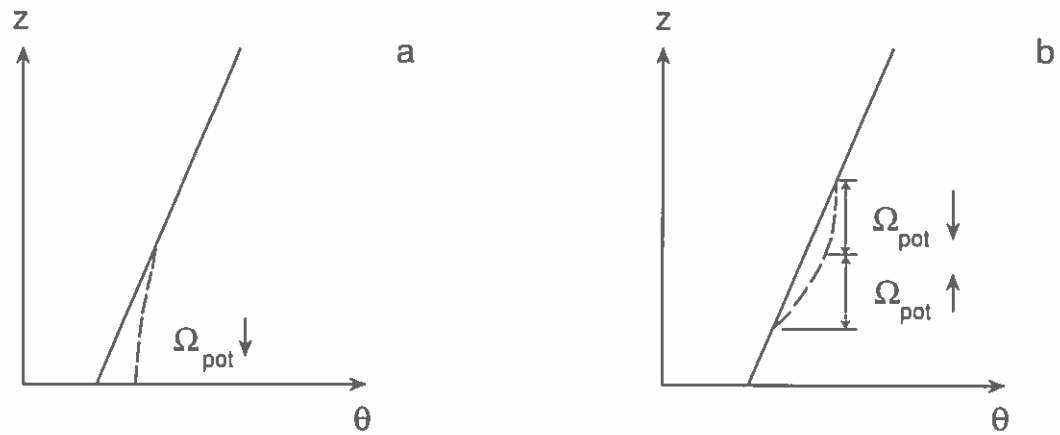

Fig. 6.21. The change in the vertical potential temperature profile (solid line: initial; dashed line: final) as a consequence of diabatic heating and the associated local change in the potential vorticity: (a) near the earth's surface and (b) somewhere higher in the atmosphere. See the text for further information.

If, indeed, the most important heat source is the sensible heat flux from the ocean, the potential vorticity will decrease steadily until it is zero. Shutts [1981] investigated the structure of a balanced vortex with zero potential vorticity. The specification of the potential vorticity distribution together with the balance conditions fixes the velocity distribution and temperature distribution. This is called the "invertibility principle" by Hoskins et al. [1985] [see also Egger 1990b]. The calculations made by Shutts [1981] reveal that the zero potential vorticity balanced vortex has a structure very similar to a real hurricane. This lends additional support to the conjecture that the hurricane is a balanced structure (close to thermal wind balance).

A vortex in the atmosphere is not a closed system. Neglecting diabatic heating, friction and other non-conservative forces, potential vorticity is materially conserved [e.g., Pedlosky 1987]. Thus, positive potential vorticity from the static barotropic environment will be drawn in at low levels and, probably also, from the stratosphere into the eye. Therefore, the potential vorticity will approach zero only in the outflow leg near the potential vorticity sink. Because the resistance to displacements in the r–z plane in a balanced symmetric vortex (the stiffness; see section 4.2) is proportional to the potential vorticity, this actually turns out to be very advantageous for further intensification of the vortex. Radial flow will only be hampered in the inflow leg, where the stiffness with respect to symmetric disturbances is high, and not in the outflow leg. This will obviously lead to a pressure decrease at low levels.

More details about the structure of a balanced vortex such as a tropical cyclone, in relation to potential vorticity can be found in papers by Shutts and Thorpe [1978], Thorpe [1985] and Schubert and Alworth [1987].

The effect of diabatic heating on cyclone growth as a function cyclone baroclinicity. The qualitative remarks discussed in the previous subsection are supported by calculations performed by van Delden [1989a,b]. Ooyama's [1969] balanced axisymmetric cyclone model (see fig. 3.4) was employed to calculate the radial circulation needed to maintain balance in the presence of self-induced diabatic heat sources in a vortex with a prescribed tangential velocity distribution. The diabatic heating in this model is parameterised by a mass flux "Q" (units: m s^{-1}), between layers 1 and 2. This mass flux functions as a sink of potential vorticity in the upper layer (2) and a source of potential vorticity in the lower layer (1)*). Therefore, considering only its effect on the potential vorticity distribution, "Q" is a more accurate parameterisation of latent heat release than of sensible heat fluxes at the earth's surface.

The model also allows for boundary layer convergence in the form of a vertical mass flux (w) into the lower layer (1) from below (see fig. 3.4). In fact, "Q" is set proportional to w by

$$\text{"}Q\text{"} = \eta w^{+} \; ; \quad w^{+} = w \quad \text{if } w > 0 \, , \quad w^{+} = 0 \quad \text{if } w \leq 0 \, . \tag{6.31}$$

A linear analysis of this model [Ooyama 1969] shows that the vortex will grow only when $\eta > 1$. That is, if there is a net mass flux out of the lower layer (1).

The central ($r = 0$) surface pressure decrease needed to maintain the model vortex in thermal wind balance is plotted in fig. 6.22 as a function of vortex baroclinicity for a vortex with a prescribed radial profile of tangential velocity,

*) The potential vorticity in an individual layer in Ooyama's model is defined as absolute vorticity divided by layer thickness (see also section 5.1). Therefore, strictly speaking, it is not the same as Ertel's potential vorticity, which apart from a factor $1/\rho$ is defined as the scalar product of the vorticity vector and the potential temperature gradient (see eq. 6.25). However, both have the property of being conserved in the absence of diabatic processes and both are proportional to the vorticity.

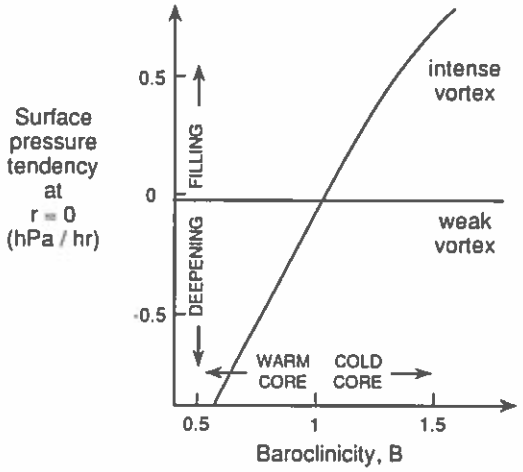

Fig. 6.22. The central deepening rate as a function of vortex baroclinicity, B, for an intense vortex (maximum tangential velocity = 30 m s^{-1}) and for a weak vortex (maximum tangential velocity = 5 m s^{-1}) [van Delden 1989b].

$$u_j = \frac{2\hat{u}_j r}{\hat{r}[1 + (r/\hat{r})^2]}, \tag{6.32}$$

where $\hat{r}$ is the radius of maximum tangential wind and $\hat{u}_j$ is the maximum tangential wind in layer j. This wind profile is very similar to that observed in hurricane Alicia, shown in fig. 5.11. The calculations were performed for two cases: a weak vortex (maximum tangential velocity 5 m s^{-1}) and a strong vortex (maximum tangential velocity 30 m s^{-1}). The radius of maximum wind was 50 km in both cases. The baroclinicity, B, is defined as $B = u_2/u_1$. In a warm-core vortex $B < 1$, since u decreases with height (see fig. 5.13). In a cold-core vortex $B > 1$. More details concerning the calculations can be found in van Delden [1989a,b].

The results show that a weak vortex will hardly deepen, independent of the baroclinicity. As expected, the deepening rate increases as the core becomes warmer. The results also show that a cold core vortex will tend to fill (at least initially) as a result of diabatic heating. The reasons for this are quite subtle. It would be going too far to discuss them here. They are discussed by van Delden [1989a,b].

On the basis of the foregoing we may conclude that an important property of diabatic heating, as far as its effect on the deepening of a balanced vortex is concerned, is its role as a *sink* of potential vorticity in the outflow leg of the radial circulation. This clearly promotes the outflow relative to the inflow and, thus, further intensification. Since the sink of potential vorticity is most effective in intensifying the cyclone if the diabatic heating is located at low levels, this explains the general finding in numerical and theoretical studies of tropical cyclones and polar lows and mid-latitude cyclones that low-level heating is more efficient at intensifying a vortex than upper-level heating [Sardie and Warner 1983, Hack and Schubert 1986].

There is of course a lot more to be said about the fascinating dynamics of tropical cyclones. For example, what happens if the outflow becomes (conditionally) baroclinically unstable (see sections 4.2 and 6.1)? Does this lead to enhanced cyclone intensification? What dynamical processes govern the

formation of convective spiral bands and the secondary wind maxima in conjunction with concentric eyewalls [Willoughby et al. 1982, 1984, Willoughby 1990a]? How do non-axisymmetric processes, especially in the outer part of the cyclone [e.g., Flatau and Stevens 1989], affect the cyclone as a whole? Remember that M_a is not conserved when there are azimuthal pressure gradients. Another question concerns the relation or feedback between the heat source and the cyclone. These questions are still under active investigation. Interested readers are referred to the books by Palmén and Newton [1969], Simpson and Riehl [1981], Anthes [1982], Elsberry et al. [1987] and Cotton and Anthes [1989], the reviews by Yanai [1964], Anthes [1974], Ooyama [1982], Willoughby [1988] and Emanuel [1991], and recent observational papers by Weatherford and Gray [1988] and Willoughby [1990a]. Other discussions of the tropical cyclone in this review can be found in chapter 2 and sections 3.3, 3.4, 5.3 and 5.5.

7. Conclusion

7.1. Prediction of meso-scale weather systems

In view of the fact that many, if not most, significant meteorological events are associated with meso-scale features, and since the prediction of the weather is an important activity of meteorologists, a short section about meso-scale weather prediction is in order.

Within this context, we should start by recapitulating the principal idea which this review attempts to convey to the reader, namely, the idea that the meso-scale represents a transition regime between two relatively well defined atmospheric flow regimes, i.e. the large-scale balanced regime and the small scale unbalanced regime (see e.g., fig. 5.4). One consequence of this fact is that no unique scaling of the basic hydrodynamic and thermodynamic equations, such as that performed by Charney [1948] and Eliassen [1948] for large-scale weather systems (for a more recent reference on this topic, see Lynch [1989]), will produce a simplified set of equations that will apply under all meso-scale meteorological conditions. A numerical model which aims to predict the weather down to the meso-scale will therefore have to be based on the complete set of equations, including a rather detailed description of the local forcing functions, such as variations in terrain, condensation heating and evaporative cooling, infrared and short-wave radiation, evaporation and conduction of heat at the earth–air interface and turbulent transfer of heat and moisture upward in the boundary layer. This obviously is a very extensive and difficult task.

The predictability of the weather is determined principally by (a) the knowledge of the initial conditions, (b) the knowledge of the boundary conditions in space, and (c) the representation of the forcing function in the model.

The *initial condition* is obtained from a combination of observations, a model prediction from a previous state (e.g., six hours earlier), which functions as a guessfield, and the requirement that the velocity field and the pressure field are in some kind of dynamic balance. This last requirement is imposed in order to prevent as much as possible the excitation of gravity waves in the model from imbalances due to observation errors. However, there is the danger that this condition also filters out real imbalances that are essential for the (further) development of certain meso-scale weather systems. Another problem with the balance condition is that the equations describing the balanced state must be of the elliptic type. Only then can a unique initial state be found (see section 5.5). This is not always the case, especially in the equatorial region, where the Coriolis parameter approaches zero [Tribbia 1981]. The paper by Heijboer et al. [1989] gives a good impression of the problems involved in initializing a

meso-scale forecasting model used in The Netherlands. Other recent papers which discuss the initialization and data assimilation problem applied to meso-scale weather prediction models are those by Briere [1982], Bijlsma and Hafkenscheid [1986] and Lilly [1990]. The opinion of many is that the spatial and especially the temporal resolution of the present upper air observation system is inadequate for numerical meso-scale weather forecasting. We will have to await the installation of meso-scale networks of radars measuring vertical profiles of wind and temperature. In the United States this is now carried out under the name NEXRAD [Lilly 1990]. It appears that soundings from satellites at this moment are so inaccurate that they hardly contribute to the quality of the weather forecast [Smith 1991]. This situation will probably improve in ten years or so with the advent of the next generation of satellites.

Due to limits on computer-power, a numerical meso-scale weather prediction model will necessarily cover a limited area. Thus, *lateral boundary conditions* are required. These boundary conditions can be obtained from the output of a numerical model with a lower resolution covering a larger area (e.g., the whole globe). An example of an operational meso-scale limited area model is described by Golding [1990]. This non-hydrostatic model, based on the model developed by Tapp and White [1976], has a horizontal grid distance of 15 km and 16 levels in the vertical between 10 m and 12010 m. It covers an area of 1400 by 1400 km. Of course, a whole spectrum of models exists. For example, the global hydrostatic models used for medium range (2 to 10 day) weather forecasting have a resolution corresponding to a finite difference grid of about 100 km with about 20 levels between the earth's surface and the top of the atmosphere ($p = 0$) [e.g., Bengtsson 1990]. Krishnamurti et al. [1990] give an extensive overview of existing limited area hydrostatic models (which lie in between the two models mentioned above) and the associated numerical techniques [see also Pielke 1984]. A study performed by Anthes et al. [1989] has shown that the lateral boundary condition is the most important factor determining the skill of a limited area model for forecast periods up to 36 h. This also demonstrates that large-scale motions have a major, if not dominant, effect on the evolution of the smaller-scale (i.e. meso-scale) motions.'

The representation of the *forcing function* depends on our theoretical knowledge of the physical processes responsible for the forcing. Finding a good representation of the forcing function, especially when this forcing is operating on a relatively small scale (such as near the earth's surface), is probably the most difficult aspect of numerical modelling of meso-scale atmospheric circulations. For example, the evolution and, therefore, the predictability of a field of stratocumulus clouds or closed convection cells depends strongly on the long-wave radiative cooling at cloud top and the short-wave radiative warming of the cloud by absorption [Driedonks and Duynkerke 1989]. Squall lines or intense thunderstorms, on the other hand, are forced very strongly by the large-scale flow and also by the terrain (see section 6.4). For the simulation and prediction of the formation of a polar low, tropical cyclone or small-scale intense mid-latitude cyclone [e.g., Shutts 1990] the representation of the forcing due to latent heat release, which may also operate on a very small scale (smaller than the distance between grid points in the model), is of crucial importance. However, we need not be too pessimistic: the study by Anthes et al. [1989] has shown that relatively simple model parameterizations of the forcing produce nearly the same forecast skill as the more complex schemes.

7.2. Final remarks

Clearly this review is not exhaustive as far as the many individual meso-scale weather systems are concerned. Meso-scale weather phenomena such as thermally driven mountain and valley winds [e.g.,

Blumen 1990], along-shore surges [e.g., Mass and Albright 1987, Dorman 1988], orographic blocking and channelling of a cold front [e.g., Hoinka and Heimann 1988], coastal fronts and coastal lows [e.g., Pike 1989, van den Berg 1987, Økland 1990, Reason and Jury 1990], drylines [e.g., Weston 1972, Schaefer 1986] and lee-side lows [e.g., Smith 1982] (see also fig. 6.9a) have received little or no attention.

As an alternative approach, we have not taken the weather phenomena themselves, but the dynamical processes which are common to these weather phenomena as the guide to the review. Examples of such dynamical processes are hydrostatic instability, conditional static instability, adjustment to hydrostatic balance, adjustment to thermal wind balance, dynamical instability and baroclinic instability. A theoretical examination of these processes, in which we decided to neglect the earth's curvature (the β-effect), provided us with several characteristic non-dimensional parameters, characteristic frequencies and wavelengths which govern the behaviour of a wide variety of circulations which come under the meso-scale. The limiting wavelengths are the depth of the flow, at the small-scale end, and the Rossby radius of deformation at the large-scale end. The limiting frequencies are the Brunt–Väisälä frequency at the high-frequency side and the Coriolis parameter at the low-frequency side. A rich variety of dynamical processes fall within these limiting time and length scales. The specific meso-scale weather phenomena have served as illustrations of these processes.

An important distinction has been made between balanced and unbalanced meso-scale circulations (see sections 5.4 and 5.5). An example of a balanced system is a tropical cyclone. An example of an unbalanced system is a thunderstorm. The meso-scale, in fact, represents the transition between the unbalanced regime and the balanced regime. Whether the atmosphere produces balanced or unbalanced systems depends on the nature (time scale and length scale) of the forcing. The concept of forcing is thus a central topic of this review.

In summary, not the weather phenomena themselves, but the dynamical processes common to all meso-scale weather events are the key to this review. Discussions of specific meso-scale weather systems are woven into the review as illustrations of these dynamical processes. I hope that this approach will give the reader a better understanding of the concept of meso-scale as well as of the similarities and differences between specific meso-scale weather phenomena.

Acknowledgements

I would like to thank Dale Durran (Seattle, USA), Dieter Etling (Hannover, Germany), Helmut Kraus (Bonn, Germany), Hans Oerlemans (Utrecht) and an anonymous reviewer for very useful comments on the first version of the manuscript. Discussions with Helmut Kraus have led to a better presentation of the reasons behind the structure of this review (the headings: Stability, Adjustment and Forcing). I would like to thank Sheila McNab for advice on the English language and Sejo Kruizinga for helping me to obtain data from the ECMWF in Reading for the case study of the thunderstorm. I am also indebted to the "Tekenkamer" of the Institute of Earth Sciences (University of Utrecht) for most of the figures; the Dutch Weather Service (KNMI) in De Bilt for the sea breeze data and the polar low data; the Belgian Weather Service in Uccle and the German Weather Service in Offenbach for data concerning the polar low (figure 5.15); and the University of Dundee for the satellite photographs. The writing of this review was done in part at the Free University of Amsterdam.

References

Abarbanel, H.D.I., D.D. Holm, J.E. Marsden and T. Ratiu, 1984, Richardson number criterion for the nonlinear stability of three-dimensional stratified flow, Phys. Rev. Lett. 52, 2352.

Adrian, G. and F. Fiedler, 1991, Simulation of stationary wind and temperature fields over complex terrain and comparison with observations, Beitr. Phys. Atmosph. 64, 27–48.

Agee, E.M., 1987, Mesoscale cellular convection over the oceans, Dyn. Atmos. Oceans 10, 317–341.

Anthes, R.A., 1971, Iterative solutions to the steady-state axisymmetric boundary-layer equations under intense pressure gradient, Mon. Weather Rev. 99, 261–268.

Anthes, R.A., 1974, The dynamics and energetics of mature tropical cyclones, Rev. Geophys. Space Phys. 12, 495–522.

Anthes, R.A., 1982, Tropical cyclones, their evolution, structure and effects, Meteorological Monographs, Vol. 41 (American Meteorological Society, Boston).

Anthes, R.A. and T.T. Warner, 1978, Development of hydrodynamic models suitable for air pollution and other meso-meteorological studies, Mon. Weather Rev. 106, 1045–1078.

Anthes, R.A., Y.-H. Kuo, E.-Y. Hsie, S. Low-Nam and T.W. Bettge, 1989, Estimation of skill and uncertainty in regional numerical models, Q. J. R. Meteorol. Soc. 115, 763–806.

Arakawa, H., ed., 1969, Climates of northern and eastern Asia, World Survey of Climatology, Vol. 8 (Elsevier, Amsterdam).

Asai, T., 1970a, Three-dimensional features of thermal convection in plane Couette flow, J. Meteorol. Soc. Japan 48, 18–29.

Asai, T., 1970b, Stability of plane parallel flow with variable vertical shear and unstable stratification, J. Meteorol. Soc. Japan 48, 129–139.

Asai, T. and A. Kasahara, 1967, A theoretical study of compensating downward motions associated with cumulus clouds, J. Atmos. Sci. 24, 487–496.

Asai, T. and I. Nakasuji, 1973, The stability of Ekman boundary layer flow with thermally unstable stratification, J. Meteorol., Soc. Japan 51, 29–42.

Asai, T. and I. Nakasuji, 1977, On the preferred mode of cumulus convection in a conditionally unstable atmosphere, J. Meteorol. Soc. Japan 55, 151–167.

Atkinson, B.W., 1981, Meso-scale Atmospheric Circulations (Academic Press, New York).

Bacmeister, J.T. and R.T. Pierrehumbert, 1988, On high drag states and nonlinear flow over an obstacle, J. Atmos. Sci. 45, 63–80.

Baines, P.G., 1987, Upstream blocking and airflow over mountains, Ann. Rev. Fluid Mech. 19, 75–97.

Baines, P.G. and B.P. Leonard, 1989, The effects of rotation on flow of a single layer over a ridge, Q. J. R. Meteorol. Soc. 115, 293–308.

Barnes, G.M. and M.A. LeMone, 1988, The third conference on mesoscale processes, 20–26 August, 1987, Vancouver B.C., Canada, Bull. Am. Meteorol. Soc. 69, 396–405.

Barry, R.G., 1981, Mountain Weather and Climate (Methuen, New York).

Batchelor, G.K., 1967, An Introduction to Fluid Dynamics (Cambridge Univ. Press, Cambridge).

Beebe, R.G. and F.C. Bates, 1955, A mechanism for assisting in the release of convective instability, Mon. Weather Rev. 83, 1–10.

Bénard, H., 1900, Les tourbillons cellulaires dans une nappe liquide, Rev. Gén. Sci, Pur. Appl. 11, 1261–1271, 1309–1328.

Bengtsson, L., 1990 Advances in numerical prediction of the atmospheric circulation in the extratropics, in: Extratropical Cyclones, eds C.W. Newton and E.O. Holopainen (American Meteorological Society, Boston) pp. 194–220.

Bennetts, D.A. and B.J. Hoskins, 1979, Conditional symmetric instability – a possible explanation for frontal rainbands, Q. J. R. Meteorol. Soc. 105, 945–962.

Bennetts, D.A. and P. Ryder, 1984, A study of mesoscale convective bands behind cold fronts, Part I. Mesoscale organization, Q. J. R. Meteorol. Soc. 105, 121–145.

Bennetts, D.A., J.R. Grant and E. McCallum, 1988, An introductory review of fronts. Part 1: theory and observations, Met. Mag. 117, 357–370.

Bergeron, T., 1928, Über die driedimensional verknüpfende Wetteranalyse, Geofys. Publ. 5 (6), 1–111.

Bergeron, T., 1954, The problem of tropical hurricanes, Q. J. R. Meteorol. Soc. 80, 131–164.

Bijlsma, S.J. and L.M. Hafkenscheid, 1986, Initialization of a limited area model: a comparison between normal mode and bounded derivative methods, Mon. Weather Rev. 114, 1445–1455.

Bjerknes, J., 1938, Saturated ascent of air through a dry-adiabatically descending environment, Q. J. R. Meteorol. Soc. 64, 325–330.

Bluestein, H.B., 1986, Fronts and jet streaks: a theoretical perspective, in: Mesoscale Meteorology and Forecasting, ed. P.S. Ray (American Meteorological Society, Boston) pp. 173–215.

Bluestein, H.B. and M.H. Jain, 1985, Formation of mesoscale lines of precipitation: severe squall lines in Oklahoma during spring, J. Atmos. Sci. 42, 1711–1732.

Blumen, W., ed., 1990, Atmospheric Processes over Complex Terrain, Meteorological Monographs, Vol. 23 (American Meteorological Society, Boston).

Bosart, L.F., C.J. Vaudo and J.H. Heldon Jr., 1972, Coastal frontogenesis, J. Appl. Meteorol. 11, 1236–1258.

Boussinesq, J., 1903, Theorie Analytique de la Chaleur 2 (Gauthier-Villars, Paris) 172.

Bradbury, T.A.M., 1990, Links between convection and waves, Met. Mag. 119, 112–120.

Bretherton, C.S., 1987, A theory for nonprecipitating convection between two parallel plates. Part II: linear theory and cloud structure, J. Atmos. Sci. 44, 1809–1827.
Bretherton, C.S. and P.K. Smolarkiewicz, 1989, Gravity waves, compensating subsidence and detrainment around cumulus clouds, J. Atmos. Sci. 46, 740–759.
Briere, S., 1982, Nonlinear normal mode initialization of a limited area model, Mon. Weather Rev. 1166–1186.
Brown, R.A., 1970, A secondary flow model for the planetary boundary layer, J. Atmos. Sci. 27, 742–757.
Brown, R.A., 1972, On the inflection point instability of a stratified Ekman boundary layer, J. Atmos. Sci. 29, 850–859.
Brown, R.A., 1980, Longitudinal instabilities and secondary flows in the planetary boundary layer: a review, Rev. Geophys. Space Phys. 18, 683–697.
Browning, K.A., 1986, Morphology and classification of middle-latitude thunderstorms, in: Thunderstorm Morphology and Dynamics, 2nd Ed., ed. E. Kessler (University of Oklahoma Press, Norman) pp. 133–152.
Browning, K.A., 1989, The mesoscale data base and its use in mesoscale forecasting, Q. J. R. Meteorol. Soc. 115, 717–762.
Browning, K.A., 1990, Organization of clouds and precipitation in extratropical cyclones, in: Extratropical Cyclones, eds C.W. Newton and E.O. Holopainen (American Meteorological Society, Boston) pp. 129–153.
Browning, K.A., M.E. Hardman, T.W. Harrold and C.W. Pardoe, 1973, The structure of rainbands within a midlatitude depression, Q. J. R. Meteorol. Soc. 99, 215–231.
Businger, S. and R.J. Reed, 1989, Cyclogenesis in cold air-masses, Weather Forecasting 4, 133–156.
Byers, H.R., and R.R. Braham Jr., 1949, The Thunderstorm (US Govt. Printing Office, Washington).
Chandrasekhar, S., 1961, Hydrodynamic and Hydromagnetic Stability (Oxford University Press, Oxford).
Chang, C.-P., 1970, Westward propagating cloud patterns in the tropical Pacific as seen from time-composite satellite photographs, J. Atmosph. Sci. 27, 133–138.
Chapman, S., and R.S. Lindzen, 1970, Atmospheric Tides, Thermal and Gravitational (Reidel, Dordrecht).
Charney, J.G., 1947, The dynamics of long waves in a baroclinic westerly current, J. Meterol. 4, 135–163 [reprinted in Lindzen et al. 1990, pp. 223–250].
Charney, J.G., 1948, On the scale of atmospheric motions, Geofys. Publ. 17(2) [reprinted in Lindzen et al. 1990, pp. 251–265].
Charney, J.G., 1973, in: Dynamic Meteorology, ed. P. Morel (Reidel, Dordrecht) pp. 97–352.
Charney, J.G. and A. Eliassen, 1964, On the growth of a hurricane depression, J. Atmos. Sci. 21, 68–75.
Chlond, A., 1988, Numerical and analytical studies of diabatic heating effect upon flatness of boundary layer rolls, Beitr. Phys. Atmosph. 61, 312–329.
Chopra, K.P., 1973, Atmospheric and oceanic flow-problems introduced by islands, Adv. Geophys. 16, 297–421.
Christie, D.R., 1989, Long nonlinear waves in the lower atmosphere, J. Atmos. Sci. 46, 1462–1491.
Clark, R.H., 1989, Sea-breezes and waves: the "Kalgoorie sea-breeze" and the "Goondiwindi breeze", Aust. Met. Mag. 37, 99–107.
Clark, T.L., 1979, Numerical simulations with a three-dimensional cloud model: lateral boundary condition experiments and multicellular severe storm simulations, J. Atmos. Sci. 36, 2196–2215.
Clark, T.L. and W.R. Peltier, 1977, On the evolution and stability of finite-amplitude mountain waves, J. Atmos. Sci. 34, 1715–1730.
Clark, T.L. and W.R. Peltier, 1984, Critical layer reflection and the resonant growth of nonlinear mountain waves, J. Atmos. Sci. 41, 3122–3134.
Cotton, W.R. and R.A. Anthes, 1989, Storm and Cloud Dynamics (Academic Press, New York).
Cotton, W.R., M.S. Lin, R.L. McAnelly and C.J. Tremback, 1989, A composite model of mesoscale convective complexes, Mon. Weather Rev. 117, 765–783.
Crook, N.A. and M.J. Miller, 1985, A numerical and analytical study of atmospheric undular bores, Q. J. R. Meteorol. Soc. 111, 225–242.
Cruette, D., 1976, Experimental study of mountain lee waves by means of satellite photographs and aircraft measurements, Tellus 28, 499–523.
Cullen, M.J.P., J. Norbury, R.J. Purser and G.J. Shutts, 1987, Modelling the quasi-equilibrium dynamics of the atmosphere, Q. J. R. Meteorol. Soc. 113, 735–757.
Dalu, G.A. and R.A. Pielke, 1989, An analytical study of the sea breeze, J. Atmos. Sci. 46, 1815–1825.
Danielsen, E.F., 1990, In defense of Ertel's potential vorticity and its general applicability as a meteorological tracer, J. Atmos. Sci. 47, 2013–2020.
Davies, H. C., 1984, On the orographic retardation of a cold front, Beitr. Phys. Atmosph. 57, 409–418.
Davies, H.C. and H. Pichler, eds, 1990, Mountain meteorology and ALPEX. Special issue of Meteor. Atmos. Phys. 43.
Davies-Jones, R.P., 1985, Tornado dynamics, in: Thunderstorm Morphology and Dynamics, 2nd Ed., ed. E. Kessler (University of Oklahoma Press, Norman) pp. 197–236.
Davies-Jones, R.P., 1991, Frontogenetical forcing of secondary circulations. Part I: The duality and generalization of the Q-vector, J. Atmos. Sci. 48, 497–509.
Davis, P.A. and W.R. Peltier, 1976, Resonant parallel shear instability in the stably stratified planetary boundary layer, J. Atmos. Sci. 33, 1289–1300.
Deardorff, J.W., 1974, Three-dimensional numerical study of turbulence in an entraining mixed layer, Boundary-Layer Meterol. 7, 199–226.
Defant, F, 1951, Local winds, in: Compendium of Meteorology, ed. T.F. Malone (American Meteorological Society, Boston) pp. 655–672.
DeMaria, M. and W.H. Schubert, 1984, Experiments with a spectral tropical cyclone model, J. Atmos. Sci. 41, 901–924.
DeMaria, M. and J.D. Pickle, 1988, A simplified system of equations for the simulation tropical cyclones, J. Atmos. Sci. 45, 1542–1554.
Dorman, C.E., 1988, Comments on the paper by Mass and Albright (1987), Mon. Weather Rev. 116, 2401–2406.

Drazin, P.G. and W.H. Reid, 1982, Hydrodynamic Stability (Cambridge University Press, Cambridge).
Driedonks, A.G.M. and P.G. Duynkerke, 1989, Current problems in the stratocumulus-topped atmospheric boundary layer, Boundary-Layer Meteorol 46, 275–303.
Dunn, G.E., 1951, Tropical cyclones, in: Compendium of Meteorology, eds T.F. Malone (American Meteorological Society, Boston) pp. 887–901.
Durran, D.R., 1986a, Another look at downslope windstorms. Part I: development of analogs to supercritical flow in an infinitely deep, continuously stratified fluid, J. Atmos. Sci. 43, 2527–2543.
Durran, D.R., 1986b, Mountain waves, in: Mesoscale Meteorology and Forecasting, ed. P.S. Ray (American Meteorological Society, Boston) pp. 472–492.
Durran, D.R., 1989, Improving the anelastic approximation, J. Atmos. Sci. 46, 1453–1461.
Durran, D.R., 1990, Mountain waves and downslope winds, in: Atmospheric Processes over Complex Terrain, ed. W. Blumen (American Meteorological Society, Boston) pp. 59–82.
Durran, D.R. and J.B. Klemp, 1982, On the effects of moisture on the Brunt–Väisälä frequency, J. Atmos. Sci. 39, 2152–2158.
Durran, D.R. and J.B. Klemp, 1982, Another look at downslope winds. Part II: Nonlinear amplification beneath wave-overturning layers, J. Atmos. Sci. 44, 3402–3412.
Durran, D.R. and J.B. Klemp, 1983, A compressible model for the simulation of moist mountain waves, Mon. Weather Rev. 111, 2341–2361.
Dutton, J.A., 1976, The Ceaseless Wind (McGraw-Hill/Dover, New York).
Dutton J.A. and G.H. Fichtl, 1969, Approximate equations of motion for gases and liquids, J. Atmos. Sci. 26, 241–254.
Eady, E.T., 1949, Long waves and cyclone waves, Tellus 1, 33–52.
Egger, J., 1989, Föhn and quasi-stationary fronts, Beitr. Phys. Atmosph. 62, 20–29.
Egger, J., 1990a, Thermally forced flows, in: Atmospheric Processes over Complex Terrain, ed. W. Blumen (American Meteorological Society, Boston) pp. 43–58.
Egger, J., 1990b, Some aspects of potential vorticity inversion, J. Atmos. Sci. 42, 1269–1275.
Einaudi, F., D.P. Lalas and G.E. Perona, 1978, The role of gravity waves in tropospheric processes, Pageoph 117, 627–663.
Eliassen, A., 1948, The quasi-static equations of motion, Geof. Publ. 17, 1–44.
Eliassen, A., 1952, Slow thermally or frictionally controlled meridional circulations in a circular vortex, Astrophysica Norvegica 5, no. 2.
Eliassen, A., 1959, On the formation of fronts in the atmosphere, in: The Atmosphere and the Sea in Motion, ed. B. Bolin (The Rockefeller Institute Press, New York), pp. 277–287.
Eliassen, A., 1962, On the vertical circulation in frontal zones, Geof. Publ. 24, 147–161.
Eliassen, A., 1971, On the Ekman layer in a circular vortex, J. Meteorol. Soc. Japan 49, 784–789.
Eliassen, A., 1984, Geostrophy, Q. J. R. Meteorol. Soc. 110, 1–12.
Eliassen, A., 1990, Transverse circulations in frontal zones, in: Extratropical cyclones, eds C.W. Newton and E.O. Holopainen (American Meteorological Society, Boston) pp. 155–165.
Eliassen, A. and E. Kleinschmidt, 1957, Dynamic Meteorology, in: Encyclopedia of Physics, Vol. 58, eds S. Flügge and J. Bartels, pp. 1–154.
Elsberry, R.L., W.M. Frank, G.J. Holland, J.D. Jarrel and R.L. Southern, 1987, A Global View of Tropical Cyclones, Naval Postgraduate School, Monterey, CA 93943, USA.
Emanuel, K.A., 1979, Inertial instability and mesoscale convective systems. Part 1: linear theory of inertial instability in rotating systems, J. Atmos. Sci. 36, 2425–2449.
Emanuel, K.A., 1982, Inertial instability and mesoscale convective systems. Part 2: symmetric CISK in a baroclinic flow, J. Atmos. Sci. 39, 1080–1097.
Emanuel, K.A., 1983a, Lagrangian parcel dynamics of moist symmetric instability, J. Atmos. Sci. 40, 2368–2376.
Emanuel, K.A., 1983b, On assessing local conditional symmetric instability from atmospheric soundings, Mon. Weather Rev. 111, 2016–2033.
Emanuel, K.A., 1983c, Elementary aspects of the interaction between cumulus convection and the large scale environment, in: Mesoscale Meteorology – Theories, Observations and Models, NATO ASI ser. C, vol. 114, eds D.K. Lilly and T. Gal-Chen (Reidel, Dordrecht) pp. 551–576.
Emanuel, K.A., 1984, First conference on mesoscale meteorology, 31 May–3 June, 1983, Norman, Oklahoma, Bull. Am. Meteorol. Soc. 65, 145–148.
Emanuel, K.A., 1986a, Overview and definition of mesoscale meteorology, in: Mesoscale Meteorology and Forecasting, ed. P.S. Ray (American Meteorological Society, Boston) pp. 1–17.
Emanuel, K.A., 1986b, An air–sea interaction theory for tropical cyclones. Part 1: steady state maintainance, J. Atmos. Sci. 43, 585–604.
Emanuel, K.A., 1991, The theory of hurricanes. An. Rev. Fluid Mech. 23, 179–196.
Emanuel, K.A. and R. Rotunno, 1989, Polar lows as arctic hurricanes, Tellus 41A, 1–17.
Erickson, C.O. and L.F. Whitney, 1973, Picture of the month. Gravity waves following severe thunderstorms, Mon. Weather Rev. 101, 708–711.
Ertel, H., 1942, Ein neuer hydrodynamischer Wirbesatz, Meteorol. Z. 59, 277–281.
Estoque, M.A., 1962, Vertical and radial motion in a tropical cyclone, Tellus 14, 394–402.
Etling, D., 1971, The stability of an Ekman boundary layer flow as influenced by thermal stratification, Beitr. Phys. Atmosph. 44, 168–186.
Etling, D., 1989, On atmospheric vortex streets in the wake of large islands, Meteorol. Atmos. Phys. 41, 157–164.
Etling, D., 1990, Mesoscale vortex shedding from large islands: A comparison with laboratory experiments of rotating stratified flows, Meteorol. Atmos. Phys. 43, 145–151.

Ewenz, C.M. and H. Kraus, 1990, An analytical exercise to elucidate quasi-geostrophic frontogenesis, Meteorol. Atmos. Phys. 42, 179–196.
Exner, F.M., 1925, Dynamische Meteorologie, 2nd Ed., (Springer Verlag, Vienna) p. 205.
Faller, A.J., 1963, An experimental study of the instability of the laminar Ekman boundary layer, J. Fluid Mech. 15, 560–576.
Fendell, F.E., 1974, Tropical cyclones, Adv. Geophys. 17, 2–100.
Fiedler, F., 1971, The variance spectrum of the horizontal wind velocity at 50 m above the ground, Beitr. Phys. Atmosph. 44, 187–200.
Fjørtoft, R., 1946, On the frontogenesis and cyclogenesis in the atmosphere: Part I – on the stability of the stationary circular vortex, Geof. Publ. 16.
Fjørtoft, R., 1950, Applications of integral theorems in deriving criteria of stability for laminar flows and for the baroclinic circular vortex, Geof. Publ. 17.
Flatau, M. and D.E. Stevens, 1989, Barotropic and inertial instabilities in the hurricane outflow layer, Geophys. Astrophys. Fluid Dyn. 47, 1–18.
Frank, W.M., 1977, The structure and energetics of the tropical cyclone. Part 1: Storm structure. Mon. Weather Rev. 105, 1119–1135.
Frank, W.M., 1983, The cumulus parameterization problem, Mon. Weather Rev. 111, 1859–1871.
Franklin, J.L., S.J. Lord and F.D. Marks Jr., 1988, Dropwindsonde and radar observations of the eye of hurricane Gloria (1985), Mon. Weather Rev. 116, 1237–1244.
Fujita, T.T., 1981, Tornadoes and downbursts in the context of generalized planetary scales, J. Atmos. Sci. 38, 1512–1534.
Gal-Chen, T. and R.C.J. Somerville, 1975, On the use of a coordinate transformation for the solution of the Navier–Stokes equations, J. Comput. Phys. 17, 209–228.
Garner, S.T., 1989, Fully Lagrangian numerical solutions of unbalanced frontogenesis and frontal collapse, J. Atmos. Sci. 46, 717–739.
Garner, S.T., 1991, The nongeostrophic structure of baroclinic waves and its relation to fronts and jetstreaks, J. Atmos. Sci. 48, 147–162.
Gill, A.E., 1982, Atmosphere–Ocean Dynamics (Academic Press, New York).
Godske, C.L., T. Bergeron, J. Bjerknes and R.C. Bundgaard, 1957, Dynamic Meteorology and Weather Forecasting (American Meteorological Society, Boston/Carnegie Institution, Washington).
Golding, B.W., 1990, The Meteorological Office mesoscale model, Met. Mag. 119, 81–96.
Goldstein, S., 1931, On the stability of superposed fluids of different densities, Proc. R. Soc. A 132, 524–548.
Gossard, E.E. and W.H. Hooke, 1975, Waves in the Atmosphere (Elsevier, Amsterdam).
Gray, W.M., 1991, Comments on "Gradient balance in tropical cyclones", J. Atmos. Sci. 48, 1201–1208.
Green J.S.A. and G.A. Dalu, 1980, Mesoscale energy generated in the boundary layer, Q. J. R. Meteorol. Soc. 106, 721–726.
Gross, G., 1985, An explanation of the "Maloja Serpent" by numerical simulation, Beitr. Phys. Atmosph. 58, 441–457.
Hasse, S.P., 1991, Numerical simulation of the bore-like cold front of 8 October 1987 in Southern Germany, Tellus 43A, 97–105.
Hasse, S.P. and R.K. Smith, 1984, Morning glory wave-clouds in Oklahoma: a case study, Mon. Weather Rev. 112, 2078–1089.
Hack, J.J. and W.H. Schubert, 1986, Nonlinear response of atmospheric vortices to heating by organized convection, J. Atmos. Sci. 43, 1559–1573.
Haderlein, K., 1989, On the dynamics of orographically retarded cold fronts, Beitr. Phys. Atmosph. 62, 11–19.
Haurwitz, B., 1931, Zur Theorie der Wellenbewegungen in Luft and Wasser, Veröff. Geophys. Inst. Leipzig 6, no. 1.
Hawkins, H.F. and D.T. Rubsam, 1968, Hurricane Hilda, 1964: II, The structure and budjets of the hurricane on October 21, 1964, Mon. Weather Rev. 99, 427–434.
Haynes, P.H. and M.E. McIntyre, 1987, On the evolution of vorticity and potential vorticity in the presence of diabatic heating and frictional or other forces, J. Atmos. Sci. 44, 828–841.
Haynes, P.H. and M.E. McIntyre, 1990, On the conservation and impermeability theorems for potential vorticity, J. Atmos. Sci. 47, 2021–2031.
Heijboer, L.C., H. Timmerman and A. van der Hoek, 1989, Description and performance of an hourly nowcasting and very short-range forecasting system, Q. J. R. Meteorol. Soc. 115, 93–125.
Heimann, D., 1986, Estimation of regional surface layer wind field characteristics using a three-layer mesoscale model, Beitr. Phys. Atmosph. 59, 518–537.
Hines, C.O., 1972, Gravity waves in the atmosphere, Nature 239, 73–78.
Hoeker, W.H., 1960, Wind speed and airflow patterns in the Dallas tornado of April 2, 1957, Mon. Weather Rev. 88, 167–180.
Hoinka, K.P. and D. Heimann, 1988, Orographic channelling of a cold front by the Pyrenees, Mon. Weather Rev. 116, 1817–1823.
Holton, J.R., 1979, An Introduction to Dynamic Meteorology, 2nd Ed. (Academic Press, New York).
Hoskins, B.J., 1974, The role of potential vorticity in symmetric stability and instability, Q. J. R. Meteorol. Soc. 100, 480–482.
Hoskins, B.J., 1975, The geostrophic momentum approximation and the semigeostrophic equations, J. Atmos. Sci. 32, 233–242.
Hoskins, B.J., 1978, Baroclinic instability and frontogenesis, in Rotating Fluids in Geophysics, eds P.H. Roberts and A.M. Sowarel (Academic Press, New York) pp. 171–302.
Hoskins, B.J., 1982, The mathematical theory of frontogenesis, Ann. Rev. Fluid Mech. 14, 131–151.
Hoskins, B.J., 1990, Theory of extratropical cyclones, in: Extratropical Cyclones, eds C.W. Newton and E.O. Holopainen (American Meteorological Society, Boston) pp. 63–105.
Hoskins, B.J. and I. Draghici, 1977, The forcing of ageostrophic motion according to the semi-geostrophic equations and in an isentropic coordinate model, J. Atmos. Sci. 34, 1859–1867.
Hoskins, B.J., M.E. McIntyre and A.W. Robertson, 1985, On the use and significance of isentropic potential vorticity maps, Q. J. R. Meteorol. Soc. 11, 877–946.
Houghton, D.D. and A. Kasahara, 1968, Nonlinear shallow flow over a ridge, Commun. Pure Appl. Math. 21, 1–23.

Houze Jr., R.A. and P.V. Hobbs, 1982, Organization and structure of precipitating cloud systems, Adv. Geophys. 24, 225–315.
Howard, L.N., 1961, Note on a paper by John W. Miles, J. Fluid Mech. 10, 509–512.
Howard, L.N. and S.A. Maslowe, 1973, Stability of stratified shear flows, Boundary-Layer Meteorol. 4, 511–523.
Hsu, Y.-J. and A. Arakawa, 1990, Numerical modeling of the atmosphere with an isentropic vertical coordinate, Mon. Weather Rev. 118, 1933–1969.
Huang, X.-Y., 1990, The organization of moist convection by internal gravity waves, Tellus 42A, 270–285.
Hunt, J.C.R., F. Tampieri, W.S. Weng and D.J. Carruthers, 1991, Air flow and turbulence over complex terrain: a colloquium and a computational workshop, J. Fluid Mech. 227, 667–688.
Igawa, M. and Y. Nagasawa, 1989, A numerical study of a dynamically induced Foehn observed in the Abashiri-Ohmu area, J. Meteorol. Soc. Japan 62, 429–458.
Ishida, H., 1990, Seasonal variations of spectra of wind speed and temperature in the mesoscale frequency range, Boundary-Layer Meteorol. 52, 335–348.
Joint Centre for Mesoscale Meteorology, 1988, report no. 1 (Meteorological Office, UK.)
Jorgensen, D.P., 1984, Mesoscale and convective-scale characteristics of mature hurricanes, J. Atmos. Sci. 41, 1268–1311.
Kasahara, A., 1974, Various vertical coordinate systems used for the numerical weather prediction, Mon, Weather Rev. 102, 509–522.
Kaylor, R. and A.J. Faller, 1972, Instability of the stratified Ekman boundary layer and the generation of internal waves, J. Atmos. Sci. 29, 497–509.
Kessinger, C.J., D.B. Parsons and J.W. Wilson, 1988, Observations of a storm containing mesocyclones, downbursts horizontal vortex circulations, Mon. Weather Rev. 116, 1959–1982.
Kessler, E., ed. 1985, Thunderstorm Morphology and Dynamics, 2nd Ed. (University of Oklahoma Press, Norman).
Keuttner, J.P., P.A. Hildebrand and T.L. Clark, 1987, Convection waves: observations of gravity wave systems over convectively active boundary layers, Q. J. R. Meteorol. Soc. 113, 445–467.
Keyser, D., 1986, Atmospheric fronts: an observational perspective, in: Mesoscale Meteorology and Forecasting, ed. P.S. Ray (American Meteorological Society, Boston) pp. 216–258.
Keyser, D. and M.A. Shapiro, 1986, A review of the structure and dynamics of upper-level frontal zones, Mon. Weather Rev. 114, 452–499.
Kingsmill, D.E. and R.M. Wakimoto, 1991, Kinematics, dynamic and thermodynamic analysis of a weakly sheared severe thunderstorm over northern Alabama, Mon. Weather Rev. 119, 262–297.
Klemp, J.B., 1987, Dynamics of tornadic thunderstorms, Ann. Rev. Fluid Mech. 19, 369–402.
Klemp, J.B. and D.R. Durran, 1987: Numerical modelling of Bora winds, Meteorol. Atmos. Phys. 36, 215–227.
Klemp, J.B. and R.B. Wilhelmson, 1978, The simulation of three-dimensional storm dynamics, J. Atmos. Sci. 35, 1070–1096.
Kocin, P.J., L.W. Uccellini and R.A. Petersen, 1986, Rapid evolution of a jet streak circulation in a pre-convective environment, Meteorol. Atmos. Phys. 35, 103–138.
Koschmeider, E.L. and S.G. Pallas, 1974, Heat transfer through a shallow convecting fluid, Int. J. Heat Mass Transfer 17, 991–1002.
Kraus, H., 1987, Specific surface climates, in Landolt-Börnstein, New Series Vol. 4c, part 1 (Springer, Berlin) pp. 29–92.
Kraus, H., J.M. Hacker and J. Hartmann, 1990, An observational aircraft-based study of sea breeze frontogenesis, Boundary-Layer Meteorol. 53, 223–265.
Krishnamurti, R., 1970, On the transition to turbulent convection. Part 1: the transition from two to three-dimensional flow, J. Fluid Mech. 42, 295–307.
Krishnamurti, T.N., A. Kumar, K.S. Yap, A.P. Dastoor, N. Davidson and J. Sheng, 1990, Performance of a high resolution mesoscale tropical prediction model, Adv. Geophys. 33, 133–286.
Kuhn, M., 1989, Föhnstudien (Wissenschaftliche Buchgesellschaft, Darmstadt).
Kundu, P.K., 1990, Fluid Mechanics (Academic Press, New York).
Kuo, H.L., 1961, Convection in a conditionally unstable atmosphere, Tellus 13, 441–459.
Kuo, H.L., 1965a, Further studies of the properties of cellular convection in a conditionally unstable atmosphere, Tellus 17, 413–433.
Kuo, H.L., 1965b, On the formation and intensification of tropical cyclones through latent heat release by cumulus convection, J. Atmos Sci. 22, 40–63.
Kurz, M., 1979, Frontogenetic processes in the lower troposphere, Beitr. Phys. Atmosph. 52, 331–347.
Kutzbach, G., 1979, The Thermal Theory of Cyclones (American Meteorological Society, Boston).
Lalas, D.P. and F. Einaudi, 1976, On the characteristics of gravity waves excited by atmospheric shear layers. J. Atmos. Sci. 33, 1248–1259.
Lawrence, G.A., 1990, On the hydraulics of Boussinesq and non-Boussinesq two-layer flows, J. Fluid Mech. 215, 457–480.
Lemon, L.R. and C.A. Doswell, 1979, Severe thunderstorm evolution and mesocyclone structure as related to tornado-genesis, Mon. Weather Rev. 107, 1184–1197.
LeMone, M.A., J.C. Frankhauser, G.M. Barnes and L.F. Tarleton, 1988a, Perturbation pressure fields measured by aircraft around the cloud-base updraft of deep convective clouds, Mon. Weather Rev. 116, 313–327.
LeMone, M.A., L.F. Tarleton and G.M. Barnes, 1988b, Perturbation pressure at the base of cumulus clouds in low shear Mon. Weather Rev. 116, 2062–2068.
Ligda, M.G.H., 1951, Radar storm observation, in: Compendium of Meteorology, ed. T.F. Malone (American Meteorological Society, Boston) pp. 1265–1282.

Lilly, D.K., 1960, On the theory of disturbances in a conditionally unstable atmosphere, Mon. Weather Rev. 88, 1–17.
Lilly, D.K., 1966, On the stability of Ekman boundary flow, J. Atmos. Sci. 23, 481–494.
Lilly, D.K., 1978, A severe downslope windstorm and aircraft turbulence event induced by a mountain wave, J. Atmos. Sci. 35, 59–77.
Lilly, D.K., 1986, The structure, energetics and propagation of rotating convective storms, J. Atmos. Sci. 43, 113–140.
Lilly, D.K., 1990, Numerical prediction of thunderstorms – has its time come?, Q. J. R. Meteorol. Soc. 116, 779–797.
Lilly, D.K. and T. Gal-Chen, eds, 1983, Mesoscale Meteorology – Theories, Observations and Models, NATO ASI ser. C, Vol. 114 (Reidel, Dordrecht).
Lilly, D.K. and J.B. Klemp, 1980, Comments on "The evolution and stability of finite amplitude mountain waves. Part II: surface wave drag and severe downslope windstorms", J. Atmos. Sci. 37, 2119–2121.
Lindzen, S., E.N. Lorenz and G.W. Platzman, (eds), 1990, The Atmosphere – a Challenge. The Science of Jule Gregory Charney (American Meteorological Society, Boston).
Lipps, F.B., 1990, On the anelastic approximation for deep convection, J. Atmos. Sci. 47, 1794–1798.
Lipps, F.B., and R.S. Hemler, 1982, A scale analysis of deep moist convection and some related numerical calculations, J. Atmos. Sci. 39, 2192–2210.
Llasat, M.C. and M. Puigcerver, 1990, Cold air pools over Europe, Meteorol. Atmos. Phys. 42, 171–177.
Lloyd, L.M., 1990, The sea-breeze at Darwin: a climatology, Met. Mag. 119, 105–112.
Long, R.R., 1953a, Some aspects of the flow of stratified fluids. I. A theoretical investigation, Tellus 5, 42–57.
Long, R.R., 1953b, A laboratory model resembling the bishop wave phenomenon, Bull. Am. Meteor. Soc. 34, 205–211.
Long, R.R., 1954, Some aspects of the flow of stratified fluids. II. Experiments with a two-fluid system, Tellus 6, 97–115.
Long, R.R., 1970, Blocking effects in flow over obstacles, Tellus 22, 471–480.
Long, R.R., 1972, Finite amplitude disturbances in the flow of inviscid rotating and stratified fluids over obstacles, Ann. Rev. Fluid Mech. 4, 69–92.
Ludlam, F.H., 1980, Clouds and Storms (Pennsylvania State University Press, University Park).
Lynch, P., 1989, The slow equations, Q. J. R. Meteorol. Soc. 115, 201–219.
Maddox, R.A., 1980, Mesoscale convective complexes, Bull. Am. Meteorol. Soc. 61, 1374–1387.
Maddox, R.A., K.W. Howard, D.L. Bartels and D.M. Rogers, 1986, Mesoscale convective complexes in the middle latitudes, in: Mesoscale Meteorology and Forecasting (American Meteorological Society, Boston) pp. 390–413.
Marks Jr., F.D. and R.A. Houze, Jr., 1987, Inner core structure of hurricane Alicia from airborne Doppler radar observations, J. Atmos. Sci. 44, 1296–1317.
Mason, P.J., 1989, Large-eddy simulation of the convective boundary layer, J. Atmos. Sci. 46, 1492–1516.
Mass, C.F. and M.D. Albright, 1987, Coastal southerlies and alongshore surges of the west coast of North America: evidence of mesoscale topographically trapped response to synoptic forcing, Mon. Weather Rev. 115, 1707–1738.
McAnelly, R.L. and W.R. Cotton, 1989, The precipitation life cycle of mesoscale convective complexes over the central United States, Mon. Weather Rev. 117, 784–808.
McNulty, R.P., 1978, On upper tropospheric kinematics and severe weather occurrence, Mon. Weather Rev. 106, 662–672.
Menard, D.M. and J.M. Fritsch, 1989, A mesoscale convective-generated inertially stable warm core vortex, Mon. Weather Rev. 117, 1237–1261.
Miles, J., 1961, On the stability of heterogeneous shear flows, J. Fluid Mech. 10, 496–508.
Miles, J., 1986, Richardson's criterion for the stability of stratified shear flow Phys. Fluids 29, 3470–3471.
Miller, P.P. and D.R. Durran, 1991, On the sensitivity of downslope windstorms to the asymmetry of the mountain profile, J. Atmos. Sci. 48, 1457–1473.
Moncrieff, M.W., 1978, The dynamical structure of two-dimensional steady convection in constant shear, Q. J. R. Meteorol. Soc. 104, 543–567.
Musil, D.J., A.J. Heymsfield and P.L. Smith, 1986, Microphysical characteristics of a well developed weak echo region in a high plains supercell thunderstorm, J. Clim. Appl. Meteorol. 25, 1037–1051.
Newton, C.W., and A. Trevisan, 1984, Clinogenesis and frontogenesis in jetstream waves. Part I: analytical relations to wave structure. J. Atmos. Sci. 41, 2717–2734.
Newton, C.W. and E.O. Holopainen, (eds), 1990, Extratropical Cyclones (American Meteorological Society, Boston).
Nieuwstadt, F.T.M. and R.A. Brost, 1986, The decay of convective turbulence, J. Atmos. Sci. 43, 532–546.
Oberbeck, A., 1879, Über die Wärmleitung die Flüssigheiten bei Berücksichtigung der Strömingen infolge von Temperaturdifferenzen, Ann. Phys. Chem. 7, 271–292.
Oerlemans, J., 1983, On the intensity of atmospheric convection, Beitr. Phys. Atmosph. 56, 341–353.
Oerlemans, J., 1986, Convection in a conditionally unstable atmosphere: a re-investigation of Bjerknes' slice method, Beitr. Phys. Atmosph. 59, 41–53.
Ogura, Y., 1964, Frictionally controlled, thermally driven circulation in a circular vortex with application to tropical cyclones, J. Atmos. Sci. 21, 610–621.
Ogura, Y. and N.A. Phillips, 1962, Scale analysis of deep and shallow convection in the atmosphere, J. Atmos. Sci. 19, 173–179.
Ogura, Y. and T. Takahashi, 1971, Numerical simulation of the life cycle of a thunderstorm cell, Mon. Weather Rev. 99, 895–911.
Økland, H., 1990, The dynamics of coastal troughs and coastal fronts, Tellus 42A, 444–462.
Ooyama, K.V., 1964, A dynamical model for the study of tropical cyclone development, J. Geofys. Intern. 4, 187–198.
Ooyama, K.V., 1966, On the stability of the baroclinic circular vortex: a sufficient criterion for instability, J. Atmos. Sci. 23, 43–53.

Ooyama, K.V., 1969, Numerical simulation of the life cycle of tropical cyclones, J. Atmos. Sci. 26, 3–40.
Ooyama, K.V., 1982, Conceptual evolution of the theory and modelling of the tropical cyclone, J. Meteorol. Soc. Japan 60, 369–379.
Orlanski, I., 1975, A rational subdivision of scales for atmospheric processes, Bull. Am. Meteorol. Soc. 56, 527–530.
Orlanski, I., 1981, The quasi-hydrostatic approximation, J. Atmos. Sci. 38, 572–582.
Orlanski, I., B. Ross, L. Polinsky and R. Shaginaw, 1985, Advances in the theory of atmospheric fronts, Adv. Geophys. 28B, 223–252.
Palmén, E. and C.W. Newton, 1969, Atmospheric Circulation Systems (Academic Press, New York).
Panchev, S., 1985, Dynamic Meteorology (Reidel, Dordrecht).
Parker, S.B., ed., 1988, Meteorology Source Book (McGraw-Hill, New York).
Parsons, D.B. and P.V. Hobbs, 1983, The mesoscale and microscale structure and organization of clouds and precipitation in midlatitude cyclones. XI: comparison between observational and theoretical aspects of rainbands, J. Atmos. Sci. 40, 2377–2397.
Pedlosky, J., 1987, Geophysical Fluid Dynamics, 2nd Ed. (Springer, Berlin).
Peltier, W.R. and T.L. Clark, 1980, Reply to comments of D.K. Lilly and J.B. Klemp, J. Atmos. Sci. 37, 2122–2125.
Peltier, W.R. and T.L. Clark, 1983, Nonlinear mountain waves in two and three spatial dimensions, Q. J. R. Meteorol. Soc. 109, 527–548.
Pettre, P., 1982, On the problem of violent valley winds, J. Atmos. Sci. 39, 542–554.
Phillips, N.A., 1951, A simple three-dimensional model for the study of large-scale extratropical flow patterns, J. Meteorol. 8, 381–394.
Phillips, N.A., 1957, A co-ordinate system having special advantages for numerical forecasting, J. Meteorol. 14, 184–185.
Physick, W.L., 1988, Mesoscale modelling in complex terrain, Earth Sci. Rev. 25, 199–235.
Pichler, H., 1984, Dynamik der Ätmosphäre (B.I. Wissenschaftsverlag, Zurich).
Pielke, R.A., 1974, A three-dimensional numerical model of the sea breezes over south Florida, Mon. Weather Rev. 102, 115–139.
Pielke, R.A., 1984, Mesoscale Meteorological Modeling (Academic Press, New York).
Pike, W.S., 1990, Persistent coastal convergence in a heavy snowfall event on the south-east coast of England, Met. Mag. 119, 21–32.
Queney, P., 1948, The problem of air-flow over mountains. A summary of theoretical results, Bull. Am. Meteorol. Soc. 29, 16–25.
Ramaswamy, C., 1956, The subtropical jetstream and its role in the development of large-scale convection, Tellus 8, 26–60.
Rao, D.B. and T.J. Simons, 1970, Stability of a sloping interface in a rotating two-fluid system, Tellus 22, 493–503.
Rasmussen, E., 1989, A comparative study of tropical cyclones and polar lows, in: Polar and Arctic Lows, eds P.F. Twitchell, E.A. Rasmussen and K.L. Davidson (Deepak, Virginia) pp. 47–80.
Rasmussen, E. and M. Lystad, 1987, The Norwegian polar lows project: a summary of the international conference on polar lows, 20–23 May 1986, Oslo, Norway, Bull. Am. Meteorol. Soc. 68, 801–816.
Rasmussen, R., P.K. Smolarkiewicz and J. Warner, 1989, On the dynamics of Hawaiian cloud bands: comparison of model results with observations and island climatology, J. Atmos. Sci. 46, 1589–1608.
Ray, P.S., ed., 1986, Mesoscale Meteorology and Forecasting (American Meteorological Society, Boston).
Rayleigh, Lord, 1880, On the stability, or certain fluid motions, Proc. London Math. Soc. 11, 57–70.
Rayleigh, Lord, 1883, Investigation of the character of the equilibrium of an incompressible heavy fluid of variable density, Proc. London Math. Soc. 14, 170–177.
Rayleigh, Lord, 1916a, On convection currents in a horizontal layer of fluid, when the higher temperature is on the under side, Phil. Mag. 32, 529–546.
Rayleigh, Lord, 1916b, On the dynamics of revolving fluids, Proc. R. Soc. A 93, 148–154.
Reason, C.J.C. and M.R. Jury, 1990, On the generation of the southern African coastal low, Q. J. R. Meteorol. Soc. 116, 1133–1151.
Reed, R.J., 1990, Advances in knowledge and understanding of extratropical cyclones during the past quarter century: an overview, in: Extratropical Cyclones, eds C.W. Hewton and E.O. Holopainen (American Meteorological Society, Boston) pp. 27–45.
Richardson, L.F., 1920, Proc. R. Soc. A 97, 354.
Riehl, H., 1951: Aerology of tropical cyclones in: Compendium of Meteorology, ed. T.F. Malone (American Meteorological Society, Boston) pp. 902–913.
Riehl, H., M.A. Alaka, C.L. Jordan, R.J. Renard, 1954, The Jet Stream, Meteor. Mon. Vol. 2 (American Meteorological Society, Boston).
Rivera, A., 1990, Las situaciones de lluvias torrenciales en el área mediterránea española y el Plan Previmet, La Meteorologia 1, 30–39.
Roeloffzen, J.C., W.D. van den Berg and J. Oerlemans, 1986, Frictional convergence at coastlines, Tellus 38A, 397–411.
Rogers, R.R. and M.K. Yau, 1989, A Short Course in Cloud Physics, 3rd Ed. (Pergamon Press, Oxford).
Rosenthal, S.L., 1963, On the problem of the diagnostic calculation of vertical and radial motions in a wet vortex, Mon. Weather Rev. 91, 453–464.
Rossby, C.G., 1937, On the mutual adjustment of pressure and velocity distributions in certain simple current systems. I, J. Mar. Res. 1, 15–28.
Rossby, C.G., 1938, On the mutual adjustment of pressure and velocity distributions in certain simple current systems. II, J. Mar. Res. 1, 239–263.
Roth, R., 1981, Der konvergenzeffekt an flachküsten, Meteorol. Rundschr. 34, 24.
Rottman, J.W. and J.E. Simpson, 1989, The formation of internal bores in the atmosphere, Q. J. R. Meteorol. Soc. 115, 941–963.
Rotunno, R., 1983, On the linear theory of the land and sea breeze, J. Atmos. Sci. 40, 1999–2009.
Rotunno, R. and K.A. Emanuel, 1987, An air-sea interaction theory for tropical cyclones. Part II: evolutionary study using a nonhydrostatic axisymmetric numerical model, J. Atmos. Sci. 44, 542–561.
Rotunno, R. and J.B. Klemp, 1982, The influence of the shear-induced pressure gradient on thunderstorm motion, Mon. Weather Rev. 110, 136–151.
Rotunno, R., J.B. Klemp and M.L. Weisman, 1988, A theory for strong, long-lived squall lines, J. Atmos. Sci. 45, 463–485.

Saitoh, S. and H. Tanaka, 1987, Numerical experiments of conditional baroclinic instability as a possible cause for frontal rainband formation. Part I. Basic experiment, J. Meteorol. Soc. Japan 65, 675–708.
Sardie, J.M. and T.T. Warner, 1983, On the mechanism for the development of polar lows, J. Atmos. Sci. 40, 869–881.
Sawyer, J.S., 1956, The vertical circulation at meteorological fronts and its relation to frontogenesis, Proc. R. Soc. A 234, 346.
Schaefer, J.T., 1986, The dryline, in: Mesoscale Meteorology and Forecasting, ed. P.S. Ray (American Meteorological Society, Boston) pp. 549–572.
Schär, C. and R.B. Smith, 1991, Shallow-water flow past high topography as a model for atmospheric vortex shedding, Proc. 8th Conf. on Atmospheric and Oceanic Waves and Stability, Denver, 14–18 October 1991 (American Meteorological Society, Boston).
Schlesinger, R.E., 1975, A three-dimensional model of an isolated deep convective cloud: preliminary results, J. Atmos. Sci. 32, 934–957.
Schmidt, H. and U. Schumann, 1989, Coherent structure of the convective boundary layer derived from large eddy simulation, J. Fluid Mech. 200, 511–562.
Schubert, W.H., J.J. Hack, P.L. Silva Dias and S.R. Fulton, 1980, Geostrophic adjustment in an axisymmetric vortex, J. Atmos. Sci. 34, 1464–1484.
Schubert, W.H. and J.J. Hack, 1982, Inertial stability and tropical cyclone development, J. Atmos. Sci. 39, 1687–1697.
Schubert, W.H. and B.T. Alworth, 1987, Evolution of potential vorticity in tropical cyclones, Q. J. R. Meteorol. Soc. 113, 147–162.
Schumann, U., T. Hauf, H. Höller, H. Schmidt and H. Volkert, 1987, A mesoscale model for the simulation of turbulence, clouds and flow over mountains: formulation and validation experiments, Beitr. Phys. Atmosph. 60, 413–446.
Schwerdtfeiger, W., ed., 1976, Climates of central and south America, World Survey of Climatology, Vol. 12 (Elsevier, Amsterdam).
Scorer, R.S., 1949, Theory of waves in the lee of mountains, Q. J. R. Meteorol. Soc. 75, 41–56.
Scorer, R.S., 1986, Cloud Investigation by Satellite, Ellis Horwood Series in Environmental Science (Ellis Horwood, Chicester).
Scorer, R.S., 1988, Lessons from observations of chaotic flow in the atmosphere, J. Mech. Theor. Appl. 7, 145–165.
Scorer, R.S. and A. Verkaik, 1989, Spacious Skies (David and Charles, London).
Seitter, K.L. and H.L. Kuo, 1983, The dynamical structure of squall line type thunderstorms, J. Atmos. Sci. 40, 2831–2854.
Shapiro, M.A., 1976, The role of turbulent heat flux in the generation of potential vorticity in the vicinity of upper-level jet stream systems, Mon. Weather Rev. 104, 892–906.
Shapiro, M.A., 1981, Frontogenesis and geostrophically forced secondary circulations in the vicinity of jet stream-frontal zone systems, J. Atmos. Sci. 38, 954–973.
Shapiro, L.J., and H.E. Willoughby, 1982, The response of balanced hurricanes to local sources of heat and momentum, J. Atmos. Sci. 39, 378–394.
Sheets, R.C., 1982, On the structure of hurricanes as revealed by research aircraft data, in: Intense atmospheric vortices, eds L. Bengtsson and J. Lighthill (Springer, Berlin) pp. 35–49.
Sheppard, P.A., 1956: Airflow over mountains. Q. J. R. Meteorol. Soc. 82, 528–529.
Shutts, G.J., 1981, Hurricane structure and zero potential vorticity approximation, Mon. Weather Rev. 109, 324–329.
Shutts, G.J., 1990, Dynamical aspects of the October storm, 1987: a study of a successful fine mesh simulation, Q. J. R. Meteorol. Soc. 116, 1315–1347.
Shutts, G.J. and A.J. Thorpe, 1978, Some aspects of vortices in rotating stratified fluids, Pageoph 116, 993–1106.
Siebert, P., 1990, South Foehn studies since the ALPEX experiment, Meteorol. Atmos. Phys. 43, 91–103.
Simpson, J.E., 1987, Gravity Currents in the Environment and the Laboratory (Ellis Horwood, Chicester).
Simpson, R.H. and H. Riehl, 1981, The Hurricane and its Impact (Louisiana State University Press, Baton Rouge).
Smith, R.B., 1979, The influence of mountains on the atmosphere, Adv. Geophys. 21, 87–230.
Smith, R.B., 1982, Synoptic observations and theory of orographically disturbed wind and pressure, J. Atmos. Sci. 39, 60–70.
Smith, R.B., 1987, Aerial observations of the Yugoslavian Bora, J. Atmos. Sci. 44, 269–297.
Smith, R.B., 1989a, Hydrostatic airflow over mountains, Adv. Geophys. 31, 1–41.
Smith, R.B., 1989b, Comments on "Low Froude-number flow past three-dimensional obstacles. Part 1: Baroclinically generated lee vortices", J. Atmos. Sci. 46, 3611–3613.
Smith, R.K., 1988, Travelling waves and bores in the lower atmosphere: the 'morning glory' and related phenomena, Earth Sci. Rev. 25, 267–290.
Smith, W.L., 1991, Atmospheric soundings from satellites – false expectation or the key to improved weather prediction, Q. J. R. Meteorol. Soc. 117, 267–297.
Smolarkiewicz, P.K., R. Rasmussen and T.L. Clark, 1988, On the dynamics of Hawaiian cloud bands, J. Atmos. Sci. 45, 1872–1905.
Smolarkiewicz, P.K. and R. Rotunno, 1989a, Low Froude number flow past three-dimensional obstacles. Part I: baroclinically generated lee vortices, J. Atmos. Sci. 46, 1154–1164.
Smolarkiewicz, P.K. and R. Rotunno, 1989b, Reply to a comment by R.B. Smith, J. Atmos. Sci. 46, 3624–3617.
Smolarkiewicz, P.K. and R. Rotunno, 1990, Low Froude number flow past three-dimensional obstacles. Part II: upwind flow reversal zone, J. Atmos. Sci. 47, 1498–1511.
Snyder, W.H., R.S. Thompson, R.E. Eskridge, R.E. Lawson, I.P. Castro, J.T. Lee, J.C.R. Hunt and Y. Ogawa, 1985: On strongly stratified flow over hills: dividing streamline concept, J. Fluid Mech. 152, 249–288.
Spiegel, E.A. and G. Veronis, 1960, On the Boussinesq approximation for a compressible fluid, Astrophys. J. 131, 442–447.
Steiner, J.T. 1972, A three-dimensional model of cumulus development, J. Atmos. Sci. 30, 414–435.
Stern, M.E., 1975, Ocean Circulation Physics (Academic Press, New York).

Stone, P.H., 1966, On non-geostrophic baroclinic stability, J. Atmos. Sci. 23, 390–400.
Sundquist, H., 1970, Numerical simulation of the development of tropical cyclones with a ten-level model, part 1, Tellus 22, 359–390.
Takeda, T., 1971, Numerical simulation of a precipitating convective cloud: the formation of a "long-lasting" cloud, J. Atmos. Sci. 28, 350–376.
Tapp, M.C. and P.W. White, 1976, A nonhydrostatic mesoscale model, Q. J. R. Metoerol. Soc. 102, 277–296.
Taylor, G.I., 1931, Effect of variation in density on the stability of superposed streams of fluid, Proc. R. Soc. A 132, 499–523.
Telford, J.W. and J. Warner, 1962, On the measurement from an aircraft of buoyancy and vertical air-velocity, J. Atmos. Sci. 19, 415–423.
Thorpe, A.J., 1985, Diagnosis of balanced vortex structure using potential vorticity, J. Atmos. Sci. 42, 397–406.
Thorpe, A.J., 1990, Frontogenesis at the boundary between air-masses of different potential vorticity, Q. J. R. Meteorol. Soc. 116, 561–572.
Thorpe, A.J. and M.J. Miller, 1978, Numerical simulations showing the role of the downdraught in cumulonimbus motion and splitting, Q. J. R. Meteorol. Soc. 104, 873–893.
Thorpe, A.J. and R. Rotunno, 1989, Nonlinear aspects of symmetric instability, J. Atmos. Sci. 46, 1285–1299.
Thorpe, A.J., M.J. Miller and M.W. Moncrieff, 1982, Two-dimensional convection in nonconstant shear: a model of midlatitude squall lines, Q. J. R. Meteorol. Soc. 108, 739–762.
Thorpe, A.J., B.J. Hoskins and V. Innocentini, 1989, The parcel method in a baroclinic atmosphere, J. Atmos. Sci. 46, 1274–1284.
Thorpe, S.A., 1981, An experimental study of critical layers, J. Fluid Mech., 103, 321–344.
Tolstoy, I., 1973, Wave Propagation (McGraw-Hill, New York).
Tribbia, J.J., 1981, Nonlinear normal mode balancing and the ellipticity condition, Mon. Weather Rev. 109, 1751–1761.
Tritton, D.J., 1988, Physical Fluid Dynamics, 2nd ed. (Oxford Sci. Publ., Oxford).
Turner, J.S., 1973, Buoyancy Effects in Fluids (Cambridge University Press, Cambridge).
Twitchell, P.F., E.A. Rasmussen and K.L. Davidson, eds 1989, Polar and Arctic Lows (Deepak, Virginia).
Uccellini, L.W., 1980, On the role of upper tropospheric jet streaks and leeside cyclogenesis in the development of low level jets in the great plains, Mon. Weather Rev. 108, 1689–1696.
Uccellini, L.W., 1990, Processes contributing to the rapid development of extratropical cyclones, in: Extratropical Cyclones, eds C.W. Newton and E.O. Holopainen (American Meteorological Society, Boston) pp. 81–105.
Uccellini, L.W. and D.R. Johnson, 1979, The coupling of upper and lower tropospheric jet streaks and implications for the development of severe convective storms, Mon. Weather Rev. 107, 682–703.
Uccellini, L.W. and S.E. Koch, 1987, The synoptic setting and possible sources for mesoscale wave disturbances, Mon. Weather Rev. 115, 721–729.
Van Delden, A., 1985, On the preferred mode of cumulus convection, Beitr. Phys. Atmosph. 58, 202–219.
Van Delden, A., 1988, On the flow-pattern of shallow atmospheric convection, Beitr. Phys. Atmosph. 61, 169–186.
Van Delden, A., 1989a, Gradient wind adjustment, CISK, and the growth of polar lows by diabatic heating, in: Polar and Arctic Lows, eds P.F. Twitchell, E.A. Rasmussen and K.L. Davidson (Deepak, Virginia) pp. 109–113.
Van Delden, A., 1989b On the deepening and filling of balanced cyclones by diabatic heating, Meteorol. Atmos. Phys. 41, 127–145.
Van den Berg, W.D. 1987, Coastal Frontogenesis in The Netherlands: Observations and Modeling, PhD thesis, University of Utrecht.
Van der Hoven, J., 1957, Power spectrum of horizontal wind speed in the frequency range from 0.0007 to 900 cycles per hour, J. Meteorol. 14, 160–164.
Van Dyke, M., 1982, An Album of Fluid Motion (The Parabolic Press, Stanford).
Veltishchev, N.K. and A.A. Zelnin, 1975, Numerical simulation of convection in air, J. Fluid Mech. 68, 353–368.
Vergeiner, I. and E. Dreiseitl, 1987, Valley winds and slope winds: observations and elementary thoughts, Meteorol. Atmos. Phys. 36, 264–286.
Vinnichenko, N.K., Kinetic energy spectrum in the free atmosphere, Tellus 22, 158–166.
Volland, H., 1988, Atmospheric Tidal and Planetery Waves (Kluwer, Deventer).
Walsh, J.E., 1974, Seabreeze theory and applications, J. Atmos. Sci. 31, 2012–2026.
Weatherford, C.L. and W.M. Gray, 1988, Typhoon structure as revealed by aircraft reconnaisance, Mon. Weather Rev. 116, 1032–1056.
Weisman, M.L. and J.B. Klemp, 1986, Characteristics of isolated convective storms, in: Mesoscale Meteorology and Forecasting, ed. P.S. Ray (American Meteorological Society, Boston) pp. 331–358.
Weisman, M.L., J.B. Klemp and R. Rotunno, 1988, Structure and evolution of numerically simulated squall lines, J. Atmos. Sci. 45, 1990–2013.
Wessels, H.R.A., 1968, De zware windhozen van 25 juni 1967, Hemel en Dampkring 66, 155–177.
Weston, K.J., 1972, The dry-line of northern India and its role in cumulonimbus convection, Q. J. R. Meteorol. Soc. 98, 513–531.
Whiteman, C.D., 1990, Observations of thermally developed wind systems in mountainous terrain, in: Atmospheric Processes over Complex Terrain, Meteorological Monographs, Vol. 23, ed. W. Blumen (American Meteorological Society, Boston) pp. 5–42.
Wihelmson, R.B. and J.B. Klemp, 1978, A three-dimensional numerical simulation of splitting that leads to long-lived storms, J. Atmos. Sci. 35, 1037–1063.
Williams, R.T., 1974, Numerical simulation of steady state fronts, J. Atmos. Sci. 31, 1286–1296.
Willoughby, H.E., 1977, Inertia-buoyancy waves in hurricanes, J. Atmos. Sci. 34, 1028–1039.
Willoughby, H.E., 1978, A possible mechanism for the formation of hurricane rainbands, J. Atmos. Sci. 35, 838–848.
Willoughby, H.E., 1979, Forced secondary circulations in hurricanes, J. Geoph. Res. 84, 3173–3182.
Willoughby, H.E., 1988, The dynamics of the tropical cyclone core, Aust. Met. Mag. 36, 183–191.
Willoughby, H.E., 1990a, Temporal changes of the primary circulation in tropical cyclones, J. Atmos. Sci. 47, 242–264.
Willoughby, H.E., 1990b, Gradient balance in tropical cyclones, J. Atmos. Sci. 47, 265–274.

Willoughby, H.E., 1991, Reply to comments by W.M. Gray, J. Atmos. Sci. 48, 1209–1212.
Willoughby, H.E., J.A. Clos and M.G. Shoreibah, 1982, Concentric eye walls, secondary wind maxima, and the evolution of a hurricane vortex, J. Atmos. Sci. 39, 395–410.
Willoughby, H.E., F.D. Marks Jr. and R.J. Feinberg, 1984: Stationary and moving convective bands in hurricanes, J. Atmos. Sci. 41, 3189–3211.
Willoughby, H.E., H.-L. Jin, S.J. Lord and J.M. Piotrowicz, 1984, Hurricane structure and evolution as simulated by an axisymmetric, nonhydrostatic numerical model, J. Atmos. Sci. 41, 1169–1186.
Wipperman, F., 1981, The applicability of several approximations in meso-scale modelling, Beitr. Phys. Atmosph. 54, 298–308.
Witney Jr., L.F., 1977, Relationship of the subtropical jet stream to severe local storms, Mon. Weather Rev. 105, 398–412.
Yamasaki, M., 1974, Finite-amplitude convection in a conditionally unstable stratification, J. Meteorol. Soc. Japan 52, 365–379.
Yamasaki, M., 1977, The role of surface friction in tropical cyclones, J. Meteorol. Soc. Japan 55, 559–571.
Yanai, M., 1964, Formation of tropical cyclones, Rev. Geophys. 2, 367–414.
Yih, C.-S., 1980, Stratified Flow (Academic Press, New York).
Zhang, D.-L. and J.M. Fritsch, 1988, A numerical investigation of a convectively generated, inertially stable, extratropical warm-core mesovortex over land. Part 1: structure and evolution, Mon. Weather Rev. 116, 2660–2687.
Zhang, D.-L. and J.M. Fritsch, 1988, Numerical simulation of the meso-β scale structure and evolution of the 1977 Johnstown flood. Part 3: internal gravity waves and the squall line, J. Atmos. Sci. 45, 1252–1268.